博士論文

**Development of Electrical Discharge Machining
System for Cutting Single Crystal SiC**

（単結晶 SiC の放電加工システムの開発）

趙　永華

Doctoral Dissertation

東京大学
THE UNIVERSITY OF TOKYO

Development of Electrical Discharge Machining System for Cutting Single Crystal SiC

（単結晶 SiC の放電加工システムの開発）

指導教員　国枝　正典　教授

東京大学大学院　工学系研究科　精密機械工学専攻

趙　永華

Development of Electrical Discharge Machining System for Cutting Single Crystal SiC

Yonghua ZHAO

The thesis describes the development of new electrical discharge machining (EDM) methods and systems for application of EDM on slicing and coring of single crystal silicon carbide (SiC) ingot.

Single crystal silicon carbide (SiC), emerging as a high-performance semiconductor material for next-generation high temperature, high frequency and high energy efficiency power devices, brings new challenges to the conventional wafer manufacturing process due to its higher hardness which is almost 2 times of that of conventional semiconductor silicon (Si). Since the hardness of SiC is approaching to that of diamond, diamond is the only tool material that is qualified for the fabrication of SiC wafer (including grinding, slicing, polishing, lapping etc.), which results in a high cost of the manufacturing process. In addition, due to its high hardness, the machining efficiency is very low when the conventionally used manufacturing process for Si is applied to SiC. On the other hand, it is possible to machine SiC by electrical discharge machining (EDM) owing to its conductivity. Besides, it was reported that wire EDM slicing of SiC wafer showed a higher machining rate and lower wafer surface damage compared to multi-wire saw method. However, the material removal mechanism and EDM characteristics of SiC are still not clear. On top of this, wire EDM, especially the currently being developed multi-wire EDM, meets several problems when it is applied to slice SiC wafer, including wire breakage, wire vibration and low productivity etc. Therefore, this thesis is devoted to clarifying the EDM mechanism and characteristics of SiC and developing new electrical discharge machining methods and systems to enhance and advance the application of EDM for cutting SiC and SiC-like materials in the future.

In Chapter 1, at first the subjects and objectives of manufacturing SiC wafer were briefly introduced and the current problems and disadvantages of the conventional standard slicing process of SiC wafer such as high cost, low efficiency, large kerf loss, and the sliced SiC wafer accuracy etc. were described. On top of these, state of the art of EDM of SiC and the development of multi-wire electrical discharge slicing (EDS) of SiC were described and the problems and difficulties of application of wire EDM for cutting SiC were described. Following this, the purpose of this research and the constitution of the thesis were described.

In Chapter 2, the differences between EDM of SiC and widely-used steel material were investigated. Experimental results showed that although SiC had a higher resistivity as semiconductor compared to steel, the material removal efficiency was much higher than that of steel. The fracture behavior of SiC by thermal shock owing to its brittleness in EDM was considered as one of the material removal mechanisms of EDM of SiC. Moreover, the influence of the high resistivity of SiC on EDM properties were revealed by conducting heat conduction analysis of single discharge using finite difference method taking into consideration the Joule heating effect in EDM of SiC. The analysis showed that Joule heating effect had a significant influence on the surface temperature at the discharge spot. However, due to the high thermal

conductivity of SiC, the surface temperature dropped quickly after the discharge ignition. In addition, the influence of the crystal anisotropy on the wire EDM cutting performance were investigated. It was found that wire EDM of SiC presented a higher machining rate when the cutting direction is parallel to the c axis. At last, the wire EDM cutting performances of SiC were evaluated in terms of area cutting speed, surface roughness and topography, sub-surface damaged layer and wire breakage. Wire breakage problem was found serious in wire EDM of SiC especially when large duty factor was used. In order to solve the wire breakage problem, foil electrode was proposed in Chapter 3.

Chapter 3 describes the machining performance of SiC by utilizing band-shaped foil tool electrode. In order to solve the wire breakage problem and reduce the wire vibration in wire EDM slicing, foil EDM of SiC was proposed for slicing SiC instead of wire electrode because foil tool electrode could be as thin as several tens micrometers while taking a larger tension force and discharge current compared to those of wire electrode. A foil tool electrode fixture was newly developed and installed on the main axis of sinking EDM machine to perform foil EDM cutting experiments like normal sinking EDM process. The feasibility of EDS of SiC by foil tool electrode was proved by experiments. Furthermore, the influences of foil tool electrode thickness, foil tool polarity, foil tool material, cut depth, pulse conditions and dielectric liquid on the foil EDM cutting performances were described. It was found that negative tool polarity and short pulse duration were more suitable for machining SiC. Thinner foil tool electrode could achieve a higher area cutting speed, however the tool wear also increased. Copper foil was found most practical for being used as the tool electrode. EDM of SiC in water could achieve a higher machining rate, however, EDM of SiC in oil presented a better surface integrity and thinner sub-surface damaged layer. The reasons for the differences between EDM of SiC in oil and in deionized water, for example, cooling effect and permittivity of the working liquid etc. were discussed. In addition, it was found that with increasing the cut depth the foil EDM cutting speed decreased probably due to deteriorated gap conditions. The foil tool electrode wear length also increased considerably, which made it impracticable to slice large diameter ingot continuously and stably. In order to improve the flushing conditions and disperse the tool length wear, reciprocating slicing of SiC by tensioned foil electrode was proposed. In the developed method, foil EDS was conducted by servo feeding the tensioned foil electrode to the workpiece which was reciprocated by a reciprocating worktable. The development of the experimental setup of reciprocating slicing method was presented and the machining experiments of foil EDS of SiC were described. Experimental results showed that reciprocating foil EDS method could disperse the tool wear along the reciprocating direction and improve the flushing conditions. The tool wear length along the reciprocating direction in the reciprocating stroke, however, was not uniform which brought about instability of the reciprocating slicing process due to frequent change of the discharge gap width.

In Chapter 4, development of stable and continuous EDS of SiC by running foil tool electrode method is described. In order to eliminate the instability of EDS of SiC caused by the uneven tool wear in the reciprocating slicing method mentioned above, running foil EDS method was developed. The running foil EDS was conducted by feeding the workpiece towards a foil tool electrode which was running in just one-direction. The mechanism of running foil EDS was based on a steady tool wear model of the running foil which enabled a stable slicing process. Analysis of the tool wear model at steady state showed that the tool wear length in running foil EDS was decided by the tool wear ratio, foil running speed and workpiece width. The development of the new experimental system of the running foil EDS method was described and the machining stability of this method was presented. The performances of running foil EDS of SiC

such as slicing speed, kerf width etc. were described. In addition, the influences of flushing effect on the running foil EDS performance were investigated. Both higher foil running speed and flushing could contribute to improve the slicing speed. An average kerf width of around 95μm was achieved by this method with foil tool electrode thickness of 30μm.

In Chapter 5, development of multi-discharge EDM of SiC by electrostatic induction feeding method is described. Aiming to improve the productivity of foil EDS, multi-foil electrical discharge slicing of SiC was proposed. In the multi-wire EDS method which is being widely developed for slicing SiC ingot currently, a single wire is wound multiple turns and the electricity is fed to each winding turn of the wire electrode at the same time. Multi-discharge is realized by introducing a large impedance into each branch of discharge circuit so that the electrical potential at each wire electrode will not be easily affected by the occurrence of one discharge at a certain wire electrode. However, introduction of large impedance brings about low energy efficiency due to the consumption of electric energy of the resistance. Besides, large impedance (mainly inductance XL) in the discharge circuit makes it difficult to generate discharges with short pulse duration which is considered necessary to perform high accuracy and efficiency slicing of SiC. In conclusion, this method is still under developing. On the other hand, EDM by the electrostatic induction feeding (EIF) method, in principle, can realize multiple discharges with an extremely simple discharge circuit (no resistance is required in the discharge circuit). In addition, in this method, only a bipolar pulse power supply is required to realize multiple discharges at the same time. Non-contact feeding of electricity can also be achieved by the electrostatic induction feeding if necessary. Therefore, the challenge of applying this method to multi-discharge EDS of SiC was proposed in this study. However, due to the limited conditions in developing the multi-foil EDS system, experimental setup of multiple-discharge EDM coring of SiC ingot was developed instead to investigate the proposed multi-discharge EDM method. The development of the new experimental setup was described and the machining experiments were presented. The multi-discharge EDM coring experiments were performed successfully. With six sets of separate tool electrodes, six discharges were generated simultaneously or sequentially in a single pulse of the pulse power supply. The discharge frequency was increased to several times of the frequency of the pulse power supple. The machining rate of multi-discharge EDM by EIF could be increased by increasing the pulse power source frequency and the number of separate feeding capacitors. Moreover, compared with the conventional single-discharge EDM by the electrostatic induction feeding method under the same total discharge energy, both the machining efficiency and the machining accuracy could be improved by the multi-discharge EDM by EIF due to the separate feeding of electricity. It is therefore considered that the same method and principle can be applied for multi-foil EDS method.

In Chapter 6, the main findings obtained in Chapter 2 to Chapter 5 are summarized as the final conclusions of this thesis. The remaining research subjects and the perspective of the future research work are described based on this research.

Table of Contents

Symbols

A : Cross-section area of electrode

B : Foil bobbin diameter

c : Specific heat

d_0 : Wire diameter

$d(t)$: Time-dependent plasma diameter

D : Electric flux density

E : Electric field intensity

E_0 : Power supply voltage

F : Tension force of foil electrode

F_r : Resultant force

h : Foil tool wear length

I_z : Inertia moment

i : Current

$\bar{i}$: Average discharge current

i_e : Discharge current

j : Current density

k : Elastic Modulus

K_s : Gauge factor of strain gauage

l : Length

L : Slicing thickness of workpiece

m : Foil electrode thickness

n : Foil electrode width

P : Torque

Q : Heat energy

$\dot{Q}$: Joule heat generated per unit time

q'' : Heat flux

$\dot{q}$	: Energy generation rate per unit volume of medium in heat transfer process
R	: Resistance
R_{max}	: Surface roughness
S	: Cross-section area of conductor / control volume
T	: Temperature
t	: Time
t_d	: Discharge delay time
t_e	: Discharge duration
t_o	: Discharge interval
U	: Open voltage
V	: Electrical potential
V_0	: Output voltage of Wheatstone Half-Bridge circuit
v	: Foil running speed
v_e	: Workpiece feed speed
U_e	: Voltage drop inside arc plasma
U_m	: Measured value of discharge gap voltage in experiments
U_t	: Voltage drop inside tool electrode
U_w	: Voltage drop inside workpiece
W	: Volume
W_e	: Tool electrode wear volume
W_w	: Material removal volume of workpiece
W_z	: Section modulus
X_L	: Inductive reactance
Z	: Impedance
λ	: Thermal conductivity
θ	: Melting point / Decomposition point
ρ	: Electrical resistivity
ρ_d	: Material density

π : Circular constant

η : Energy distribution ratio of anode in single discharge

τ : Tool wear ratio

ε : Strain

ε_d : Dielectric constant (permittivity)

ε_0 : Vacuum dielectric constant

σ : Stress

σ_{ts} : Tensile strength

σ_{max} : Maximum normal stress

Chapter 1   Introduction

1.1   Electrical Discharge Machining [1, 2, 3]

Electrical Discharge Machining (EDM), known as a non-traditional manufacturing process, removes material by melting and/or evaporating of the workpiece by a series of rapidly recurring discharges generated between two electrodes in a dielectric medium (oil, deionized water, air, etc.). One of the electrodes is called tool electrode, while the other is called workpiece. By placing the tool electrode oppositely to the workpiece at a distance of several μm to several tens μm and applying a high voltage between them, arc discharge with intense heat can be generated at a certain point by the breakdown of the dielectric. The high temperature of the arc plasma (around 7000K) of discharge can melt and/or evaporate the workpiece material and form a discharge crater on the workpiece surface. The material is removed by accumulation of the discharge craters. However, since the arc plasma heats the tool electrode while removing material from the workpiece, tool wear exists in EDM as the normal machining process.

In general, EDM is classified into two main categories, which are well known as sinking EDM and wire EDM respectively, according to their different specialty and application. Sinking EDM process, also referred to as die sinking EDM, is generally used to machine a workpiece with desired shape by utilizing a reversely shaped tool electrode as shown in **Fig. 1.1**. Therefore, sinking EDM is widely used in the mold industry and also for machining intricate shapes. On the other hand, wire EDM, as shown in **Fig. 1.2**, uses a metal wire (brass, molybdenum, tungsten, etc.) with diameter of 20μm ~300μm as the tool electrode to cut the workpiece like wire saw process. Either very thin and flexible metal or very thick metal can be cut precisely and easily by wire EDM. Particularly, since the wire is running during machining and new wire is supplied from the wire bobbin all the time, tool wear is not a problem in wire EDM. **Table 1.1** lists the general differences between sinking EDM and wire EDM process.

Table 1.1 Differences between sinking EDM and wire EDM [3]

	Material of Tool electrode	Discharge current waveform	Workpiece polarity	Dielectric
Sinking EDM	Copper, Copper tungsten, Graphite, Tungsten, Tungsten carbide	Relatively low discharge current with long discharge duration	Mostly $(-)$	EDM oil
Wire EDM	Brass wire, Tungsten wire, Zink and Brass coated steel wire	Extremely high discharge current with short pulse duration	$(+)$	Deionized water, EDM oil
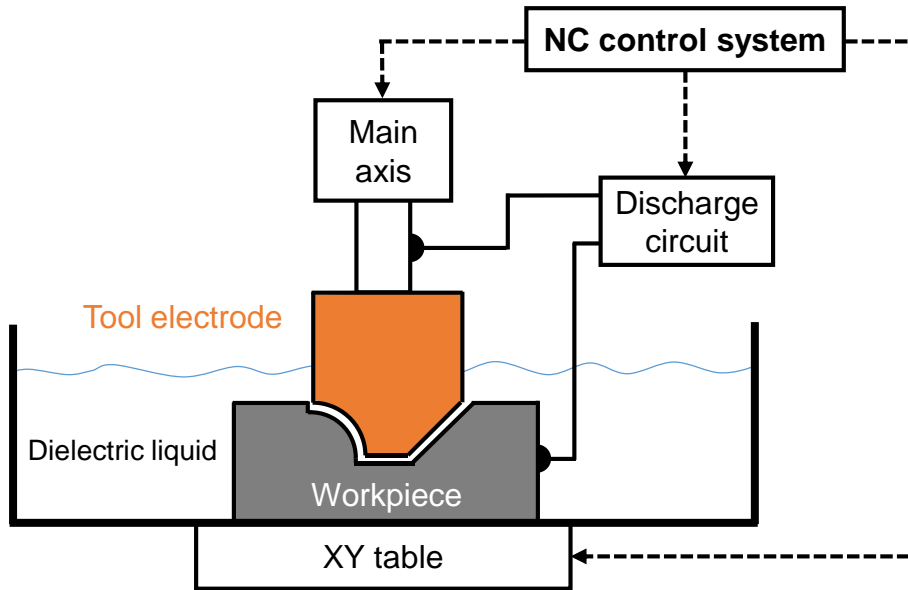
Fig. 1.1 Diagram of sinking electrical discharge machining
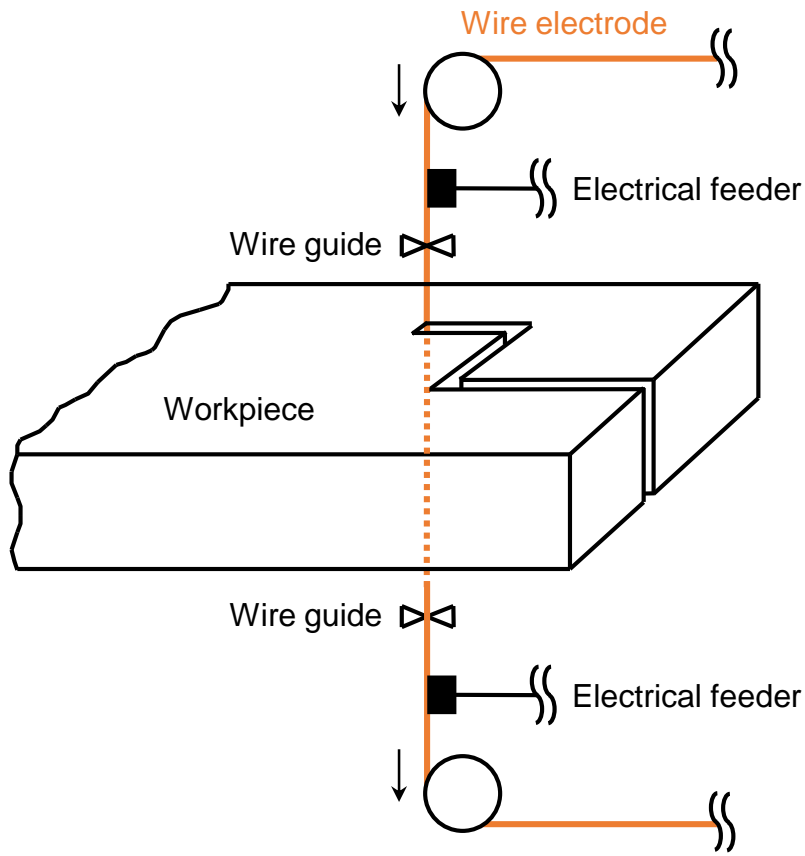
Fig. 1.2 Diagram of wire electrical discharge machining

In principle, any conductive materials can be machined by EDM. Compared to conventional mechanical cutting process, since EDM removes materials by means of heat energy instead of mechanical deformation, EDM is capable to machine any material with conductivity regardless of the hardness. In terms of machining reaction force, since EDM is no contact machining, workpiece with high aspect ratio can be achieved. In addition, machining of micro intricate parts can also be performed owing to small reaction force.

1.2 Principle of electrical discharge machining [1, 2, 3, 4, 5]

In EDM discharge is generally considered as arc discharge. In a single pulse (duration longer than several microseconds), single discharge is generated randomly at one spot on electrode surfaces. At the discharge spot, discharge current (current density approaching to $10^8 \sim 10^9 \text{A/m}^2$) flows through the arc column which is formed by the breakdown of dielectric medium. Super high heat flux generated from the arc column flows into the local areas on electrode surfaces where the arc column exists and results in melting and/or evaporation of the electrode materials. The melted electrode material is then cooled and removed by the flushing of dielectric liquid and leaves a discharge crater on the electrode surfaces. The removal volume of single discharge is very small and the machining is accomplished by accumulating small discharge craters through rapidly repeated discharges. In detail, it is considered that the formation of discharge and removal of material are done as illustrated in **Fig. 1.3**.

(a) Generation of arc discharge

Setting tool electrode (cathode) and workpiece (anode) facing each other at a distance of several tens to several hundred μm, if high voltage (around 100V) is applied to the gap between the two electrodes, free electrons existing in the gap (dielectric medium) will be excited and accelerated and dash against the anode by the electric field, while collide with other neutral particles existing in the dielectric medium. Neutral particles will lose electrons due to collision and changes into positive ions. In consequence the number of free electrons increases which further promote the ionization of dielectric by more severe collision in the gap, which is considered as avalanche ionization. The increased positive ions generated by ionization will also be accelerated by the electrical field and collide with the cathode, of which the collision energy will result in secondary electron coming out from the cathode surface. Thus dielectric medium breaks down and current flows through the gap. With the further increase of current density at the cathode surface, the cathode surface temperature will increase and cause thermionic emission of electrons. Together with the electrons existing in the electrical field, the supply of electrons in the gap will be explosively increased and arc discharge is formed in the gap.

(b) Removal of electrode material and generation of bubble

The plasma generated in the gap has a temperature of 6000K~7000K [6]. Once the arc plasma column is generated, heat flux will be applied to the discharge spots on the tool and workpiece surfaces which has a power density of around 10^9W/m^2. The material of tool electrode and workpiece will be melted and evaporated by the heat flux of arc plasma column. In the meantime, the dielectric liquid near the arc plasma column will also be evaporated due to its high temperature. Together with the evaporation of electrode materials, volume of bubble generated in the gap around the arc column will increase sharply after the

ignition of arc discharge. The generated bubble shows extremely high pressure and expands rapidly towards the surrounding dielectric liquid, which can achieve a speed of 25m/s at the boundary of the bubble. In the end, the radius of the bubble around the arc column center can reach up to several millimeters. The melted materials are cooled and re-solidified by the surrounding dielectric liquid and change into small balls which are generally referred to as EDM debris and removed with the flushing of dielectric liquid.

(c) Recovery of dielectric strength

The generated arc discharge finishes when the pulse power source supply is off. With the finish of arc discharge, the temperature at discharge spot decreases and electrons and ions recombine together. Consequently the conductivity of the dielectric liquid will be decreased significantly which is usually referred to as recovery of dielectric strength or extinguish of arc plasma. In order to avoid discharge concentration and localization, the dielectric strength of the working liquid must be fully recovered before the next pulsed discharge. Generally it takes about 5μs or less [7] for the center temperature of the arc plasma to drop under 5000K, which is considered as the temperature at which the dielectric breakdown strength is sufficiently recovered in sink EDM with pulse duration of several tens μs.

(d) Formation of discharge crater

The melted material on the tool and workpiece surface cannot be removed completely. The left unremoved material is re-solidified and forms a discharge crater on the tool/workpiece surface. Therefore, the top layer of discharge crater is generally considered as re-solidified layer. Beneath the re-solidified layer, there is a heat affected layer.

a) Generation of arc discharge

4
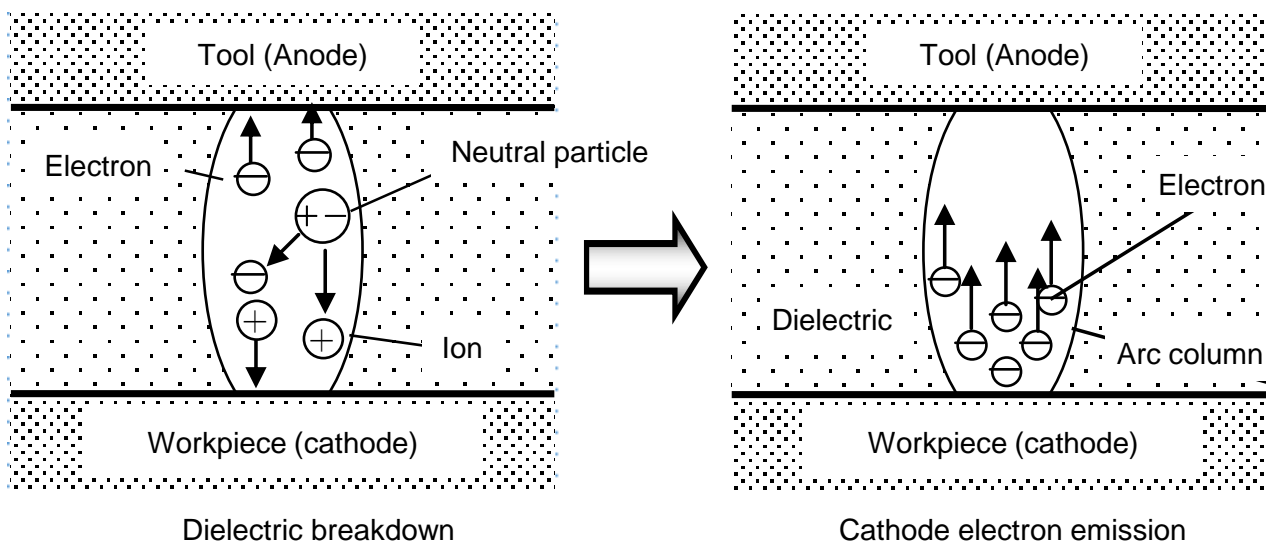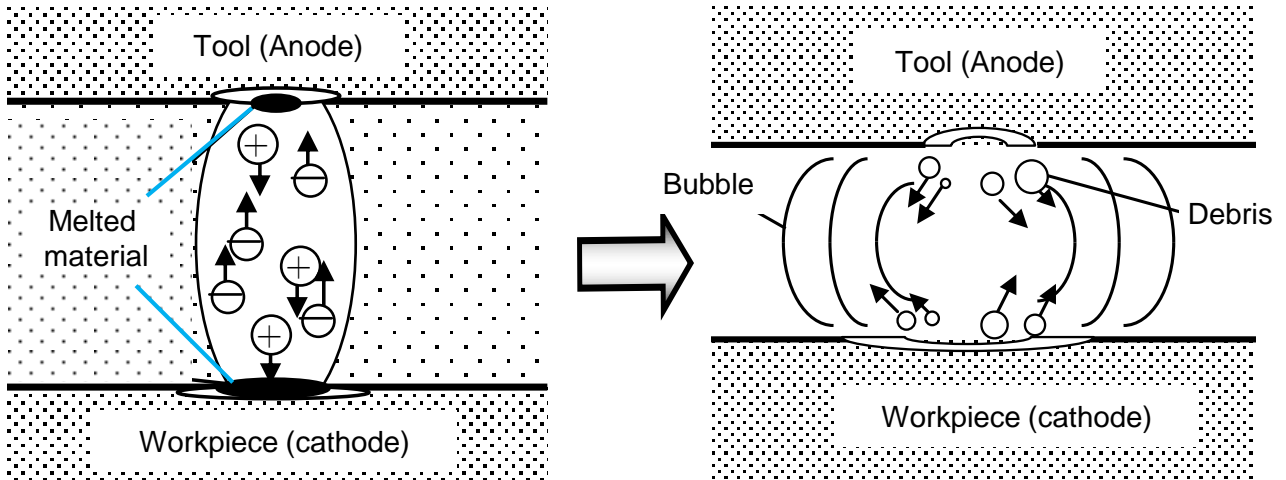
b)   Material removal and generation of bubble
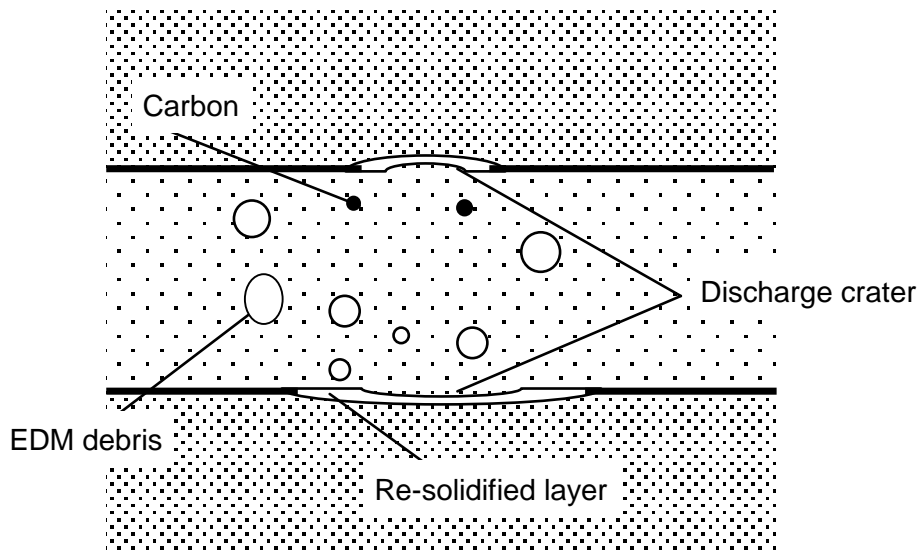
c)   Recovery of dielectric and formation of discharge crater

Fig. 1.3 Illustration of electrical discharge machining mechanism

1.3 Discharge circuit

This section describes the discharge circuit and discharge waveforms from the perspective of the mechanism of sinking EDM and wire EDM respectively.

1.3.1   Discharge circuit in sinking EDM

In EDM, pulsed discharges must be generated to realize stable and high precision machining. In normal sinking EDM, transistor type pulse generators are generally used to generate discharge pulses.

Fig. 1.4 shows the general discharge circuit in sinking EDM which is usually referred to as transistor type discharge circuit. Pulsed discharges are generated by switching on/off the transistors in the circuit orderly. The discharge current and discharge gap voltage can be measured by using current sensor and voltage probe respectively, as shown in **Fig. 1.5**. The typical discharge waveforms are shown in **Fig. 1.6**.

i) Applying voltage to discharge gap

 When the transistors are switched on, the open voltage U of the power source (around 100~200V) will be applied to the discharge gap which results in an electrical potential difference between the tool electrode and the workpiece. However, discharge doesn't occur immediately. As shown in **Fig. 1.6**, there is usually a discharge delay time before discharge occurs and the discharge delay time depends on the gap conditions (gap width, existence of other particles, etc.). If the gap width becomes shorter, usually the discharge delay time will become shorter. However, if the gap distance becomes zero, short circuiting will occur, showing 0V gap voltage as marked in **Fig. 1.6**. When the dielectric breakdown strength is not recovered during the discharge interval, the next discharge occurs at the same place as the previous discharge, reducing the dielectric breakdown strength further. In this situation also, the discharge delay time becomes zero, which is usually considered as abnormal discharge.

ii) Occurrence of discharge and control of discharge duration

After the discharge gap is broken-down, the discharge current flows from the power source to the discharge gap and the gap voltage is dropped to around 20V, which is usually referred to as discharge voltage U_e, regardless of the discharge current. The discharge current can be determined by the resistance in each branch circuit and/or the number of transistors which are set on at the same time. The occurrence of discharge can be detected by the pulse control circuit. The discharge current flows in a preset time t_e, which is referred to as discharge duration. After t_e, the pulse control circuit will forcibly turn off the transistor and stop the current. By controlling the discharge duration the same, the material removal volume of single discharge can be kept the same so that high accuracy finished surface can be accomplished in EDM.

iii) Discharge interval

After discharge, the transistor will be kept off for a time of t_o, which is referred to as discharge interval time. During the compulsory discharge interval time t_o, the arc plasma of the previous discharge is extinguished completely and the dielectric strength is fully recovered so that the next discharge will be generated at different places. In other words, the discharge interval time is essential to the dispersion of discharge locations in EDM to avoid discharge concentration.

After the discharge interval when the dielectric strength is fully recovered, the transistor will be switched on again by the pulse control circuit to apply voltage to the discharge gap. The machining is conducted by repeating the process from i) to iii).

The percentage of actual discharge time in machining is usually evaluated by duty factor (*D. F.*), which is defined as the following equation (Eq. 1.1), where $<t_d>$ indicates the average discharge delay time.
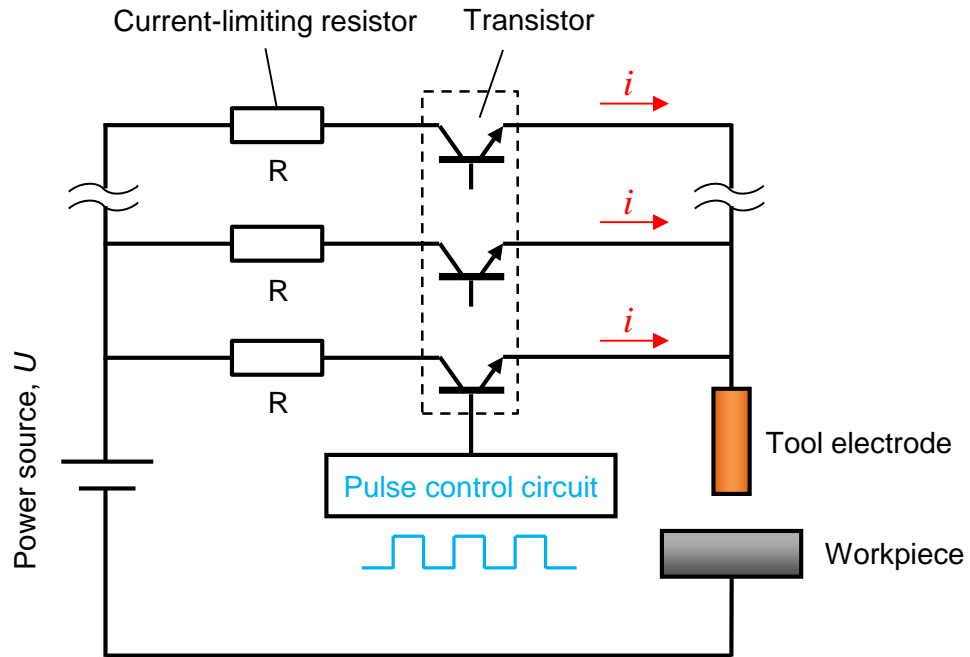
Fig. 1.4 Discharge circuit with transistor type pulse generator
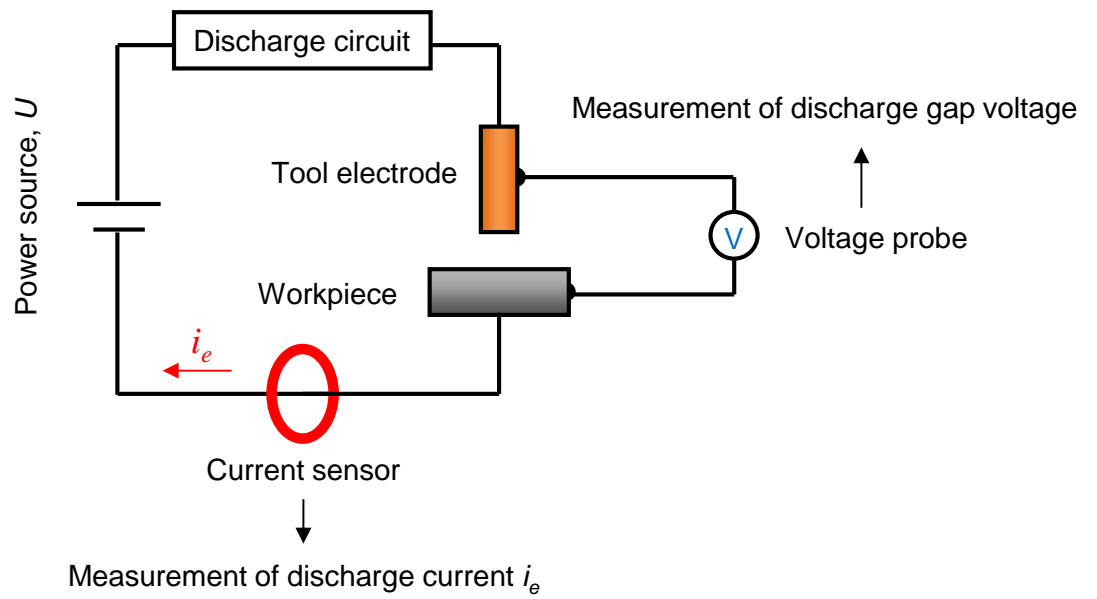
Fig. 1.5 Illustration of measurement method of discharge current and discharge gap voltage in EDM
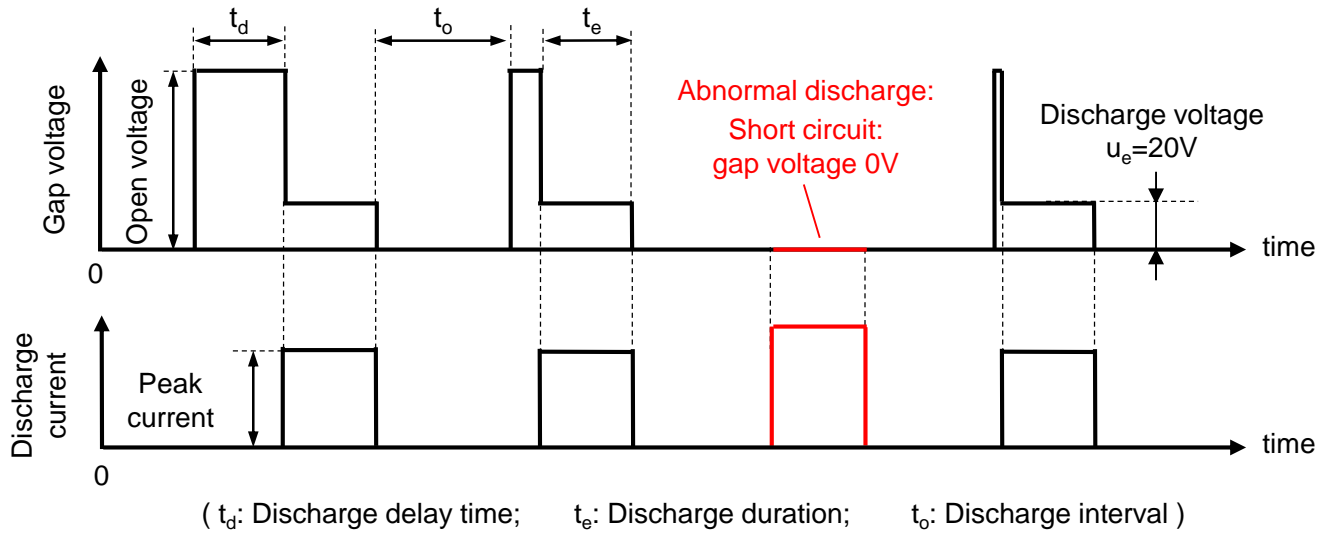
Fig. 1.6 Discharge voltage and current waveforms in transistor type discharge circuit

Generally, the larger the D.F. is, the higher material removal rate can be achieved. However, too large D.F. will cause instability of EDM process due to insufficient discharge interval time.

$$D.F. = \frac{t_e}{<t_d> + t_e + t_o}$$
Eq. 1.1

1.3.2 Discharge circuit in wire EDM

Wire EDM also utilizes transistor type discharge circuit. However, the discharge circuit and discharge waveform are different from those of sinking EDM due to their different characteristics and applications. One of the most significant characteristics distinguishing wire EDM from sinking EDM is tool wear (tool wear is not a problem in wire EDM since new wire is supplied continuously), which brings about great differences of discharge circuit and discharge waveforms between wire EDM and sinking EDM.

The schematic diagram of the discharge circuit of wire EDM used in this research is shown in **Fig. 1.7**. **Fig. 1.8** shows the corresponding discharge waveforms.

In the discharge circuit, bipolar pulse power source with a relatively low open voltage (around 80V) is applied to the discharge gap to ignite the discharge. The reason is as the following. In wire EDM, deionized water is more preferable to hydrocarbon dielectrics to be used as the working liquid considering fire hazards. However, since the workpiece in wire EDM is usually set as plus to improve the machining rate, the electrolytic action of deionized water must be avoided to improve the machining accuracy. To realize this, the workpiece polarity is set to minus periodically by the bipolar pulse power source.

8

On the other hand, however, after the discharge gap breaks down, the high open voltage (around 280V) power source with high current output is applied to the discharge gap to supply a very high peak and short duration (0.5~5µs) pulse current to improve the material removal rate, as shown in **Fig. 1.8**. In addition, to increase the machining rate, the workpiece polarity is always set as anode when the high current is applied. Moreover, the discharge gap voltage is slightly higher than 20V when the high open voltage power source is acting due to significant current density.

Pulse condition with short discharge duration and high peak current is commonly used in wire EDM to achieve a high machining efficiency because it can generate larger heat flux compared with the pulse condition of smaller discharge current and longer pulse duration under the same discharge energy. Although the tool wear will also increase under this condition, it is not a problem in wire EDM because new wire electrode is being supplied all the time during machining. In sinking EDM, however, the pulse duration are usually longer while discharge current is lower to reduce the tool wear as shown in **Table 1.1**. On top of this, the short pulse duration in wire EDM can provide better surface integrity due to small discharge energy of single discharge.
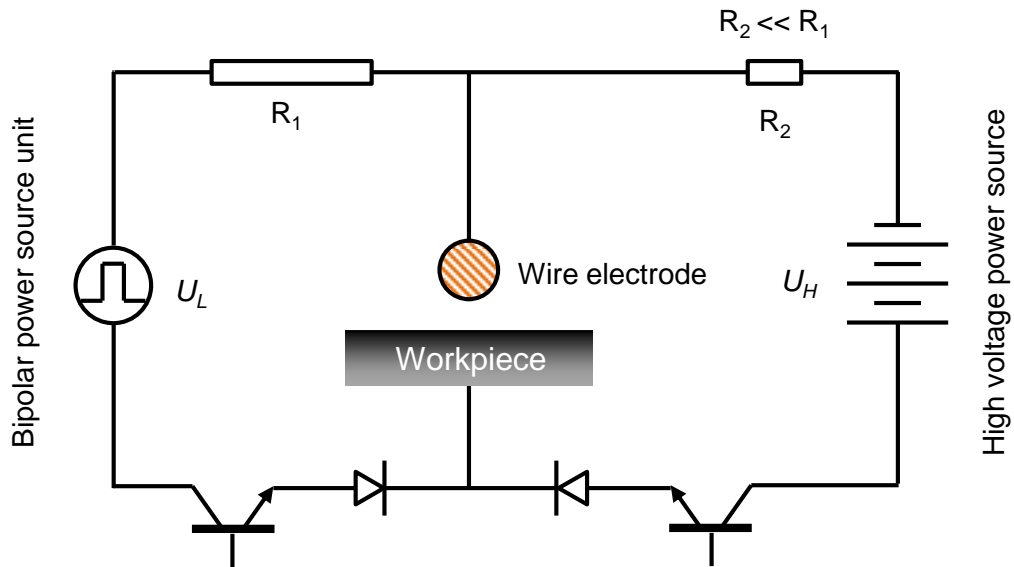
Fig. 1.7 Schematic diagram of discharge circuit in wire EDM
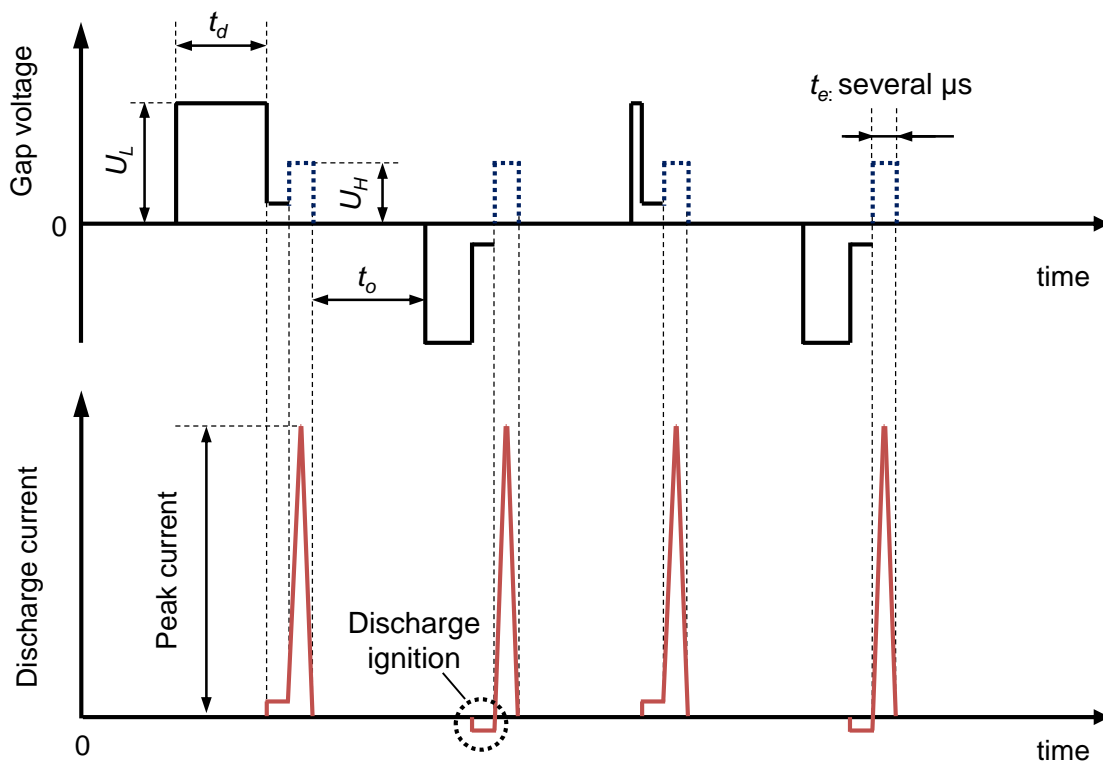
Fig. 1.8 Schematic diagram of discharge circuit in wire EDM

1.4 Servo feed control mechanism

In EDM, the tool electrode feed speed is not constant but changing adaptively according to the discharge gap conditions while in the conventional machining methods the cutting tools are fed at a constant speed. The control method of tool feed in EDM is referred to as servo feed control. The target of the servo feed control is to maintain the discharge frequency at a constant and optimal value to achieve the maximum machining efficiency. However, the discharge gap width is critical to the discharge frequency. Too large discharge gap will result in a low discharge frequency while too small discharge gap may cause discharge concentration or short circuit. In other words, the servo feed control system tries to maintain a proper discharge gap width during machining.

Thus, the servo feed system in EDM controls the tool feed speed based on the difference between the measured average gap voltage and the preset servo reference voltage. The average gap voltage (the average value of the discharge gap voltage in a certain time) is obtained by the control unit of the EDM machine during machining at a sampling frequency of several tens Hz. To be specific, the servo feed speed is proportional to the voltage difference between the measured average discharge gap voltage and the preset servo reference voltage.

Fig. 1.9 shows the principle of servo feed control in EDM which can keep the discharge gap width at the proper width. On one hand, if the tool feed speed is too slow, the gap width will increase. Increased gap width will result in a longer discharge delay time due to larger gap breakdown strength. In consequence, the discharge delay time will become longer and cause a higher average gap voltage. If the measured average gap voltage is higher compared to the preset servo reference voltage, the tool will be fed by the servo control unit. On the other hand, however, if the feed speed is too fast, the gap width will become smaller, resulting in a shorter discharge delay time. In consequence, the measured average gap voltage will become lower than the preset servo reference speed and the tool electrode will be retracted back. By repeating this process, the gap width and discharge frequency in EDM is controlled at a proper value.

With regard to the preset servo reference voltage, on one hand, if it is set too high, the discharge gap width will be kept at a large value which can facilitate the removal of EDM debris. However, the replication accuracy of the tool shape will decrease due to the large gap width. In addition, the machining rate will also decrease due to decreased discharge frequency at a large gap width. On the other hand, if the servo reference voltage is set too low, the discharge gap will be maintained at a small width due to too high servo feeding speed. Too small gap width will increase the probability of discharge concentration or short circuit. In practice, the reference voltage is usually selected based on experimental or empirical data.
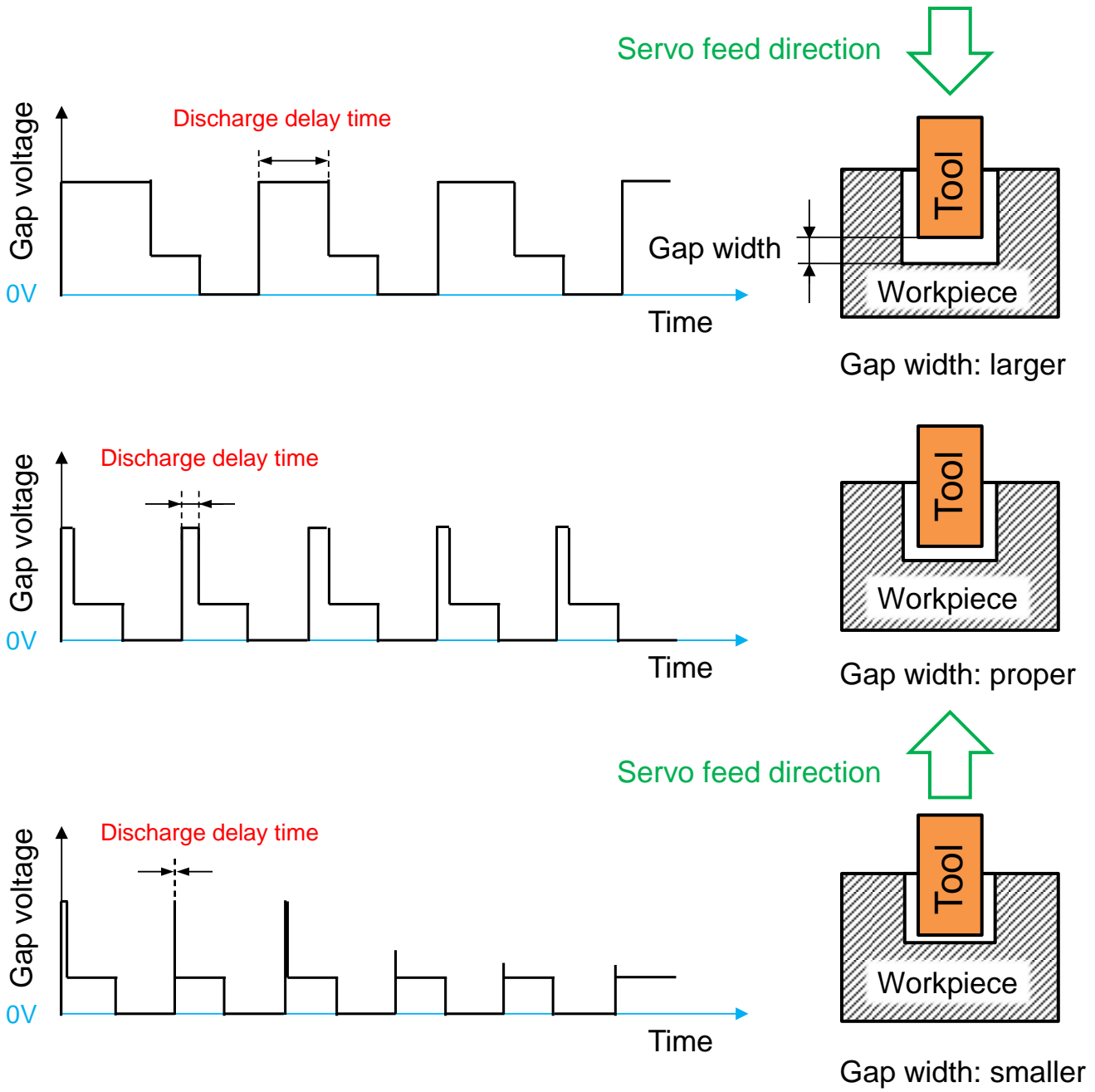
Fig. 1.9 Principle of servo feed control in EDM

1.5   Manufacturing of single crystal silicon carbide wafer

This section describes the background of the development of SiC wafer manufacturing process. Wafer is a thin slice of semiconductor material, such as a crystalline silicon carbide, widely used in electronics as the most essential element for the fabrication of integrated circuits (ICs) etc. The wafer serves as the substrate for microelectronic devices built in and over the wafer. This research focuses on the fabrication of single crystal silicon carbide wafer, which is emerging as a promising semiconductor material for the next-generation power devices.

1.5.1   Introduction of SiC material

Single crystal silicon carbide (SiC) (see **Fig. 1.10**), is an extremely hard and inert IV-IV compound semiconductor material presenting a hexagonal close-packed crystal structure. As one of the well-known semiconductors, SiC is drawing more and more attention in recent years because of its high suitability for high performance semiconductor devices (high power, high temperature, high frequency, etc.) where conventional semiconductors such as Si, GaAs etc. are reaching their limits.

For SiC, a Si-C pair is considered as one unit of atoms in the close-packed structure. Variation of the occupation sites of atoms results in a number of crystal structures of SiC which are called polytypes (more than 200) [8]. There are three main polytypes of SiC: 4H-SiC, 6H-SiC and 3C-SiC. **Table 1.2** shows a comparison of the material properties between SiC, Si and some other semiconductor materials. As can be seen, SiC has superior electrical and physical properties over commonly used single crystal Si semiconductor such as wider band-gap (3 times of that of Si), larger critical electric field intensity (10 times of that of Si), higher thermal conductivity and higher electron saturation drift velocity etc. Owing to its large dielectric breakdown strength, SiC presents a high withstand voltage and a low energy loss. The wide energy band gap makes SiC capable to work under high temperature. Furthermore, due to its high electron saturation drift velocity, SiC devices are capable of operation with high frequency. In addition, the high thermal conductivity of SiC makes the dissipation of heat of the devices easy. Therefore, the cooling of SiC based devices becomes needless which makes it possible to further miniaturize the machinery. To summarize these attractive features described here, SiC has been regarded as able to function well under very hostile environments such as high voltage, high temperature and high frequency conditions at which conventional semiconductors cannot work adequately [9, 10].

On the other hand, to prevent the growing serious problem of global warming, the spread of products such as automobile (electricity / hybrid), photovoltaic power generation, information appliance and household electrical appliance and so forth which utilize many high efficiency power electronics is expected more and more. However, with the further development of electronic devices, Si semiconductor is approaching its performance limit due to intrinsic material properties, especially in applications related to high-power, high temperature and high frequency devices [8]. Therefore, SiC based power devices are drawing more and more attentions due to its high energy efficiency and low energy loss. It is highly expected that the performances of a great variety of applications and systems can be improved significantly by utilizing SiC-based electronics. Therefore the research and development of single crystal silicon carbide (SiC) based devices have been advancing rapidly in recent years to meet the constantly emerging versatile demands of semiconductor industry.

However, it meets great challenges to scale out the application of SiC-based semiconductor devices in the semiconductor industry due to its high price. This is mainly resulted from the high manufacturing cost of SiC wafers, which will be described in the following section. Currently Si still dominates nearly all semiconductor applications for economic reasons. SiC has little chance of being widely used unless its cost is the same as or lower than that of Si [10]. To stimulate the development of SiC semiconductors and extend their applications, reduction of the cost of manufacturing SiC is considered to be of great importance.

Applications:

1) SiC Diode

2) SiC MOSFET

3) SiC power module

Fig. 1.10 SiC wafer and its applications

Table 1.2 Physical properties of SiC, Si, GaAs and GaN at room temperature

Properties	4H-SiC	6H-SiC	Si	GaAs	GaN
Crystal structure	Hexagonal	Hexagonal	Diamond	Zinc blende	Wurtzite
Energy band gap [eV]	3.02	2.86	1.12	1.43	3.39
Dielectric breakdown field [MV/cm]	3.5	3	0.3	0.4	2
Thermal conductivity [W/cm·K]	4.9	4.9	1.51	0.54	1.3
Saturation drift velocity [cm/s] x 10^7	2.7	2	1	2	2.7

1.5.2 State-of-the-art of manufacturing process of SiC wafer

The high manufacturing cost of single crystal SiC semiconductor is considered to be resulted from the not fully developed fabrication processes of SiC. This section describes the state-of-the-art of the manufacturing process of SiC wafer.

1.5.2.1 Manufacturing processes of SiC wafer

Wafer manufacturing includes a series of processes. **Fig. 1.11** shows the general processes of manufacturing of semiconductor wafers, beginning with crystal growth and ending with wafer. The processes are simply classified into three main categories as in the following:

▪ Crystal growth

The first process is to grow bulk crystal. In the case of SiC, seeded sublimation recrystallization growth, which is usually referred to as physical vapor transport (PVT) growth method, is used to grow bulk crystal SiC.

▪ Wafer forming

Once the bulk crystal ingot is grown, it is processed to form wafers and substrates, which is referred to as wafer forming procedure. In the wafer forming procedure, at first both ends of the grown ingot is cropped (the tail end tends to have higher impurity) and the ingot is trimmed to obtain a cylindrical shape with consistent cross-section area [8]. Then the ingot is sliced into thin slices of wafers by various methods which will be discussed in the following sections.

▪ Wafer finishing

After slicing, the wafer is subjected to wafer finishing process (generally including grinding, lapping, polishing and chemical mechanical polishing (CMP)) to achieve the final high precision wafer surface (submicron surface roughness, damage-free). Specifically, at first, grinding process which utilizes diamond tools is applied to remove the surface waviness produced by the slicing process with a high efficiency (especially when the wafer diameter is becoming larger). Lapping is a mechanical free abrasive machining (FAM) process (the abrasives are suspended in slurry) which can remove the surface roughness and subsurface damage of sliced wafer. Usually after lapping process, an initial global planarization can be achieved. Chemical-mechanical polishing (CMP) is usually the standard process to achieve a large flat damage free surface [8].

After this, the wafer (prime wafer) is ready for photolithography and microelectronics fabrication to produce microelectronics chips.
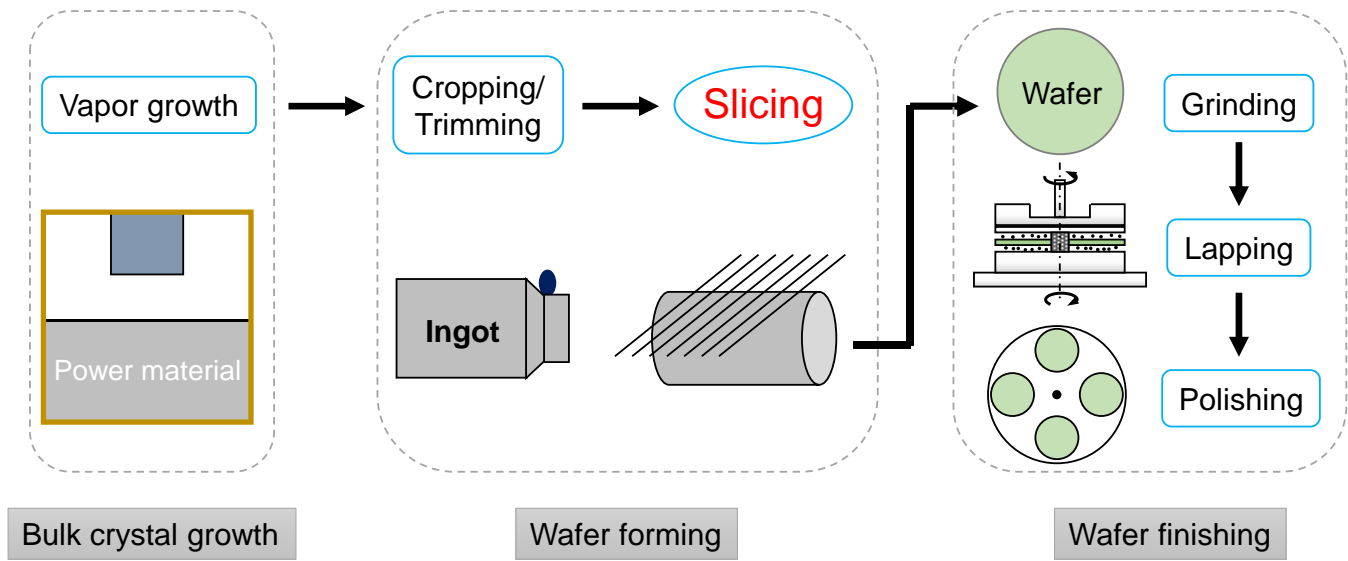
Fig. 1.11 Manufacturing process of single crystal SiC wafer [8]

The manufacturing objectives of SiC wafer are summarized as the following:

1) High wafer quality:

Manufactured wafer must be tested for function defects before it is sent to make devices. There are several specifications to evaluate the quality of manufactured wafer. The major specifications are listed as the following: crystallization defects (micro-pipe defects, planar defects, etc.), crack defects, geometric accuracy of the machined wafer such as total thickness variation (TTV), local thickness variation (LTV), SORI (wafer warp), surface orientation etc. All of these have put forward strict requirements to the SiC wafer manufacturing process.

2) Large wafer size:

Wafer size (diameter of wafer) is of great importance to increase the throughput and reduce the cost of semiconductor devices. This is because a larger wafer diameter enables producing more ICs from a single wafer, enhancing the productivity and the efficiency. Taking Si wafer for instance, the Si wafer diameter has been increased from 100mm to 300mm in the past 20 years, followed by 450mm diameter Si wafer which is considered to be coming up soon in the next few years. With regard to SiC single crystal, currently SiC wafer with diameter of 3~4inch has been available on the market. 6inch SiC wafer is being developed and the success of making 6inch SiC wafer has been reported. However, it is considered that the diameter of SiC wafer will be expanded gradually and continuously with the development of semiconductor industry in the future by simple analogy with that of Si wafer.

3) Low wafer cost:

In the mass production of semiconductor wafers, except for the wafer quality and wafer size, the cost of wafer is also an important factor determining the spread of practical applications of wafer.

16

1.5.2.2 Difficulties in manufacturing of SiC wafer

However, unfortunately, the machining efficiency of the fabrication processes of SiC wafer is very low which results in a very high manufacturing cost of SiC. The main reason is due to the high hardness and brittleness of SiC, which would bring greater difficulties compared to the conventional mechanical machining process. As shown in **Table 1.3**, single crystal SiC has a much higher hardness and atomic bonding energy compared to the conventionally used Si and GaAs semiconductors, which makes it a difficult-to-machine material using the conventional machining methods [11]. Taking wafer slicing process for instance, the multi abrasive wire saw method, which is a mechanical machining process commonly used for slicing Si wafer, is significantly time- and cost- consuming when it is applied to wafering SiC ingot, especially when the ingot diameter becomes larger. Moreover, since the hardness of SiC is approaching to that of diamond, diamond is the only option as the tool to machine SiC, which results in a further increase of the machining cost of SiC. In summary, the manufacturing cost accounts for one third of the finished SiC wafer price [13]. In addition, the difficulties of wafer manufacturing increase with increasing the diameter of SiC wafer, which will be inevitable in the future.

Table 1.3 Comparison of hardness and atomic bonding energy of Si, GaAs, and SiC [11, 12]

Semiconductor	Knoop hardness [kg/mm^2]	Bonding energy [kJ/mol]
Diamond	5500-8500	-
SiC	2480	451.5
Si	1100-1400	326.8
GaAs	750	209.6

Except for the high cost of SiC manufacturing process, the price of the bulk material of single crystal SiC is also very high because growth of SiC single crystal is based on vapor growth, high temperature vapor growth and their variants. Currently the standard method that has been implemented by industry to grow single crystal SiC is seed sublimation recrystallization method, commonly known as the modified Lely method. In this method, crystal growth of SiC is performed in an environment with super-high temperature (reaching to 2500ºC) in a crucible. In the high temperature environment, raw material is decomposed by the heating and turn into SiC sublimation gas. Then the gas is transported to near the seed crystal which is preset at certain area where the temperature is relatively lower. SiC single crystal is obtained by the recrystallization of SiC sublimation gas on the seed crystal. The instrumentation and the technology involved in SiC crystal growth is very complex due to the factor that the operating temperatures are extreme, and the monitoring and control of the growth conditions are difficult [8]. In addition, preventing the mixing of impurities into the crystal also increases the difficulty of crystal growth. Therefore, even today, the availability of SiC is still limited since only a few companies are capable of producing SiC successfully [8]. These are considered as the main reasons for the high price of the raw material of SiC bulk crystal. Hence, it is of great importance to reduce the material loss at maximum during the manufacturing

processes of SiC wafer in order to decrease the wafer cost, especially the kerf loss in wafering slicing process, which will be described later.

In conclusion, both the high manufacturing cost and the high material cost of SiC result in the high price of SiC. Therefore, advances of the manufacturing technology of SiC wafer are inevitable to reduce the wafer cost and improve the wafer quality.

1.5.2.3   State-of-the-art of wafer slicing process

Slicing is the first post-growth process to produce a wafer, as shown in **Fig. 1.11**. In all the manufacturing processes of wafer, slicing is considered as the most important and critical procedure because wafer shape is firstly formed by the slicing process and the slicing accuracy of wafer, such as the bow and warpage of wafer (SORI), wafer total thickness variation (TTV) etc. has significant influences on the subsequent processes (grinding, lapping, polishing processes) for making wafer. On the other hand, the kerf loss (material loss in the kerf) due to the slicing process is also critical to reduce the wafer cost. **Fig. 1.12** illustrates the definition of kerf loss and wafer thickness in the slicing process. A smaller kerf loss can result in a higher throughput of wafers of single SiC ingot. Therefore, this research mainly focuses on the improvement of SiC wafer slicing process.

The objective of efficient slicing is to obtain a high quality of the resulting wafer with a high throughput. Specifically, a uniform wafer thickness, a small kerf width and little surface damage are required to achieve high accuracy slicing of SiC. On the other hand, high slicing speed, which determines the wafering time, is critical to reduce the wafer cost.
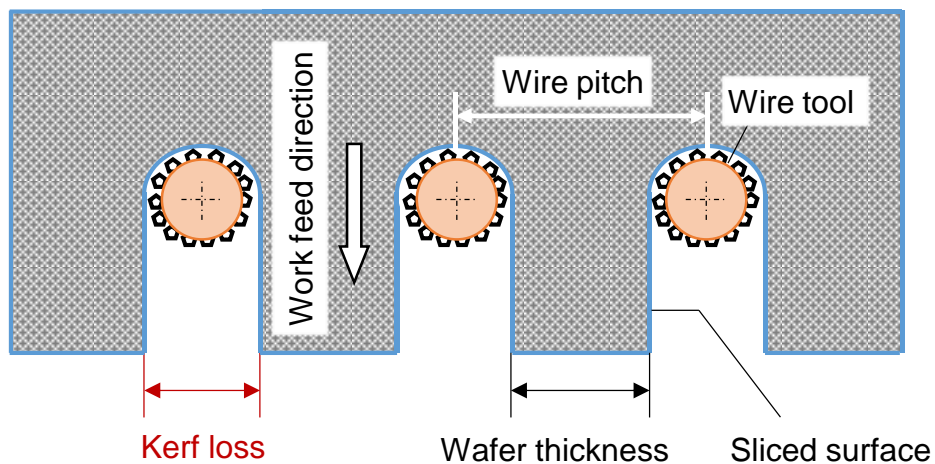
Fig. 1.12 Illustration of machining parameters in wafer slicing process (taking diamond coated wire saw for example)

Comparisons of possible methods for slicing SiC are listed in **Table 1.4**. From the perspective of the feasibility (kerf loss, wafer productivity etc.) and the cost of the slicing methods (operating cost, equipment cost etc.), the multi wire saw method is being widely used as the main slicing methods for mass

production of SiC wafer nowadays. On the other hand, wire electrical discharge machining (wire EDM) method is also being developed to slice SiC wafers in recent years taking advantage of its high machining efficiency and accuracy [14].

Table 1.4 Characteristics of different slicing method for SiC [14]

Wafer slicing method	Characteristics
Peripheral blade saw method Blade band saw method	Difficulties in reducing kerf-loss and realizing multi-cut
Laser cutting method	Bad efficiency and high cost of equipment & running
Water jet cutting method	Difficulties in reducing wafer thickness and Bad TTV with large diameter wafer
Multi-wire saw method	High throughput; Low machining efficiency; high cost
Electrical discharge cutting method	High accuracy; high cutting speed Low mass productivity;

This section mainly states the characteristics and the state of the art of the development of the two main methods for slicing SiC wafer: multi wire saw method and wire electrical discharge machining method.

▪ Free abrasive multi wire saw

So far, free abrasive wire saw is widely applied to slice SiC crystal ingot. **Fig. 1.13**(a) shows the schematic diagram of multi wire saw method. A single piano wire made from tempered (cold-drawn) high-carbon steel (high tensile strength) is commonly used as the tool to cut the workpiece and the wire diameter usually varies from 100 to 300μm. The piano wire tool is wound many turns over several grooved cylinder wire guides to form a wire web surface. Slurry consisting of a suspension of hard abrasive abrasives is fed continuously onto the wire web surface by the manifolds on both sides of the ingot. The slicing is conducted by feeding the crystal ingot (mounted on a holding jig) in the downward direction perpendicular to the wire web which is moving unidirectionally or bidirectionally at high speed and carrying the abrasive slurry to remove the material from the surface of ingot. The material removal is accomplished by pressing the abrasive grain to the workpiece by the wire and moving the abrasive grain along the workpiece surface by the wire movement, as illustrated in **Fig. 1.13**(b). In the case of SiC, due to its high hardness, diamond grits are generally used as the abrasive to improve the machining efficiency. The multi-turns of wire allows large-scale simultaneous process of the workpiece [8].

Kao [15] and Moeller [16] examined the microscopic aspects of the free abrasive wire sawing process and described the removal mechanism during the wire sawing process as a free abrasive machining (FAM) process, which is a rolling-indenting process as illustrated in **Fig. 1.13**(b). The main difference to the common FAM process (lapping etc.) is that lapping pressure is created by pressing the flexible wire tool to the workpiece.

One of the disadvantages of the free abrasive wire saw method is the necessity of slurry treatment due to environmental concerns.
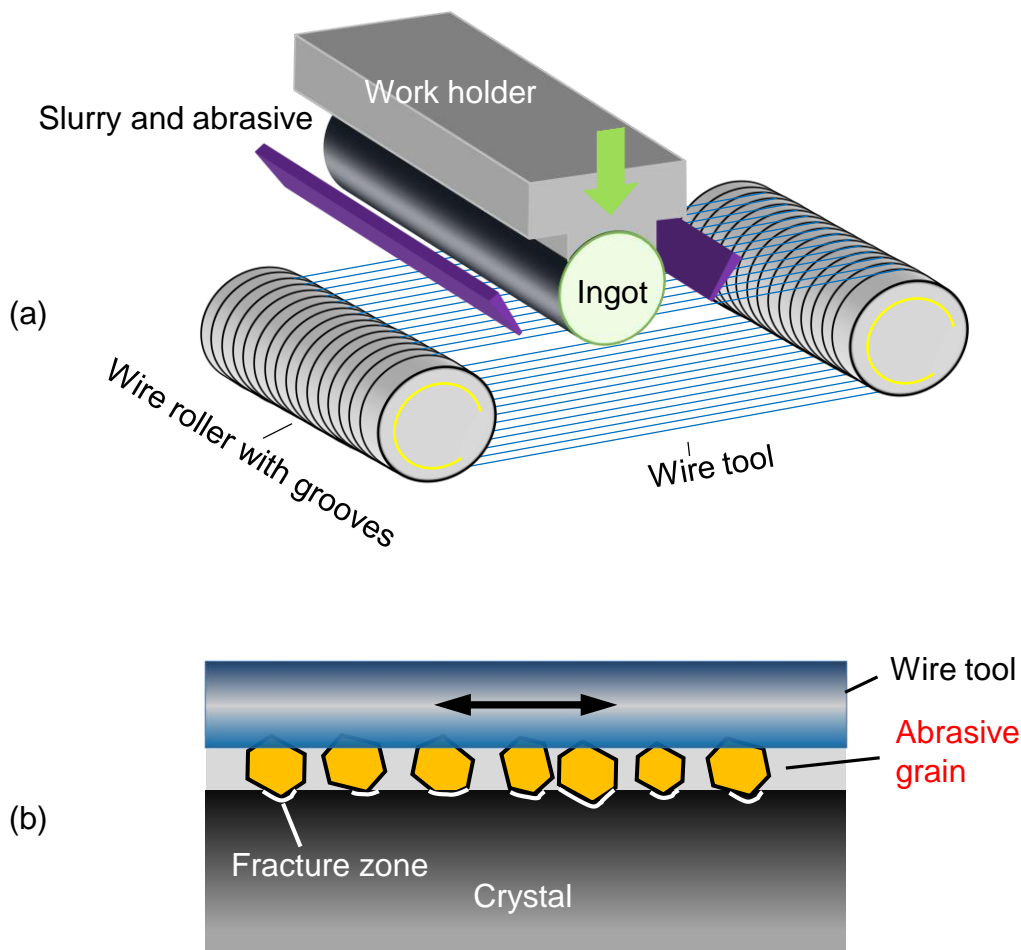
Removal mechanism: similar to lapping / polishing process

Fig. 1.13 (a) Schematic diagram of multi wire saw method; (b) Enlarged view of discharge gap indicating the material removal mechanism of multi wire saw [8, 16].

- Fixed abrasive multi wire saw

Fixed abrasive wire saw method performs slicing by utilizing abrasive-impregnated wire tool. The apparatus and slicing method are similar to the free abrasive method as shown in **Fig. 1.13**(a). Since abrasive particles (typically industrial diamond) are impregnated on the circumferential surface of the wire (by electroplating method etc.) for slicing, no slurry is required in this method.

However, it is important to note that, fundamentally, the manufacturing model of fixed abrasive wire saw is entirely different from that of free abrasive wire saw. Instead of the rolling–indenting free abrasive machining process of the free abrasive wire saw method, the fixed abrasive wire saw method removes material by means of a ploughing process (shear-dominated process similar to the orthogonal machining process) using the impregnated diamond particles on the wire tool, which is considered as a more brutal machining process. Furthermore, the diamond grains on the wire tool surface can be stripped off, resulting in the loss of the ability for the wire to perform further slicing operations [8].

Table 1.5 contrasts the free abrasive wire saw and fixed abrasive wire saw [8]. The consumables in the table refers to the wire tool, the slurry and the abrasive grains used in the wire saw process. The comparison indicates that generally free abrasive wire saw is more suitable for most slicing operations because it provides a higher slicing accuracy (smaller damage and smaller wafer waviness) and lower cost. However, when the ingot hardness is high, taking SiC for example, fixed abrasive is suggested to be used to improve the slicing efficiency. The comparison of the standard slicing time of different size SiC ingots by the two methods is shown in **Table 1.6** [17]. Therefore, diamond-impregnated wire saw method is now being widely developed for slicing SiC due to its high efficiency. However, with the expansion of SiC wafer diameter to 6inch in the future, it is considered that the machining efficiency will be reduced furthermore which brings about new difficulties to the wire saw process. In recent years, in order to improve the slicing rate, diamond coated multi-wire saw with high running speed (1000~4000m/min) and high tension force (25~45N) is being developed [18, 19]. Experimental results show that by increasing the wire running speed, the machining time of SiC wafer can be further reduced and it is expected to be applied to slice 6inch SiC wafer in the future. However, there is a trade-off between the improvement of machining speed and machining accuracy in the wire saw method.

Table 1.5 General comparisons between the free abrasive wire saw and the fixed abrasive wire saw [8]

Property	Free abrasive wire saw	Fixed abrasive wire saw
Machining model	Rolling-indenting	Ploughing
Abrasive grains	Free abrasives, re-utilization	Lost forever once stripped off wire
Depth of damage	Uniform, 5-15μm	Variable, 20-30μm
Sliced wafer waviness	Smaller	Larger
Cost of consumables per wafer	Lower	Higher
Slicing of very hard material	Less effective, longer time	More effective, shorter time
Kerf loss (typically)	180-210μm	250-400μm
Impact on environmental	Larger	Smaller

Table 1.6 The standard slicing time of different diameter SiC wafer [17]

		Free abrasive wire saw	Fixed abrasive wire saw
Diameter of abrasive grains		3~12μm	30~60μm
Wafer size	2inch	More than 24h	More than 3h
	3inch	More than 60h	More than 6h
	4inch	More than 90h	More than 9h

1.5.3 Research trend on wire EDM cutting of semiconductor wafer

As described above, due to the high hardness and brittleness of SiC, with the mechanical machining process of SiC by diamond tool, there is always a trade-off between the machining efficiency and accuracy. It is difficult to obtain both high efficiency and high accuracy at the same time [19]. In order to meet the challenges with the expansion of wafer diameter and the development of the semiconductor industry in the future, the SiC slicing process must be advanced. On the other hand, owing to the conductivity of SiC

semiconductor, EDM can be applied to machine SiC material. Since EDM is a non-contact machining process and it can removal any conductive materials regardless of the hardness, it is expected that the machining efficiency and accuracy of wafer can be improved by applying EDM process. Furthermore, since the wire EDM slicing process has no limitation to the wafer diameter, it has great potential for slicing larger diameter wafer in the future. In addition, it is expected that the process cost can be reduced by EDM because diamond is not used in EDM [17].

EDM was firstly applied to slice traditional semiconductor materials like Si and Ge etc. Okada et al. [20] proposed to apply wire electrical discharge machining (wire EDM) method to slice monocrystalline Si ingot and experimentally investigated the machining properties such as speed and surface roughness etc., which showed that wire EDM could achieve the same slicing accuracy as that of multi wire saw method. In addition, it was concluded that higher slicing efficiency could be achieved if multi wire EDM slicing could be realized. Peng et al. [21] also verified that as long as the discharge parameters match the material characteristics, the wire breakage can be avoided and the slicing efficiency is acceptable if the demand of wafer amount is small. The surface roughness is reasonable and the geometric errors are quite satisfactory. Bamberg et al. [22] applied wire EDM for machining single crystal germanium (Ge) with a resistivity of $0.01\Omega cm$ without using any means for increasing the conductivity of the germanium ingot. Under the discharge energy of 0.111mJ, germanium can be cut without inducing any kind of subsurface damage (detected by scanning electron microscope (SEM)) despite its extreme brittleness. However, under this condition, the slicing rate is relatively slow [23]. Takino et al. [24] investigated the influence of the dielectric in wire EDM slicing of Si. Experimental results indicated the importance of dielectric. It was found that wire EDM in oil is better than that in water for cutting polished single crystal Si to obtain high-quality surfaces.

The research of EDM slicing of SiC started in the recent years. At first the feasibility of applying EDM to slice SiC was proved. Kato et al. [25] characterized EDM of single crystal SiC in terms of EDM surface condition and damage condition. It was reported that smooth surfaces without any scratches with surface roughness Ra=1~2μm was obtained. Moreover, by analyzing the EDM's surface of SiC using X-ray photoelectron spectroscopy (XPS), it was found that the EDM'd surface of SiC was composed by mixture of silicon oxide (SiO_2) and graphite (C). The mixture layer was observed as a porous layer with thickness of around 1-10μm. In addition, the maximum cutting speed of 2inch SiC wafer reached about 500μm/min (area cutting speed: $19.6mm^2$/min). In terms of the EDM damage layer, in general the damage depth (heat affected zone) resulted from EDM process depends on the machining conditions (mainly discharge energy). Nevertheless Kato et al. [25] reported that the surface damage caused by EDM is extremely low compared with mechanical polishing damage of SiC. In addition, wafer polishing experiments showed that the (0001) silicon and carbon surfaces of SiC wafer changed to atomically flat surfaces by removing only 10-15μm and 22-25μm thick from the EDM top surfaces respectively. However, the EDM conditions are not mentioned here.

Yamada et al. [26] also reported that higher cutting speed, smaller surface roughness, smaller warpage and smaller kerf loss could be obtained by wire EDM compared with those of the diamond wire saw method. In the case of EDM of high resistivity SiC material ($20\Omega m$), high electric field effect and high temperature effect (decreasing workpiece resistivity by increasing the temperature of the workpiece) can be applied to increase the discharge current for performing the machining [27].

With regard to the sub-surface damage of SiC (crystal damage), Ishikawa et al. [28] investigated the cross-section of as-sliced 6H-SiC by cross-sectional transmission electron microscopy (TEM) and found that EDM induces little crystal disorder in hexagonal SiC by slicing process. However, there is formation of silicon, carbon, 3C-SiC, and cracks due to the decomposition of SiC material by the discharge energy, which should be removed by following mechanical treatments.

However, as discussed above, it is found that the material removal mechanism of EDM of SiC has not been investigated, which is considered very important to optimize the EDM slicing process of SiC. In addition, the fundamental research on EDM of SiC is considered insufficient to understand the mechanism and properties of EDM of SiC. Therefore in this research the difference of wire EDM characteristics between SiC and metal material, the surface topography of wire EDM, the influences of Joule heating effect, the influence of crystal orientation on EDM of SiC etc. are comprehensively investigated in Chapter 2.

1.5.4 Research trend on development of multi-wire electrical discharge slicing of SiC

On the other hand, however, wire EDM is not practical to be used for slicing SiC ingot due to its low productivity. In all the cases discussed above, only one wafer can be cut at one time, as illustrated in **Fig. 1.14**. Even if the wire electrode is wound many turns like shown in **Fig. 1.13**(a), in principle, the converted machining time of single wafer is still the same as that of conventional wire EDM without winding of wire. This is because, there is only one discharge location in one pulse of wire EDM no matter how much turns the wire electrode is winded. Therefore, it is of great necessity and importance to develop multiple discharge EDM method to improve the machining efficiency of wire EDM for mass production.

In the recent years (2008~), aiming to improve the slicing throughput of SiC, multi-wire electrical discharge slicing (hereafter referred to as multi-wire EDS) methods have been proposed and multi-wire EDS machines are being widely developed.
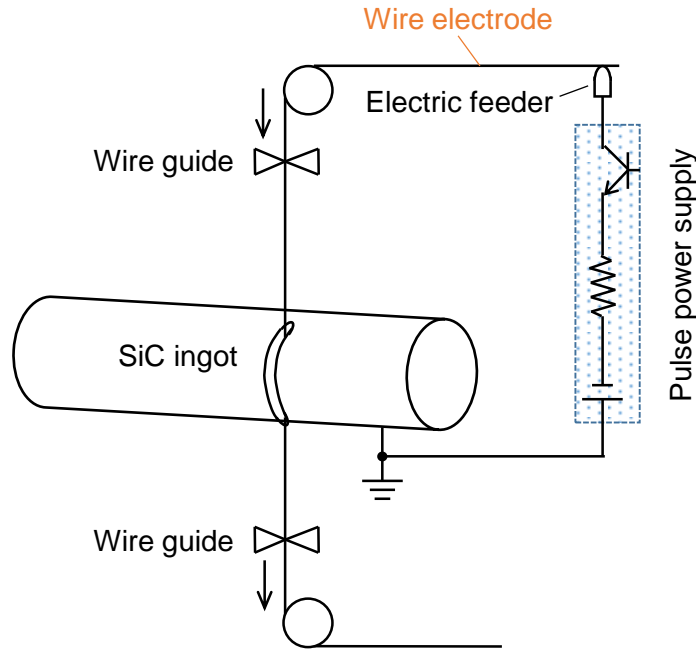
Fig. 1.14 Illustration of conventional wire EDM used for slicing of SiC

As a new method, so far there is still no standard definition of multi wire EDS, and the mechanism and structure of multi wire EDS are still under development. Nevertheless, the purpose of multi-wire EDS is very clear: realization of multiple discharges between the multiple wire electrodes and the workpiece at the same time to improve the slicing efficiency. **Fig. 1.15** shows a schematic diagram of the basic structure of multi-wire EDS method. A single wire tool electrode (steel wire, brass wire, etc.) is drawn from a wire supply spool and wound around grooved wire guides to form a wire web, similar to that of the multi wire saw method. The workpiece (ingot) is fixed on a stage which is submerged into the dielectric liquid and fed perpendicular to the wire web for slicing. The distance between the ingot and the wire web is adjusted by a feed control system. By applying pulsed voltage to the gap between the wire web and the ingot, discharges can be generated. The wire electrode after use is collected by the take-up spool and new wire is supplied continuously to the working area for machining. In order to improve the utilization of wire, reciprocating motion can be applied to the wire to realize reutilization of the wire electrode. In order to remove the EDM debris in the cut slit, in some case, dielectric liquid is flushed into the machining slit during machining like the single wire EDM processes [29-35].

Okamoto et al. [29] firstly developed a multi-wire EDM slicing equipment with a single wire and a multi-power supply unit which can realize 3 cuts at the same time. In this method, the maximum number of wire electrode was set three based on the number of the multi-power supply unit, which could generate three individual discharge pulses simultaneously. It is found that higher wire running speed results in smaller kerf width and high slicing speed because higher wire running speed can improve the removal of EDM debris. In addition, in terms of supplying dielectric liquid to the working area, EDM slicing by immersion in the dielectric provides a better slicing results compared with the nozzle flushing method of dielectric.

Following this, multi-wire EDS equipment for slicing 2inch SiC ingot was developed, which achieved a cutting speed of 400μm/min [32]. However, the corresponding machining conditions were not disclosed. Analysis result of the as-sliced SiC wafer shows that the sliced surface by multi-wire EDS was not flat but with convex or concave. The reason was considered to be caused by the wire vibration during slicing, which could be reduced by increasing the wire tension force. However, with increasing the wire tension force, wire breakage will become a serious problem. To prevent the wire breakage during slicing, Ogawa et al. [33] improved the electric discharge pulse control system and succeeded in slicing of 4inch SiC ingot with 10 multi-wires. In addition, it was pointed out that the multi-wire EDM equipment could be practically used to slice ingot with diameter larger than 4inches by effective removal of machining debris from the discharge gap. Therefore, in this research it is considered that high wire running speed and high running stability is necessary to realize precise slicing of larger diameter wafers in the future.

Itokazu et al. [34, 35] from Mitsubishi Electric Corporation also succeeded in the development of multi-wire EDS equipment which realized 40 cuts of poly-crystal SiC at the same time without wire breakage. The slicing conditions are shown in **Table 1.7**. An average kerf width of around 208μm was achieved in the experiment.

Table 1.7 Machining conditions of multi-wire EDS of polycrystalline SiC [34, 35]

Wire electrode	Brass coated steel wire
Wire diameter	Φ0.1 [mm]
Wire pitch	0.6 [mm]
Feed speed of slicing	80 [μm/min]
Workpiece thickness	Around 100 [mm]
Workpiece resistivity	0.02 [Ω·cm]

However, with increasing the wire turns furthermore, it is considered that the slicing speed per wafer will be decreased and the probability of wire breakage will increase due to larger wear of wire tool.

Although there are different ways to realize multi-discharge EDM [29, 31, 34, 35], the general principle of multi-discharge EDM to realize multi-wire EDS is the same, as shown in **Fig. 1.16**. The pulse power is fed to multi wire electrodes (wire web) at the same time through the electrical feeders. Multi-discharge is realized by introducing a large impedance into each branch of discharge circuit so that the electrical potential at each wire electrode will not be easily affected by the occurrence of one discharge at a certain wire electrode. At the beginning, multi-discharge machining was realized by connecting multiple discharge circuits to the single wire electrode [29]. In this method, the discharge current is controlled by the

impendence inside the discharge circuit. However, with increasing the wire turns, the system becomes very complicated due to the increased electric feeders and so forth. In order to reduce the number of electric feeders and simplify the discharge system, unified feeding of electricity method was developed which fed electricity to the wire electrode by just using a single piece of electricity feeder, as shown in **Fig. 1.15**. The discharge current was controlled by taking advantage of the impedance of wire electrode itself between the electric feeder and the discharge spot [31, 34, 35].

However, it is considered that there is a disadvantage of this method: introduction of large impedance in the discharge circuit will cause low energy efficiency due to the consumption of energy of the resistance. Furthermore, the increased impedance (mainly inductance X_L) in the discharge circuit will make it difficult to generate discharges with short pulse duration based on the following equation while short pulse discharge is considered to be of great importance to realize high precision machining.

$$U = X_L \frac{di_e}{dt}$$

<div align="right">Eq. 1.2</div>
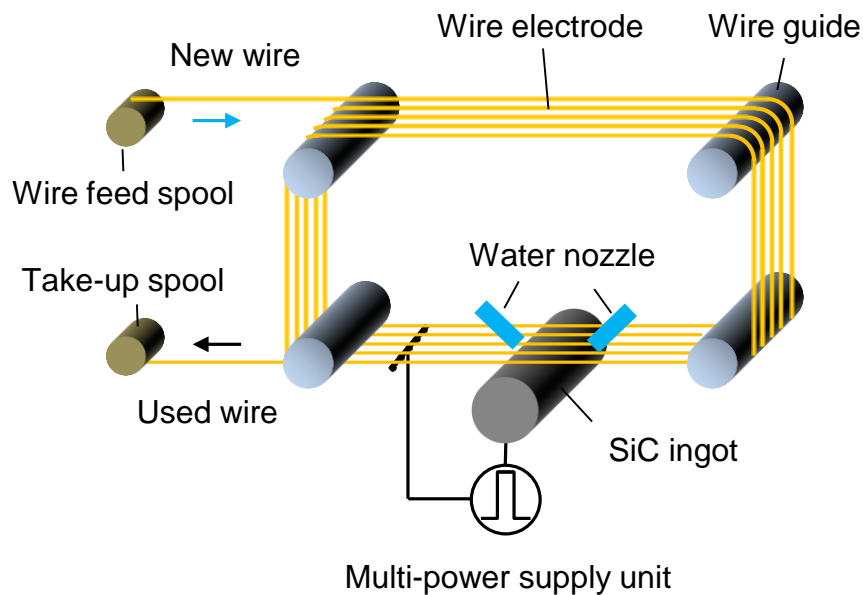
Fig. 1.15 Illustration of multi-wire EDM slicing method [29~35]

Electric feeder

$$Z = \sqrt{R^2 + X_L^2}$$

Impedance Z

Wire electrode

Electric feeder

Pulse power supply

Single crystal SiC ingot
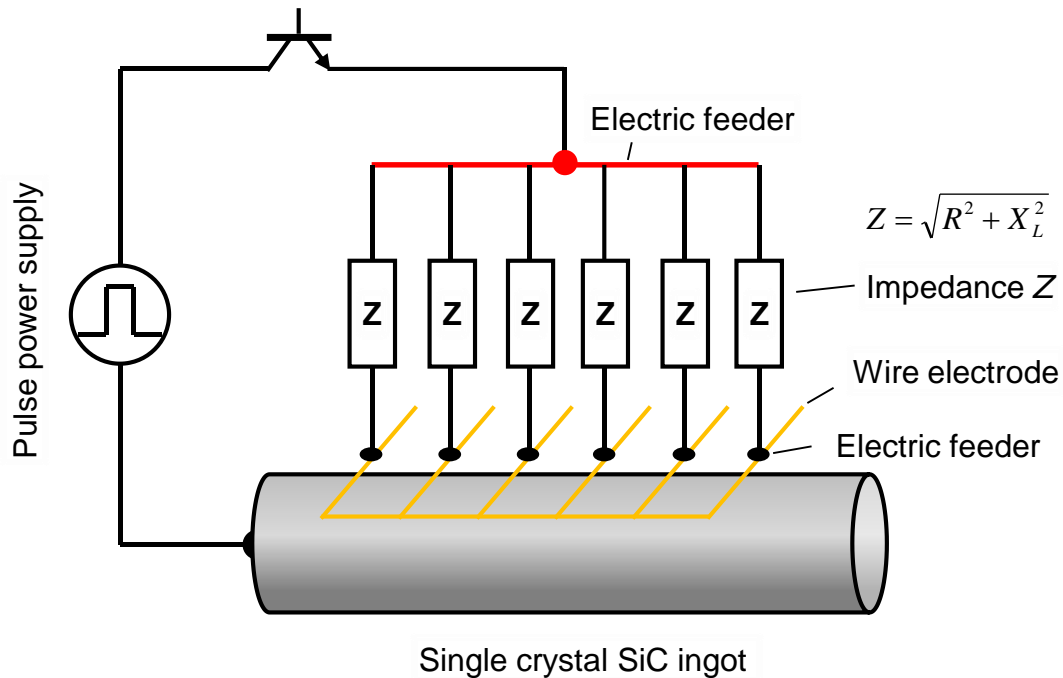
Fig. 1.16 Mechanism of multi-discharge machining in multi-EDS process [31]

With regard to this, a new multi-discharge EDM method by utilizing electrostatic induction feeding method is proposed and investigated in this research (Chapter 5), which can simplify the discharge circuit and improve the energy efficiency at the same time.

Fig. 1.17 shows a comparison of the slicing capacity per single turn (winding) of wire tool in different wafer slicing method. It can be found that although multi-wire EDM slicing method can improve the total area cutting speed (number of wire winding × cutting speed of single winding), the cutting speed of single turn of wire (feed speed) decreases to about half of that of single wire EDM. With regard to the reason of this, on one hand, it is considered that in the multi-wire EDS method, the multiple discharge frequency cannot be increased in proportion to the increase of wire turns. On the other hand, the lower cutting speed per single wafer in multi-wire EDS is probably due to the limited discharge current since large discharge current cannot be applied to the wire electrode in multi-wire EDS in order to prevent wire breakage. Currently, the multi-wire EDS shows a lower area cutting speed compared with that of multi-wire saw method. It is therefore considered that the potential of multi-wire EDS method is not fully realized and multi-wire EDS method must be enhanced and improved to achieve a better slicing performance. However, it should be pointed out here that in **Fig. 1.17**, the diameter of the wire tool (not disclosed in the literatures) might be different.
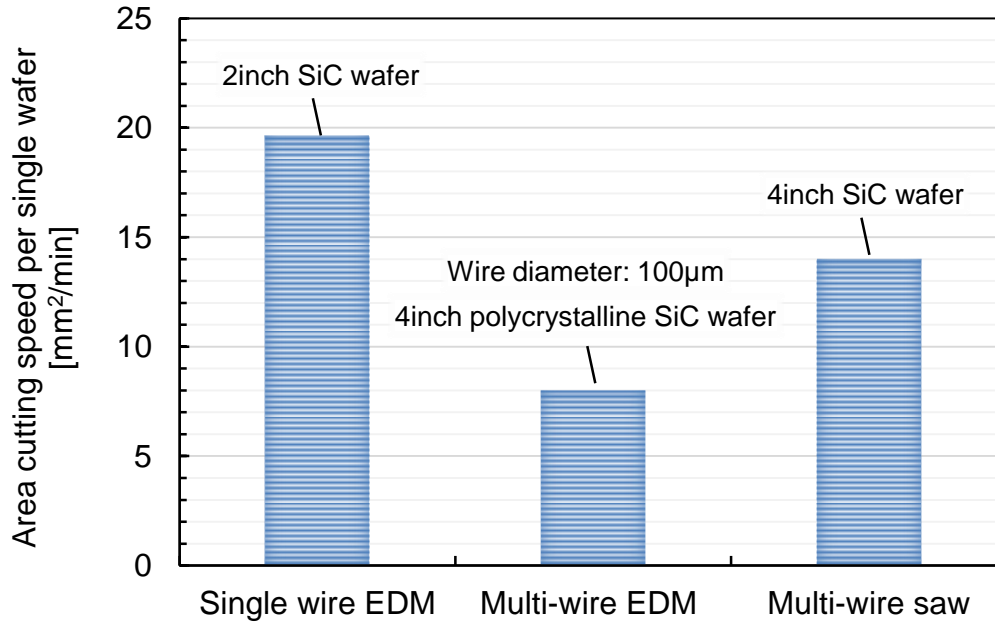
Fig. 1.17 Slicing capacity of single turn of wire in different wafer slicing method [14, 17, 35]

In conclusion, as a quite new manufacturing process, the multi-discharge EDS process shows great potential for application of SiC wafer slicing. However, this technology is still under development and there are still many subjects that should be improved and advanced as the followings:

1) Clarification of the EDM characteristics and material removal mechanisms of SiC.

2) Improving the wire electrode running speed and running stability.

3) Increasing the number of wire electrodes furthermore and preventing the wire breakage problem.

4) Improvement of the multi-discharge EDM method to realize high efficiency and low cost.

1.5.5 Progress of wire electrode for EDM slicing of SiC

In EDM cutting process, wire electrode is generally used as the electrode, which is the reason why this process is referred to as wire EDM. Brass wire is generally used in wire EDM due to its low price and high discharge performance. However, there is a common problem of wire EDM process: wire breakage, especially when the wire diameter is small. Many factors can lead to the wire breakage problem such as a decrease in flushing pressure, inefficient removal of erosion debris and some other stochastic phenomena appearing during the machining [36]. In principle, discharge concentration at a certain point of the wire electrode during machining which causes an increase in the localized temperature is considered as the main reason for the wire breakage [2]. Wire breakage during machining must be avoided because it would cause a discontinuous machining process and in consequence a low machining efficiency and a

29

productivity. In addition, if the wire breaks in the middle of machining due to any reason, it is impossible to reset the wire electrode at the same position, which will decrease the accuracy of the machined profile and leave a remarkable stripe on the machined surface [37]. In order to prevent the wire breakage, several approaches can be taken in wire EDM process:

1) Increasing wire running speed.

2) Flushing dielectric liquid to discharge gap and making dielectric flow surround the wire electrode.

3) Improving the machining stability and reducing the short circuit (for example, using zinc coated wire).

4) Using wire that has a high tensile strength under high temperature.

5) Development of adaptive control system providing an online identification of abnormal discharge conditions and a control strategy preventing the wire breakage without compromising the various wire EDM performance measures [38].

Except for these, automatic wire connection technology has also been developed to solve this problem.

Although the recent advance of prevention technology of wire breakage on wire EDM machine is remarkable, it is not always sufficient to satisfy the users, especially in the case of the newly developing technology: multi-wire electrical discharge machining technology. Because the wire breakage problem will become more serious in multi-wire EDM process due to the increased load of machining per unit length of wire electrode. In order to prevent the wire breakage, too thin wire electrodes cannot be used. In addition, in multi-wire EDM, the wire arranging and winding system is much more complex compared with that of the conventional wire EDM, which makes the reset of wire after breakage and the automatic wire connection more difficult. So far, no automatic wire connection method has been developed in the multi-wire EDM method. For these reasons, currently, in multi-wire EDM slicing method of SiC ingot, brass coated steel wire electrodes with diameter no smaller than 100μm are being used [29, 30, 34, 35] in order to avoid the wire breakage.

Reduction of the diameter of the wire electrode, however, is another important aspect in wire EDM slicing of SiC wafer in order to improve the slicing accuracy and productivity. In order to perform small kerf loss EDM slicing, very thin diameter wire electrode is required. In general wire EDM, tungsten wire or molybdenum wire (Φ 0.03- Φ 0.1) are generally used due to their high tensile strength. However, the price of tungsten wire is very expensive. Moreover, with the thin diameter wire, the machining parameters (discharge current etc.) and the wire tension force must be decreased to prevent wire breakage which will result in a low machining rate and machining accuracy.

On the other hand, the wire vibration during running must also be reduced in order to achieve a high geometrical accuracy cutting. Although there are many reasons causing the wire vibration such as the mechanical forces produced by the pressure from the generated bubbles of discharges, the hydraulic forces induced by the flushing, the axial forces applied to straighten the wire, the electrostatic forces acting on the wire etc. [38], it has been found out that by increasing the wire tension force, the wire vibration amplitude can be reduced and the wire EDM machining rate can be improved due to a smaller kerf width [39].

Therefore, in order to prevent the wire breakage and reduce the wire vibration, Okamoto et al. [30] employed a wire electrode with track-shaped section (as shown in **Fig. 1.18**) to increase the tension force so that the

running stability of wire can be improved while keeping a small diameter. Experimental results showed that with increasing the tension force, stable wire running could be performed which resulted in a better kerf shape. However, since the gap distance between the track-shaped wire electrode and the workpiece in one side was still large (35-40µm) compared with that of normal round wire electrode (10-15µm), it is considered that further stabilization of wire running is necessary.

In order to further reduce the wire diameter and increase the wire tension force to perform high efficiency, high accuracy machining, it is considered of significant necessity to improve the wire electrode in terms of the electrode material and electrode shape. In this study, foil electrode is proposed in place of wire electrode to be used for EDM cutting of SiC.
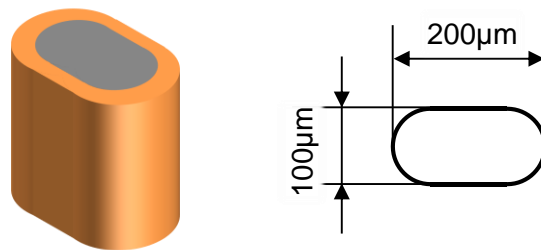
Fig. 1.18 Brass coated steel wire electrode with track-shaped section [30)]

1.6 Objective of the dissertation

As a hard and brittle material, single crystal SiC is classified into hard-to-machine material for the conventional mechanical machining process as described above. With the continuous development of semiconductor industry, it is inevitable to advance the wafer manufacturing processes to improve the wafer accuracy while having a low price. Especially, the wafer slicing process, which is considered as a critical process in all the wafer manufacturing processes, is expected to be improved furthermore since currently the slicing efficiency of SiC by multi wire saw is quite low and the cost is very high. Therefore in recent years EDM has been proposed to machine SiC due to its unique machining characteristics such as non-contact machining, regardless of the workpiece hardness etc. It is highly expected that the multi-wire EDM slicing process can be developed as a high accuracy, high efficiency and low cost wafer slicing process. Currently the EDM slicing process is still under development and there is still many subjects to be improved. The objective of this research is to advance the EDM slicing method to realize high efficiency and high accuracy machining of SiC ingot and SiC-like hard brittle materials. By researching on EDM of SiC, it is expected that new EDM machine can be developed for machining new materials coming up in the continuously developing industry.

At first, material removal mechanism and characteristics of EDM of SiC should be clarified. As a semiconductor material, EDM of SiC distinguishes itself from the traditional metal materials by its high resistivity. In addition, the high brittleness of SiC makes it very challenging to machine SiC with high accuracy by EDM because cracks and fractures may occur due to the thermal shock by EDM process which will deteriorate the cutting accuracy and wafer quality. In the recent years, there are several researches on the characterization of EDM performance, including the cutting speed, EDM'd surface composition, subsurface damage induced by EDM, etc. [13, 14, 25, 26, 28]. However, since most of the researches focused on the application of EDM of SiC, the fundamental researches, such as the material removal mechanism of SiC, the influence of EDM conditions on machining performances, the influence of the material properties (high resistivity of SiC, crystal anisotropy of SiC etc.) on the machining performances, the influence of dielectric liquid on the machining performance etc. are still unclear. In addition, there is no published study discussing about the optimal machining conditions of EDM of SiC, such as the optimal pulse conditions, optimal duty factor, etc. It is therefore considered that the current existing researches are not sufficient enough to completely understand the EDM properties of SiC. Hence, one of the objectives of this research is to clarify the EDM characteristics of SiC and optimize the machining conditions of EDM of SiC.

On the other hand, this research aims to develop a new EDM slicing system to advance the current multi-wire EDS method. Multi-wire EDS is now being widely developed to cut SiC as a new wafer slicing process. However, as described previously, there are several problems existing. The first problem is the limitation of wire running speed and wire tension. Increasing the wire speed can result in higher cutting speed and lower kerf loss owing to the improved gap flushing condition [29]. However, too high wire running speed brings about the problem of wire vibration which would reduce the cutting accuracy [30]. The wire vibration can be reduced by increasing the wire tension force. However, there is a trade-off between the reduction of wire diameter and the increase of wire tension. On one hand, smaller wire diameter is always expected in order to reduce the kerf loss and increase the slicing throughput; on the other hand, smaller wire diameter will reduce the wire tension force to avoid wire breakage. Second

problem is the limitation of discharge energy. In general, larger discharge current can result in higher machining rate. In the case of multi-wire EDS process, however, the discharge current must be limited to a certain value to avoid the wire breakage. Compared with the single wire EDM process, the load of machining time per unit length of wire electrode is larger in the multi-wire EDS process, which will cause a higher probability of wire breakage. Therefore, one of the objectives of this research is to develop a new EDM slicing method by utilizing thin foil electrodes instead of wire to solve the wire breakage problem and improve the EDM slicing performance to achieve a lower kerf loss and a higher machining rate.

In addition, the research aims to reduce the cost and improve the energy efficiency of the multi-wire EDS method. As discussed in section 1.5.4, in the current multi-wire EDS method for slicing SiC ingot, multi-discharge EDM is realized by introducing large impedances in the discharge circuits which will result in low energy efficiency due to the consumption of energy of the resistance. This research proposes a new alternative method, which is referred to as multi-discharge EDM method by electrostatic induction feeding method in this research, to realize multi-discharge EDS with lower cost and higher energy efficiency in the future.

1.7 Constitution of the dissertation

This dissertation consists of 6 chapters. The summary of each chapter is as the following.

Chapter 1: Introduction

In this chapter, at first the mechanism and characteristics of EDM process are briefly introduced. Following this is an overview of the development of SiC single crystal semiconductor and the problems hindering the applications of SiC-based devices. Next, the state-of-the-art of the development of SiC wafer manufacturing processes, especially the slicing processes are described. The research trends on electrical discharge machining (cutting, slicing etc.) of SiC, the development of multi-wire EDS method and the existing problem in wire EDM slicing of SiC are described. Based on the background, the objectives of this research are described.

Chapter 2: Characterization of wire EDM slicing of single crystal SiC

In this chapter, the fundamental characteristics of EDM of SiC are comprehensively investigated and compared with those of steel, including discharge waveform, machining rate, surface integrity, EDM debris, anisotropy of machining speed etc. Moreover, heat conduction analysis of single discharge of SiC is conducted taking into account Joule heating effect to clarify the basic EDM behaviors of SiC. Based on these, the material removal mechanism of EDM of SiC is discussed. Considering the practical use, the wire EDM slicing performance of SiC are comprehensively evaluated, inducing the influence of anisotropy property of SiC on the machining speed, surface roughness, surface topography etc. At the end, problems of wire EDM cutting of SiC are discussed.

Chapter 3: EDM cutting of SiC ingot by foil tool electrode

In this chapter, a new EDM cutting method of SiC ingots by utilizing foil electrode instead of wire electrode is proposed to overcome the shortcomings of wire EDM slicing method. The development of the experimental setup for realizing foil EDM cutting is described and the feasibility and performances (tool wear, kerf loss, machining rate etc.) of foil EDM cutting of SiC are discussed through experiments. The influences of foil material, pulse condition and dielectric liquid are described. Furthermore, foil EDM cutting of SiC with reciprocating the worktable is proposed and the experiment study results are discussed.

Chapter 4: Development of foil running system for EDM slicing of SiC

This chapter describes the development of running foil EDM slicing system. A new method of electrical discharge slicing (EDS) of SiC by utilizing running foil tool electrode is proposed to achieve a constant and stable machining process. The principle of the proposed method is described and the experimental setup for realizing running foil EDS is developed. The machining characteristics are experimentally investigated using the developed experimental setup.

Chapter 5: Multi-discharge EDM cutting of SiC ingot by electrostatic induction feeding

In this chapter, multi-foil EDS by the electrostatic induction feeding method is proposed to realize multi-slice of SiC ingot. The principle of the proposed multi-foil EDS method. In order to confirm the feasibility of the proposed multi-discharge EDM method, a special experimental setup for realizing multi-discharge EDM is developed and the multi-discharge EDM performances are described.

Chapter 6: Conclusion

In this chapter, the main findings obtained in Chapter 2 to Chapter 5 are summarized as the final conclusions of this thesis. The remaining research subjects and the perspective of future research work that are related to this thesis are discussed.

Chapter 2 Characterization of wire EDM slicing of single crystal SiC

2.1 Introduction

This chapter describes the fundamental EDM characteristics of SiC and the material removal mechanism of SiC in EDM process. In addition, the wire EDM performances for cutting SiC are discussed.

As a semiconductor, the high resistivity of SiC distinguishes itself from the conventional metal material in EDM process. At first, in order to clarify the EDM characteristics of SiC, a comparison study between wire EDM of SiC and widely-used metal material is conducted to find out the difference. Based on the experimental results, the material removal mechanism of EDM of SiC is discussed. Then how the high resistivity influences the EDM characteristics of SiC is described based on a theoretical analysis. Lastly, basic experimental studies of wire EDM of SiC are described to evaluate the EDM performances for machining SiC.

2.2 Characteristics of wire EDM cutting of SiC

2.2.1 Differences of wire EDM characteristics between SiC and steel

It is well known that the material properties, especially the electrical and thermo-physical properties, have a considerable influence on the EDM process. As a semiconductor, the material properties of SiC are significantly different from those of the metal materials, as shown in **Table 2.1**, which contrasts the physical properties between single crystal SiC and Fe (principal constituent of steel). It is therefore considered that the EDM behavior of SiC should be different from metal materials.

In order to clarify the EDM characteristics of SiC, comparison experiments between wire EDM of SiC and common tool steel SKD11 were conducted. **Fig. 2.1** shows the schematic diagram of the experiment setup. The experiments were conducted on a commercial wire EDM machine (*Sodick AP200L)*. As described in Chapter 1 (Section 1.3.2), the wire EDM machine has a low voltage circuit to ignite the electric discharge and a high voltage circuit to supply a discharge current with high peak and short duration after the gap breaks down in order to increase the machining rate. The workpiece used in the experiments was 4H-SiC single crystal and cold tool steel SKD11 respectively. The general specifications of 4H-SiC are shown in **Table 2.2**. The machining conditions in the experiments were preset exactly the same for both two workpiece materials, as shown in **Table 2.3**.

2.2.1.1 Discharge waveform

At first the discharge waveform was observed. **Fig. 2.2** shows the differences of discharge current and gap voltage between wire EDM of SiC and SKD11 material under the same preset machining conditions. In the case of SiC, the timing of switching to the high voltage power supply is delayed compared to that of steel. This is because the detection of the discharge occurrence is done based on the reduction of the gap voltage below a threshold voltage. It can be seen that the discharge current was much smaller in the case

37

of SiC under the same preset machining conditions. In addition, the measured discharge gap voltage of SiC was around 50V, about 2 times higher compared with that of SKD11. Moreover, when the high voltage power supply was applied, the gap voltage of SiC reached to about 125V. The reason is considered that the higher resistivity of SiC material caused a high voltage drop inside SiC which consequently resulted in a higher measured gap voltage and a lower discharge current. Due to the high voltage drop inside SiC, Joule heat will be generated inside SiC. The influences of the Joule heat generation on EDM process will be discussed later.
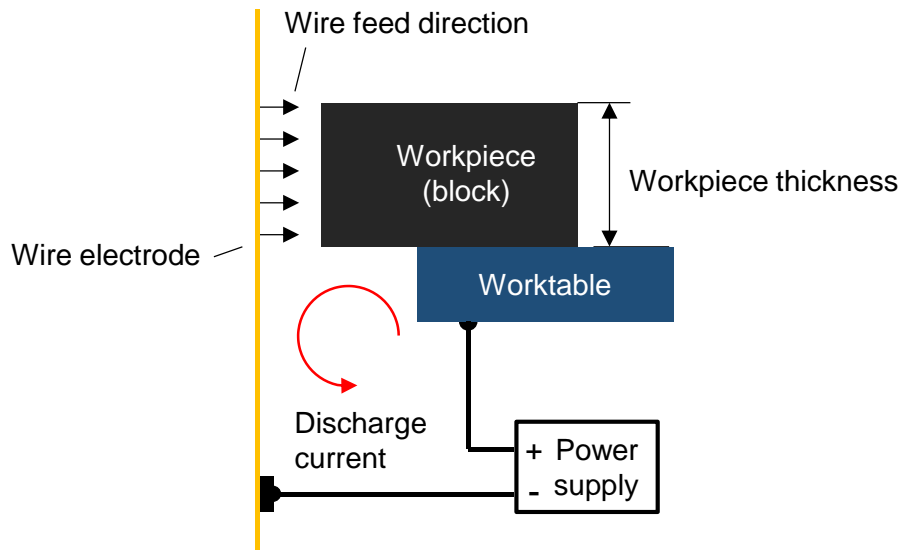
Fig. 2.1 Illustration of wire EDM cutting

Table 2.1 Physical properties of SiC and Fe

|	Electrical resistivity [Ω cm]	Thermal conductivity λ [W/m·K]	Melting point θ [K]	$\lambda\theta^2$ [x10^6]
SiC	0.013~0.025	490	3000	4410
Fe	9.71×10^{-6}	80.2	1772	251.8

Table 2.2 General specifications of SiC single crystal

Polytype	4H
Surface orientation	(0001)
Conduction type	N type
Resistivity	0.013～0.025 [Ω·cm]

Table 2.3 Preset wire EDM conditions for comparison experiments of cutting SiC and SKD11

|	
Wire electrode	Brass wire, φ200μm
Workpiece polarity	(+)
Dielectric liquid	Deionized water
Cut length [mm]	10
Cut direction	// c surface
Workpiece thickness [mm]	10
Duty factor	9.1 [%]
Open voltage [V]	80
Servo voltage [V]	58
Wire running speed [m/min]	8
Wire tension [N]	8
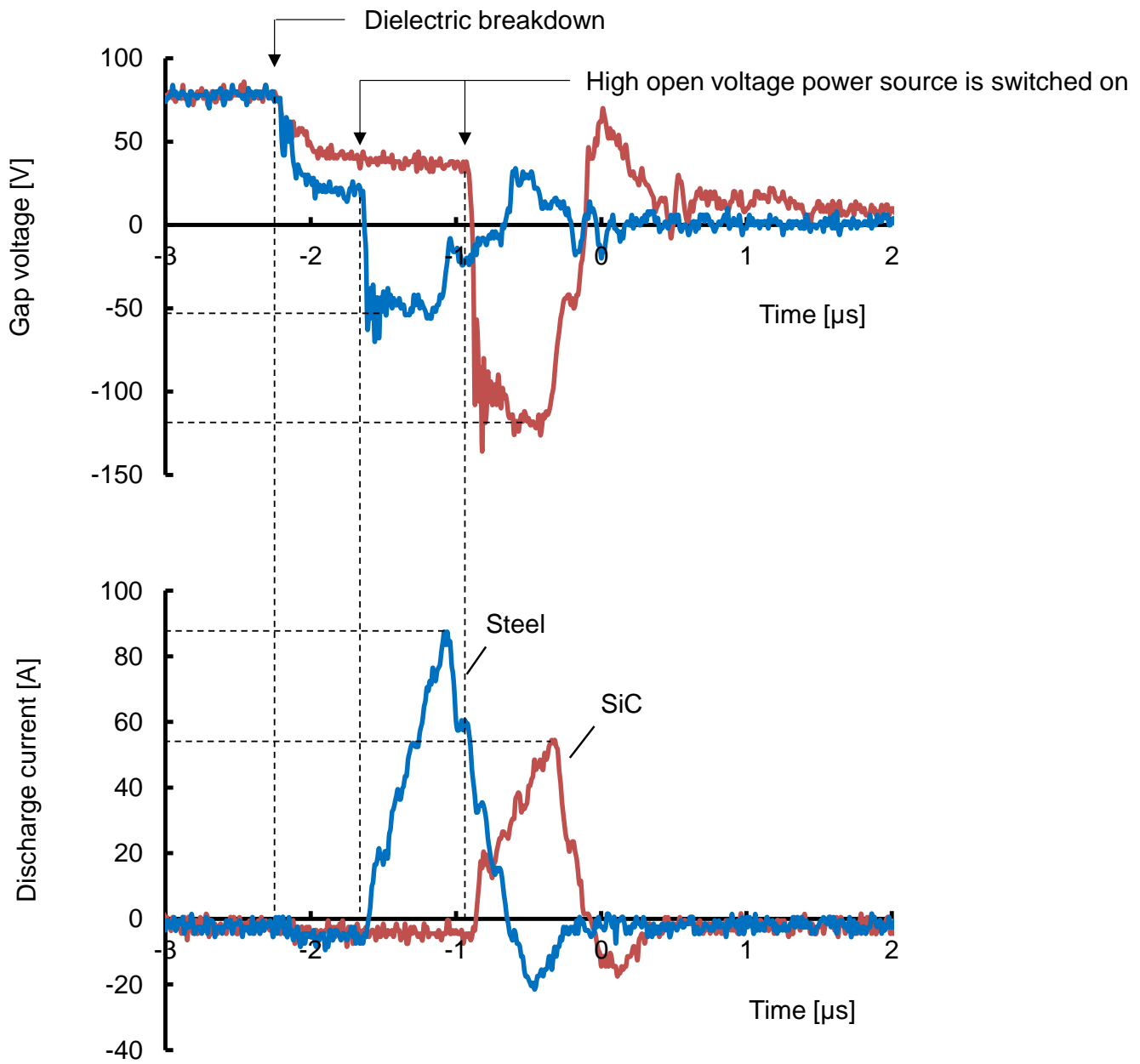
Fig. 2.2 Discharge current and gap voltage difference between wire EDM of SiC and SKD11 under the same preset machining conditions

2.2.1.2 Machining characteristics

The material removal volume was obtained from the product of length of cut, workpiece thickness and kerf width. Since the gap voltage of SiC is different from that of steel due to the voltage drop in the SiC workpiece, under the same servo voltage, the discharge frequency will be different between the two materials (Refer to Chapter 1, Section 1.4: servo feed control mechanism). Therefore, the material removal volume per single pulse discharge was investigated taking into account the difference in discharge frequency between the two different materials. Specifically, the discharge number in machining was counted using a universal counter (*Hewlett Packard 53131 A*) and the total material removal volume divided by the total discharge number was taken as the material removal volume per single pulse discharge.

The experimental results of material removal rate (MRR) difference between the two materials are shown in **Fig. 2.3**. The points connected by dashed lines indicate the same preset machining conditions. Under the existing conditions of the wire EDM machine, with increasing the discharge current, the discharge duration was also increased to some extent, as marked in the figure. Nevertheless, it can be seen that under the same presetting of discharge current, the measured discharge current of SiC was much lower than that of SKD11 because of its higher electrical resistivity. Moreover, the discharge duration is slightly shorter in the case of SiC compared with that of steel. However the material removal volume per single discharge of SiC material was several times higher than steel and the value increased more rapidly with increasing discharge energy.

The surface roughness of the machined surface was measured using a surface texture measuring instrument (*Tokyo Seimitsu, Surfcom*). **Fig. 2.4** shows the difference of surface roughness R_{max} between SiC and SKD11. Under the same discharge current, SiC surface presents a much larger surface roughness compared with that of the machined steel surface. Furthermore, the surface roughness of SiC deteriorates with increasing the discharge current. The reasons is considered that, as mentioned above, the material removal volume per single discharge of SiC is larger than that of steel which would cause a larger discharge crater on the workpiece surface. Also, as shown in **Fig. 2.5**, under the same discharge current, the cut kerf width of SiC was larger than that of steel indicating a larger discharge gap width.
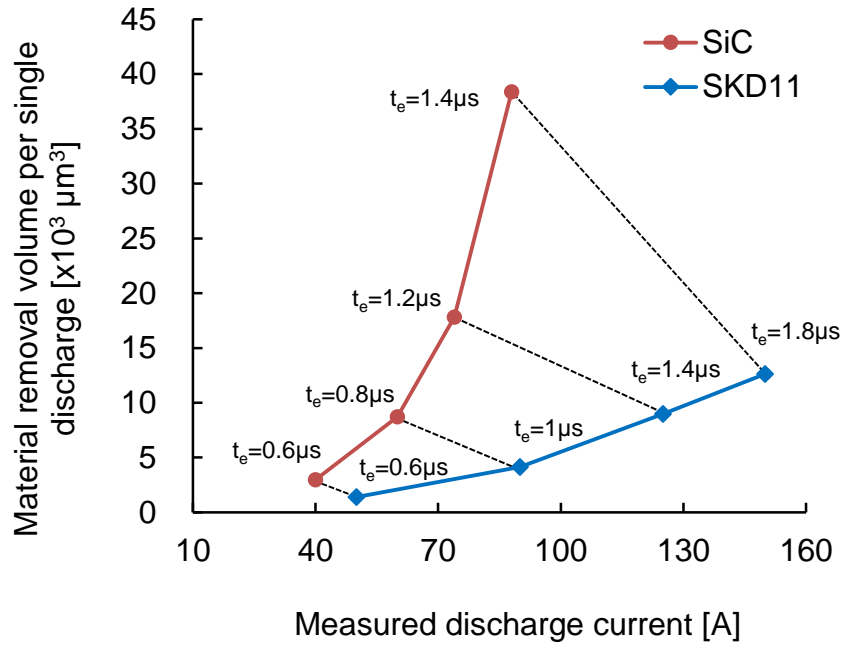
Fig. 2.3 Material removal rate difference between wire EDM of SiC and cold tool steel SKD11
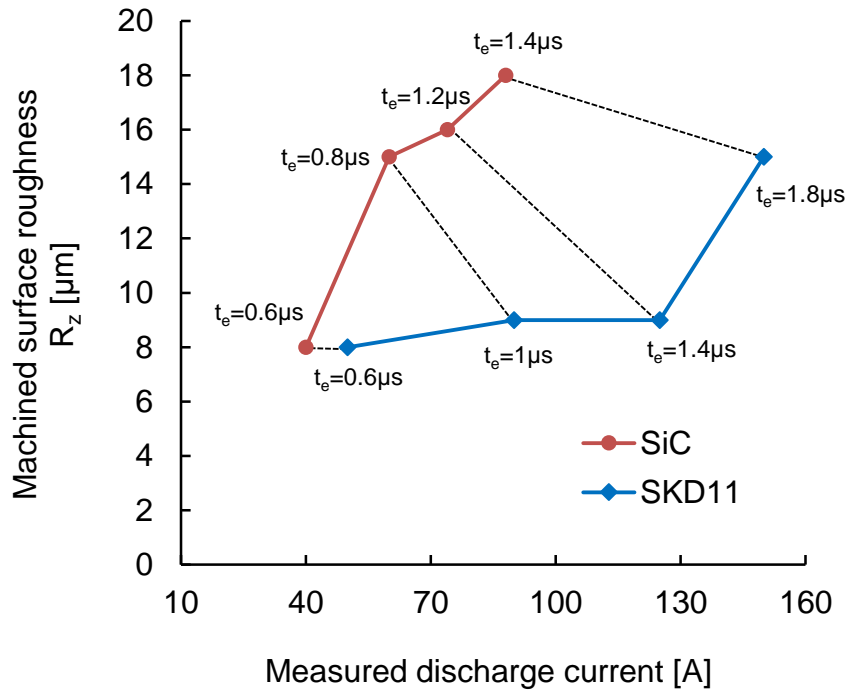
Fig. 2.4 Surface roughness difference between wire EDM'd surface of SiC and cold tool steel SKD11
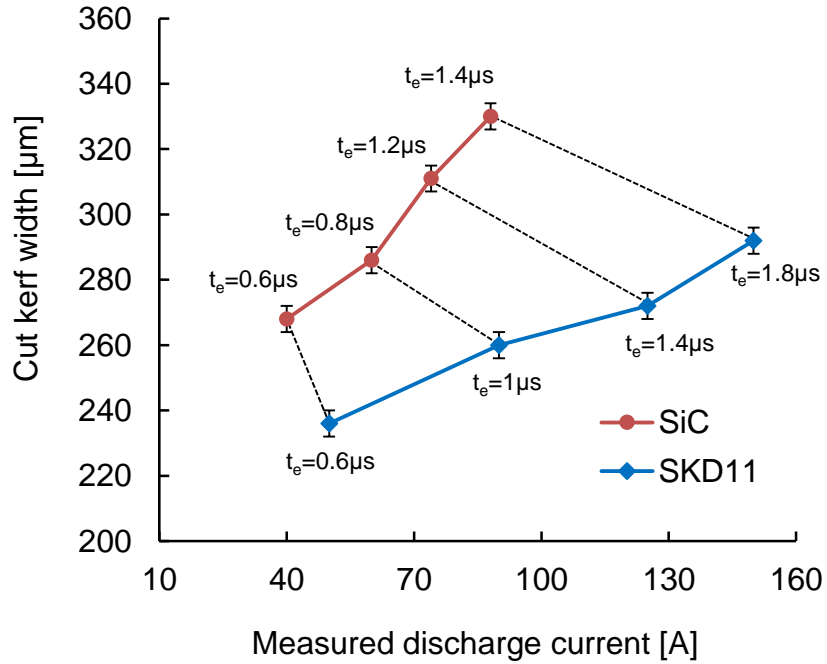
Fig. 2.5 Cut kerf width difference between wire EDM of single crystal SiC and cold tool steel SKD11

2.2.2 Material removal mechanism of EDM of brittle SiC

To find out the reasons for the different EDM behaviors of these two different materials, the material removal mechanism of SiC need to be investigated. It is well known that the material removal rate is closely related to the material properties of the workpiece. Yamashita et al. [40] investigated the influences of material properties on the material removal rate in sinking EDM processes. The required time t for the workpiece surface to be melted right after the dielectric breakdown was considered as the main parameter determining the MRR. The time t, as shown in Eq. 2.1, was derived by solving the one-dimensional heat conduction equation:

$$t = \left(\frac{\rho c \pi}{4} \right) \frac{\lambda \theta^2}{q''^2} \qquad \text{Eq. 2.1}$$

Here ρ is the material density; c is the specific heat; λ is the material thermal conductivity; θ is the material melting point (Since SiC has no melting point, θ here refers to the decomposition point of SiC) and q'' is the heat flux from the arc plasma of the discharge. Specifically the factor $\lambda \theta^2$ in Eq. 2.1 was found to be inversely proportional to the material removal rate by experiments for the majority of pure metal materials, which means that the material with higher thermal conductivity and melting point is more difficult to be

43

machined by EDM. According to **Table 2.1**, however, this value $\lambda\theta^2$ of SiC is almost 20 times larger than that of Fe (principal constituent of steel), which means that SiC should be a difficult-to-machine material by EDM method. It is therefore considered that the higher machining speed of SiC may be caused by other material removal mechanism.

On one hand, considering that SiC single crystal is of high electrical resistivity, the voltage drop in the workpiece was considerable (around 30V, as can be seen in **Fig. 2.1**), while in metal materials the voltage drop is usually negligible. When an electric current passes through a conductor, there will be heat released from the conductor, which is referred to as Joule heating effect. Hence Joule heat would be generated in EDM of SiC because of the high voltage drop in the workpiece. Together with the heat conducted from the arc plasma, the surface temperature of SiC was probably higher compared with that of steel. In consequence, the workpiece material of SiC was more easily to be removed, resulting in a higher material removal rate [41]. This will be discussed further in detail in the following section.

On the other hand, SiC material is of high brittleness. It has been reported that the material removal mechanism of advanced conductive ceramics was based on not only melting or vaporizing but also spalling [42]. Therefore the brittle structure of SiC may also contribute to its higher machining rate by cracks generation due to the thermal stress in EDM process.

Based on this assumption, experiments of EDM of SiC in clean deionized water in a clean tank by sinking EDM were conducted under the machining conditions shown in **Table 2.4**. The EDM debris was collected and observed by scanning electron microscope (SEM). **Fig. 2.6** shows the image of the observed EDM debris of SiC which reveals the evidence of multangular SiC debris particles. These kinds of small fragments were considered to be generated by the fracture of the workpiece due to the thermal cracks caused by electrical discharges. The multi-angular debris particles had nearly hexagonal or square shapes with crystallographically oriented sharp edges. The shape may be caused by cleavage fracture along crystal planes of SiC with sizes ranging from several microns to around 100μm. The larger the current density, the larger the heat flux will become, which will increase the thermal stress in the workpiece and make stress crack failure easier. This was considered as another main mechanism for the higher material removal rate of EDM of SiC. From this point of view, it is considered that optimal machining conditions should be selected in EDM of single crystal SiC in order to balance the material removal rate and the generation of cracks and fractures.
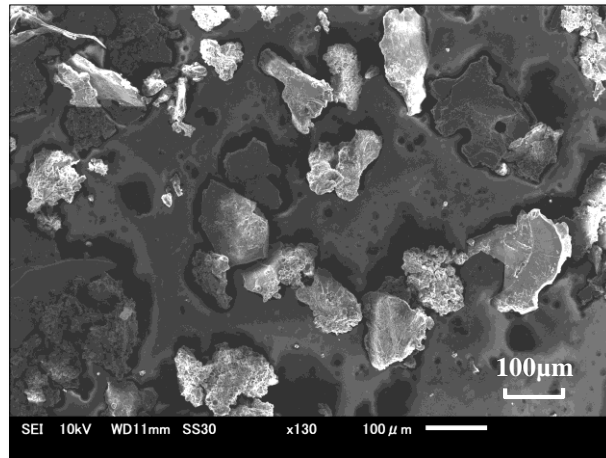
Fig. 2.6 SEM image of EDM debris of SiC in deionized water

Table 2.4 Machining conditions used for observing the EDM debris

Open voltage [V]	120
Tool polarity	(-)
Pulse duration [μs]	10
Pulse interval [μs]	50
Discharge current [A]	14
Dielectric liquid	Deionized water
Machining method	Sinking EDM

2.3 Heat conduction analysis of single discharge of SiC considering Joule heating effect

2.3.1 Introduction

This section describes the study on material removal mechanism of EDM of SiC in terms of temperature distribution by conducting heat transfer analysis of single discharge of SiC taking into consideration of Joule heat generation inside workpiece.

It is well known that EDM is a thermal process, removing material by melting and/or vaporization of the workpiece taking advantage of the energy input from discharges. Therefore, the temperature distribution of the workpiece near discharge spot during machining will be critical to the material removal rate. In general, higher working surface temperature can improve the machining rate by facilitating the melting and vaporization of material.

In the previous wire EDM experiments, however, it was found that under the same machining conditions, material removal rate of single crystal SiC was dozens of times higher than that of cold tool steel SKD11, although SiC featured a characteristic of higher melting point and higher thermal conductivity compared to that of steel. On the other hand, since SiC is a high resistivity material compared to metal, Joule heat generated during discharges inside the workpiece may contribute to the material removal process by increasing the workpiece temperature.

Saeki et al. [41] studied the influence of Joule heating effect on the EDM performances of Si_3N_4, which was a kind of ceramic material with high resistivity and low thermal conductivity, and found that temperature distribution inside workpiece could be significantly affected by the Joule heat. Similarly, it is considered in this paper that the Joule heating effect due to the resistance of SiC during discharges may be one of the main reasons for the higher material removal rate of SiC. However, since the thermo-properties of SiC is totally different from that of ceramic material, it is necessary to clarify the influence of Joule heating effect on the machining performance by calculating the temperature distribution inside the workpiece in EDM of SiC taking into account the Joule heating effect.

2.3.2 Heat transfer analysis algorithm and analysis model

Since it is almost impossible to obtain the 3-dimensional temperature distribution inside EDM workpiece through experimental methods, heat transfer analysis is conducted to calculate the temperature of workpiece during machining. Finite difference method (FDM), a numerical analysis method, was employed to perform the heat transfer analysis to obtain the temperature distribution in this study.

2.3.2.1 Analysis algorithm

This study focuses on the analysis of temperature distribution inside workpiece (SiC) resulted from single discharge.

Fig. 2.7 shows the analysis procedure for calculating the temperature distribution. Firstly the electrical potential distribution inside the workpiece is computed due to its high resistivity. Then based on the calculated electrical potential distribution, the Joule heat generation can be calculated by analyzing the current density distribution inside the workpiece. Next considering the energy input from both the generated Joule heat and the heat flux from discharges, unsteady heat conduction analysis is accomplished to compute the time-dependent distribution of workpiece temperature. To improve the accuracy of calculation, the arc column diameter change along with the passage of time due to the expansion behavior of arc plasma is also taken into consideration in every time step [41].
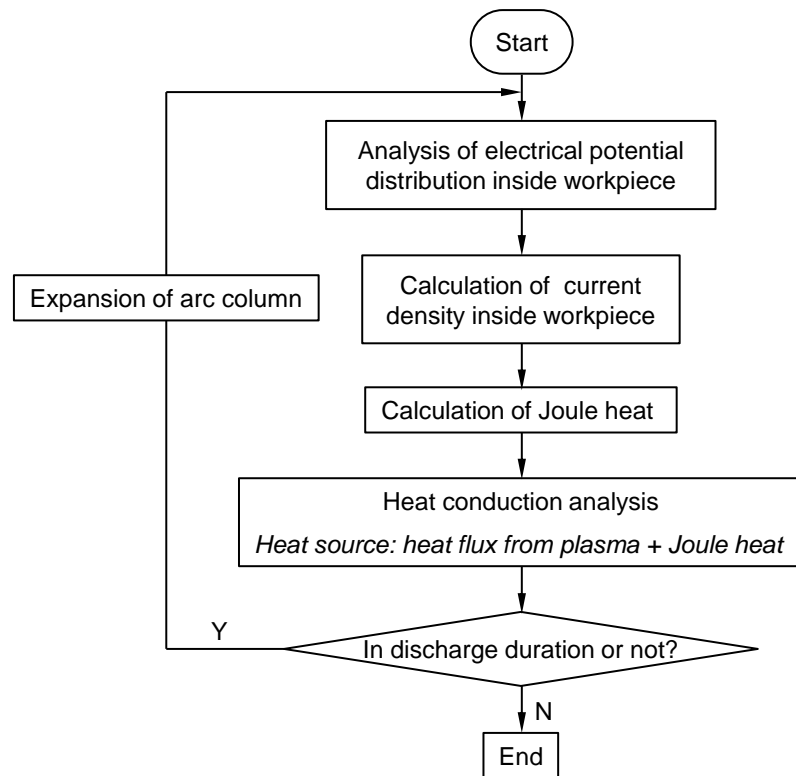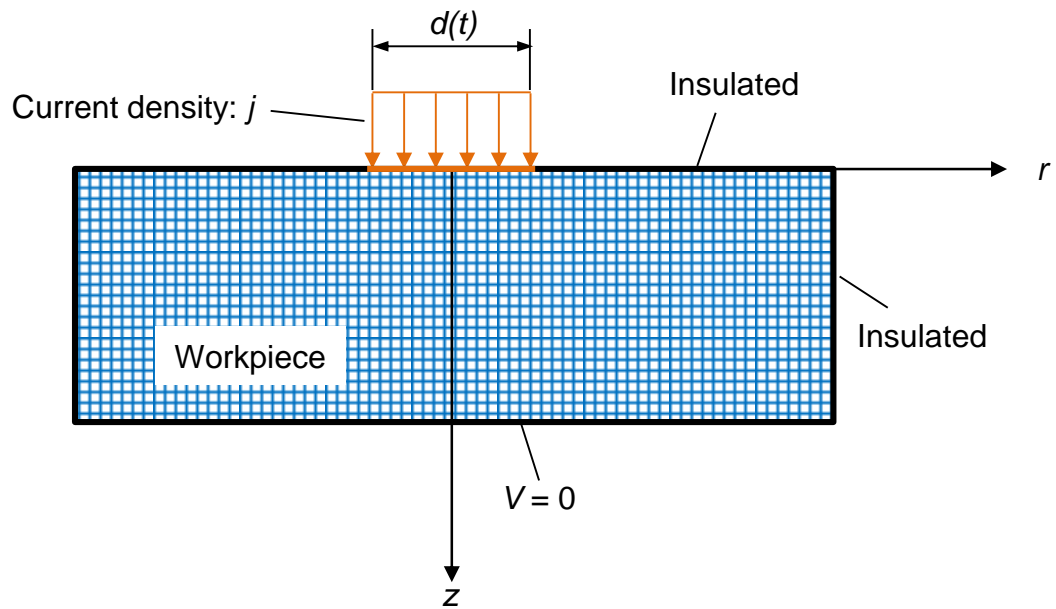

Fig. 2.7 Flow chart of numerical analysis of temperature distribution inside workpiece of single discharge

2.3.2.2   Analysis model

Fig. 2.8 shows the analysis model. For numerical solution of both electrical potential distribution and temperature distribution, the same analysis model is utilized.

In consideration of single discharge, the current and heat from the discharge flows axis-symmetrically into the workpiece. Therefore, the shape of the workpiece model is set as cylinder and cylindrical coordinate system is used for the calculation as shown in **Fig. 2.8**. The model for arc plasma column is also assumed

to be a cylinder. The arc column is set right at the center of the workpiece top surface (machining area). The brown area on the working surface indicates the energy input region where the current density, j, and heat flux q'' from the arc plasma are considered to be uniform.

Fig. 2.8 Illustration of the heat transfer analysis mode

2.3.3 Electrical potential distribution analysis

2.3.3.1 Governing equation

With regard to the 3D model discussed above in **Fig. 2.8**, since it is axisymmetric, no electrical charges (current) will flow along the circumferential direction. Therefore, the analysis model can be simplified as a two dimension model as shown in **Fig. 2.9**.

Considering a specific control volume around node [m, n] as shown in **Fig. 2.10**, based on the law of charge conservation, the algebraic sum of current flowing from the adjacent control volumes into the control volume [m, n] should be zero, as expressed in Eq. 2.2.

$$i_1+i_2+i_3+i_4=0$$

Eq. 2.2

48

Fig. 2.9 Simplified analysis model of electric potential distribution of single discharge EDM
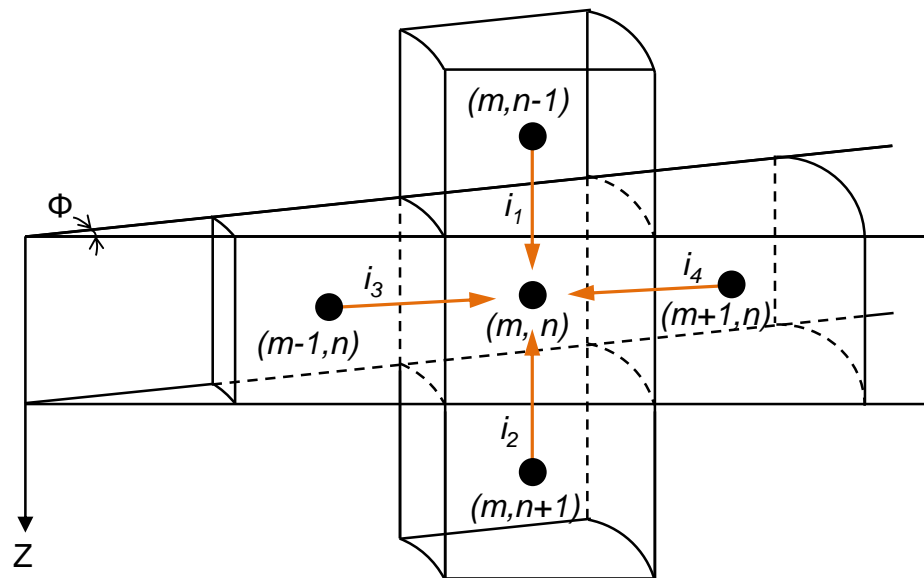
Fig. 2.10 Illustration of current flow into control volume [m, n]

Here, i_1~i_4 refers to the current flowing into control volume [m, n] from the adjacent ones as shown **Fig. 2.10**. On the other hand, according to the Ohm's law, current i can be expressed by Eq. 2.3. Here, ρ, l, S refers to resistivity, length and cross-section area of conductor respectively and ΔV is the potential difference in conductor.

$$i = \frac{S}{\rho l} \Delta V \qquad \text{Eq. 2.3}$$

In **Fig. 2.10**, assuming the inflow area of current into control volume [m, n] from the adjacent control volumes is S_1, S_2, S_3, S_4 respectively, the following equation (Eq. 2.4) concerning the electrical potential V, of each node can be obtained by calculating i_1~i_4 by Eq. 2.3 and substituting i_1~i_4 into Eq. 2.2.

$$\frac{S_1 \cdot (V_{m,n-1} - V_{m,n})}{\rho \Delta z} + \frac{S_2 \cdot (V_{m,n+1} - V_{m,n})}{\rho \Delta z} + \frac{S_3 \cdot (V_{m-1,n} - V_{m,n})}{\rho \Delta r} + \frac{S_4 \cdot (V_{m+1,n} - V_{m,n})}{\rho \Delta r} = 0 \qquad \text{Eq. 2.4}$$

Consequently, Eq. 2.4 can be taken as the governing equation of every node to calculate its electrical potential. Based on the boundary conditions described in the next sections, the electrical potential at every node can be obtained by solving the set of simultaneous equations.

2.3.3.2 Boundary conditions

The main boundary conditions have been noted in the analysis model shown in **Fig. 2.9**. The electrical potential at the nodes on the bottom surface of the workpiece is maintained as zero (ground level). Except for the energy input region, all the other surfaces are considered to be insulated. The density of current flow inside the arc column is assumed to be uniform in the whole discharge area for simplicity, which equals to the value of current divided by the arc column area as shown in Eq. 2.5. Here, i_e refers to the discharge current and $d(t)$ is time-dependent diameter of the circular energy source. As one of the boundary conditions, $d(t)$ is of great importance to realize a correct calculation of electrical potential distribution.

$$j = \frac{i_e}{\pi (\frac{1}{2} d(t))^2} \qquad \text{Eq. 2.5}$$

Kojima et al. [43] investigated the temporal change of plasma diameter through experimental observation and expressed the plasma diameter as a function of discharge time and current as shown in Eq. 2.6. This equation is based on the empirical equation obtained by Saito et al. [44] and Ikai et al. [45] assuming that heat source diameters are equal to discharge craters diameters which were measured in experiment as Eq. 2.7.

$$d(t) = 1.7 \times 10^{-3} \times t^{0.35} \times i_e^{0.48} \qquad \text{Eq. 2.6}$$

$$d(t) = 2.4 \times 10^{-3} \times t^{0.4} \times i_e^{0.4}$$

Eq. 2.7

Here, the units of $d(t)$, t and i_e are [m], [s] and [A] respectively. In simple words, the energy source diameter should be exactly the same as that of the arc plasma. However, since the temperature distribution in the plasma is not uniform, the degree of ionization is not uniform. In consequence, the current density may be more concentrated near the center axis of the cylinder plasma, resulting in effective heat source diameter smaller than that of the plasma diameter. Therefore, for simplicity, $d(t)$ in Eq. 2.7 is in some cases used as the energy source diameter instead of the plasma diameter.

However, as mentioned before, since the EDM characteristics of SiC is significantly different from that of metal material due to the large voltage drop inside SiC for instance, it is considered that the $d(t)$ in Eq. 2.7 is improper to be used for analyzing the temperature distribution in SiC. Hence, in this paper, the accurate energy source diameter is determined by solving the inverse problem of electrical potential analysis in SiC of which the details will be described in the following section.

The thermo-physical properties of workpiece are listed in **Table 2.5**. For simplicity, the dependency of the material properties on temperature is not considered here.

Table 2.5 Material properties used for simulation

| Material		SiC	Steel
Resistivity	[Ω·cm]	2e-2	1.5e-5
Thermal conductivity	[W/(m·K)]	490	45
Density	[kg/m^3]	3210	7850
Specific heat	[J/(Kg·K)]	656	469

2.3.3.3   Inverse solution of plasma diameter in EDM of SiC

i) Measurement of voltage drop inside SiC in EDM:

In EDM of SiC, due to the high resistivity of SiC, there is usually a high voltage drop inside SiC. The measured discharge gap voltage U_m in experiments in EDM is usually composed of three parts (see **Fig. 2.11**): voltage drop in tool electrode U_t, voltage drop in arc plasma U_e and voltage drop inside workpiece U_w. It is well known that, as good conductors, the voltage drop in tool electrode (copper) and workpiece of metal materials is very little and can be neglected. The discharge voltage measured in EDM of steel is

usually considered as the voltage drop in the arc plasma. Hence, by subtracting the measured discharge voltage of steel from that of SiC under the same discharge current, as illustrated in **Fig. 2.12**, the voltage drop in workpiece of SiC can be obtained. In this paper, the discharge voltage of EDM of steel is taken as 20V for simplicity.

On the other hand, however, it was found that the voltage drop in SiC differs depending on the gap conditions. **Fig. 2.13**(a) and (b) show two different types of discharge waveforms observed in machining experiments of SiC. **Table 2.6** shows the experimental conditions for measuring the discharge waveforms of SiC. It can be seen that the gap voltage in **Fig. 2.13**(a) is much higher compared to that in **Fig. 2.13**(b) after the discharge is ignited. In addition, the gap voltage is not constant but decreasing with passage of discharge time due to the expansion of arc plasma. In the case of **Fig. 2.13**(b), the decreasing speed of gap voltage is quicker compared to that in **Fig. 2.13**(a). The reason is considered that discharges may occur in bubble (air), in oil or at the interface between bubble and oil through debris particles and the plasma behavior may be different in different cases, resulting in different voltage drop in SiC. For comparison, the plasma diameters in both two cases are calculated in this paper and the heat conduction analysis under both two calculated plasma diameters are conducted.


$$U_m = U_t + U_e + U_w$$
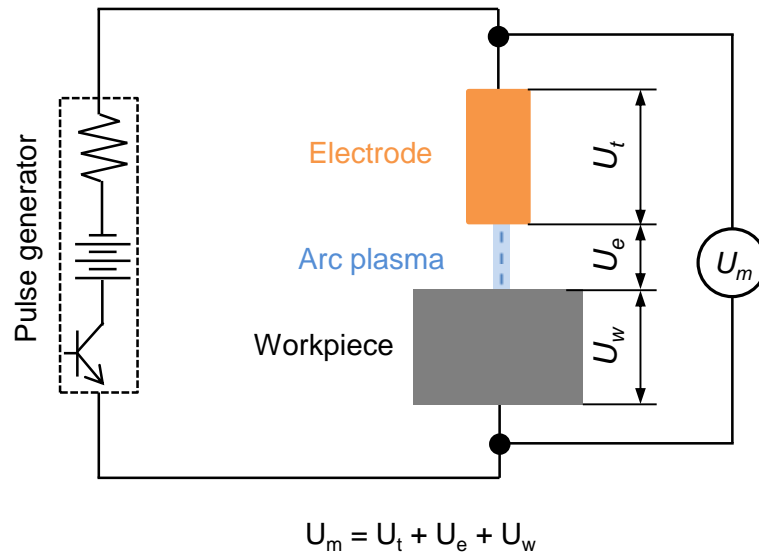
Fig. 2.11 Illustration of measure discharge voltage in EDM
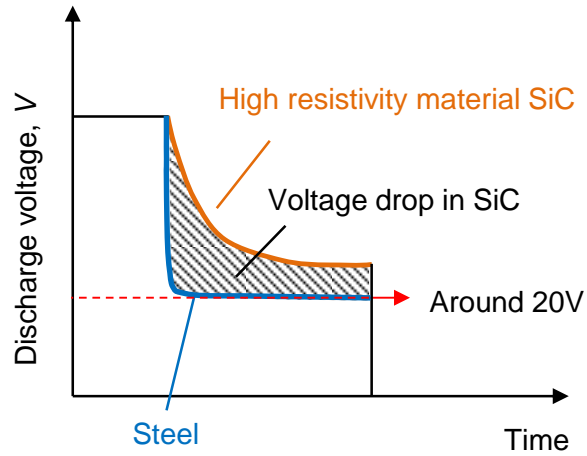
Fig. 2.12 Discharge waveform difference in EDM of SiC and steel

.

Table 2.6 Experimental conditions

Tool electrode	Copper rod, Φ5mm
Workpiece	SiC wafer, thickness: 0.5mm
Open voltage [V]	120
Preset discharge current [A]	30
Discharge duration [μs]	10
Discharge interval [μs]	2500
Servo voltage [V]	100
Dielectric liquid	EDM oil
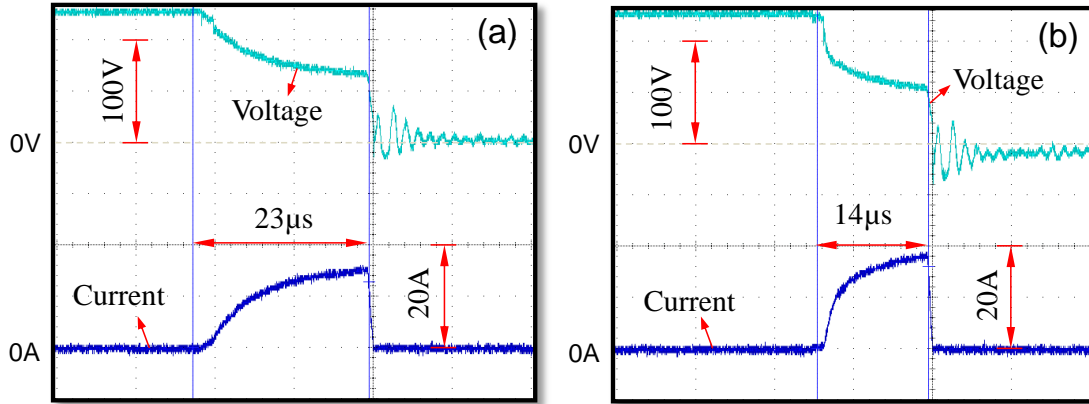
Fig. 2.13 Discharge waveform of SiC by sinking EDM: (a) High gap voltage; (g) Low gap voltage

ii) Analysis procedure for calculating the plasma diameter:

Fig. 2.14 shows the analysis method for calculating the plasma diameter. As the start, the actual discharge current and voltage waveforms are measured through experiments as shown in **Fig. 2.13**. Based on the measured data of discharge voltage and current, the voltage drop inside SiC, U_w , at certain time t (here t refers to the passage of time after the ignition of discharge) and the corresponding discharge current can be obtained. These data are used as the boundary conditions to calculate the plasma diameter at time t.

In the iteration of the program (**Fig. 2.14**), the arc column diameter, $d(t)$, is set to be changing from 0 to 200 μm with an interval of 0.01 μm. At each assumed value of $d(t)$, the voltage drop inside SiC is calculated based on the method described in Section 2.3.3.1. At certain time t, if the calculated voltage drop inside SiC agrees with the measured value, the program will end and the assumed $d(t)$ will be taken as the plasma diameter at time t. By repeating the program and changing the boundary conditions, $d(t)$ at different time can be calculated. The calculated result of plasma diameter is shown in **Fig. 2.15**. The approximate curve in the figure is taken as the equation to express the change of arc plasma diameter along with time.
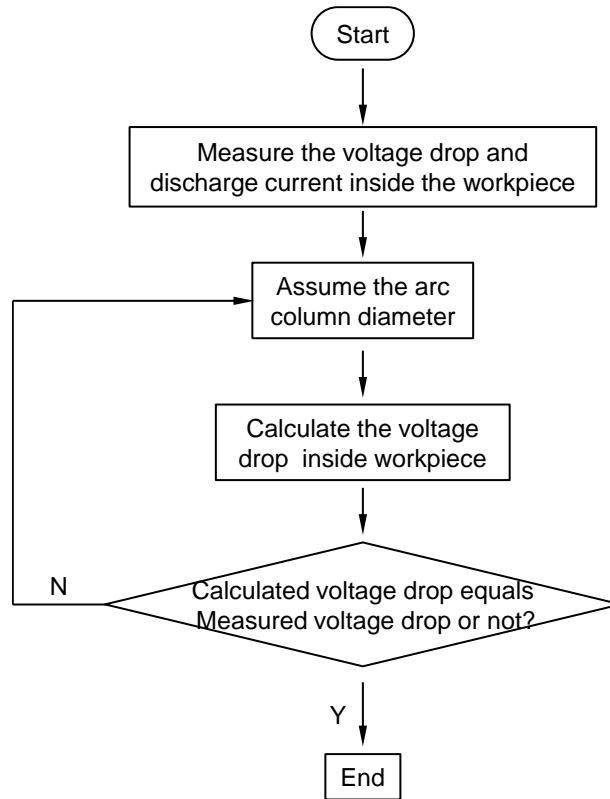
**Fig. 2.14** Procedures for inverse solution of plasma diameter in EDM of SiC
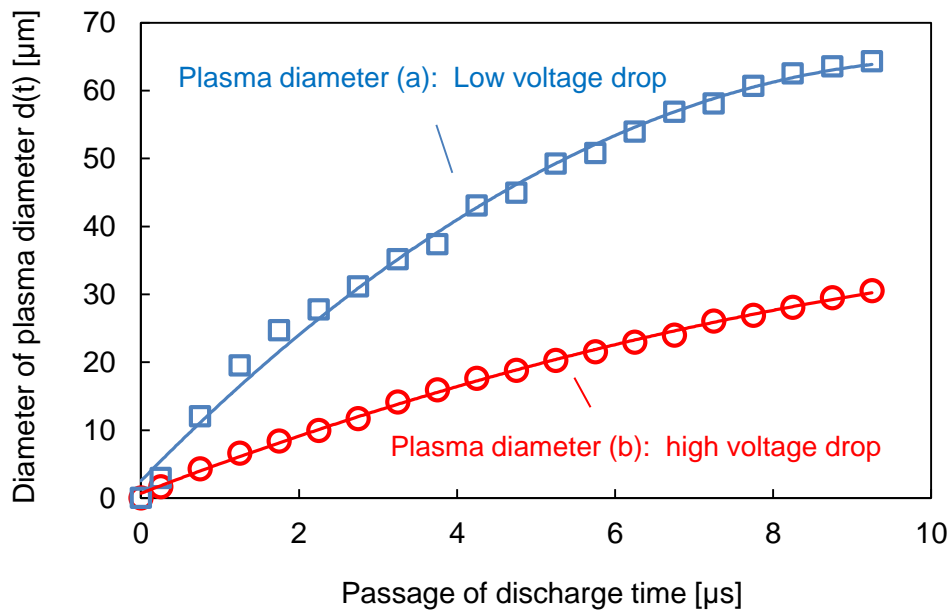
**Fig. 2.15** Calculation result of diameter expansion of energy source

2.3.3.4 Analysis result of electrical potential distribution

Fig. 2.16 shows the equipotential charts of electrical potential distribution inside SiC based on the calculated plasma diameter. For comparison, the electrical potential distribution in carbon steel is shown in **Fig. 2.17**. It should be noted that the plasma diameter *d(t)* in Eq. 2.7 was used for calculating the electrical potential distribution in carbon steel. From these two figures, it can be found that the voltage drop inside SiC, around 40V, is significantly larger compared to that of steel which is almost zero and the voltage drop mostly occurred in the vicinity of the discharge spot where the current density is highest in both two cases.

Fig. 2.18 shows the influence of workpiece length on the voltage drop in the workpiece of SiC under the same discharge conditions. The voltage drop increases with increasing the workpiece length due to the increased resistance of the workpiece. However, since voltage mostly drops near the discharge spot, the workpiece length influence on the voltage drop is not significant.
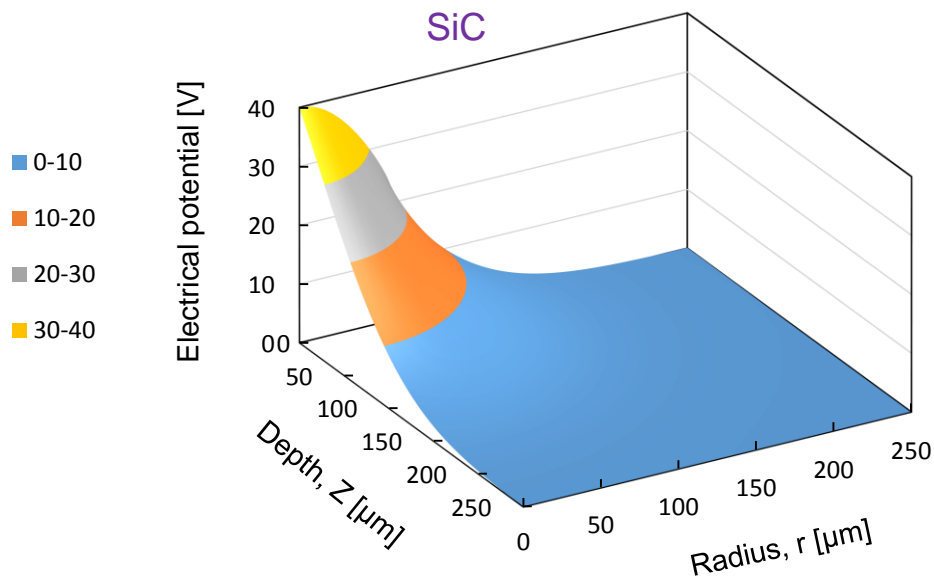
Fig. 2.16 Electrical potential distribution inside SiC of single discharge at t=10μs
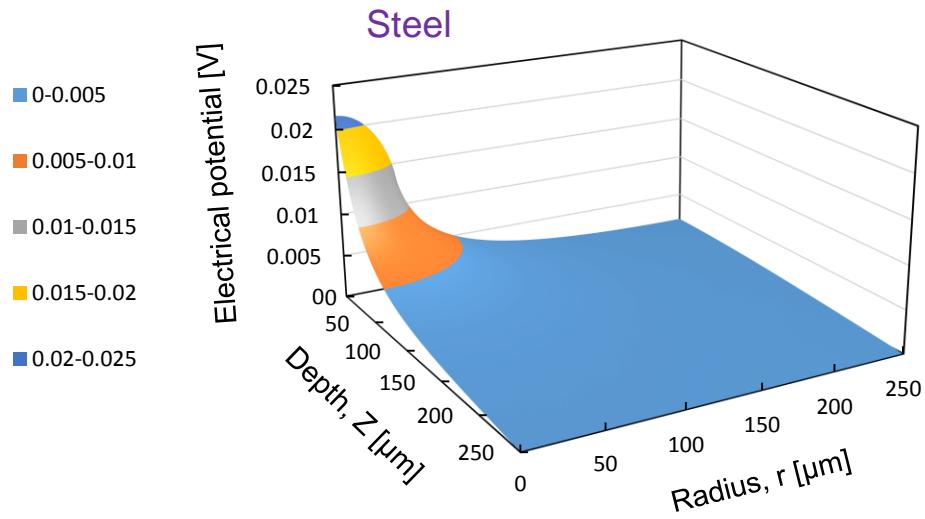
Fig. 2.17 Electrical potential distribution inside steel of single discharge at t=10μs
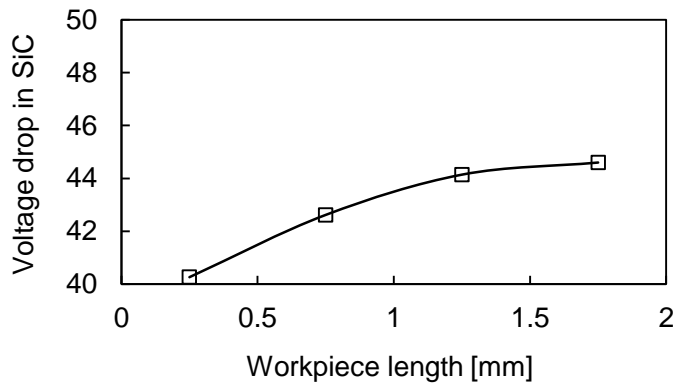
Fig. 2.18 Workpiece length influence on the voltage drop inside SiC

2.3.3.5 Calculation of Joule heat

When an electric current passes through a conductor, there will be heat released from the conductor, which is referred to as Joule heating effect. The Joule heat generated per unit time $\dot{Q}$ in a conductor with resistance R can be calculated by Joule's laws as expressed in the following equation, where i refers to the current flowing through the conductor.

$$\dot{Q} = i^2 R \qquad\qquad \text{Eq. 2.8}$$

In the case of one specific control volume [m, n] in the analysis model, the current density flowing in the radius direction $j_{r_{m,n}}$ and depth direction $j_{Z_{m,n}}$ can be calculated based on the analysis results of electrical potential distribution in the last section, as expressed in the following equations, where ρ is the resistivity of workpiece material.

$$
\begin{aligned}
j_{r_{m,n}} &= \frac{V_{m-1,n} - V_{m+1,n}}{2\rho\Delta r} \\[2mm]
j_{z_{m,n}} &= \frac{V_{m,n-1} - V_{n+1,n}}{2\rho\Delta Z}
\end{aligned}
\qquad\qquad \text{Eq. 2.9}
$$

Then the total current density flowing through control volume [m, n] can be expressed as

$$j_{m,n} = \sqrt{j_{r_{m,n}}^{\ 2} + j_{Z_{m,n}}^{\ 2}} \qquad\qquad \text{Eq. 2.10}$$

The Joule heat generated per unit time in each control volume [m, n], $\dot{Q}_{m,n}$ can be calculated by the following equation based on the equations described above, where $W_{m,n}$ is the volume of the control volume.

$$\dot{Q}_{m,n} = \rho W_{m,n} j_{m,n}^2 \qquad\qquad \text{Eq. 2.11}$$

## 2.3.4 Temperature distribution analysis

2.3.4.1 Governing equation

The analysis model for temperature distribution, as shown in **Fig. 2.19**, is the same as the model used for electrical potential distribution except for the boundary conditions. The temperature distribution inside workpiece can be calculated by solving the time-dependent heat conduction equation in the cylindrical model as expressed in the following equation (Eq. 2.12).

$$\rho_d c \frac{\partial T}{\partial t} = \frac{1}{r}\frac{\partial}{\partial r}\left(\lambda r \frac{\partial T}{\partial r}\right) + \frac{\partial}{\partial z}(\lambda \frac{\partial T}{\partial z}) + \dot{q}$$

Eq. 2.12

Here, ρ_d is density of the workpiece, c is specific heat, λ is thermal conductivity of the workpiece and T is temperature and $\dot{q}$ is the rate at which energy is generated per unit volume of the medium.

With regard to one specific control volume [m, n], as shown in **Fig. 2.20**, the heat conduction equation can be expressed as equation Eq. 2.13 based on the energy conservation law, where $W_{m,n}$ refers to the volume of the control volume, Q^p refers to the heat input per unit time due to conduction. $\dot{Q}_{m,n}$ is the heat generated in control volume [m, n] per unit time by Joule heating effect and $T^p_{m,n}$ indicates the temperature of control volume [m, n] at time t^p ($= p \times \Delta t$).

$$\rho_d c W_{m,n} \frac{T^{p+1}_{m,n} - T^p_{m,n}}{\Delta t} = Q^p + \dot{Q}_{m,n}$$

Eq. 2.13
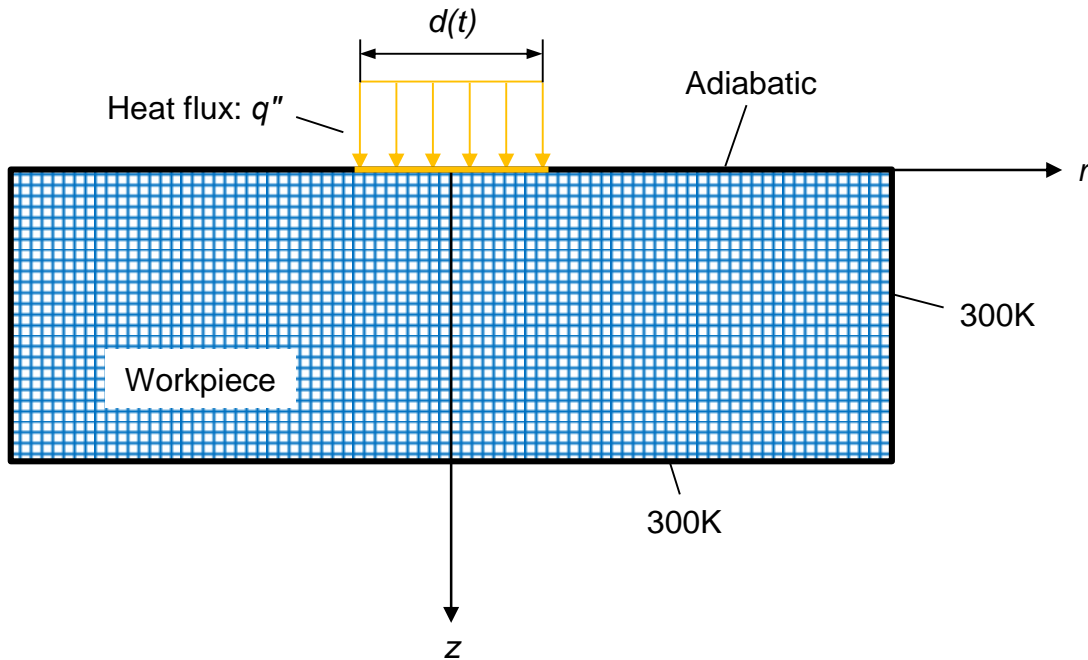
Fig. 2.19 Heat conduction analysis model of single discharge of SiC
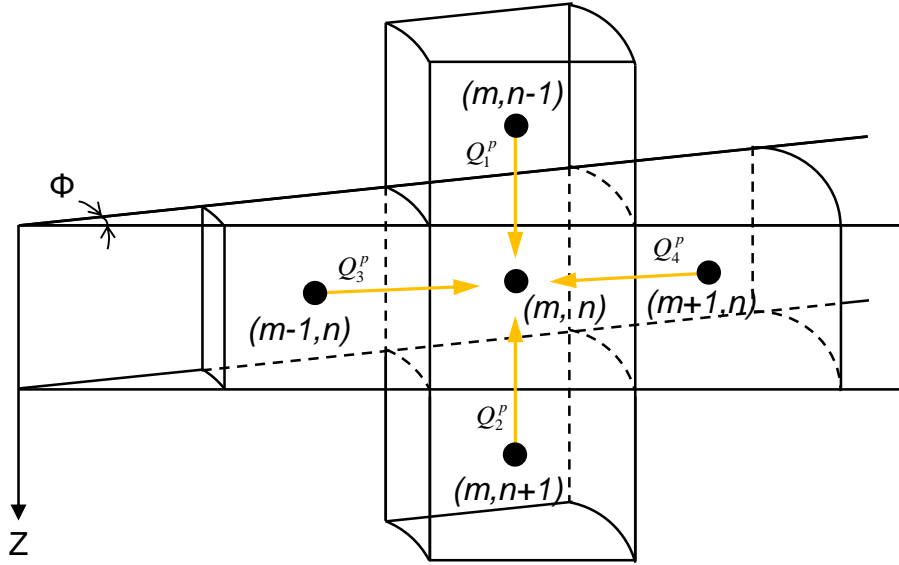
Fig. 2.20 Illustration of heat flow into control volume [m, n]

The input heat of control volume [m, n] through conduction can be expressed as in Eq. 2.14, where $Q_1^p \sim Q_4^p$ indicates the heat flowing into control volume [m, n] from the adjacent control volumes per unit time as shown in **Fig. 2.20**.

$$Q^p = Q_1^p + Q_2^p + Q_3^p + Q_4^p \qquad \text{Eq. 2.14}$$

Here, $Q_1^p \sim Q_4^p$ can be express as the following equation by Fourier's Law of heat conduction.

$$Q_1^p = \lambda \frac{T_{m,n-1}^p - T_{m,n}^p}{\Delta z} S_1$$

$$Q_2^p = \lambda \frac{T_{m,n+1}^p - T_{m,n}^p}{\Delta z} S_2$$

$$Q_3^p = \lambda \frac{T_{m-1,n}^p - T_{m,n}^p}{\Delta r} S_3 \qquad \text{Eq. 2.15}$$

$$Q_4^p = \lambda \frac{T_{m+1,n}^p - T_{m,n}^p}{\Delta r} S_4$$

Substituting Eq. 2.14 and Eq. 2.15 into Eq. 2.13, the heat conduction equation at node [m, n] can be obtained as expressed in the following equation (Eq. 2.16), which indicates that the temperature at time t^{p+1} at node [m, n] can be calculated by the temperatures of its adjacent nodes at time t^p.

60

$$T_{m,n}^{p+1} = \frac{\lambda \Delta t}{\rho_d c W_{m,n}} \left(\frac{T_{m,n-1}^p - T_{m,n}^p}{\Delta z} S_1 + \frac{T_{m,n+1}^p - T_{m,n}^p}{\Delta z} S_2 + \frac{T_{m-1,n}^p - T_{m,n}^p}{\Delta r} S_3 + \frac{T_{m+1,n}^p - T_{m,n}^p}{\Delta r} S_4 \right) + T_{m,n}^p + \frac{\Delta t}{\rho_d c W_{m,n}} \dot{Q}_{m,n} \quad \text{Eq. 2.16}$$

2.3.4.2   Boundary conditions

In the analysis model shown in **Fig. 2.19**, it was assumed that the discharge is generated at the center of the top surface of the workpiece. The workpiece polarity is set as anode in order to be consistent with the workpiece polarity used in the previous wire EDM experiments. The heat flux $q^{"}$ generated by arc plasma flows into the workpiece from the discharge surface. Within the area of plasma column of diameter $d(t)$, heat flux is assumed to be uniform. Given discharge current i_e and discharge voltage u_e, the heat flux $q^{"}$ can be expressed as the following equation (Eq. 2.17), where η is the ratio of energy distributed into the anode.

$$q^{"} = \frac{\eta \cdot u_e \cdot i_e}{\pi (\frac{1}{2} d(t))^2} \qquad \text{Eq.2.17}$$

With regard to the energy distribution ratio η, Xia et al. [46] found out that the ratio of total discharge energy distributed into anode is around 40% when copper was used for both anode and cathode. On the other hand, Hayakawa [47, 48] found out that the thermal conductivity of the electrode material had a considerable influence on the energy distribution ratio η due to the energy diffusion effect. In this research, the discharge energy distribution into SiC was not measured. However, since the thermal conductivity of 4H-SiC ($490 W{\cdot}m^{-1}{\cdot}K^{-1}$) is close to that of copper ($401 W{\cdot}m^{-1}{\cdot}K^{-1}$), the energy distribution ratio of SiC (anode) is set as 40% referring to that of copper obtained by Xia et al. [46].

The initial temperature of all the nodes was set at room temperature (300K). Except for the discharge area, the top surface of the workpiece was considered to be adiabatic, which means that no heat flows in or out the surface. All the other surface temperatures of the workpiece were maintained constant at room temperature. Material removal was not considered in the analysis for simplicity. Moreover, due to the lack of relevant data, the latent heat of decomposition of SiC was not taken into account.

With the calculation method described in the previous section and the boundary conditions, the temperature at every node can be obtained.

2.3.4.3   Analysis results

2.3.4.3.1   Influence of Joule heating on temperature distribution

Fig. 2.21 shows the comparison results of the temperature distribution inside workpiece at t=2μs with and without taking into consideration the Joule heating effect utilizing the calculated plasma diameter (a) (refer to **Fig. 2.15**). It can be seen that in the case without considering Joule heat effect, the surface temperature

of SiC at discharge spot drops to 1831K after 2μs of discharge occurrence, which is below the decomposition temperature of SiC (about 2700K). On the other hand, however, taking into consideration of Joule heating effect, the surface temperature of SiC at the discharge spot is increased significantly to about 4268K. Therefore, it is considered that the Joule heating effect has a great impact on the removal of SiC.
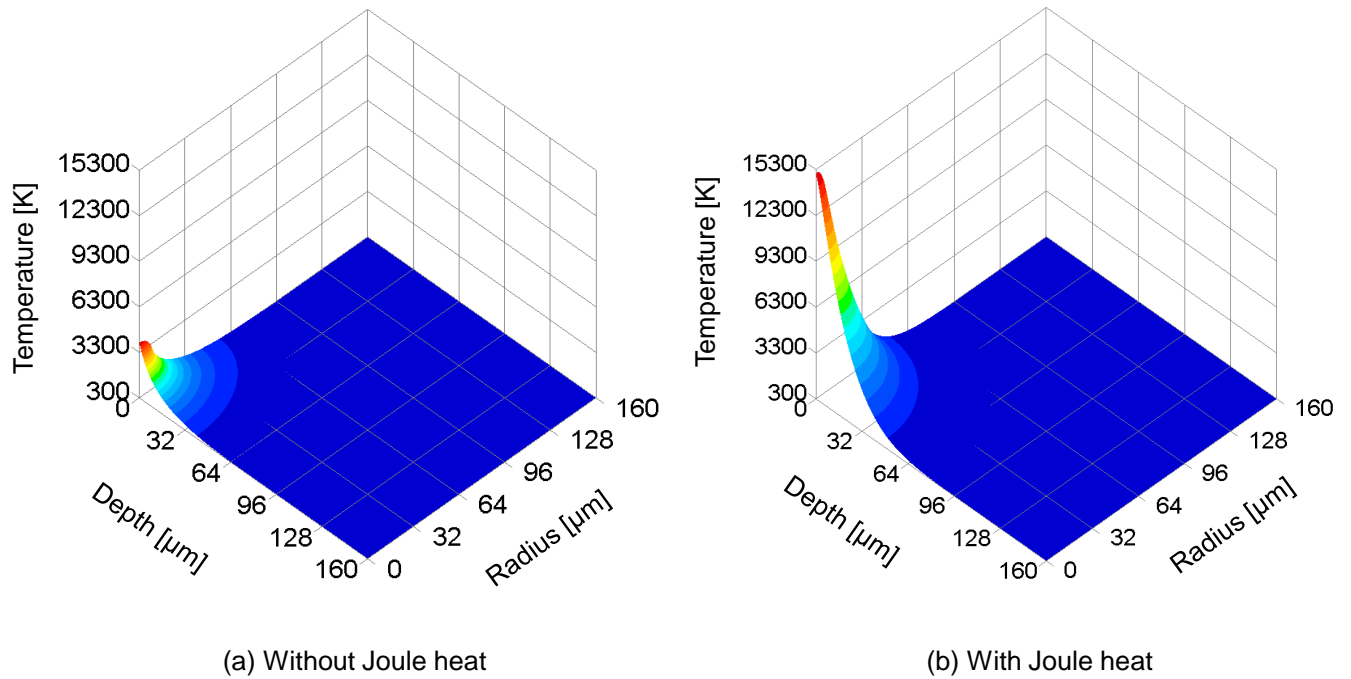

(a) Without Joule heat   (b) With Joule heat
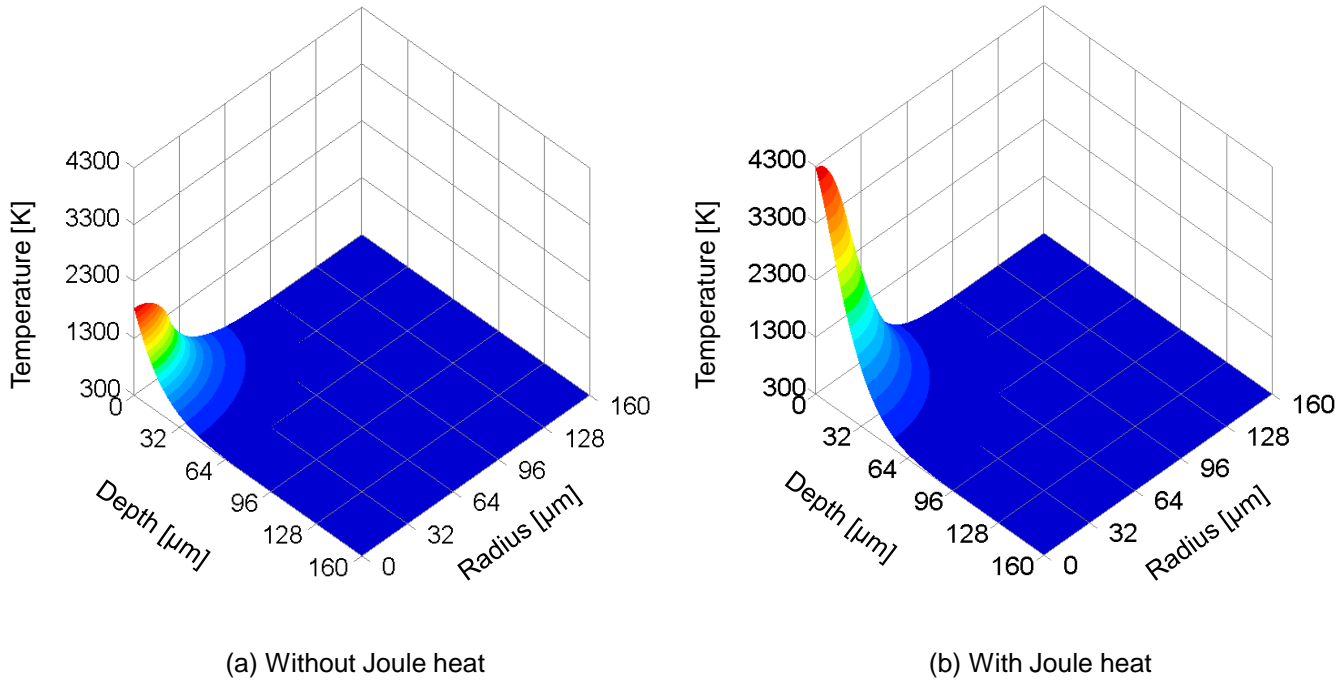
Fig. 2.21 Calculated temperature distribution by using plasma diameter (a) at t=2μs

Fig. 2.22 shows the calculated temperature using plasma diameter (b). The temperature is much higher compared with those shown in **Fig. 2.21**. This is because the plasma diameter (b), as shown in **Fig. 2.15**, is much smaller compared to plasma diameter (a) which results in a much larger heat flux under the same input energy. Besides, the Joule heat effect will become more significant with smaller plasma diameter due to the larger current density. On the other hand, it is found that the peak temperature in **Fig 2.22**(b) is approaching to 15000K. The reason why the peak temperature of the workpiece surface is beyond the plasma temperature (around 7000K) is considered that the material removal is not considered in the analysis.

2.3.4.3.2 *Temperature decrease with passage of time*

Fig. 2.23 shows the decrease of peak temperature at $r = z = 0$ (heat source center on the working surface) along with the passage of time after the ignition of discharge. It can be seen that the peak temperature drops below the decomposition temperature, 3000K, of SiC in about 4μs due to the high thermal

conductivity of SiC and the expansion of heat source diameter. Therefore, it is considered that long pulse duration may not contribute to the material removal rate of SiC. This conclusion is verified by machining experiments of SiC which will be described in Chapter 3.

(a) Without Joule heat   (b) With Joule heat

Fig. 2.22 Calculated temperature distribution by using plasma diameter (b) at t=2μs
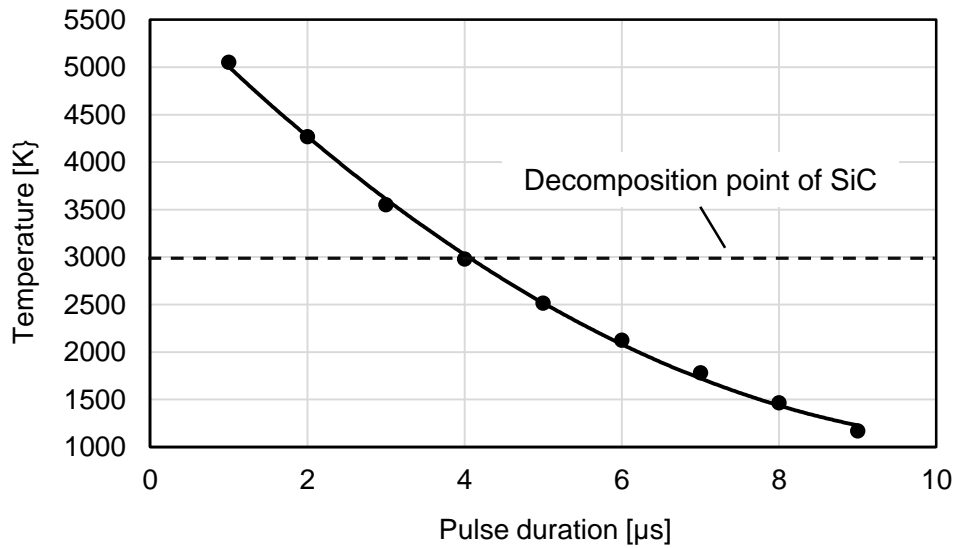

Fig. 2.23 Peak temperature vibration with the passage of discharge time on the discharge surface (by plasma diameter (a) considering Joule heating effect)

2.3.4.4 Comparison of single discharge between EDM of SiC and SKD11

To find out the reason for the differences of the material removal rate between EDM of SiC and carbon steel SKD11, comparison study on temperature distribution between single discharge of SiC and SKD11 was conducted. In both cases of SiC and SKD11, the same heat source diameter and discharge current (calculated plasma diameter (a)) was used. The latent heat was taken into consideration in the heat conduction analysis of carbon steel SKD11 while in the case of SiC it was not considered because of the lack of relevant data.

Fig. 2.24 (a) and (b) show the analyzed results of temperature distribution in SiC and steel respectively at time t=1μs. The area of high temperature region in the case of SiC was larger due to the Joule heating effect inside the workpiece compared with that of steel, which probably makes the extinction of plasma more difficult in EDM of SiC. In consequence, discharge concentration occurs more easily in EDM of SiC, which results in a higher probability of wire breakage in wire EDM of SiC compared to that of SKD11. On the other hand, however, the peak temperature at the heat source center on the discharge surface in the case of SiC was lower compared to that of steel due to its higher thermal conductivity.

(a) SiC   (b) Steel
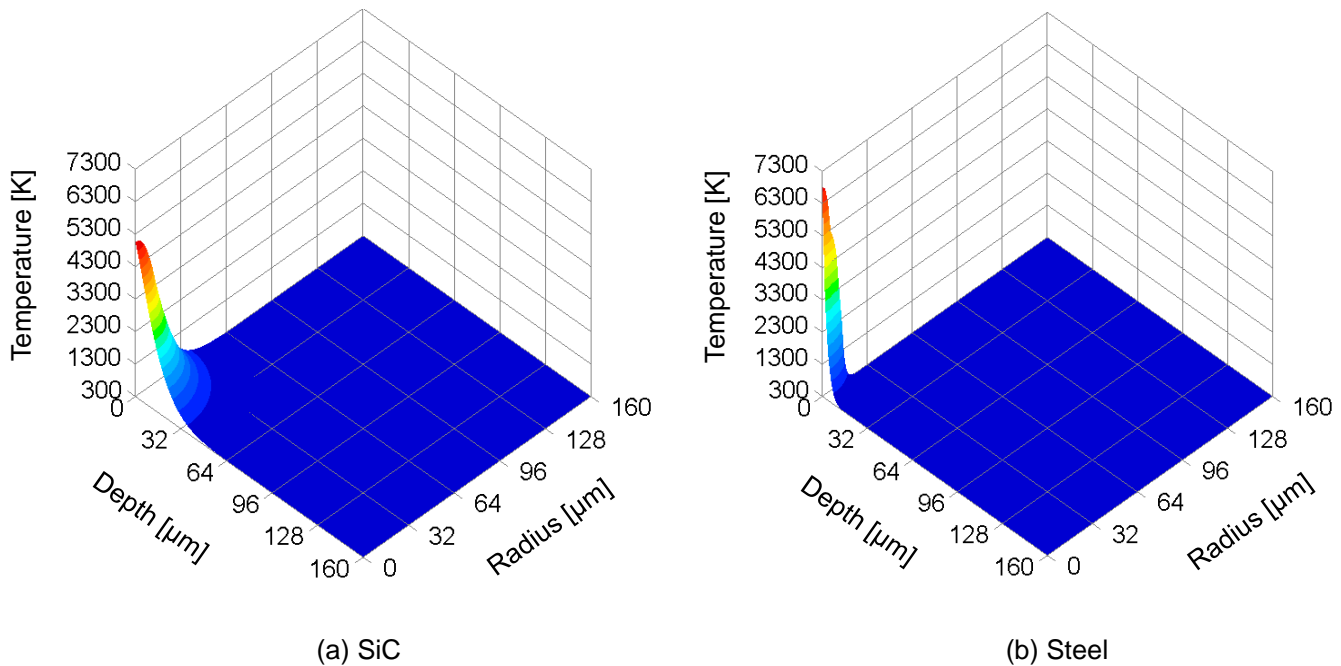
Fig. 2.24 Comparison of temperature distribution between single discharge of SiC and steel at t=1μs

On the other hand, it should be noted that in actual experiments with the same machining conditions, the heat flux input into SiC and steel is probably different. In the case of SiC, since the discharge voltage is high, under the same servo voltage, the discharge frequency should be high. Therefore, it is considered that the discharge gap width should be smaller compared with that of steel in order to achieve a higher discharge frequency. A smaller discharge gap width will result in a smaller plasma diameter [43], which in consequence brings about a higher heat flux in single discharge of SiC compared with that of steel. This probably is another reason for the higher material removal rate of SiC.

2.4 Evaluation of wire EDM slicing performance of SiC

Electrical discharge machining of single crystal SiC can be performed successfully owing to its conductivity. The following sections evaluate the performances of wire EDM slicing of SiC ingot for practical use.

2.4.1 Influence of crystal orientation on machining characteristics

4H-SiC has a hexagonal close-packed crystal structure, of which the main crystallographic orientations and planes are shown in **Fig. 2.25**. The *c* axis marked in the figure refers to the crystal growth axis of SiC. It has two preferred cleavage planes: the (11-20) and (1-100) plane respectively, as can be seen in **Fig. 2.25**, and cleavages along the cleavage plane (1-100) are more reproducible to make [49]. It is therefore considered that in EDM process, the thermal cracks resulted from electrical discharges inside the workpiece will propagate more easily along the cleavage planes. In other words, the machining speed along these crystal planes will be higher. On the other hand, it has been reported [50] that the machining speed depends significantly on the machining direction in the micro-EDM process of monocrystalline tungsten under the finish machining conditions. Therefore, this section aims to clarify the influences of the anisotropy of SiC on the EDM slicing performances.

2.4.1.1 Experimental method

To investigate the influence of the anisotropy of SiC on the EDM characteristics, 4H-SiC single crystal was cut by wire EDM along different crystal orientations. Defining the crystal direction <11-20> and <1-100> as 0˚ and 90˚ respectively, as shown in **Fig. 2.26**, SiC ingot was cut every 15˚ in between the two directions to investigate the difference of machining speed.

The experiments were conducted under the rough machining conditions as shown in **Table 2.7**. The schematic diagram of the experimental setup is shown in **Fig. 2.27**. Since the off-axis angle of the SiC wafer surface orientation was 4˚±0.5˚, before the experiment, the SiC ingot was intentionally positioned to make the crystal axis, *c* , parallel to the wire electrode. Machining was done by servo control feeding the workpiece to the wire electrode. However, it should be noted here that the workpiece feed speed should be properly selected. Because too high feeding speed will cause instability of machining due to too small gap width. On the contrary, too low feeding speed will impose restrictions on the maximum machining speed. Therefore, in order to reduce the influence of the servo feed speed on the machining rate, optimal machining conditions were investigated through machining trials. Results obtained from trial machining showed that under the preset rough machining conditions, the maximum feed speed of SiC along either direction was lower than 2.5mm/min. Therefore, the feed speed of the worktable was preset at 2.6mm/min, a little faster than the actual maximum machining speed of SiC.
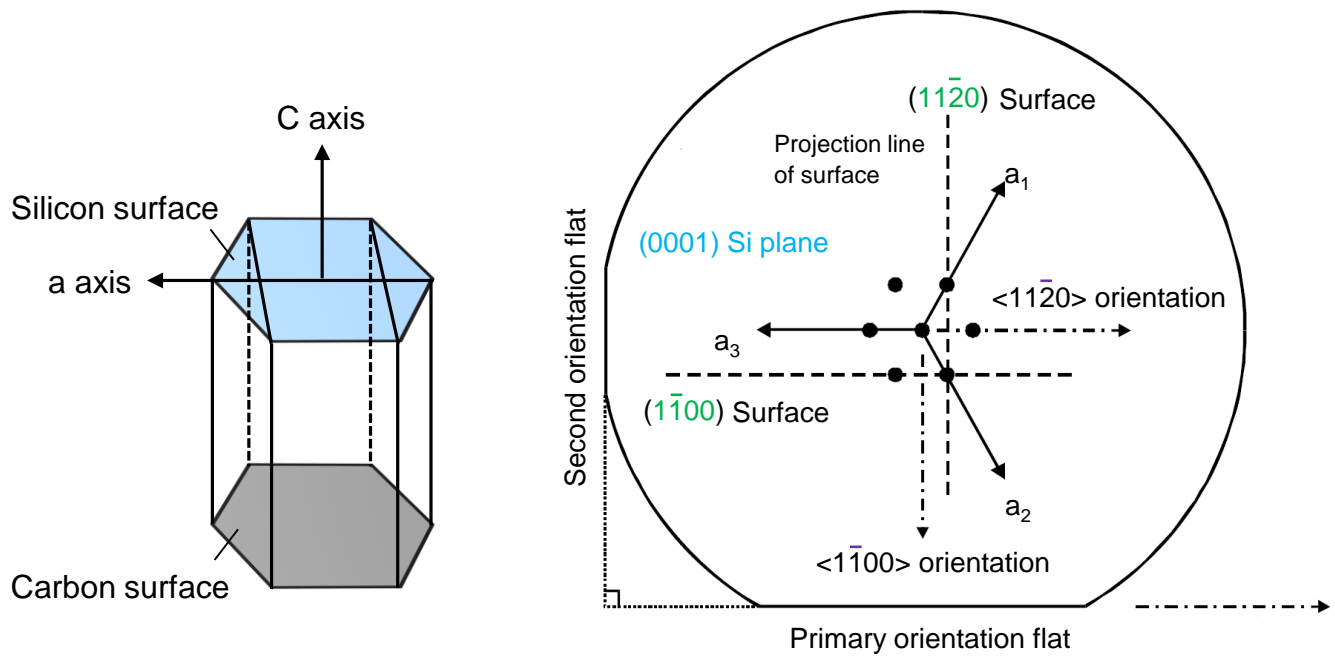
**Fig. 2.25** Crystal orientations and crystal planes of 4H-SiC
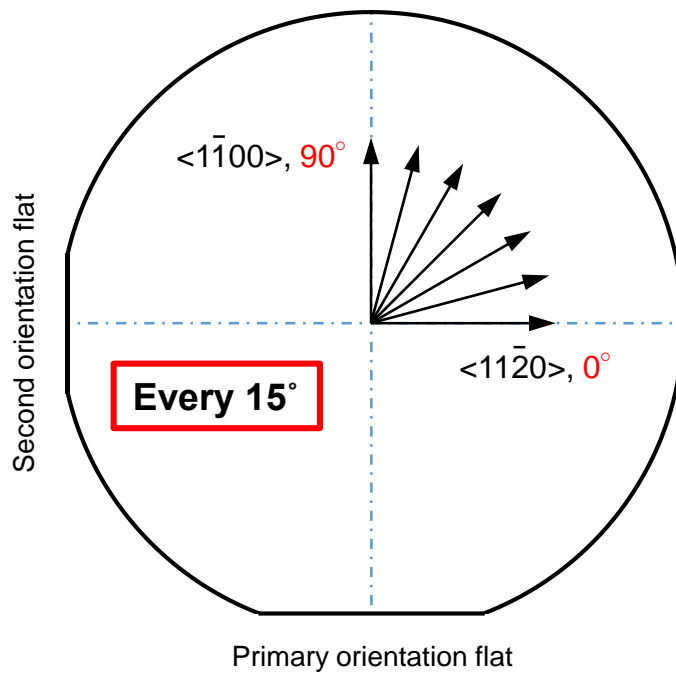
Fig. 2.26 Illustration of cutting directions of wire EDM of SiC

66

Table 2.7 Machining conditions

| Workpiece	SiC ingot
Workpiece thickness [mm]	18
Wire electrode	Brass wire, $\Phi 200\mu m$
Discharge duration [μs]	Around 0.6
Discharge current [A]	65
Cutting length [mm]	10
Wire tension [N]	8
Wire running speed [m/min]	8
Dielectric liquid	Deionized water
Specific resistance of dielectric [$\Omega \cdot cm$]	106000
Flushing method	Submerging + flushing
Nozzle position to the workpiece	Close
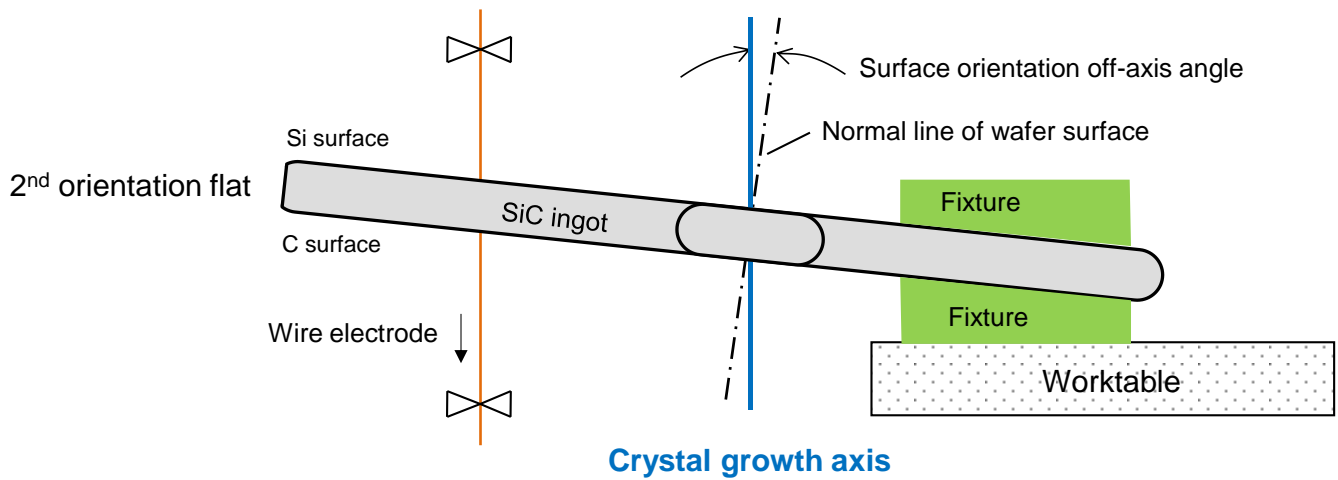
(a) Schematic diagram of the experimental setup
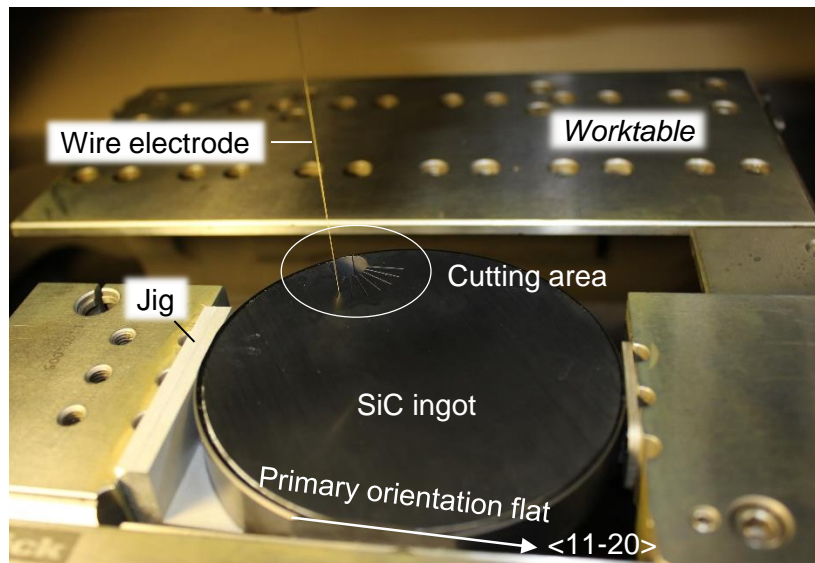
(b) Image of the experimental setup

Fig. 2.27 Experimental setup for wire EDM cutting of SiC along different crystal orientations

2.4.1.2　Experimental results

Fig. 2.28 shows the machining time variation with the change of cutting directions. No significant difference of the machining time (deviation of machining time: within 10s) was found, which probably

indicated that the influence of the anisotropy of crystal orientation in the c surface ($\perp c$ axis) on the machining rate was negligible in EDM of SiC.
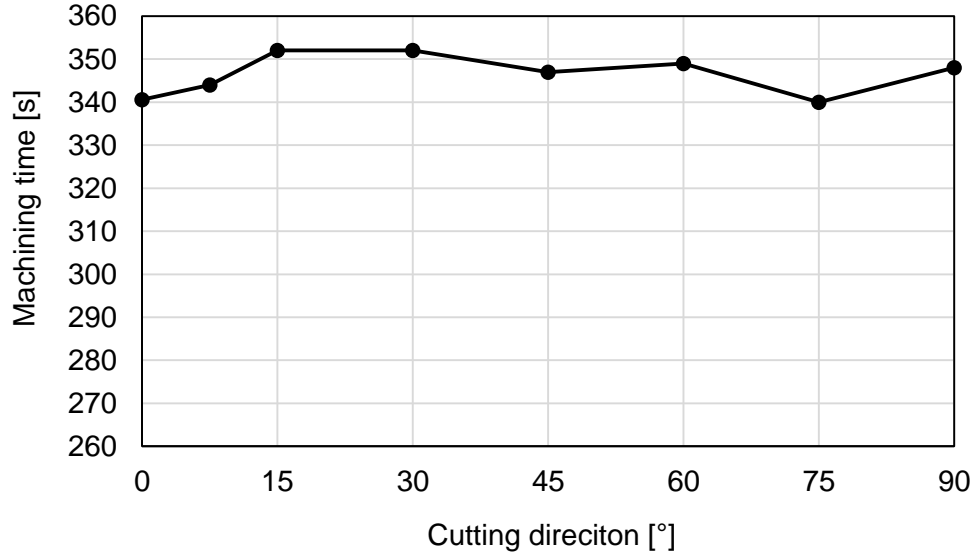

**Fig. 2.28** Wire EDM cutting speed variation with varying the cutting direction.

On the other hand, however, it was found that the wire EDM cutting speed of SiC showed a difference between the cutting direction of (a) perpendicular to the c axis and (b) parallel to the c axis as illustrated in **Fig. 2.29**. The experiment result is shown in **Fig. 2.30**. Wire EDM of SiC with cutting direction parallel to the c axis presented a slightly higher area cutting speed compared with the cutting direction perpendicular to the c axis under the same machining conditions. Here, the area cutting speed, as expressed in the following, refers to the cut surface area of the workpiece per unit time.

$$\text{Area cutting speed} = \frac{\text{Machined area of workpiece}}{\text{Machining time}}$$

Moreover, the EDM'd surface topography of SiC along these two directions also showed a large difference as shown in **Fig. 2.31**. The EDM'd surface of SiC had much less fracture pits when the cutting direction was perpendicular to the c axis (see **Fig. 2.31**(a)), which was considered as an advantage in the practical application of wire EDM slicing of SiC ingot. However, the surface roughness shown in **Fig. 2.31** presents no obvious difference. Both of the machined surface had large fracture pits resulting in a large surface roughness. The large fracture pits were probably caused by discharge concentrations during machining. Nevertheless, it can be seen that the wire EDM'd surface with cutting direction parallel to the c axis is slightly rougher compared with that of the cutting direction perpendicular to the c axis due to more fracture pits.
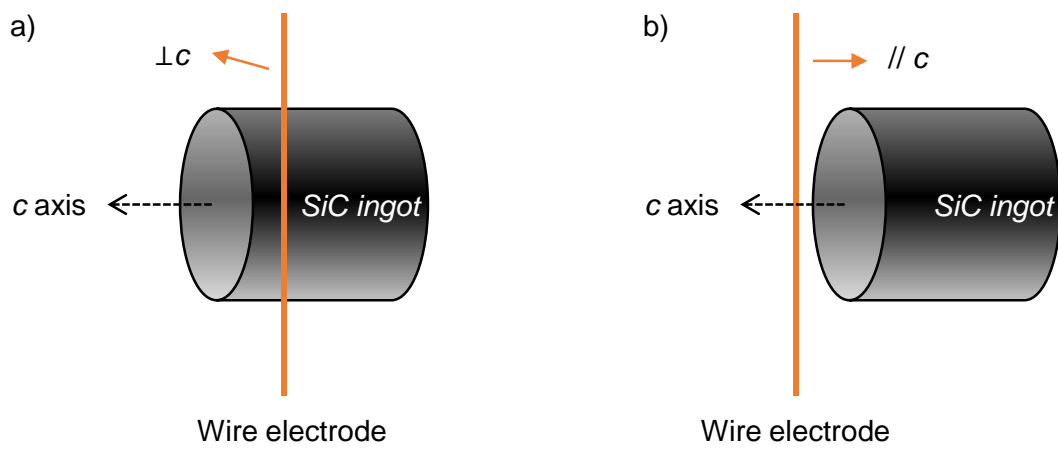
Fig. 2.29 Illustration of wire EDM directions of SiC: a) perpendicular to *c* axis; b) parallel to *c* axis
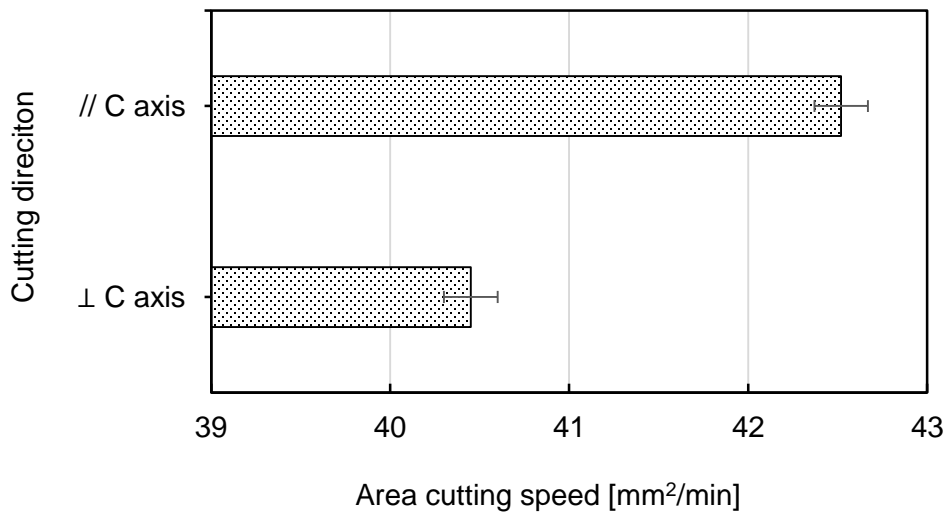
Fig. 2.30 Variation of machining rate along different cutting directions
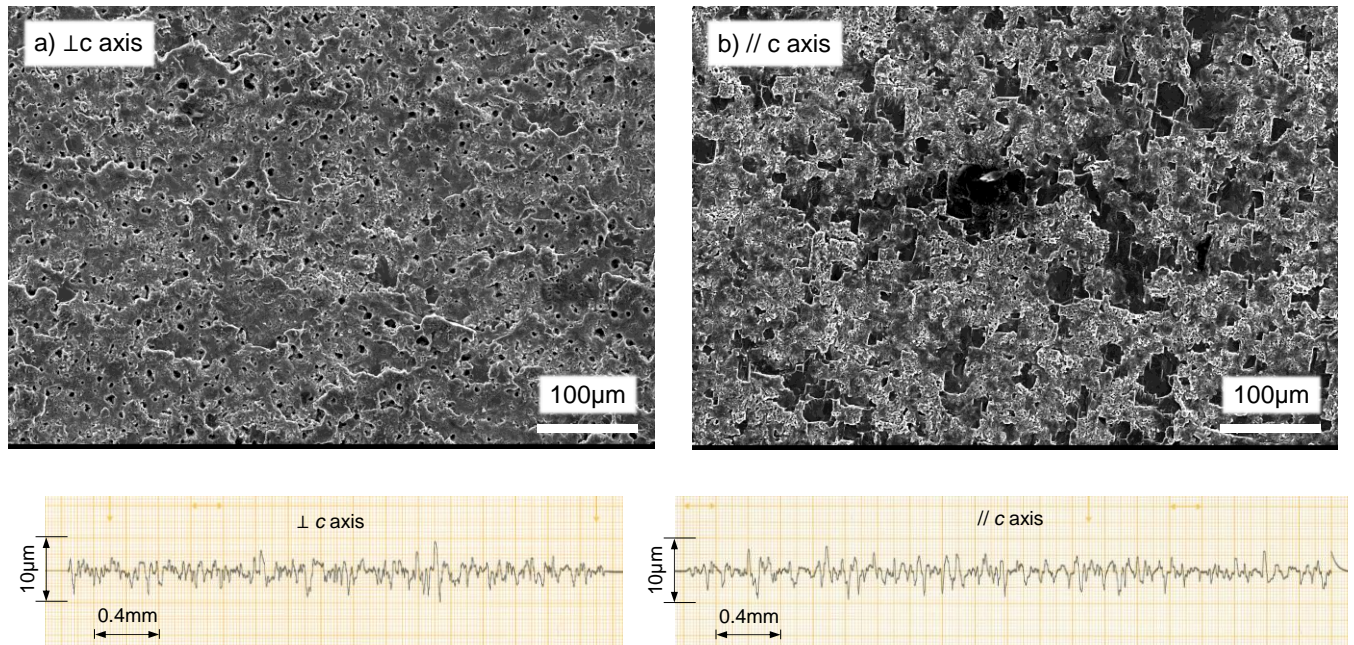
Fig. 2.31 Micro topography and surface roughness profile of wire EDM'd surface of SiC

a) Cutting direction perpendicular to *c* axis; b) Cutting direction parallel to *c* axis

With regard to the reason for the differences, on one hand, it is probably caused by the thermal anisotropy properties of SiC single crystal. Wutimakun et al. [51] has reported that the thermal diffusivities of the <1-100> and <11-20> orientations ($\perp$ *c* axis) were higher than those of the <0001> orientation (// *c* axis). Therefore, it is considered that the heat conduction process will be slower in the direction parallel to the *c* axis, which will cause a high probability of the occurrence of crack and fracture.

On the other hand, it is considered that when the cutting direction is parallel to the crystal axis, the crack failure was easier to occur. **Fig. 2.32** shows an SEM image of the wire EDM'd surface in deionized water under discharge current i_e =85A and discharge duration t_e =1µs. Micro pores around 1µm diameter and micro pits were observed on the machined surface. Furthermore, large rectangular pits with fractured walls existed on the surface aligning with each other along crystal orientations.
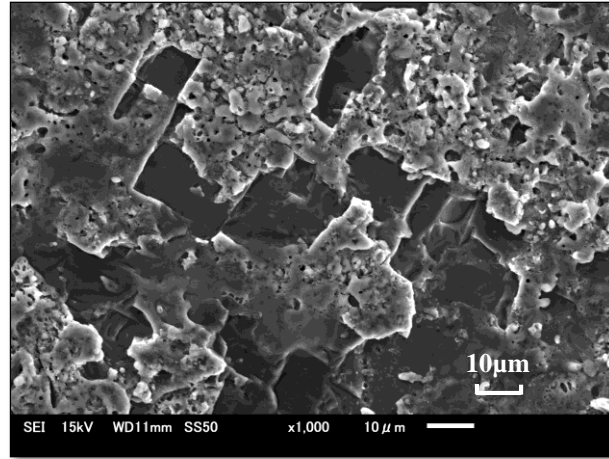
Fig. 2.32 Surface morphology of fracture of SiC by EDM (i_e =85A, t_e =1μs)

2.4.2 Balance of slicing speed and surface roughness

This section describes the wire EDM slicing speed and achievable surface roughness considering the practical use.

It has been reported that wire EDM cutting of SiC ingot can achieve a higher cutting speed and smaller surface roughness than that by conventional diamond wire saw method [26]. However, no detailed investigation has been done to show the influences of the discharge parameters on the cutting performance of SiC and the optimal machining conditions etc. Hence, in this research, the wire EDM cutting performances of SiC are investigated by experiments. The machining experiments were done on a commercialized wire EDM machine (*Sodick AP200L*). In the experiments, the discharge current was changed and all the other machining conditions were kept the same as shown in **Table 2.8**. The workpiece polarity was set as plus in order to increase the cutting speed based on the energy distribution principle in EDM that more discharge energy is distributed into anode [46, 47, 48], which is a general principle in wire EDM.

Fig. 2.33 shows the experimental results of area cutting speed and the corresponding surface roughness of SiC. It can be found out that with increasing the discharge current, the area cutting speed of SiC by wire EDM increases owing to the increased discharge energy per single discharge. On the other hand, however, with the increased discharge energy, the surface roughness deteriorates too. When the discharge current is set as 10A, small surface roughness of around 5μm can be achieved with the area cutting speed of 5mm^2/min.

Base on the experimental results, it is considered that in practical EDM slicing of SiC ingot, the area cutting speed and the surface roughness must be balanced. For example, too large discharge energy cannot be applied for slicing SiC wafer if a good surface roughness is required.

Table 2.8 Machining conditions of wire EDM of SiC

Workpiece polarity	(+)
Workpiece thickness [mm]	15
Cut length [mm]	15
Cut direction	$\perp c$ axis
Wire electrode	Brass, $\phi200\mu m$
Pulse duration [µs]	$\fallingdotseq 1$
Pulse interval [µs]	25
Servo voltage [V]	40
Wire speed [m/min]	8
Wire tension [N]	8
Dielectric liquid	Deionized water
Flushing method	Submerging + flushing
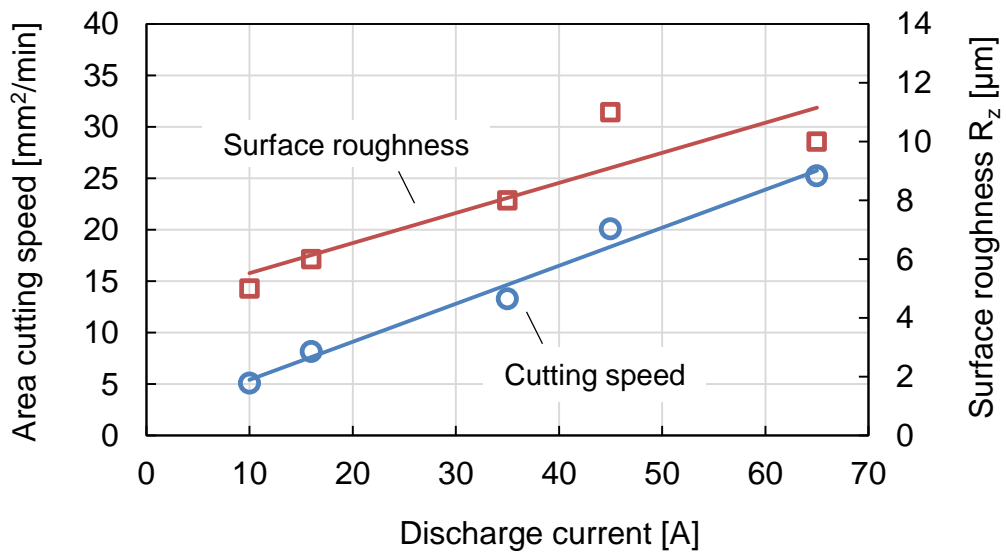
Fig. 2.33 Influences of discharge current on the area cutting speed and surface roughness of SiC

2.4.3　EDM'd surface topography and subsurface damaged layer of SiC

The wire EDM'd surface topography of SiC under two different discharge currents was observed by SEM respectively as shown in **Fig. 2.34**. As can be seen, the EDM'd surface of SiC presented a porous morphology with many holes on it. In addition, with increasing the discharge current, the average diameter of the hole became larger. This is probably resulted from the decomposition of SiC in machining. On the other hand, since SiC has no melting point, no clear discharge crater can be found on the surface of SiC which is a significant difference from the EDM'd surface of conventional metals. Furthermore, a few fracture pits can be found on EDM'd surface of SiC (marked by the yellow circle in **Fig. 2.34**), which is considered to be caused by the thermal fracture of SiC resulted from local discharge concentrations. In addition, it is found that the size and quantity of the fracture pits tend to increase with increasing the discharge current, which may contribute to the reduced mechanical integrity of the machined surface.

With regard to the elemental composition of the EDM'd surface of SiC, Kato et al. [25] analyzed the EDM'd surface of SiC using X-ray photoelectron spectroscopy (XPS) and found that the EDM'd surface of SiC was composed by mixture of silicon oxide (SiO_2) and graphite (C) due to the decomposition of SiC and oxidation of Si. Ishikawa et al. [28] also reported that the EDM'd 6H-SiC surface is not pure SiC but silicon crystal (Si) and carbon resulted from the decomposition of SiC.

To find out the damaged layer by wire EDM process under the machined surface, the cross section of the machined surface was observed by SEM. **Fig. 2.35** is an illustration of the method of observation. The machined surface was first cut at a certain angle by wire EDM to enlarge the damaged layer thickness with a magnification factor of 4.1. Then the section was polished by a high precision lapping machine (*FACT-200*) which used diamond slurry to eliminate the influenced surface by the wire EDM process. The observation result is shown in **Fig. 2.36**. It can be seen that the wire EDM process caused a clear damaged layer on the workpiece, of which the top is a porous layer with many pores in it. Under the porous layer there are many cracks which are probably caused by the thermal stress generated by the EDM process. Due to the discharge energy, the discharge surface usually has a higher temperature compared with that of the material inside the workpiece. Thus, the high compressive thermal stress near the surface is released due to yielding and removing of the material during discharge. After the discharge, when the high temperature discharge surface is rapidly cooled by the dielectric liquid, contraction of the discharge surface will occur. However, the material inside the workpiece has no contraction due to its low temperature. Therefore, tension stress will be generated inside the workpiece because only the discharge surface is contracted, which probably causes the generation of cracks. Taking into consideration the magnification factor, the damaged layer thickness was found to be approximately around 7μm. With decreasing the discharge energy, the damaged layer thickness also decreased. In conclusion, it was considered that the subsurface damaged layer depth by wire EDM was around 1~10μm depending on the machining conditions. Furthermore, the single discharge crater of EDM of SiC was observed, as shown in **Fig. 2.37**. The single discharge experiment was conducted in EDM oil. From **Fig. 2.37**, it can be confirmed that multiple cracks aligning along the crystal orientations of SiC are resulted from the single discharge due to the thermal shock.

On the other hand, however, except for the cracks, it was reported that EDM induced little crystal disorder [28]. This is probably because that SiC is removed by decomposition but not by melting.
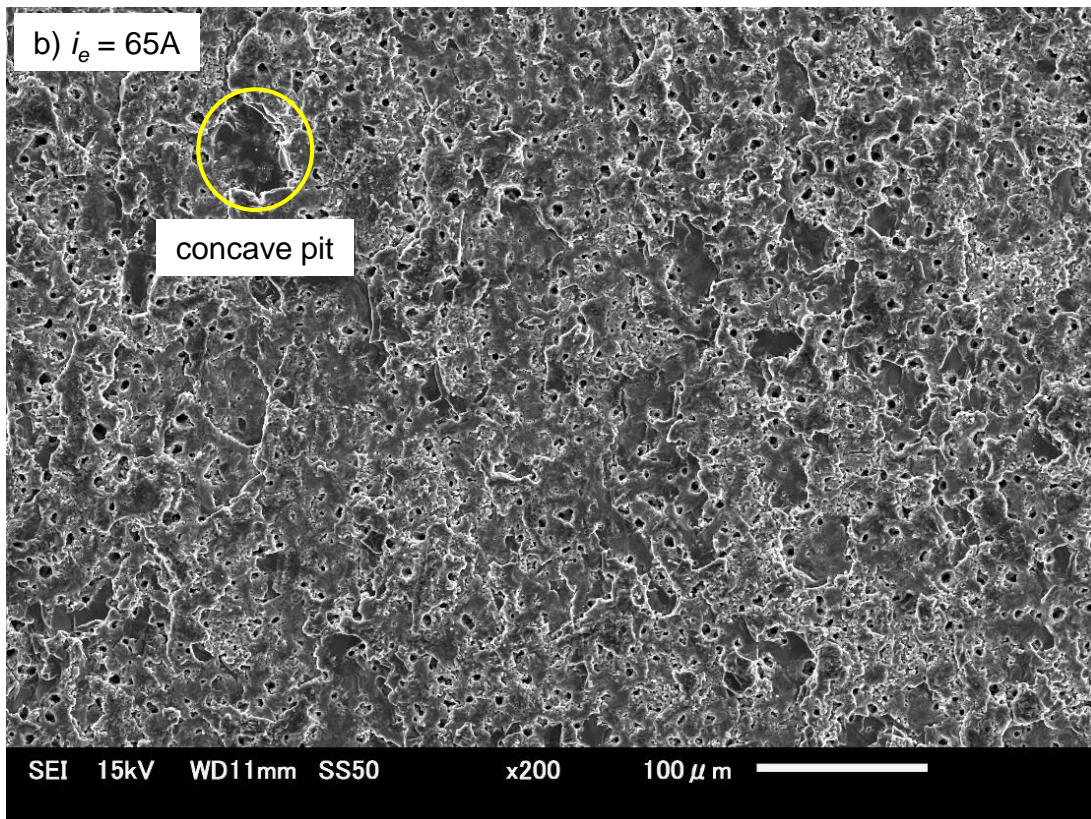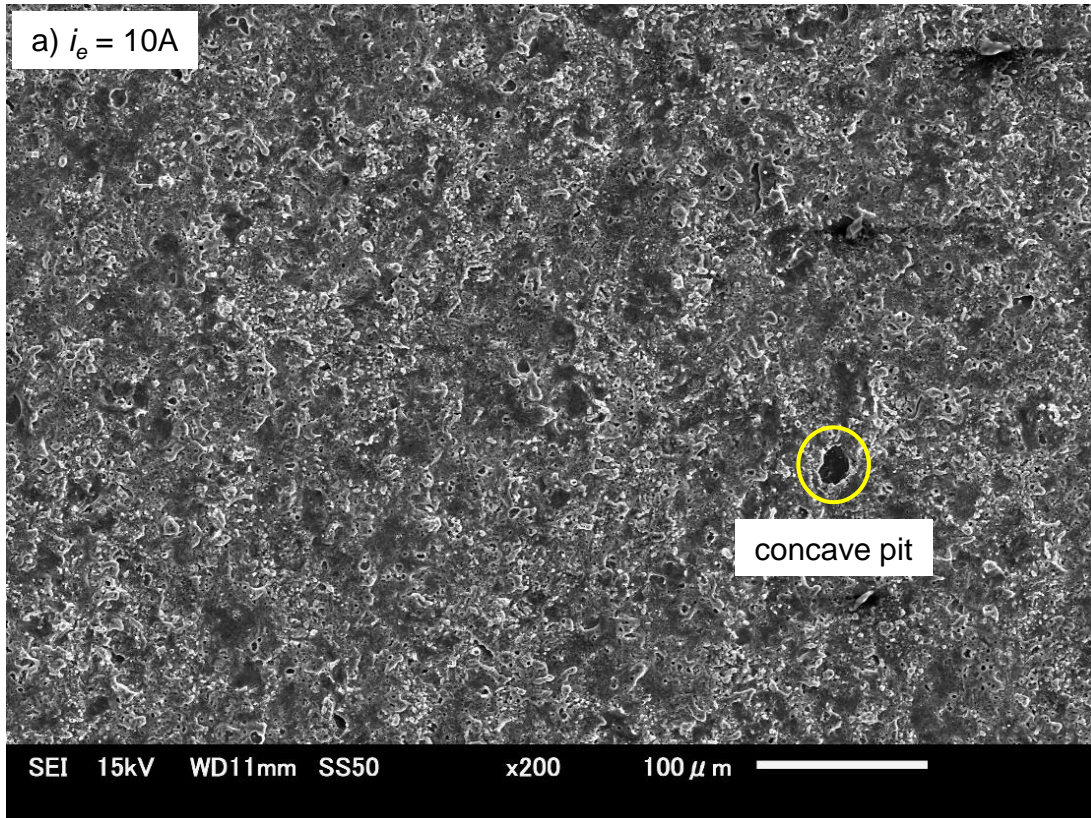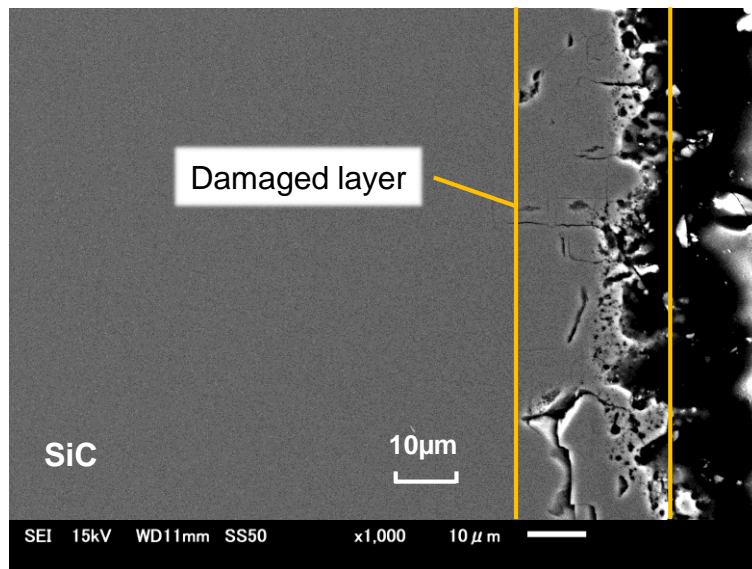
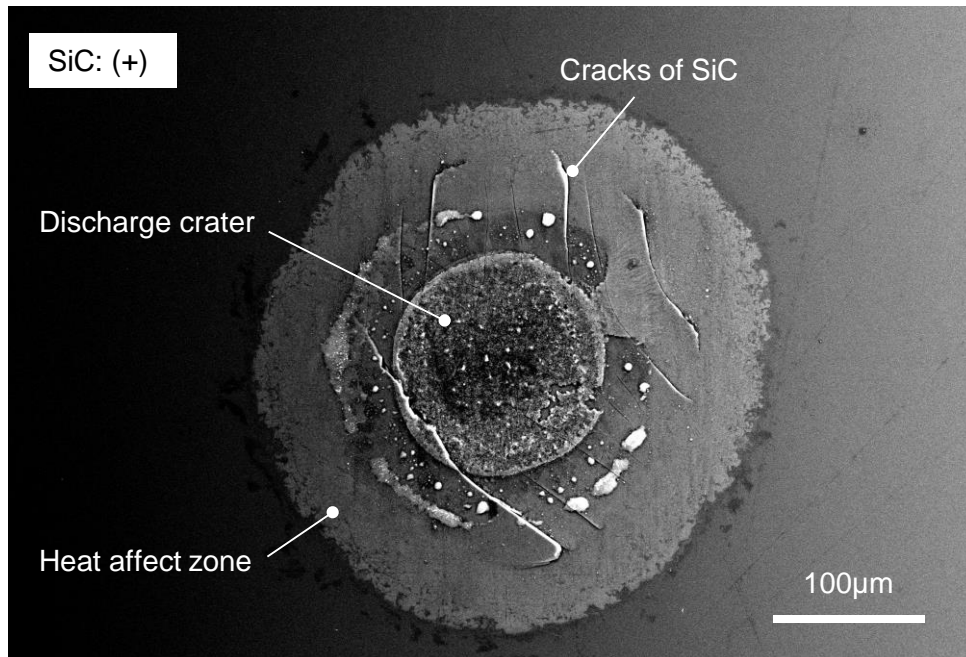**Fig. 2.34** Surface topography of wire EDM'd surface of SiC single crystal: (0001) crystal surface
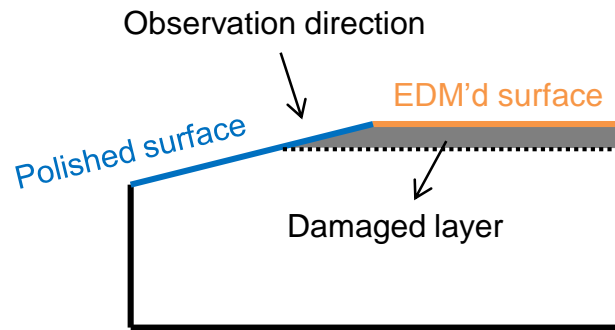
Magnification factor of damage layer: 4.1

Fig. 2.35 Illustration of the method for observing EDM damaged layer of SiC

Fig. 2.36 SEM observation of cross section of wire EDM'd surface of SiC

(Machining conditions: $i_e = 85$A, $t_e = 1\mu$s)

Fig. 2.37 Discharge crater of SiC by single discharge in EDM oil (i_e=20A, t_e=100μs)

2.4.4 Wire breakage problem of wire EDM of SiC

Wire breakage is a common problem in wire EDM. Usually when large discharge energy and low wire running speed is applied, there will be a higher risk of wire breakage due to larger heat flux per unit length of wire. Moreover, discharge concentration will cause wire breakage even the discharge energy is small. In order to clarify the probability of wire breakage in wire EDM slicing of SiC, comparison experiments between wire EDM of SiC and SKD11 were conducted with varying the parameter of discharge current. The preset machining conditions were the same as shown in **Table 2.9**. For each condition, the cutting experiment was repeated for 5 times.

The experiment results showed that, when the duty factor was set at 30%, EDM of steel was possible and stable without any wire breakage. In the case of SiC, however, although the actual discharge current was much smaller, the machining was not possible. Wire breakage occurred every time within 20 seconds after the machining started in all 5 trials, even if the discharge current was reduced to 50A. In other words, under the same setting conditions, the wire breakage rate of wire EDM of SiC was 100% while the wire breakage rate in wire EDM of SKD11 was zero.

The reason for this is considered to be the Joule heating effect in EDM of SiC. Due to the high resistivity of SiC, the Joule heating effect is considered serious at the discharge spot, which would cause a higher temperature rise in the vicinity of discharge spot compared to that of steel. In consequence, the plasma extinction will become difficult which results in discharge concentrations due to the high temperature. The discharge concentration will cause localized temperature rise on the wire electrode surface and induce

the breakage of wire [2, 41]. Therefore, it is concluded that the pulse interval in EDM of SiC must be set long enough for the complete extinction of arc plasma to achieve a stable machining process.

On the other hand, however, under the same servo voltage, due to the high voltage drop inside SiC, the gap voltage measured by the servo control system in the case of SiC is larger compared to that of steel. Therefore, the servo feed speed will be high in the case of SiC compared to steel due to the larger gap voltage, which will cause a smaller gap width. The smaller gap width is probably another reason for the easy occurrence of wire breakage in EDM of SiC since smaller gap width will result in a higher probability of discharge concentration.

Table 2.9 Experimental conditions of wire EDM of SiC and SKD11 for comparison

Workpiece	Workpiece thickness [mm]	Duty factor	Measured discharge current [A]	
			Experiment No.1	Experiment No.2
SKD11	22.5	30%	125	80
SiC	22.5	30%	100	50

In conclusion, in wire EDM of SiC, the servo voltage should be set larger and the discharge interval should be set longer to improve the machining efficiency and prevent the wire breakage. Currently, in practical application of wire EDM slicing of SiC, the wire diameter used is no larger than 100µm in order to prevent wire breakage. It is therefore considered that the risk of the wire breakage and the wire vibration has undermined the full potential of wire EDM process drastically by reducing the machining efficiency and accuracy. In addition, small kerf width cutting cannot be performed due to the risk of wire breakage of using thin wire electrode.

2.5 Conclusions of Chapter 2

The chapter mainly described the fundamental characteristics of EDM of SiC. The differences of EDM characteristics between SiC and widely-used metal material were investigated by experiments. In addition, the material removal mechanisms of EDM of SiC was clarified. Heat conduction analysis taking into account Joule heating effect was conducted to investigate the influence of Joule heat on the EDM characteristics of SiC. Furthermore, the influence of crystal anisotropy on the EDM properties of SiC was investigated. At last, aiming to apply EDM for slicing SiC in practical use, the EDM slicing performances of SiC by conventional wire EDM were evaluated. The main conclusions were as the following:

(1)   Under the same preset machining conditions, EDM of SiC showed a higher discharge voltage and lower discharge current compared with those of steel due to its higher resistivity. Therefore, theoretically, EDM of SiC was supposed to show a lower machining rate due to the lower discharge energy compared to that of steel. In addition, under the same servo voltage, EDM of SiC should have a higher discharge frequency due to its higher discharge gap voltage. However, experimental results showed that EDM of SiC had a much higher material removal rate and a larger surface roughness compared to that of steel.

(2)   The EDM debris of SiC included multi-angular particles, which indicated that the material removal mechanism of EDM of SiC included not only decomposition and evaporation but also cracking and fracturing. This was considered as one reason for the higher machining efficiency of SiC compared to that of steel.

(3)   Heat conduction analysis of single discharge of SiC showed that Joule heating effect considerably contributed to increase the surface temperature (near discharge spot) which could facilitate the material removal of SiC. On the other hand, however, due to the high thermal conductivity of SiC and the expansion of plasma diameter after the discharge ignition, the surface temperature dropped quickly with increasing the discharge time after the discharge ignition. It was therefore considered that long pulse duration would cause a low machining efficiency compared with that of short pulse duration under the same duty factor.

(4)   Influences of anisotropy of SiC on the EDM rate of SiC was investigated. No significant dependency of the machining rate on the crystal orientation was found when the machining was conducted in the surface perpendicular to the c axis. However, it was found that slightly higher machining speed could be obtained when the machining direction was parallel to the c axis compared with that perpendicular to the c axis. Moreover, fracture pits occurred more on the machined surface when the cutting direction was parallel with the c axis of SiC.

(5)   Wire EDM cutting of SiC could achieve an area cutting speed of 5mm^2/min with a machined surface roughness of 4µm (R_z). The area cutting speed increased with increasing the discharge current, while the surface roughness deteriorated. The EDM'd surface of SiC presented a porous morphology with many holes on it. Fracture pits were generated on the machined surface of SiC probably caused by thermal shock resulted from discharges and/or discharge concentration. A damage layer with many cracks in it was found beneath the machined surface (thickness around 1-10 µm).

(6)   Wire breakage was a significant problem in wire EDM cutting of SiC, especially when large duty factor was applied due to discharge concentration. To avoid the wire breakage, small discharge current, small duty factor and high servo voltage were considered necessary, which, however, would influence the machining efficiency. In the case of multi-wire EDS method, since the load of machining time per unit length of wire is increased, it is considered that the wire breakage problem will become more serious.

Chapter 3   EDM cutting of SiC ingot by foil tool electrode

3.1   Introduction

This section describes the fundamental properties of EDM cutting of SiC utilizing foil electrodes.

As discussed in previous chapters, wire breakage is a significant problem limiting further improvement of wire EDM cutting performance. Especially, prevention of the breakage of the wire electrode during machining is considered as the most important task in the development of the multi-wire EDS method considering the machining efficiency. Because the wire breakage problem will become more serious in multi-wire EDS method with increasing the number of winding turns of wire electrode in the future (refer to **Fig. 1.15**) since discharge frequency on unit length of wire electrode will increase significantly. On the other hand, however, in the multi-wire EDS method, realization of automatic wire connection is considered of great difficulties which probably further decreases the machining efficiency.

Except for the wire breakage, it is considered that in the newly developed multi-wire EDS method, there will be several other problems of using wire electrode. Here, the problems or disadvantages of using wire electrode which should be solved and advanced in the future are discussed as the following:

1) Increase of wire tension force

Wire tension has a considerable influence on the wire vibration which will influence both the cutting time and the cutting accuracy [32]. Usually, larger wire vibration amplitude results in larger kerf width and in consequence longer machining time. The wire vibration can be reduced by increasing the wire tension force. Okamoto et al. [30] has reported that with wire electrode of track-shaped section, a uniform and straight kerf shape can be accomplished by increasing the tension force. Therefore, on the premise of no wire breakage, tension force of the wire electrode should be set as high as possible. However, thin wire electrode cannot sustain very large tension force which limits the improvement of wire vibration.

2) Improvement of wire running stability

It has been found out that higher running speed of wire electrode in multi-wire EDS could result in higher machining rate and smaller kerf width due to the improvement of flushing condition under high running wire speed [29, 30]. However, higher wire running speed will brings about larger wire vibration. In order to solve the problem, Okamoto et al. [30] employed a track-shaped wire electrode with thickness of 100μm (see **Fig. 1.18**) to increase the tension force and reduce the wire vibration. However, the gap distance between wire and workpiece in one side was still larger (35-40μm) compared to that of normal round shape wire EDM (10-15μm) and the kerf width was between 150-200μm in the experiments.

Therefore, as described above, higher tension force is considered of high necessity in order to reduce the vibration of wire electrode under high wire running speed.

3) Reduction of wire diameter

In order to enhance the advantages of EDS, especially to reduce the kerf loss and improve the productivity of wafer per ingot, it is considered that the wire diameter should be reduced furthermore in the future while capable of taking a large tension fore.

Therefore, in this research foil electrodes are proposed to substitute wire electrodes to cut SiC ingots aiming to further reduce the electrode dimension (determining the kerf loss) and increase the tension force (determining the cutting accuracy and cutting time) to improve the cutting speed and accuracy at the same time.

3.2   EDM characteristics by foil tool electrode

### 3.2.1   Introduction of foil tool electrode

Foil electrode is introduced in replace of wire in EDM slicing of SiC wafer due to its advantages over wire electrode in several aspects as listed in **Table 3.1**. For easy understand, **Fig. 3.1** shows an illustration of comparison between foil electrode and wire electrode. In the first place, smaller kerf loss can be achieved by utilizing foil electrode of which the thickness can be reduced to as small as several tens μm as shown in **Fig. 3.1**. Second, the tension force of foil can be much larger by increasing the foil width compared with that of wire electrode due to increased cross section area. Therefore, the foil vibration during foil running can also be reduced under the larger tension force. On the flip side, with the same cross section area, foil with smaller thickness can be obtained. Third, the resistance of wire electrode can be decreased considerably by using foil electrode taking advantage of the increased cross section area of foil, which make it possible to apply larger discharge current to the discharge circuit to improve the material removal rate. At last, it is considered that wire breakage problem can be prevented in the case of foil electrode by increasing the foil width.

On the other hand, however, there are downsides of utilizing foil electrode. At first, the larger side surface area of foil, as illustrated in **Fig. 3.1**, will cause a higher probability of secondary side-surface discharges in EDM (also referred to as discharge surface area effect), which will result in a larger kerf loss. Second, larger side surface area probably makes the flushing difficult and may cause a worse gap condition during machining. In addition, with regard to the tool wear, decrease in the foil thickness will cause a larger tool wear ratio. These problems and the optimization of the foil width and thickness will be discussed furthermore in detail in Chapter 4.

With regard to the foil electrode material, there are several options, such as copper foil, brass foil, tungsten foil, stainless foil, etc. However, considering from the aspects of cost and foil tool wear, copper foil was selected as the electrode material to investigate the foil EDM method in this research.

Table 3.1 Advantages of foil electrode compared with wire electrode

	Foil electrode	Wire electrode
Dimension	Thickness: 10μm~	Diameter: 100μm~
Tension force	◎	×
Resistance	Small	Large
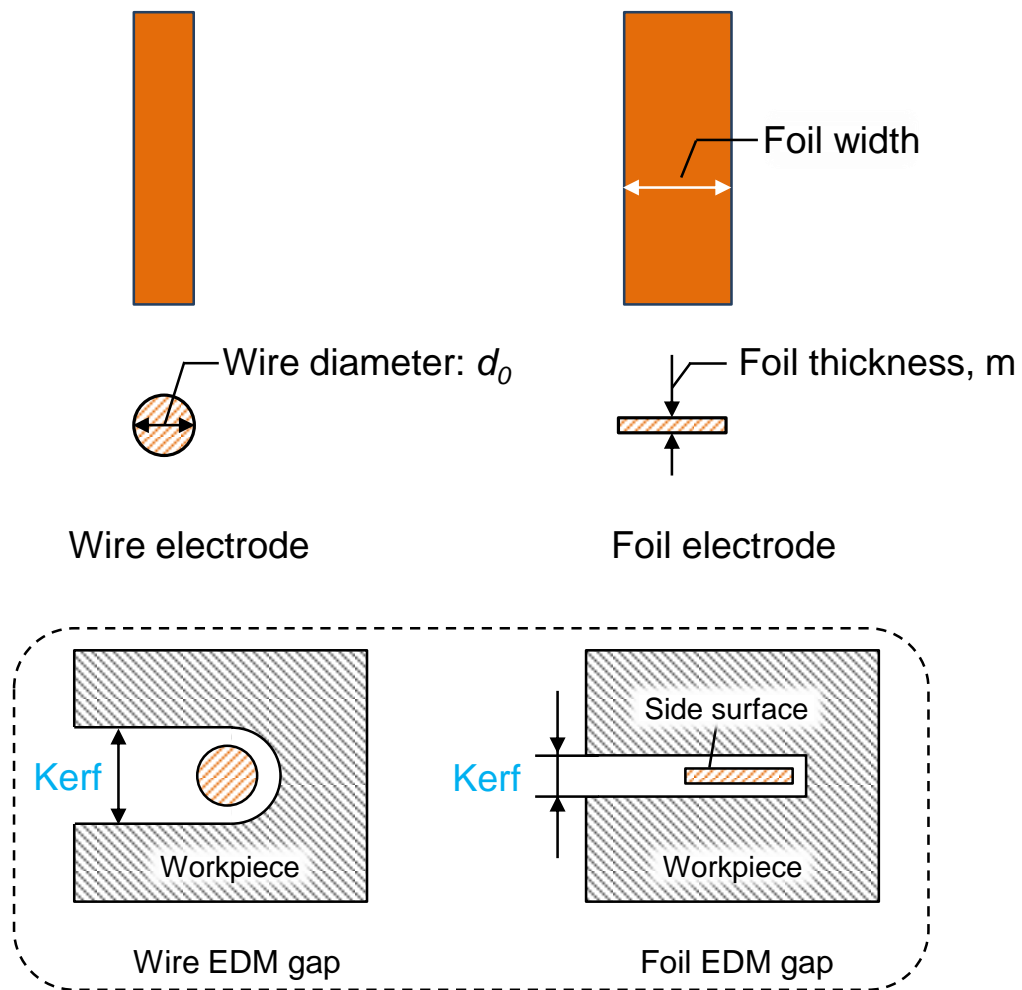
Fig. 3.1 Comparison of dimension and gap condition difference between wire and foil electrode

3.2.2 Experimental method of foil EDM

Fig. 3.2 shows the schematic diagram of the experimental setup used for investigating the EDM characteristics of SiC by foil electrode. A thin rectangular foil electrode cut by wire EDM was used as the tool electrode and it was fixed by a precise vice to maintain the flatness. In order to reduce the vibration of the thin foil electrode during feeding, the length of the foil electrode was kept less than 5mm and a slit with depth of around 2.5mm was machined in dielectric oil. The machining experiments were done on a standard sinking EDM machine (*Sodick C32*). Cutting was conducted by servo feeding the foil tool to the workpiece like the normal die-sinking EDM process. Besides, jump motion was applied to facilitate the removal of EDM debris in the gap for a stable machining process.

Discharge current and foil thickness were chosen as the parameters to investigate the foil EDM performances, including the foil tool wear, cutting speed and achievable kerf width. The main machining conditions are shown in **Table 3.2**. Short discharge duration was selected in the experiments to obtain a stable machining process. Since the standard dielectric of the existing sinking EDM machine (*Sodick C32*) is EDM oil, the experiments were firstly conducted in oil. The foil EDM cutting experiments in deionized water based on a developed external deionized water circulating system will be described later.

### 3.2.3 Machining properties of foil EDM

3.2.3.1 Rectification effect of EDM of SiC

In EDM of SiC, the connection between electrical feeders of EDM machine and workpiece (single crystal SiC) forms a metal-semiconductor contact. Generally metal-semiconductor contact presents a rectifying effect instead of common Ohmic contact characteristics in electrical circuit due to the existence of Schottky barrier at the metal-semiconductor interface [52, 53].

In machining experiments of EDM of single crystal SiC, it was found that the discharge current was slightly higher when single crystal SiC workpiece was set as negative. However, the rectification effect of SiC was found not significant probably due to its relatively high conductivity.

#### 3.2.3.2 Area cutting speed and Kerf loss

The influence of tool polarity on EDM rate of SiC is shown in **Fig. 3.3**. The tool polarity effect was obvious, providing a higher material removal rate when the workpiece was set as positive due to larger discharge energy distribution into the anode in every single discharge [46, 47]. The material removal rate increased almost linearly with increasing the discharge current.
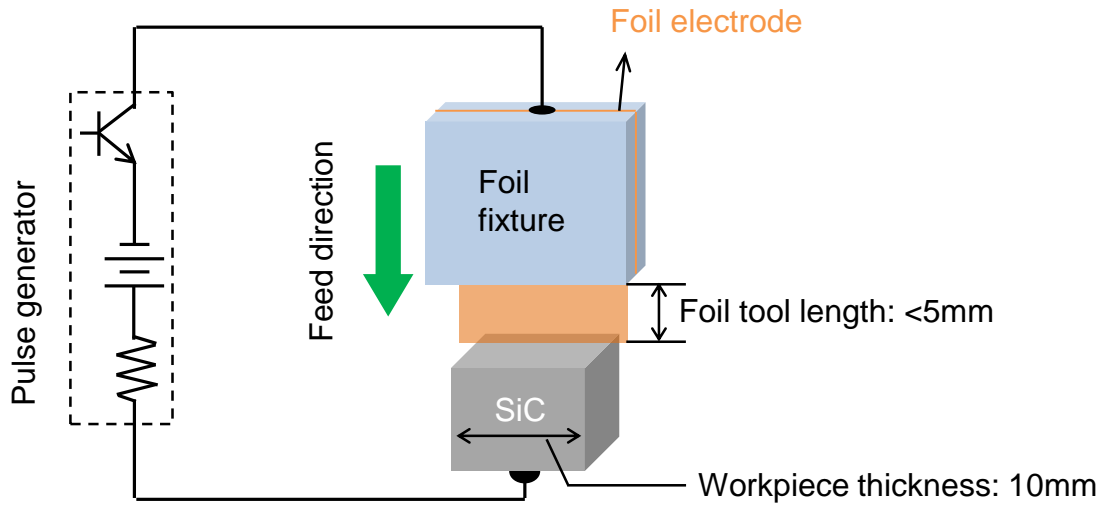
**Fig. 3.2** Schematic diagram of experimental setup for foil EDM cutting

Table 3.2 Machining conditions used in foil EDM cutting experiments

|	
Workpiece	SiC single crystal
Workpiece thickness [mm]	10
Electrode	Copper foil
Tool polarity	[+], [-]
Open voltage [V]	120
Servo voltage [V]	90
Preset discharge current [A]	8, 16, 24, 31.5
Discharge duration [µs]	3
Duty factor	9.1%
Dielectric liquid	EDM oil
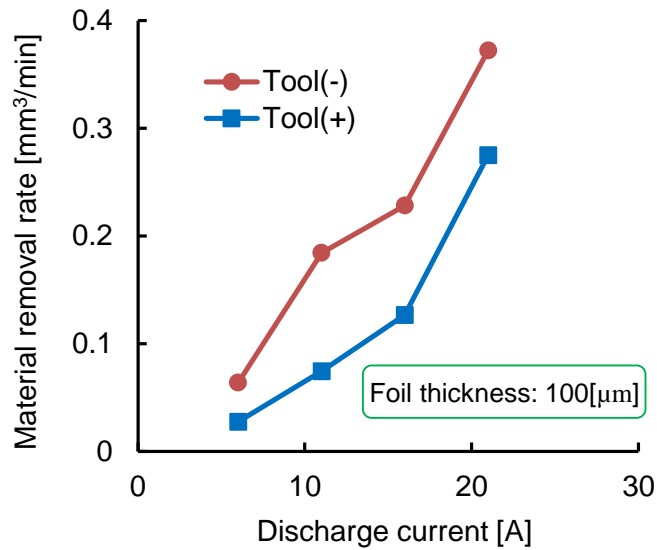
Fig. 3.3 Material removal rate increases with increasing discharge current; Negative tool polarity leads to higher material removal rate.

In application of slicing SiC ingot, average area cutting speed, of which the definition is the same as that in wire EDM (Refer to Chapter 2, Section 2.4.1.2), is considered as the important factor determining the wafer slicing time. Therefore, in the experiments, the average area cutting speed with different foil tool electrodes thicknesses was investigated. The preset discharge current was 12A, while the measured discharge current was 9A. **Fig. 3.4** shows the experiment results. It was found that thinner foil tool electrode could achieve a higher area cutting speed due to smaller kerf width. The cutting speed increased when foil thickness was decreased due to a smaller kerf width, which was an advantage for slicing SiC ingots using thinner foil electrodes. Tool polarity effect featuring higher machining speed with negative polarity was confirmed. However, since jump motion was applied in the cutting experiments, machining efficiency was not high here, presenting a area cutting speed lower than $1mm^2$/min.
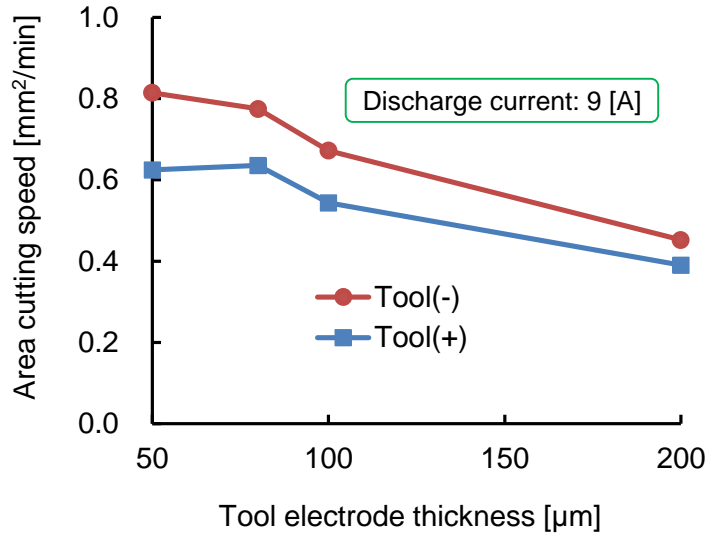
Fig. 3.4 Area cutting speed increases with decreasing foil thickness and utilizing negative polarity
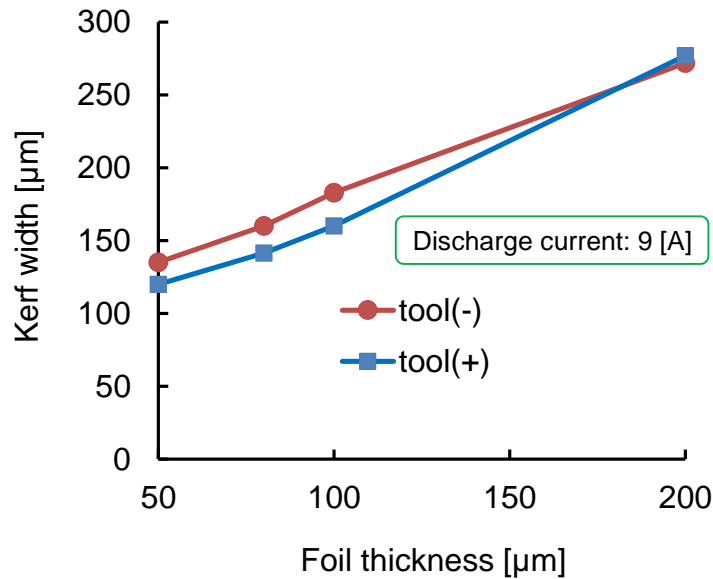
Fig. 3.5 Kerf width decreases with decreasing foil thickness; negative polarity results in larger kerf width.

The inlet width of machined kerf by different thickness foil electrodes under different polarities is shown in **Fig. 3.5**. When the tool polarity was set as negative, the cut kerf width was slightly larger than that under positive polarity due to the higher material removal volume per single discharge. However, the difference was not large since the gap width of foil EDM was mainly decided by the open voltage. By using the thinnest foil electrode with thickness of 50μm, a minimum kerf width of about 130μm was

obtained. Hence the one-side discharge gap width was about 40µm. Due to the area effect, it was considered that the secondary discharge phenomenon between the side surface of foil tool electrode and workpiece was more significant compared to that of wire electrode. In addition, the vibration of foil tool electrode during machining probably also exerted influence on the cut kerf width. It was therefore considered that insulating the tool electrode side surface and flushing away the EDM debris effectively from the discharge gap would help to decrease the kerf width and improve the machining performance.
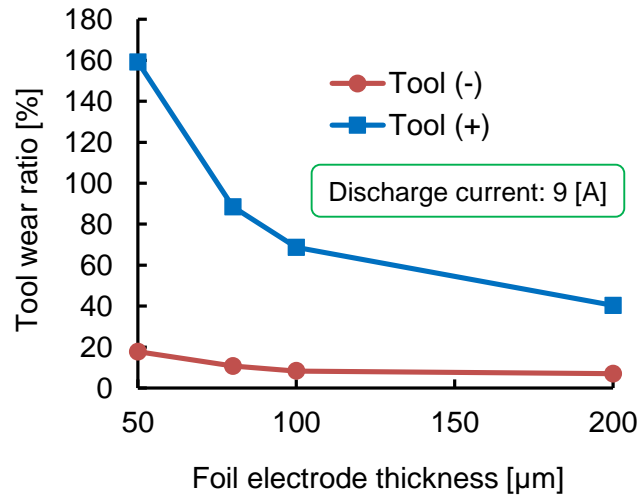
3.2.3.3   Tool wear ratio

On the other hand, however, using thinner foil electrode would cause a higher tool wear ratio, as shown in **Fig. 3.6**. Here, the tool wear ratio was defined as the following:

$$\text{Tool wear ratio} = \frac{\text{Volume of tool electrode wear}}{\text{Volume of workpiece material removal}}$$

The volume of the tool electrode wear was obtained by multiplying the foil tool wear length by the foil thickness. The foil tool wear in the thickness direction was not considered in this chapter. It was confirmed that the tool wear ratio was significantly lower when the tool was set as cathode compared to anode due to smaller discharge energy distribution into the cathode [46, 47]. Moreover, it was found that the tool wear ratio increased rapidly when the foil electrode thickness was decreased. One of the reasons was considered that smaller working area of the thinner foil tool would suffer from more frequent discharge per unit area, resulting in higher surface temperature due to higher average heat flux.

Except for higher average heat flux, foil thickness would also influence the temperature distribution of foil of single discharge. To clarify this, heat conduction analysis of single discharge in foil tool electrode was conducted. **Fig. 3.7** shows the analysis model. Heat flux by single discharge was applied to the top surface center of the cube shape foil electrode. With regard to the heat flux diameter, Eq. 2.7 was used. By the same analysis method described in Chapter 2, heat conduction equation was solved. The foil tool material used in the analysis was copper and the discharge current and duration were 30A and 2µs respectively. Latent heat was also taken into consideration in the analysis.

Fig. 3.8 shows the analyzed results of temperature distribution at time $t = 2$µs on the cross section marked in yellow color in **Fig. 3.7** which passes through the center of the heat source. By comparing these two figures, it can be found that the high temperature area of the foil electrode working surface is much larger when foil thickness is 40µm compared to that of 100µm, which in consequence results in a higher tool wear ratio. Besides, the temperature at the heat source center has reached to the boiling point of copper, which would result in a large tool wear.

**Fig. 3.6** Tool wear ratio increases with decreasing foil thickness and utilizing positive tool polarity

3.2.3.4 Tool wear ratio difference between foil EDM of SiC and steel

To compare the EDM characteristics of SiC and steel material in terms of tool wear, comparison experiments between EDM of SiC and SKD11 using foil electrodes were conducted. The thickness of the foil tool was 100μm and the polarity was set as negative. All the other machining conditions were set the same as shown in **Table 3.2**.

Fig. 3.9 shows the tool wear ratio difference in machining the two different materials. The plots connected by the dashed lines were under exactly the same preset machining conditions as shown in **Table 3.2**. The actual discharge current of cold tool steel SKD11 was larger than that of SiC because of its lower electrical resistivity. However the tool wear ratio of EDM of steel was much higher than that of SiC. The reason was considered as the following. In the first place, the energy efficiency of material removal was higher in the case of EDM of SiC because the material could be removed not only by decomposition and evaporation but also cracking and fracturing. On the other hand, in EDM, the temperature of plasma is independent of electrode materials. Therefore, for the workpiece with higher thermal conductivity, more discharge energy can be conducted into the workpiece which would improve the machining efficiency and consequently reduce the tool wear ratio [47, 48]. From **Fig. 3.9** it can also be seen that the tool wear ratio of foil EDM of SiC in the experiments was lower than 20% under different discharge current.

Fig.3.7 Heat conduction analysis model of single discharge
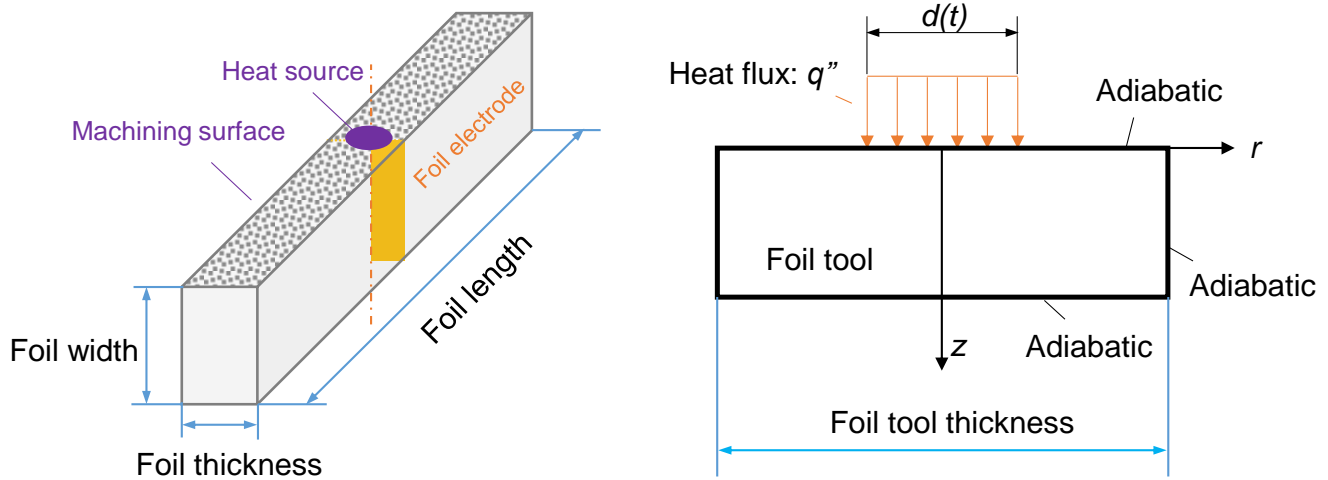
(a) Foil thickness: 100 [μm]

(b) Foil thickness: 40[μm]
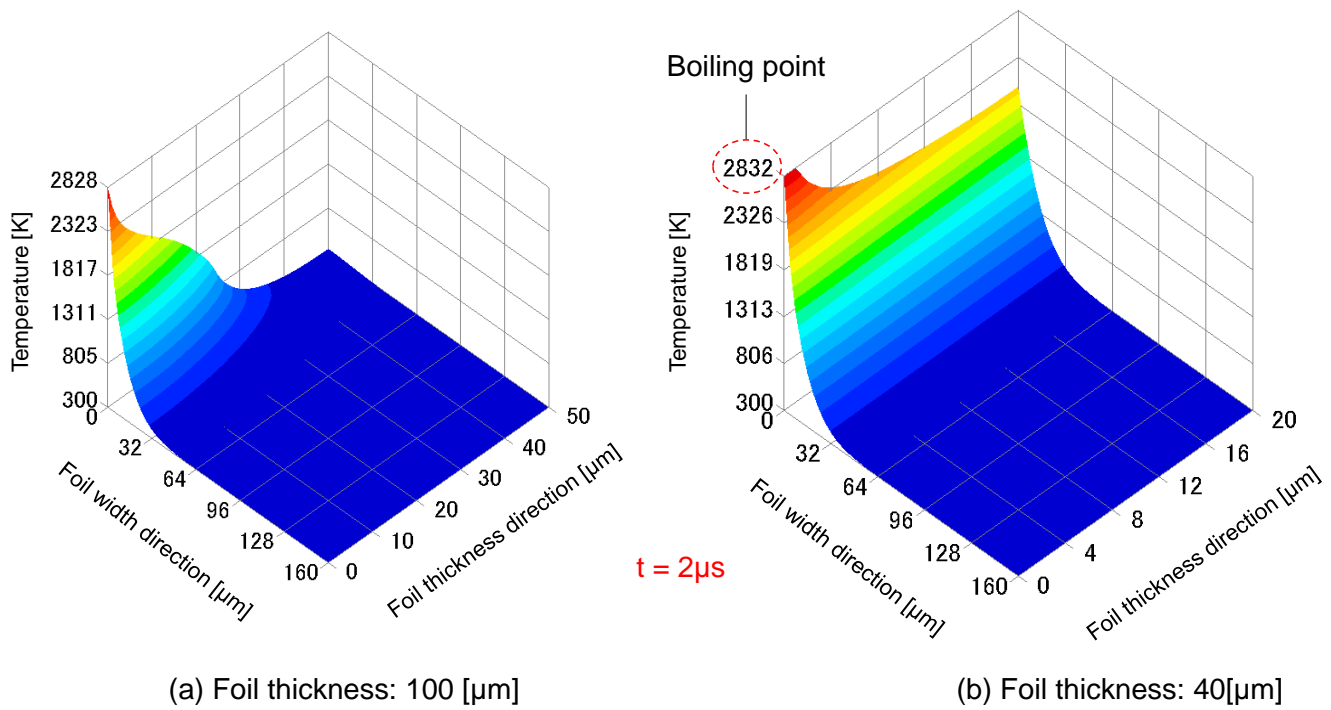
**Fig.3.8** Simulated temperature distribution in foil electrodes with different foil thickness at time t=2μs.
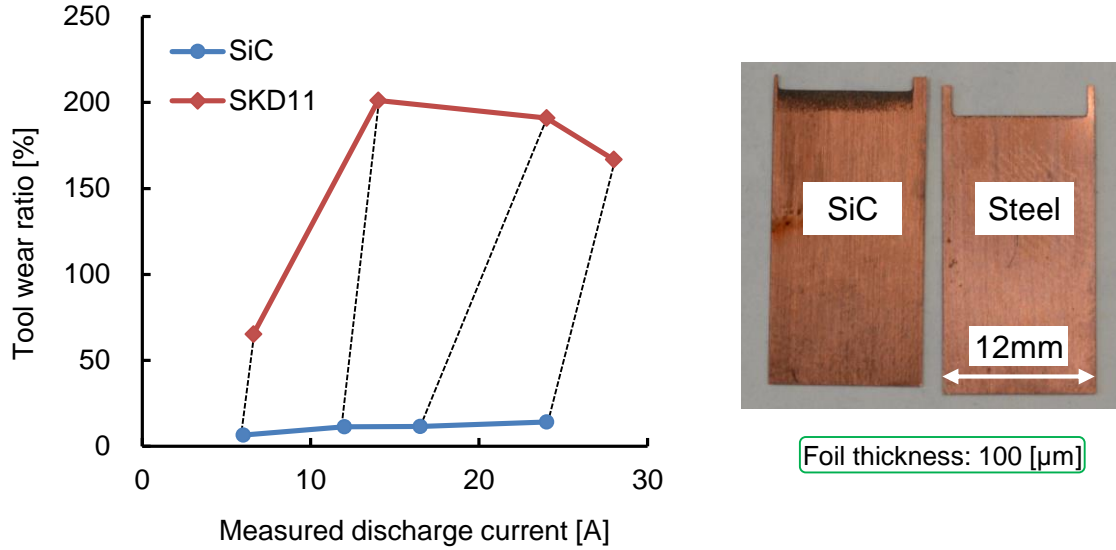
Fig. 3.9 Tool wear ratio difference between foil EDM cutting of SiC and SKD11

## 3.3   Improvement of cutting performance by utilizing tension loaded foil electrode

3.3.1   Design of foil tool electrode fixture

In order to eliminate the vibration of the foil and improve the positioning accuracy of the foil electrode, a foil tensioning fixture, as shown in **Fig. 3.10**, was developed which could not only position the foil electrode but also apply tension to the foil. **Fig. 3.11** shows the schematic diagram of the experimental setup of foil EDM cutting. The foil tool electrode was loaded in tension by the developed foil tensioning fixture to maintain the flatness of the foil electrode and avoid its vibration. The tool fixture was installed on the Z-axis of sinking EDM machine and the cutting was conducted by servo feeding the tool to the workpiece. CCD laser displacement sensor (*Keyence, LK-G10*) was used to detect the parallelism error between the foil plane and the feeding axis in the cutting direction before machining, which was found to be smaller than 10µm.

The influences of tool material, pulse duration, pulse interval, cut depth on the machining characteristics based on the improved experimental setup were investigated. Aiming to reduce the kerf width, foil electrode with thickness of 50µm was used. In addition, jump motion was applied in order to achieve a stable machining process. All the other experimental conditions, as shown in **Table 3.3**, were selected based on the experimental results obtained in the previous section. Most importantly, foil tool electrode polarity was set as negative to improve the cutting speed.

91
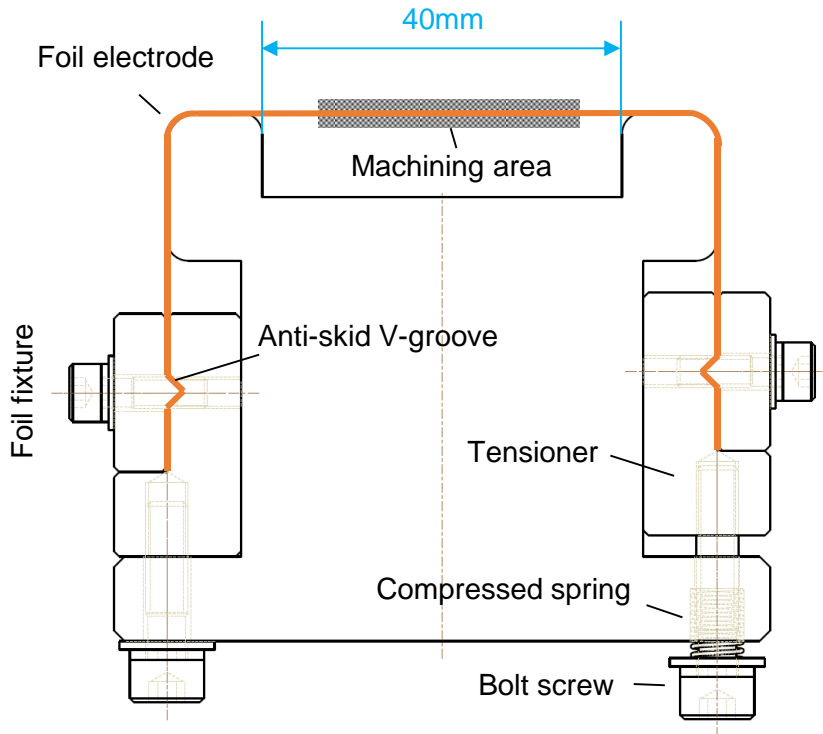
Fig. 3.10 Mechanism of tensioning of foil fixture
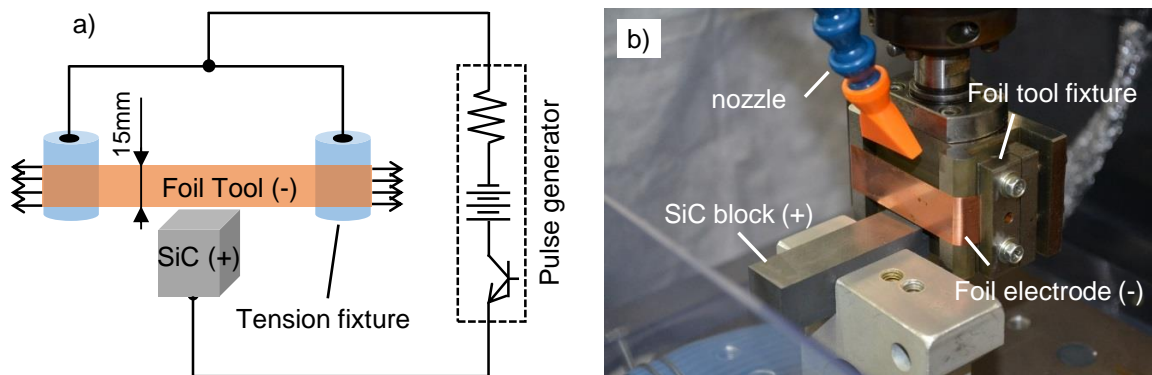
Fig. 3.11 Experimental setup of foil EDM cutting by tensioned foil tool electrode: a) schematic diagram, b) image

Table 3.3 Experimental conditions

Tool electrode	Copper foil; Tungsten foil
Tool polarity	[-]
Foil thickness [μm]	50
Cut depth [mm]	5
Workpiece thickness [mm]	20
Open voltage [V]	120
Discharge duration [μs]	2
Duty factor	20%
Tool jump speed [m/min]	6
Jump-up time [s]	0.2
Jump-down time [s]	0.4
Dielectric liquid	EDM oil

3.3.2   Experimental results

3.3.2.1   Influence of foil electrode material

Foil material is critical to the foil tool wear ratio and maximum tension force. Especially, the thermal properties of foil material are considered of great importance from the perspective of achieving low tool wear ratio. **Table 3.4** lists four kinds of foil materials that can be employed as foil electrode. Tungsten foil electrode has the highest tensile strength, highest melting point and highest value of $\lambda\theta^2$ of the four materials, which makes it quite attractive to be used as the foil material in order to reduce the tool wear, although the cost of tungsten foil is high. On the other hand, the copper foil has the highest thermal conductivity, which makes it another choice to be used as foil electrode.

With regard to brass foil which is widely used as the material of wire electrode in wire EDM, although it has a higher tensile strength compared to that of copper, the lower thermal conductivity would cause a high tool wear ratio, especially when thin foil of several μm is used. Stainless steel is usually not used as electrode in EDM because of its low thermal conductivity, therefore, stainless steel foil is not used as foil electrode in this study. The study made a special effort to investigate the difference of machining performances by using copper foil and tungsten foil respectively. Machining conditions shown in **Table 3.3** were used in the experiments.

However, experimental results shown in **Fig. 3.12** (a), (b) and (c) show that tungsten foil electrode resulted in a lower area cutting speed, higher tool length wear ratio and larger kerf loss compared with those of copper electrode. Here, tool length wear ratio is used to evaluate the foil tool electrode wear in EDM slicing, which is defined as the following:

$$\text{Tool length wear ratio} = \frac{\text{Foil tool wear length}}{\text{Actual cut depth of workpiece}}$$

The reason why tool length wear ratio is used in this research is that tool length wear ratio is a more obvious and simple way to characterize the foil tool electrode wear in foil EDM cutting process compared with the foil tool (volume) wear ratio. The tool wear along the foil thickness direction is not considered here.

It was found that after machining tungsten foil was delaminated due to the thermal stress caused by the thermal energy of discharges, which probably resulted in the higher tool length wear ratio. Moreover, by observing the discharge waveforms through oscilloscope during machining, short circuiting was found frequently, which indicated that tungsten was not suitable for machining SiC due to the instability of discharge between tungsten and SiC. Therefore, in this study, copper foil was used as the tool electrode for cutting SiC.

Table 3.4 Comparison of material properties of different foil materials

	Copper foil	Tungsten foil	Brass foil (Cu6Zn4)	Stainless foil (SUS303)
Melting point θ, [K]	1357	3680	1205	1725
Thermal conductivity λ, [W/m·K]	401	174	123	16
$\lambda\theta^2$ [x 10^6]	738.4	2356.4	178.6	47.6
Tensile strength [MPa]	220	1510	500	520
Cost	◎	×	◎	◎

Tool wear length
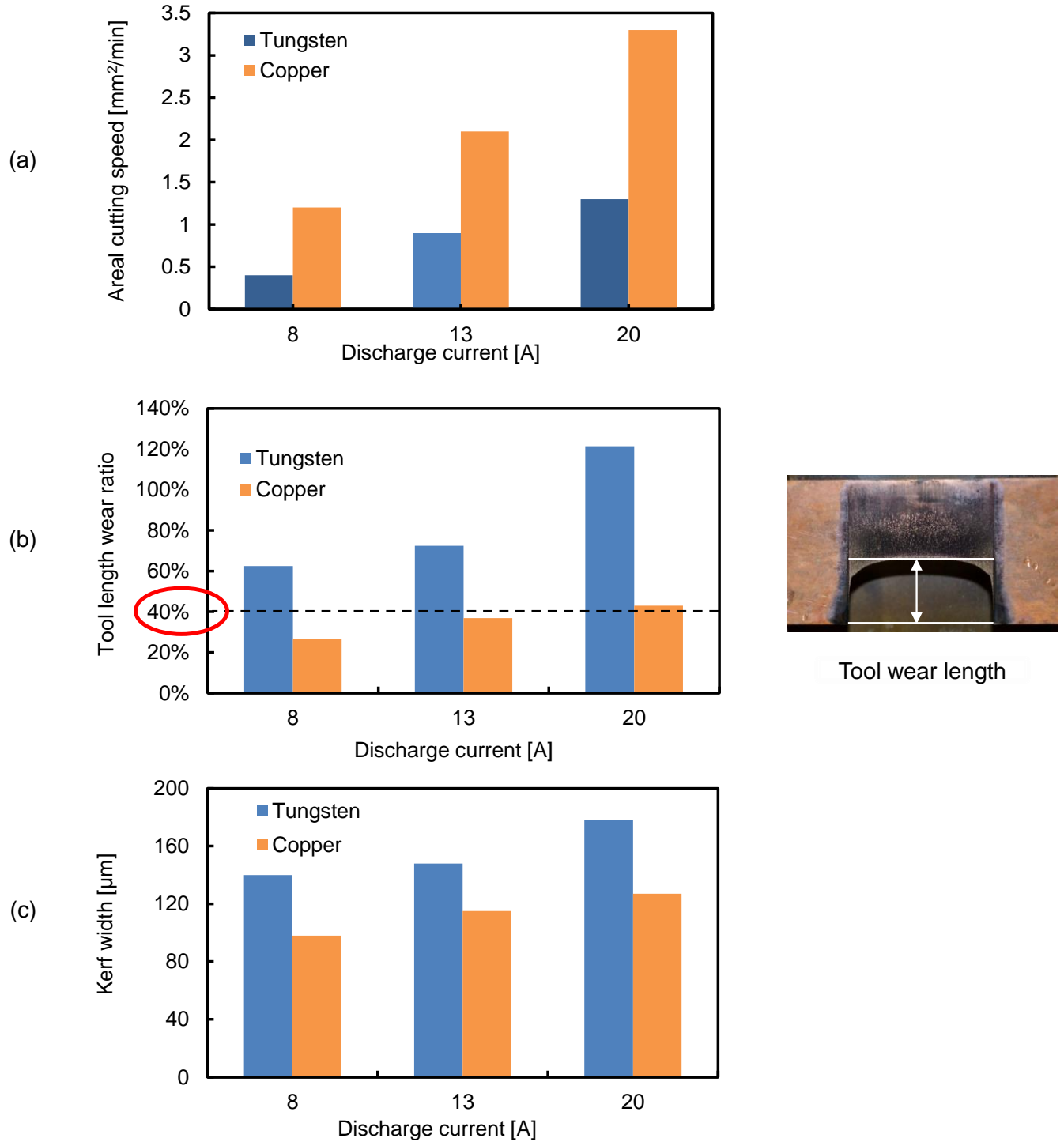
Fig. 3.12 Comparison between foil EDM of SiC by copper foil electrode and tungsten foil electrode: a) cutting speed; b) tool length wear ratio; c) kerf width.

3.3.2.2   Influence of pulse duration

Influences of pulse duration on the cutting performances were investigated under the machining conditions shown in **Table 3.5**. **Fig. 3.13** shows the experimental result which indicates that under the same duty factor, the machining rate decreases and tool wear increases with increasing the discharge duration. The main reasons are considered as the following description. The first reason is considered that since the surface temperature of the workpiece SiC, as shown in **Fig. 2.23**, drops rapidly below the decomposition temperature of SiC after discharge ignition due to its high thermal conductivity and the expansion of plasma diameter, increase of pulse duration would not contribute to remove the material but actually decrease the energy efficiency in machining of SiC. On the other hand, long pulse duration would increase the energy of single discharge and cause a larger material removal compared to that of short pulse duration under the same discharge current, which will increase the probability of crack generation in EDM of SiC. Consequently, generation of larger size debris particles by thermal fracture of which the size may be several tens μm would be severe due to the larger discharge energy. The existence of large size debris particles in the gap would easily cause short circuit or discharge concentration in EDM and result in further deterioration of machining. By repeating machining trials in experiments, it was confirmed that under either plus or minus polarity, long pulse duration resulted in concentrated discharge easily and machining became extremely unstable.

Therefore, in the region of short pulse durations (1~10μs), pulse duration was changed to clarify the influence of pulse duration. In the experiments here, the duty factor was set as 6.5%. **Fig. 3.14**(a), (b) and (c) show the variations of area cutting speed, kerf width and tool length wear ratio with varying discharge current under two different pulse durations. The actual cut depth under different machining conditions was different due to different amounts of tool wear under the same feed distance of Z-axis. For comparison, however, the actual cut depth was kept constant at around 3.5mm by adjusting the feed distance considering the tool electrode wear.

It was confirmed that even if the discharge duration was just increased from 1μs to 6 μs, the tool wear ratio was deteriorated significantly and kerf width became very large indicating a large discharge gap width. Also, cutting speed decreased greatly under long discharge duration. On the other hand, it was also confirmed that larger discharge current led to a higher cutting speed but both the cutting kerf width and tool wear increased because of the increased material removal volume in single discharge.

To under this phenomenon, the EDM debris under different pulse duration were observed in experiments. For the simplicity of collection of the EDM debris, the comparison experiments were conducted in deionized water instead of oil. All the other machining conditions were the same as that shown in **Table 2.4**. However, no big difference was found between the size of the EDM debris under the short pulse duration and the long pulse duration, as shown in **Fig. 3.15**, which shows the observed EDM debris of SiC under pulse duration of 2μs and 10μs respectively. The EDM debris shape of SiC was not spherical but multi-angular with size of several tens micrometers which was probably resulted from thermal fracture of SiC during EDM under both short and long pulse duration.

On the other hand, it has been reported that in EDM of TiB_2 (fine ceramic), with shorter pulse duration t_e, machined surface with less cracks could be obtained due to a short existing time of arc plasma per single discharge. This might be another reason why short pulse duration was better for machining SiC [2]. In

conclusion, it is considered that short pulse duration (shorter than 3µs, the short the better) is more suitable for EDM of SiC considering both the machining stability and the machining accuracy.

**Table 3.5** Experimental conditions used to investigate the influence of pulse duration

Tool electrode	Copper, (-)
Workpiece thickness [mm]	20
Foil thickness [µm]	50
Measured cut depth [mm]	3.5
Discharge current [A]	11
Duty factor	12.5%
Servo voltage [V]	40
Dielectric liquid	EDM oil
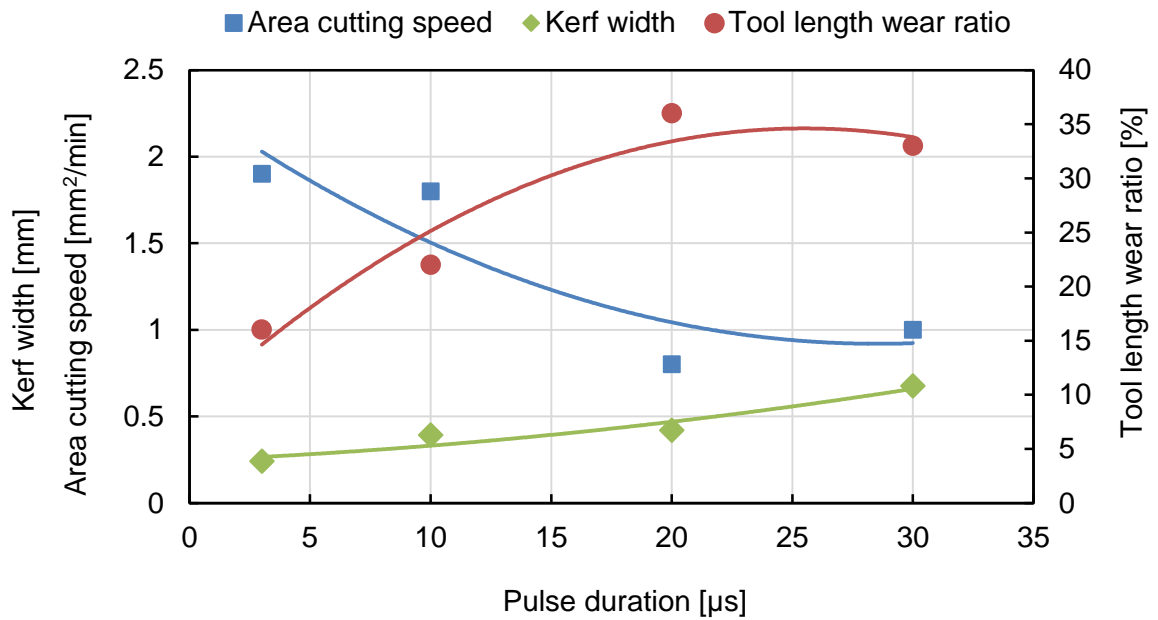
**Fig. 3.13** Pulse duration effect on the cutting performance
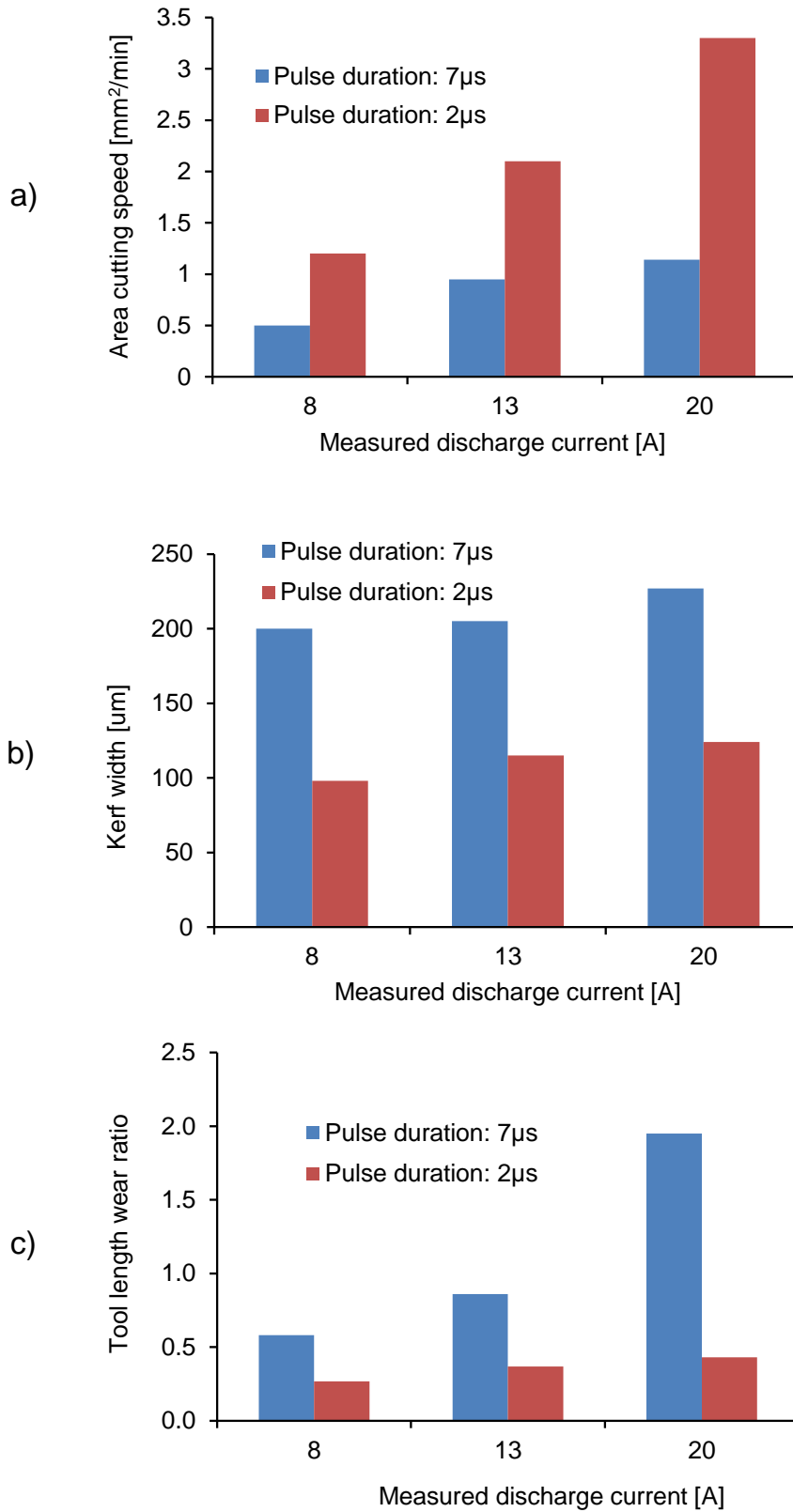
Fig. 3.14 Influence of pulse duration on the cutting performance: a) area cutting speed; b) kerf width; c) tool length wear ratio (Duty factor: 6.5%)
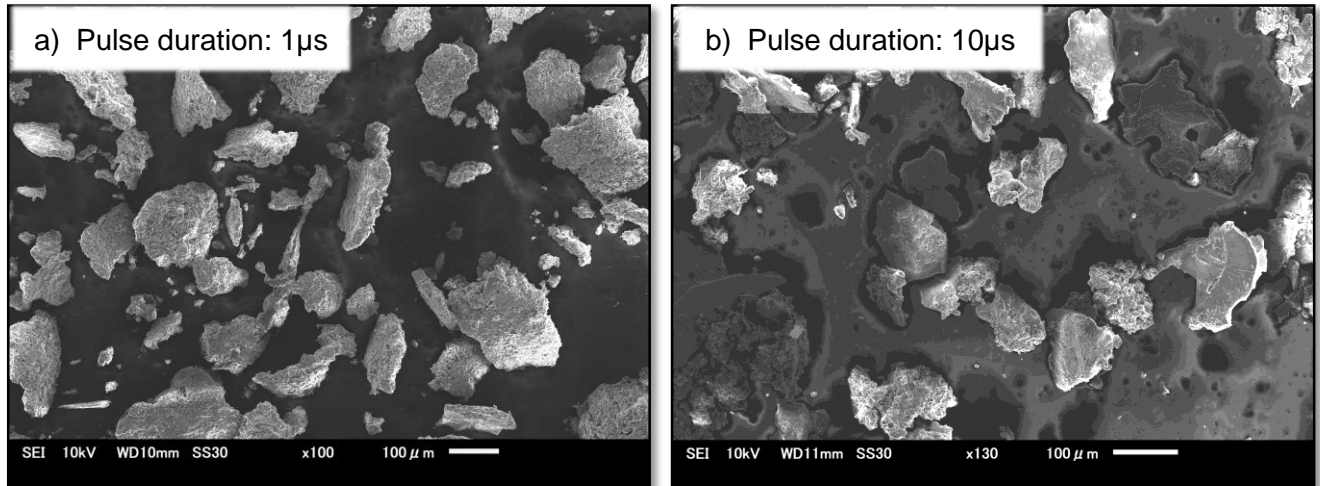
Fig. 3.15 Pulse duration influence on EDM debris of SiC (Discharge current: around 14A)

3.3.2.3 Influence of pulse interval

Considering the Joule heating effect, for a stable machining process, EDM of SiC probably requires a relatively long pulse interval for the plasma to extinguish completely before the next discharge. To find out the optimal pulse interval for EDM of SiC, the influence of pulse interval on the cutting speed and tool wear were investigated. **Fig. 3.16** shows the experiment results of the machining rate and tool length wear ratio variation under different pulse interval in deionized water (which will be described furthermore in the following sections). The optimal pulse interval was found to be around 15µs. However, in the meantime it was found that the tool length wear ratio in deionized water was around 60%.
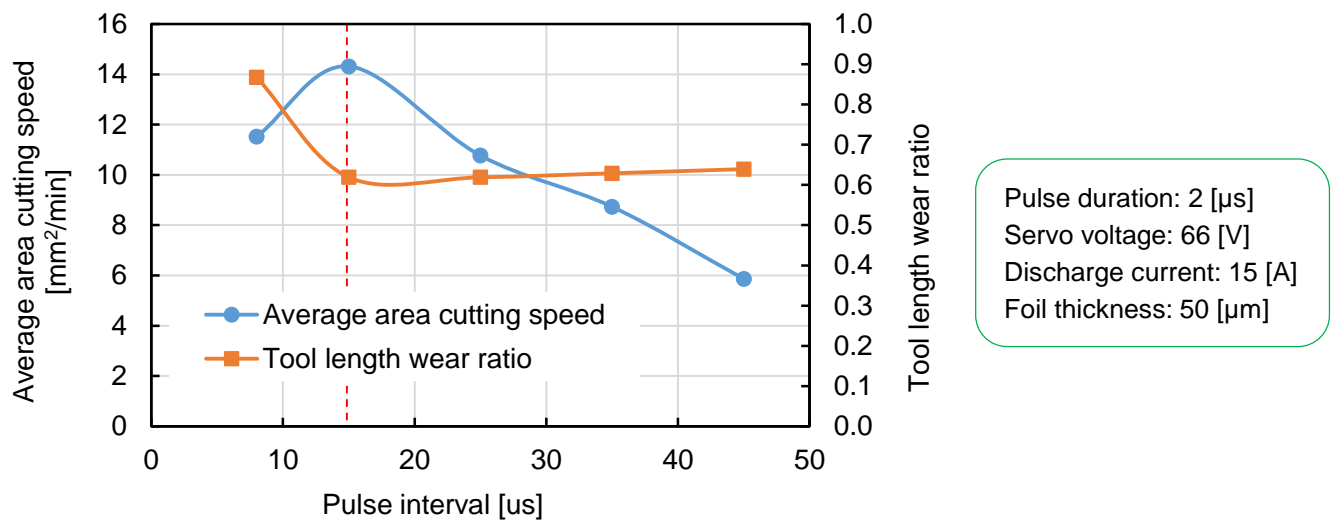
Fig. 3.16 Pulse interval influences on the machining performances (in deionized water)

99

3.3.2.4 Influence of cutting depth

In foil EDM slicing process, it is considered that the gap conditions will become worse due to the difficulty of effectively removing away EDM debris from the gap when the cut depth is larger. Therefore the influence of cutting depth on the cutting performance was investigated in this section. **Table 3.6** shows the experimental conditions.

**Table 3.6** Machining conditions used to investigate the influence of cut depth

Tool polarity	(-)
Foil thickness [µm]	50
Discharge duration [µs]	2
Discharge interval [µs]	15
Preset cut depth [mm]	7, 19
Dielectric liquid	EDM-oil

The cutting performances including average cutting speed, kerf width and tool length wear ratio with the variation of discharge current were compared under two different cut depths as shown in **Fig. 3.17**(a), (b) and (c) respectively. Experimental results showed that the kerf width increased with increasing the cutting depth. The reason is considered that when the cutting depth was increased, the whole foil tool was in the slit, which could cause a higher likelihood of lateral surface discharge. Furthermore, the average area cutting speed decreased significantly, which indicated that the gap conditions were deteriorated when the cutting depth became large. Hence it is considered that sufficient flushing of the dielectric liquid to the working gap will be of great importance to improve the cutting speed in this method. According to **Fig. 3.17**(c), the tool length wear ratio was larger than 30% and it became larger when the cutting depth and discharge current were increased. It was considered that the foil tool length wear ratio was too large for applying to slice SiC wafer. It was therefore proposed to apply a relative movement between tool and workpiece, taking reciprocating motion of the workpiece for instance, to reduce/disperse tool length wear, enhance the flushing effect and improve the cutting speed at the same time, which will be described in Section 3.5.
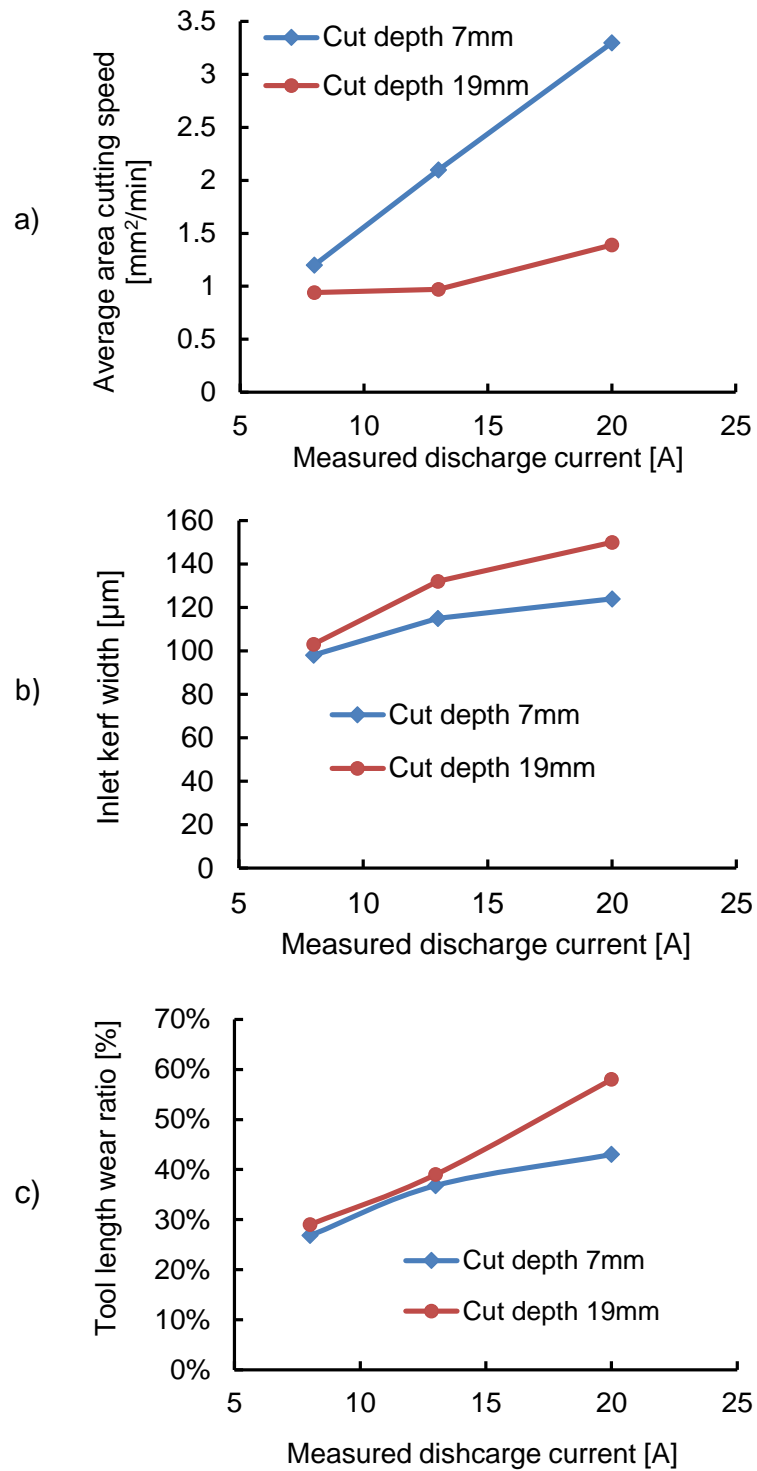
Fig. 3.17 Influence of cut depth on the cutting performance: a) average area cutting speed; b) inlet kerf width; c) tool length wear ratio

Fig. 3.18 shows the cross section profile (taken by optical microscope) of the machined kerf with a preset cut depth of 19mm under different machining conditions. The kerf width was not uniform. At the entrance side of the cutting (inlet), the kerf width was much larger than that at the bottom side due to secondary discharges occurring between the side surfaces of foil tool and workpiece. This can be avoided by insulating the side surface of the tool electrode. The minimum kerf width obtained at the inlet was 100μm when the current was around 8A. This was an important improvement regarding the decrease of the kerf width in slicing of SiC ingots because currently in all other wafer slicing methods the cut kerf width is typically around 200μm [30, 35]. If the cut depth is larger than the width of the foil, the machining will become steady and the kerf width at the inlet will not increase anymore even if the cut depth is increased.
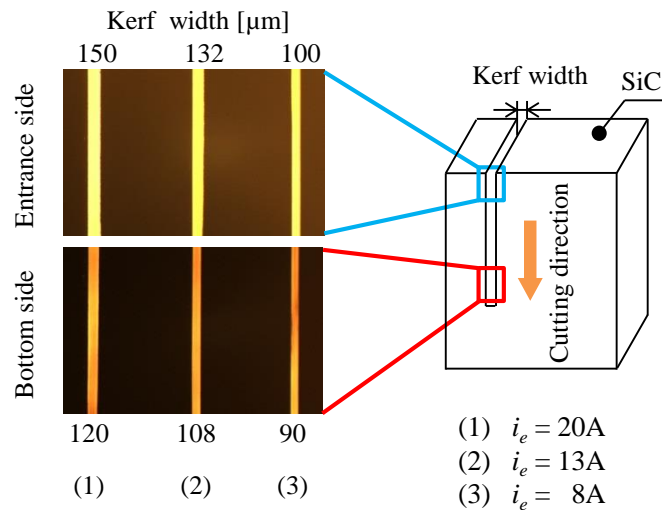
Fig. 3.18 Cross section profile of cut kerf and kerf width variations under different discharge current

3.4 Comparison between foil EDM of SiC in deionized water and in EDM-oil

It is well known that dielectric liquid has a significant impact on EDM performance. **Table 3.7** shows the general difference between EDM in oil and in deionzied water. In order to clarify the influence of dielectric on foil EDM of SiC, comparison experiments of EDM cutting of SiC between in deionized water and EDM oil utilizing the band foil tool electrode were conducted. The tool wear ratio, area cutting speed, kerf width and surface integrity were experimentally investigated.

3.4.1 Experimental setup and method

The experiments were conducted using the same setup as in **Fig. 3.11**. When conducting machining in EDM-oil, the SiC workpiece was submerged in EDM-oil and jump motion was applied to the foil electrode to facilitate the removal of EDM debris in the working gap. Since only oil could be used as the working liquid in sinking EDM machine, machining experiments of SiC in deionized water was done in an extra deionized water tank which was installed on the original sinking EDM machine. In order to maintain the

resistivity of the working dielectric, deionized water was poured to discharge gap instead of submerging by a deionized water circulation system. **Fig. 3.19** shows the schematic diagram of the developed deionized water recycling system used in the experiments. For simplicity, the deionized water of the wire EDM machine (*Sodick AP200L*) which was of high resistivity was used as the working liquid and flushed to the machining area by a flushing pump. The used deionized water was then circulated back to the wire EDM service tank through a filter and a circulating pump as shown in the figure. By this deionized water circulating system, the resistivity of deionized water was maintained at a high and constant value to ensure a stable machining process.

To find out the influence of different dielectric liquids, the EDM cutting speed and machined surface integrity in oil and water respectively were investigated by varying the pulse duration and cut depth. **Table 3.8** shows the experimental conditions**.** It should be noted that in **Table 3.8**, the actual discharge duration should be 1μs longer than the discharge duration setting due to the inductance of the electric circuit.

Table 3.7 Influences of dielectric liquid on EDM performance [3)]

	Machining speed	Surface roughness	Gap width	Tool wear	Fire risk rating
EDM oil	Low	Small	Narrow	Low under long pulse duration	High
Deionized water	High	Larger than in oil	Wide	High	No risk
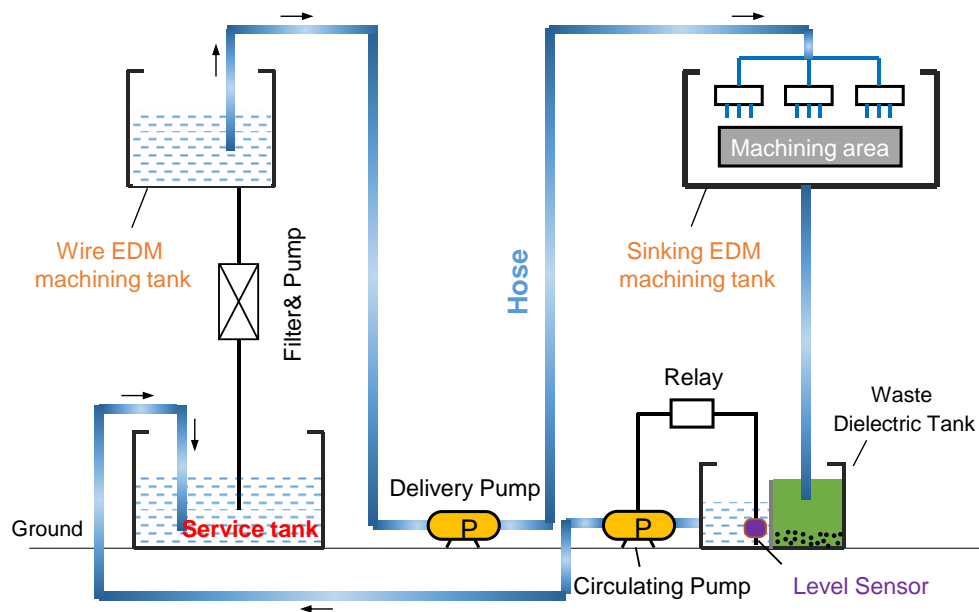
Fig. 3.19 Schematic diagram of deionized water circulation system of actual experiment setup

103

Table 3.8 Experimental conditions

Working liquid	EDM-oil; Deionized water (Resistivity: 3MΩ·cm)
Electrode	Copper foil, thickness: 50μm
Polarity of foil electrode	(-)
Preset pulse duration [μs]	1, 6
Duty factor	6.25%
Preset discharge current [A]	14
Servo voltage [V]	45
Workpiece thickness [mm]	20
Jump frequency [Hz]	≈1.3

3.4.2 Experimental results and discussion

3.4.2.1 Discharge waveform

The influence of dielectric liquid on the discharge current and gap voltage waveforms of foil EDM cutting of SiC was investigated using an oscilloscope. It was observed however that, the discharge current and voltage showed no significant difference between in EDM-oil and deionized water.

Fig. 3.20 shows the discharge current and voltage waveforms of foil EDM of SiC in deionized water by sinking EDM machine. For comparison, the discharge waveforms of EDM of cold tool steel SKD11 under the same machining conditions are also shown here. The peak current value was smaller in the case of SiC due to the higher voltage drop in SiC.
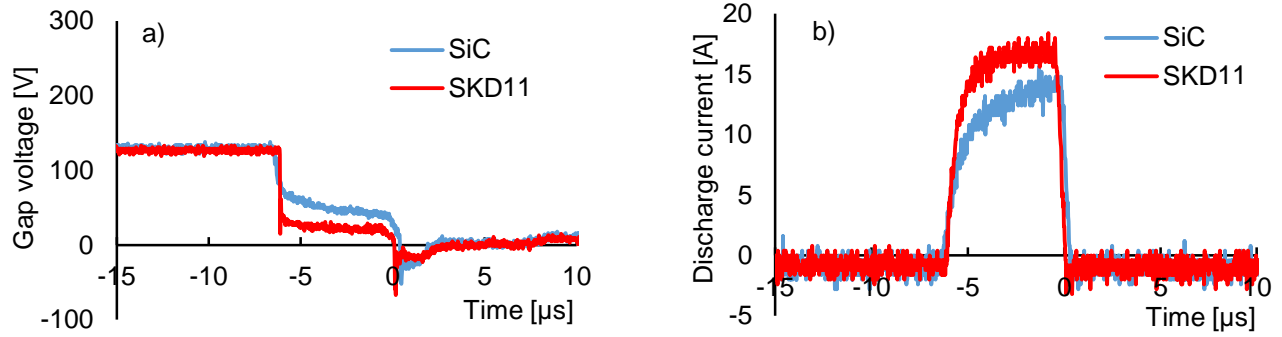
Fig. 3.20 Discharge waveform of EDM of SiC in deionized water by sinking EDM

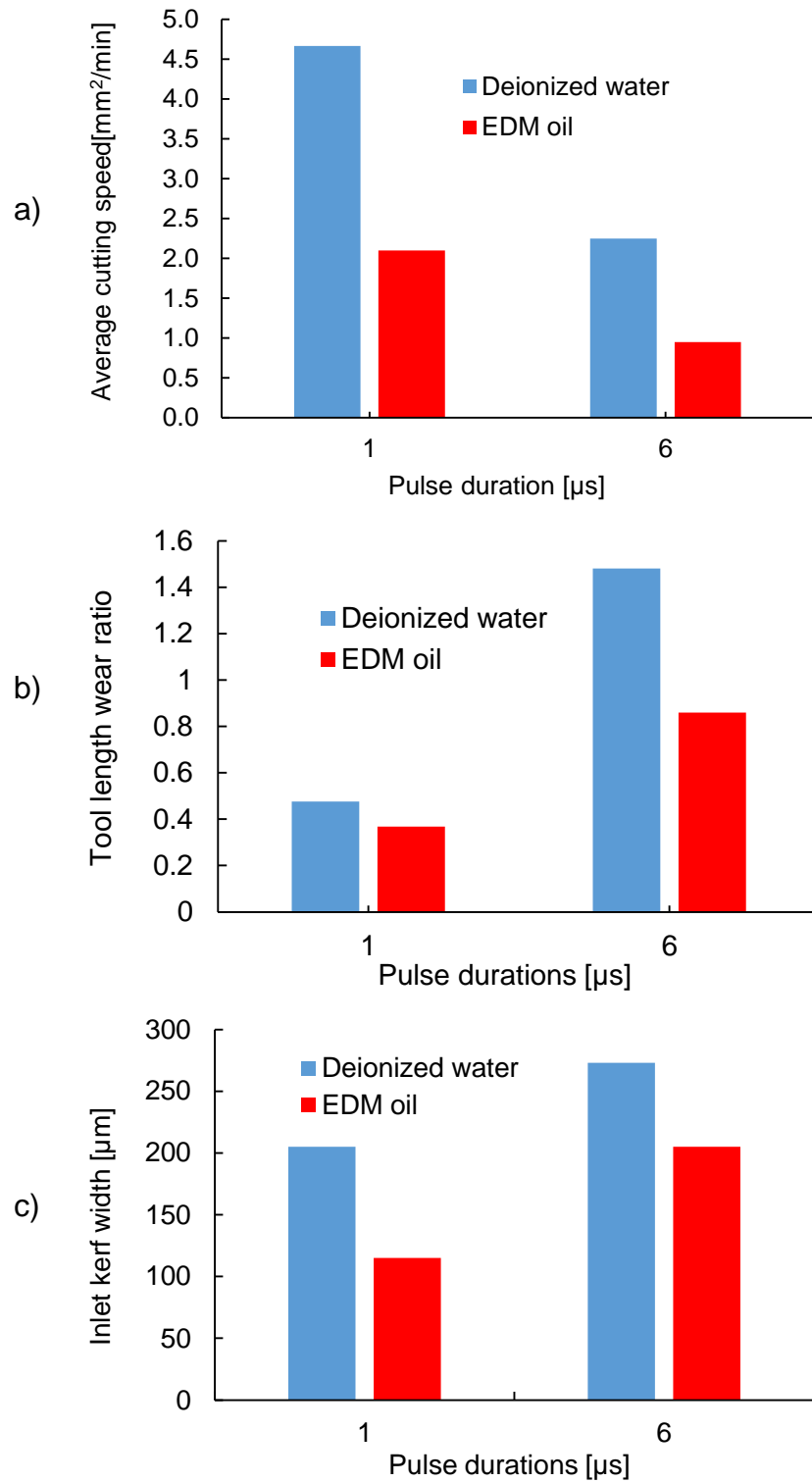### 3.4.2.2 Comparison of cutting performance between in EDM-oil and in deionized water

The polarity effect of EDM of SiC was confirmed when machining was conducted in deionized water. When the discharge duration was set as 6μs and tool electrode was set as positive, the machining speed was 2 times lower and the tool length wear ratio was 5 times higher than that of negative polarity.

To investigate the influence of dielectric liquid, experiments of EDM cutting of SiC both in oil and in deionized water were conducted under different pulse durations. **Fig. 3.21** shows the comparison results of the cutting performances. It was found that average area cutting speed was approximately 2 times higher in deionized water than that in oil under both short and long pulse duration. However, the tool wear ratio also increased in deionized water, almost 2 times higher than that in oil when pulse duration was 6μs.

On the other hand, the shape of the cut kerf was tapered in deionized water and the inlet kerf width was around 200μm, much larger than that in oil. Since the thickness of the foil tool was 50μm, the one-side gap width was 75 μm. The larger permittivity of deionized water was considered as one main reason for the larger kerf width which will be described furthermore in the next section. Except for this, the area effect and the secondary discharge phenomena between the side surface of the foil tool and the workpiece were considered as the other reasons resulting in the large kerf width. It is therefore considered that the removal of debris in the EDM gap during machining should be enhanced in order to decrease the kerf width.

Fig. 3.22 shows the comparison of EDM'd surfaces (SEM image) between in EDM-oil and in deionized water under the same machining conditions (preset pulse duration: 1μs). The EDM'd surface in EDM-oil featured a smoother surface topography without large pits caused by thermal shock compared with the surface machined in deionized water. Considering that the discharge energy was almost the same, it may indicate that the material removal volume of single discharge in deionized water was larger than that in oil. The reason was considered that the cooling effect of deionized water was more significant compared to that of oil which resulted in more intense thermal stress on the machined surface after discharge and promoted the generation of cracks after machining. In the case of oil, however, the machined surface temperature could not decrease immediately due to the worse cooling effect of oil which would restrain the formation of cracks. The surface roughness R_z of the workpiece machined in oil was 8μm, much smaller than that of 22μm in deionized water under the same machining conditions.
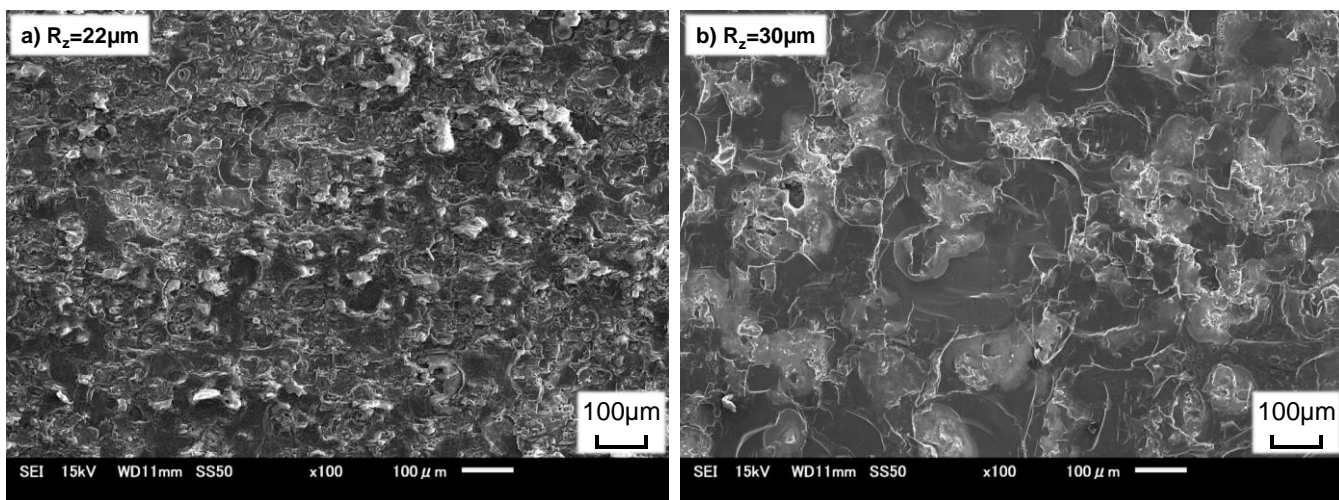
The EDM'd surfaces in deionized water under two different pulse durations were observed by SEM as shown in **Fig. 3.23**. It can be seen that under both pulse durations, the EDM'd surface in deionized water was characterized by many pits. When the pulse duration was longer, the size of such flake pits on the machined surface was larger and the surface roughness also increased, which was considered to be caused by the larger discharge energy of single discharge under the longer pulse duration. Larger discharge energy would cause a larger discharge crater and result in more significant generation of cracks and fracture. This is also one reason why short pulse duration is better for machining SiC.

Fig. 3.21 Comparison of foil EDM cutting performances of SiC in different dielectric liquids
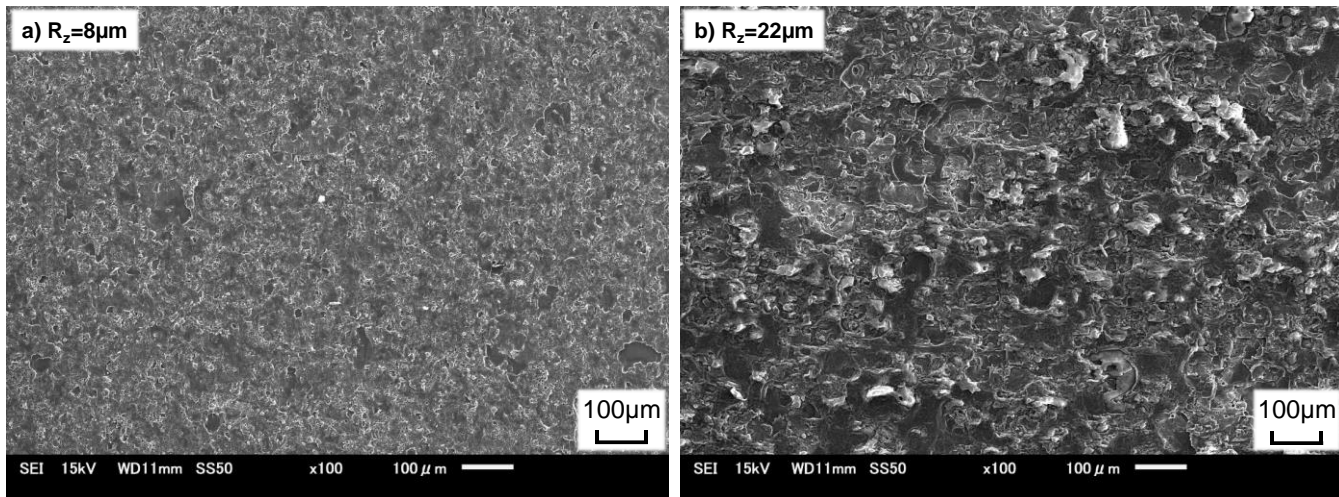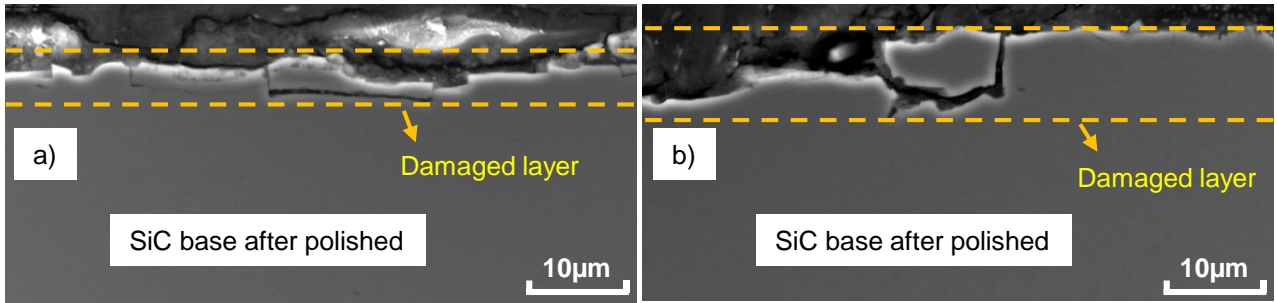
Fig. 3.22 Foil EDM'd surface of SiC in different dielectric liquids: a) EDM-oil; b) Deionized water
(Preset pulse duration: 1μs)

**Fig. 3.23** Foil EDM'd surface of SiC in deionized water under different pulse duration: a) 1μs; b) 6μs

The corresponding subsurface damage layer of SiC caused by EDM process is shown in **Fig. 3.24**. Cracks along specific crystal orientation can be seen in the damaged layer. But a defined white layer of re-solidified material cannot be observed. The subsurface damaged layer depth in EDM-oil was around 5μm, while in deionized water, the damage layer depth was around 8μm, a little larger than that in EDM-oil.

Fig. 3.25 shows the influence of cut depth on the machining performance in both EDM-oil and deionized water. The pulse duration setting in this experiment was 1μs. When the cut depth was increased, in both dielectric liquids, the machining speed decreased and the tool wear ratio increased, indicating that the machining became unstable when the cut depth was larger perhaps due to difficulty in flushing the debris particles.

108

Fig. 3.24 Subsurface layer of SiC by EDM in different dielectric liquids: a) EDM-oil; b) Deionized water
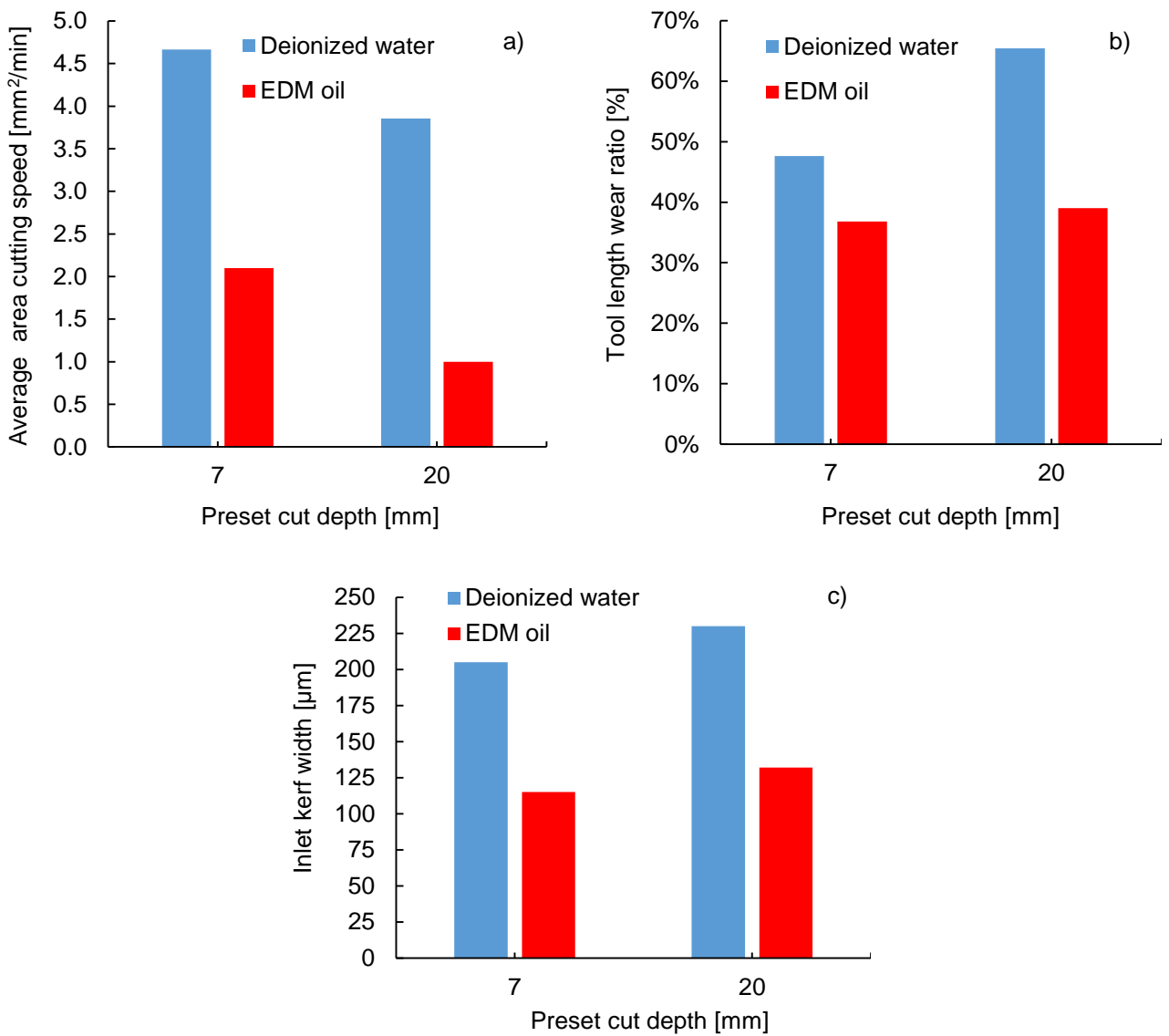

Fig. 3.25 Influence of cut depth on foil EDM cutting performance

3.4.2.3 Discussion of the influence of dielectric liquid

The experimental results in last section showed that the EDM of SiC in water resulted in a larger kerf width compared with that in oil. To clarify the experimental results, the discharge atmosphere is discussed in this section as the following.

The schematic diagram of the discharge gap between tool electrode and workpiece in normal EDM is shown in **Fig. 3.26**. The discharge gap is usually filled with bubbles (generated by discharges during continuous machining) and dielectric liquid. The diameter of bubble generated by single pulse discharge can reach up to several millimeters, several tens of times larger than the discharge gap [5]. Moreover, in continuous EDM process, most of the working area (more than 50%) will be occupied by bubbles [54], as shown in **Fig. 3.26**. Therefore, much of the time discharges are enforced to be generated in the bubbles due to the large area ratio of bubbles in the discharge gap. On the other hand, however, generation of discharges in gas is usually more difficult (requires smaller gap distance) due to its higher dielectric strength compared with that of conventional EDM in dielectric liquid [55].
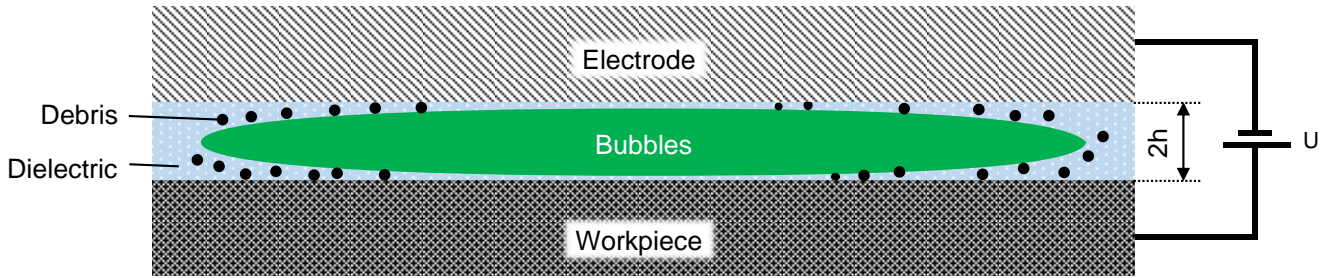
Fig. 3.26 Schematic diagram of discharge gap with bubbles in EDM

The easiness of generation of discharges (the dielectric breakdown) inside the bubble is decided by the electric field intensity inside the bubbles. The section considers the influence of dielectric liquid on the electric field intensity inside the bubble. For simplicity, the discharge gap boundary conditions are simplified as shown in **Fig. 3.27**.

Assuming that the height of bubbles is h and the discharge gap width is $2h$. Voltage of U is applied to the discharge gap. The electric field intensity in dielectric liquid E_d and in bubble (air) E_b should be different. E_b depends on the permittivity of the dielectric liquid. The electric flux density in dielectric liquid and bubble is defined as D_d and D_b respectively. The permittivity in bubble (air) and dielectric is defined as ε_0 and ε_d respectively. According to the equation for electric flux density, we can get the following formulas:

$$E_d = \frac{D_d}{\varepsilon_d}, \ E_b = \frac{D_b}{\varepsilon_0} \qquad \text{Eq. 3.1}$$

Since the electric flux density in the gap is uniform, namely $D_d = D_b$, Eq. 3.2 can be derived:

$$\varepsilon_d \cdot E_d = \varepsilon_0 \cdot E_b \qquad \text{Eq. 3.2}$$

On the other hand, the gap voltage U is expressed as Eq. 3.3:

$$U = E_d \cdot h + E_b \cdot h \qquad \text{Eq. 3.3}$$

Then we can derive the electric field intensity in the bubble as shown in Eq. 3.4:

$$E_b = \frac{U}{h \cdot (1 + \dfrac{\varepsilon_0}{\varepsilon_d})} \qquad \text{Eq. 3.4}$$

Assuming the gap condition is the same, since the ratio of permittivity of deionized water to the permittivity of EDM-oil $\varepsilon_{water} : \varepsilon_{oil}$ is approximately 80:1, the electric field intensity inside the bubble in deionized water is much larger than that in oil, which indicates that the total average dielectric strength of the discharge gap in deionized water should be much lower than that in oil.

Moreover, the area ratio of bubble of the discharge gap in deionized water is much smaller than that in oil, which further reduces the dielectric strength. Therefore it is concluded that discharges can occur more easily in deionized water than in EDM-oil, which is considered as the main reason for the larger kerf width of EDM of SiC in deionized water.
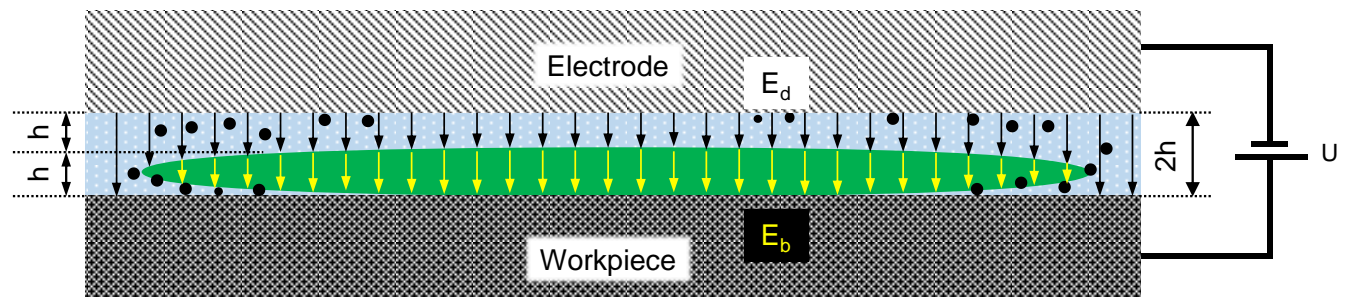
Fig. 3.27 Simplified schematic diagram of the discharge gap

On the other hand, the machined surface in deionized water presented a larger surface roughness and damaged depth. Since under the same preset servo voltage, the discharge frequency in oil and water were almost the same, it was considered that the material removal efficiency of single discharge of EDM of SiC in deionized water was larger than that in oil, which could result in a higher machining speed. The reason was probably due to the better cooling effect of deionized water. In addition, the machining stability in deionized water may be better than that in oil which could result in a better machining efficiency.
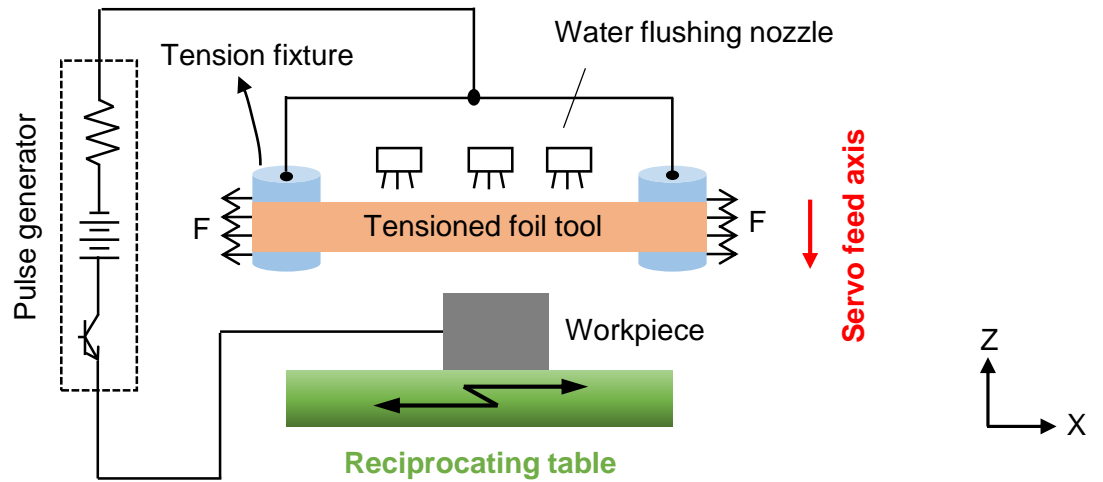
3.5 Reciprocating slicing of SiC by foil EDM utilizing reciprocating worktable

In the previous sections, it has been found that foil EDM cutting became unstable when the cut depth increased due to the deterioration of gap conditions. In addition, since the foil tool electrode was stationary but not running during machining, the foil tool wear length was significant, which was not feasible for practical use. In order to improve the foil EDM cutting performance, a relative motion between foil tool and workpiece is considered necessary to improve the discharge gap condition and reduce the length wear ratio. Therefore, it is proposed to apply a reciprocating motion to the workpiece along the foil length direction to disperse the foil tool length wear. By applying reciprocating motion to the workpiece, it is also expected that the cutting speed can be improved by improving the gap conditions.

3.5.1 Experimental setup

The schematic diagram of the experimental setup of reciprocating slicing of SiC is shown in **Fig. 3.28**. A reciprocating table, of which the reciprocating speed and stroke could be changed, was fixed on the worktable of the machine. **Table 3.9** shows the specifications of the developed reciprocating worktable. The workpiece was fixed on the reciprocating worktable and reciprocated together with the table. The foil tool electrode was installed on the Z axis of a standard sinking EDM machine (*Sodick C32*). The machining was conducted by servo feeding the foil tool electrode to the workpiece along the -Z direction while the workpiece is reciprocating along the X axis direction.

However, since the worktable was reciprocating at a high speed during machining, it was difficult to perform experiments by submerging the worktable (together with the workpiece) in the dielectric liquid. Therefore, in the experiments, dielectric was supplied to the machining area by flushing. In flushing method, EDM oil could not be used due to a high risk of fire. Hence deionized water was used as the working liquid. In order to ensure the resistivity of deionized water could maintain at a high and constant value for stable machining, a deionized water circulating system was developed as illustrated in **Fig. 3.29**. The machining was conducted by flushing the deionized water to the machining area while the workpiece was reciprocated by the worktable.

112

Fig. 3.28 Schematic diagram of the experimental setup of foil EDM reciprocating slicing of SiC
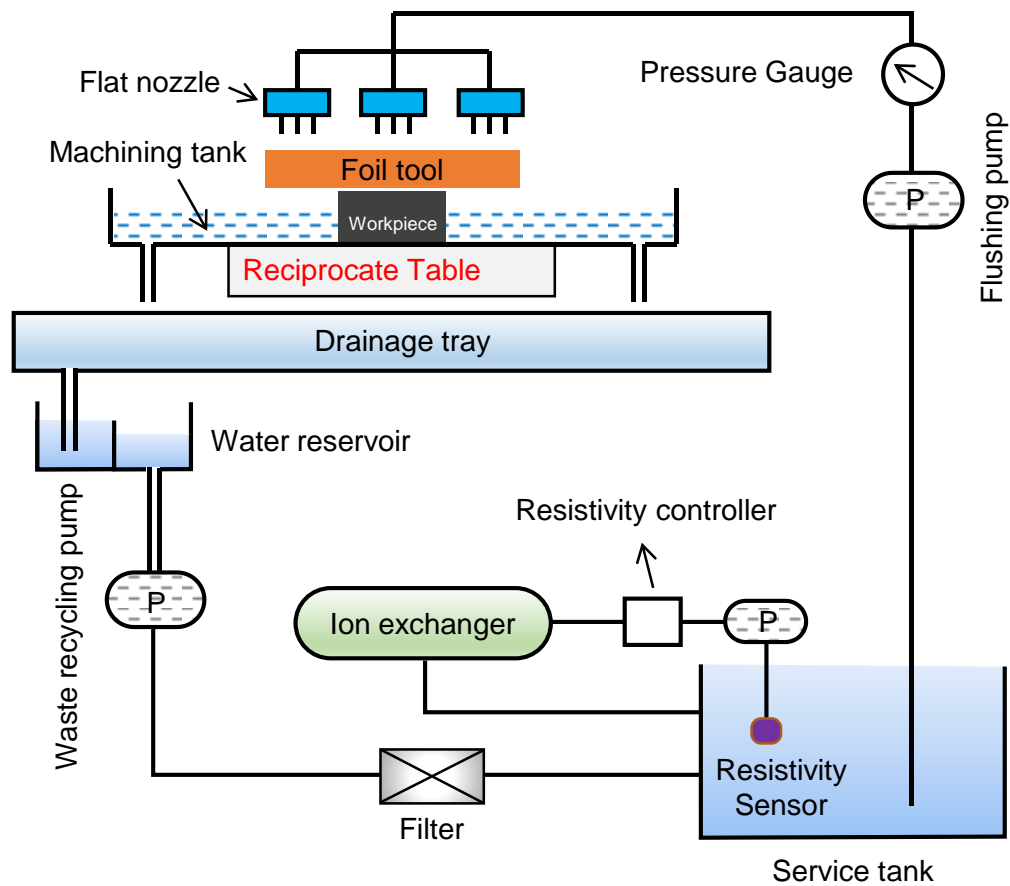

Fig. 3.29 Development of experimental system for reciprocating slicing of SiC

**Table 3.9** Specifications of the reciprocating worktable

Maximum reciprocating stroke [mm]	180
Maximum reciprocating speed [m/min]	36
Positioning accuracy [μm]	0.1
Acceleration/Deceleration time	Configurable

The foil tool electrode fixture used in the experiments is shown in **Fig. 3.30**. In order to realize reciprocating slicing of SiC, the length of the copper foil electrode was increased to 150mm. The tensioning mechanism of the foil tool fixture was the same as that shown in **Fig. 3.10**. Deionized water was flushed to the foil tool electrode by three swivel nozzles from above. **Fig. 3.31** shows the side view of the flushing method used in the experiments.

The parallelism error between the foil tool plane and the reciprocating motion trajectory was critical to the machining accuracy. Therefore, in the experiments, the parallelism error was detected by utilizing CCD laser displacement sensor (*Keyence, LK-G10*) and reduced by adjusting the angle of installation of the tool fixture to make sure that the parallelism error was less than 4μm within the stroke. In addition, before the experiment, the lower edge of the foil tool was dressed on-the-machine by a copper-tungsten electrode at the beginning to obtain an even gap between the foil tool and the workpiece. **Fig. 3.32** is a photograph of the actual experimental setup.
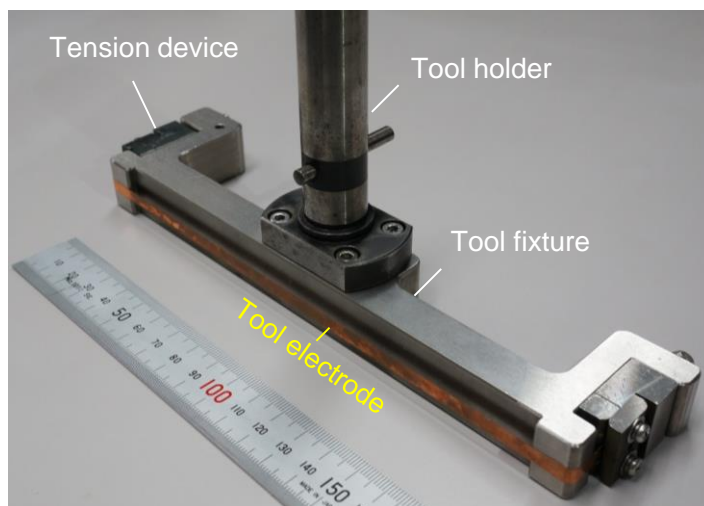
Fig. 3.30 Tool electrode fixture used for reciprocating slicing of SiC
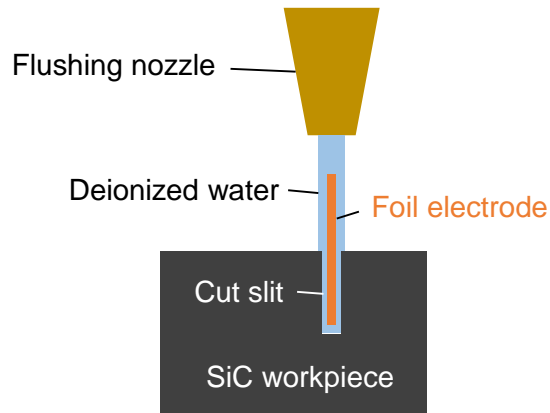
Fig. 3.31 Illustration of flushing method in reciprocating slicing of SiC
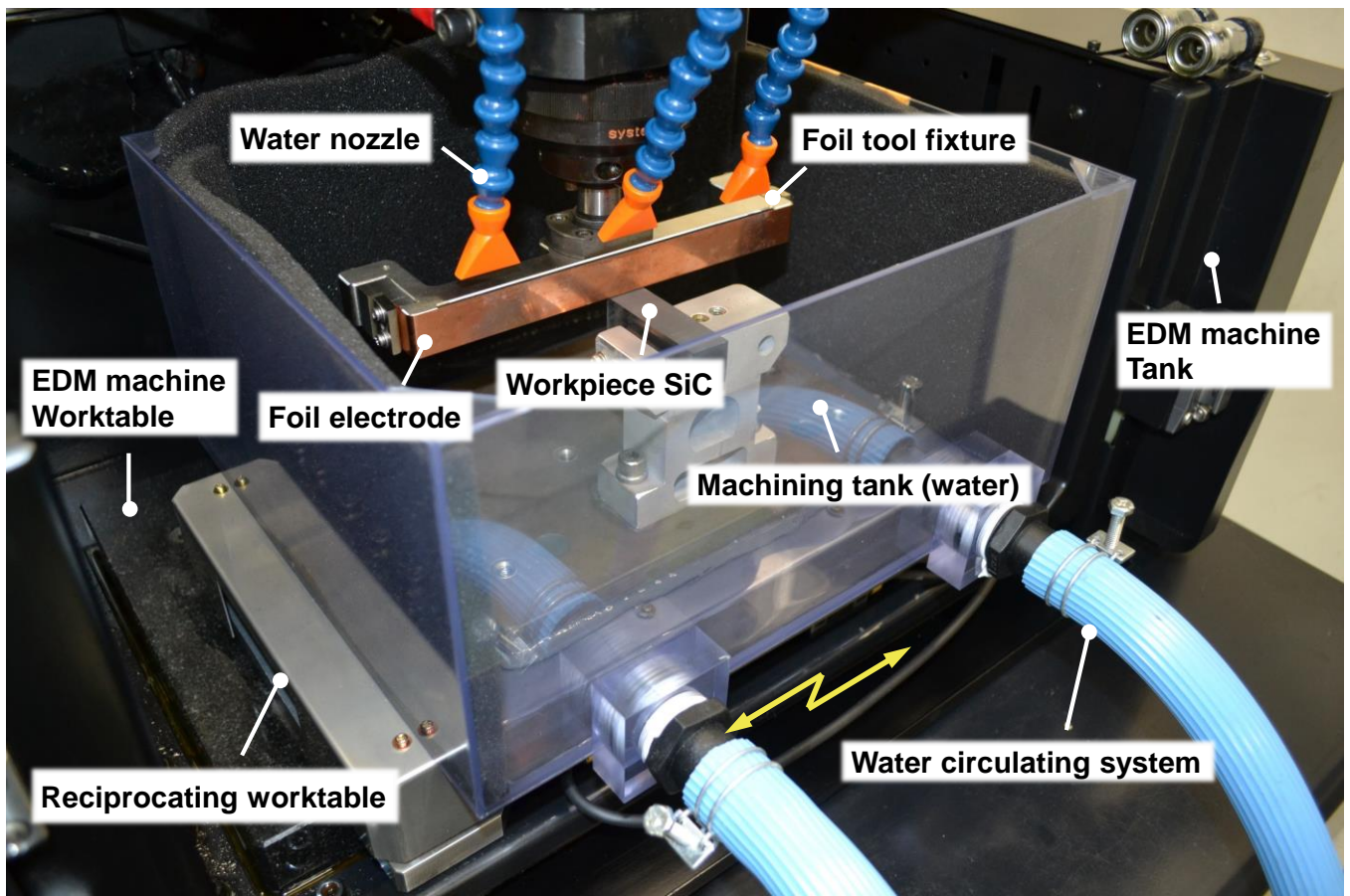

Fig. 3.32 Photograph of experimental setup of foil EDM reciprocating slicing of SiC

3.5.2 Experimental method

Influence of the reciprocating motion on the cutting performance was investigated under the optimized machining conditions shown in **Table 3.10**. **Fig. 3.33** is an illustration of the machining conditions used in the experiments.

Table 3.10 Experimental conditions

Dielectric liquid	Deionized water
Foil tool polarity	(-)
Foil thickness [μm]	80
Open voltage [V]	120
Servo voltage [V]	55
Discharge current [A]	14
Preset pulse duration [μs]	1
Pulse interval [μs]	15
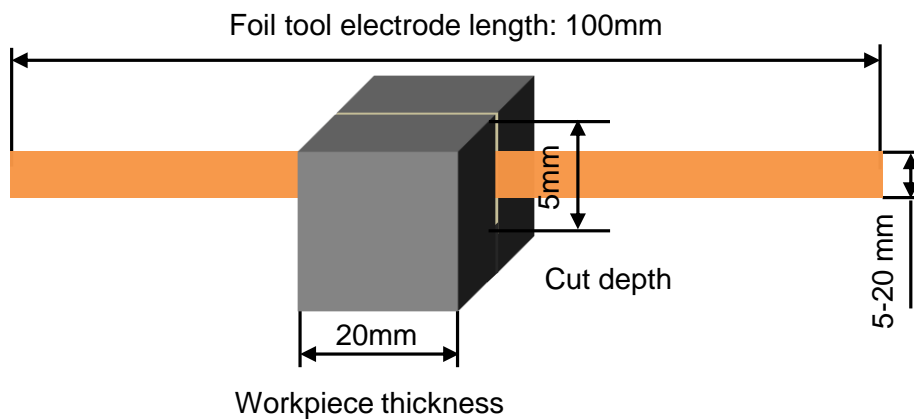
Fig. 3.33 Illustration of machining conditions in the reciprocating slicing method of SiC

3.5.3 Experimental results and discussion

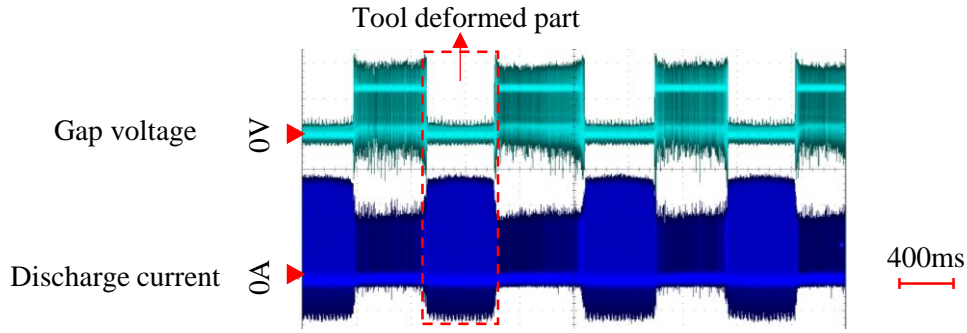3.5.3.1 Machining stability under different machining modes

To find out the stable machining conditions, different machining modes were performed as shown in **Table 3.11**. During machining, the discharge waveforms of different machining modes were measured by an oscilloscope to evaluate the machining stability.
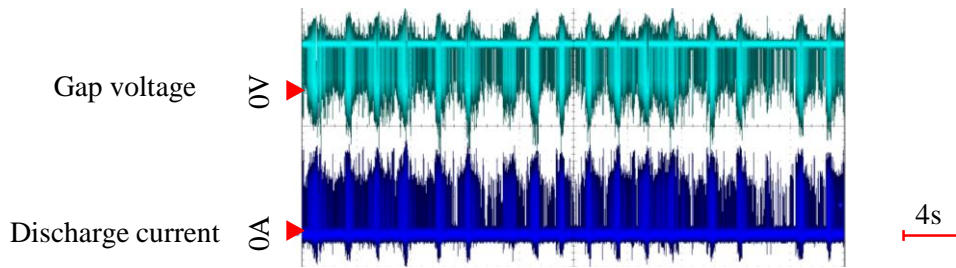
Table 3.11 Different machining modes

Mode 1	Reciprocating motion
Mode 2	Reciprocating motion + Jump motion

In machining mode 1, considering that the debris could be removed by the reciprocating motion of the workpiece, jump motion was not applied to obtain a continuous machining process without any interruption. However the machining could not proceed stably because of frequent short circuit, of which the reason will be discussed later. **Fig. 3.34**(a) shows the discharge waveforms measured during machining. With regard to the discharge waveform, as described in Section 1.3.2, the time when the gap voltage became zero indicated that short circuiting occurred during machining. In **Fig. 3.34**(a), periodic short circuiting can be seen clearly.

To achieve a stable machining, mode 2 was tried out. In mode 2, jump motion (with the same direction as the servo direction) with high frequency but small height was applied to investigate the machining performance. The jump up and down time was 0.01s and 0.2s respectively. Jump speed was 16.7mm/s (jump height $\approx$167μm). From the discharge waveform shown in **Fig. 3.34**(b), it can be found that no clear short circuit exists in the discharge waveform, which probably indicates that the stability of machining is improved. The collision problem of tool and workpiece could be alleviated because the gap condition could be detected by the machine every time when the jump motion returned back to the original servo place. Although the short circuit could be avoided, the machining became discontinuous due to the frequent interruption of discharges by the jump motion. When the jump frequency was decreased too much, the collision and short circuiting problem occurred again. In the experiments, the frequency of jump was kept higher than 5Hz to obtain a machining process without frequent short circuit.

Tool deformed part

Gap voltage — 0V

Discharge current — 0A

400ms

(a) Short circuiting in machining mode 1

Gap voltage — 0V

Discharge current — 0A

4s

(b) Stable discharge in machining mode 2 (Jump frequency>5Hz)

**Fig. 3.34** Machining stability under different machining methods

3.5.3.2 Disperse of tool electrode wear

By reciprocating motion, foil tool electrode wear could be dispersed as shown in **Fig 3.35**. Tool wear length was reduced considerably compared to that without reciprocating motion. However, unfortunately, it was found that the tool wear length was not uniform. Especially at the two sides of the electrode, which was also the start/end of the reciprocating stroke, the tool wear length was much smaller compared to that at the center part of the electrode. This phenomenon was caused by the shorter machining time of the workpiece (stand-by time of the workpiece) at the start/end of the reciprocating stroke. However, the tool wear shape could be changed by adjusting the reciprocating speed. As shown in **Fig. 3.36**, by increasing the stand-by time of the workpiece (delay time of the reciprocating motion) at the start and end stage of the reciprocating stroke, the tool wear length became more even compared to that without controlling the speed. Nevertheless, it was difficult to control the tool wear shape completely even.

During slicing, uneven tool electrode wear would result in a rapidly changing gap distance when the workpiece was applied the reciprocating motion, which probably caused the instability of machining by frequent short circuit as described before. This will be discussed further in the following section.
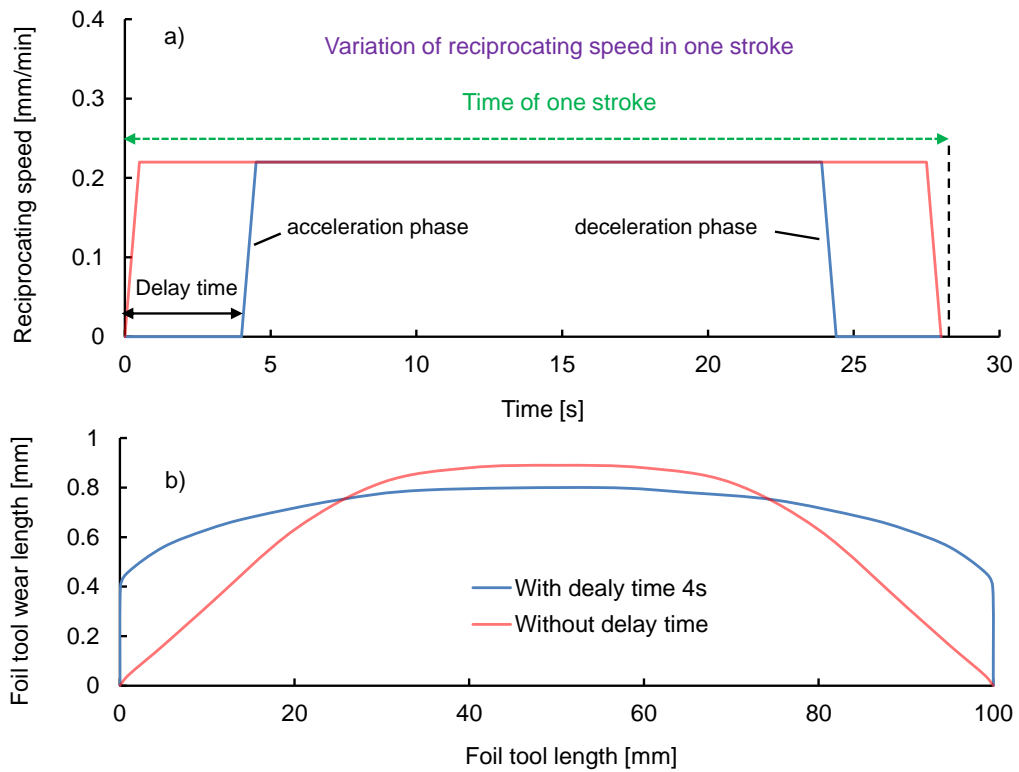
118

(a) Photograph of foil tool wear in reciprocating slicing of SiC
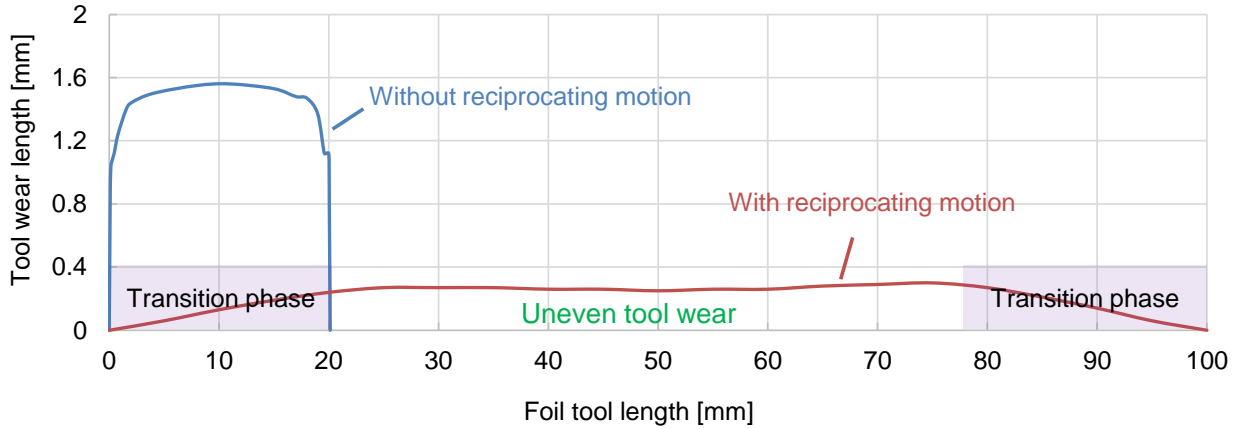
(b) Measurement of tool wear shape

**Fig. 3.35** Tool wear shape in the reciprocating slicing method

Fig. 3.36 Influences of reciprocating speed on the tool wear shape

119

3.5.3.3 Influence of reciprocating motion

In the experiments, the workpiece reciprocating speed was changed to investigate its influence on the cutting speed. The experimental results are shown in **Fig. 3.37**. The reciprocating stroke was set as 80mm. The green point shown in **Fig. 3.37** indicates the tool length wear ratio of foil EDM without reciprocating motion and jump motion. In the case of reciprocating slicing method, it was expected that the slicing speed could be improved since the gap conditions would be improved by the reciprocating motion of the workpiece. Experimental results showed that, however, the average cutting speed increased a little when the reciprocating motion of the workpiece was applied at a very low reciprocating frequency. With increasing the reciprocating frequency furthermore, the cutting speed decreased. At a certain point, machining could not proceed due to the collision between the foil tool and the workpiece, resulting in deformation of foil tool. The reason was considered as the following.

During machining, the servo feed axis, as shown in **Fig. 3.28**, was perpendicular to the reciprocating direction of the workpiece. Due to the uneven tool wear along the reciprocating direction, the gap change was very rapid during machining. The servo respond speed must be high enough to detect the rapidly changing gap condition for a stable machining process. On one hand, too frequent gap change would aggravate the load of the servo control system and result in a low machining speed. On the other hand, if the reciprocating frequency was increased too much, the gap change speed would exceed the capacity of servo control system and the servo feed could not work normally, which was considered as the reason why collision occurred between the foil tool and the workpiece when the reciprocating frequency was increased too large.
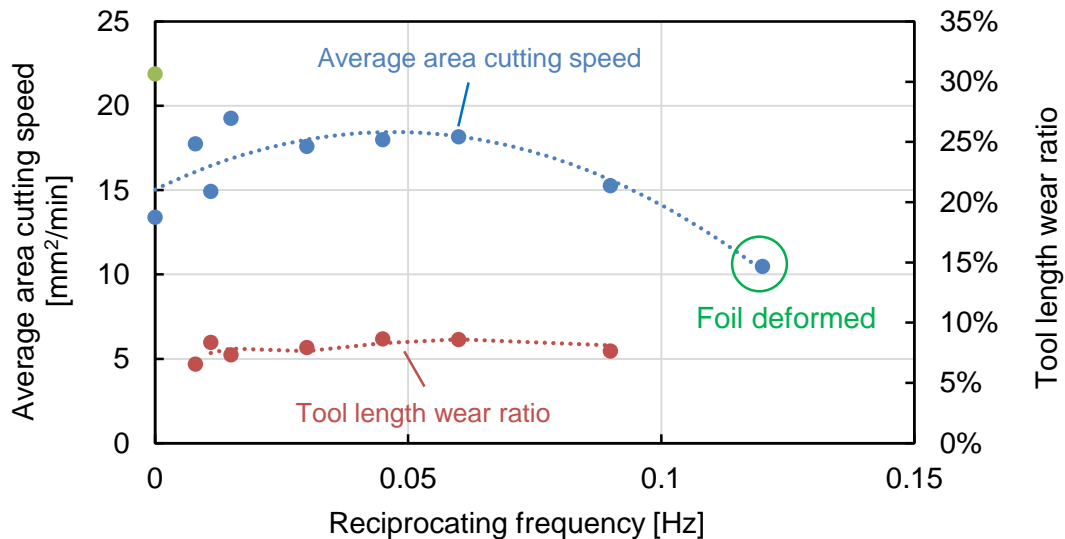
Fig. 3.37 Influences of reciprocating speed on the slicing performance

3.5.3.4   Cut kerf width

Fig. 3.38 shows the cut kerf width under different reciprocating frequency, which indicates that with increasing the reciprocating frequency, the kerf width did not decrease but increased even though the flushing conditions were better with higher reciprocating frequency. It was therefore considered that the deterioration of the kerf width was due to the deformation of the foil tool electrode caused by the collision between the foil tool and the workpiece.
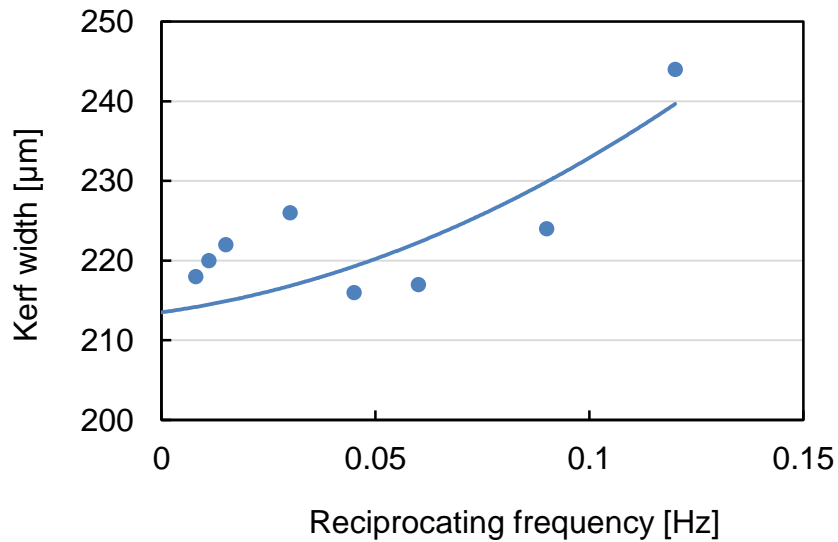
Fig. 3.38 Kerf loss in the reciprocating slicing method

3.6 Conclusions of Chapter 3

In Chapter 3, foil electrode was proposed in place of wire electrode for cutting SiC. Foil EDM slicing experiments were conducted by utilizing a specifically developed foil tool electrode fixture which could apply tension force to the foil and keep the foil flatness. The performances of foil EDM cutting of SiC including the cutting speed, kerf width, foil tool wear etc. were experimentally investigated. In addition, the dielectric influences on the foil EDM performance of SiC were investigated. At last, aiming to reduce the foil tool electrode wear length, reciprocating slicing of SiC method, which was similar to conventional multi-blade saw method, was proposed. The experimental setup for the proposed reciprocating slicing method was developed and the characteristics and feasibility of this method were investigated. The main conclusions were as the following:

1) The development of foil tool electrode fixture was accomplished. Based on the developed fixture, foil positioning error (including the foil flatness error) less than 10μm was achieved. Foil EDM cutting of SiC was performed successfully on a commercial sinking EDM machine by utilizing 50μm foil electrode. A minimum kerf width of 100μm was achieved by using the 50μm thick foil electrode.

2) Foil tool electrode length wear ratio was around 0.25~0.4 in foil EDM cutting by 50μm thick foil electrode when the discharge current was changed from 8A~20A with discharge duration of about 2μs. It should be noted here that jump motion of the foil tool electrode was applied during machining in order to improve the machining stability. In addition, it was found that the tool wear ratio of SiC was more than 2 times lower compared with that of steel material under the same preset machining conditions. The higher material removal efficiency and higher thermal conductivity of SiC were considered as the reasons.

3) The optimal machining conditions of foil EDM of SiC were investigated. It was found that negative polarity of tool electrode and short pulse duration was better for foil EDM of SiC with higher machining speed and smaller tool wear ratio. On the contrary, long pulse duration was confirmed not suitable for EDM SiC due to a lower machining efficiency and severe discharge concentration.

4) The foil EDM performances between in EDM oil and in deionized water were compared. It was found that under the same machining conditions, EDM in deionized water featured higher cutting speed, higher tool wear ratio and larger kerf width compared to those in EDM-oil. The EDM'd surfaces of SiC in deionized water and in EDM-oil also presented significant difference. The surface machined in EDM-oil had a smoother surface topography while the surface machined in deionized water had many fracture pits on it. The surface roughness obtained from EDM in oil was much smaller compared to that in deionized water. In addition, the subsurface damaged layer depth in deionized water was slightly larger than that in EDM-oil. The reasons were considered as the following. Comparing with EDM oil, the higher permittivity of deionized water decreased the dielectric strength. In consequence, discharge occurred more easily in deionized water than in oil, which probably resulted in the larger kerf width of EDM of SiC in deionized water. In addition, it was considered that due to the better cooling effect of deionized water compared with that of EDM oil, the material removal efficiency of single discharge was higher in deionized water than in oil, which would result in a higher machining rate and a larger surface roughness.

5) Since the foil tool wear length ratio was up to 0.2~0.4 in the experiments, reciprocating slicing of SiC was proposed in the research to disperse the foil tool length wear in foil EDM slicing of SiC. The development of the experimental setup of EDM slicing of SiC by foil electrode utilizing a reciprocating worktable was accomplished. Experimental results showed that the foil tool electrode length wear could be decreased considerably due to the reciprocating motion. In addition, with increasing the frequency of the reciprocating motion, the average cutting speed increased due to the improved flushing conditions of the discharge gap. However, further increase of the reciprocating frequency would cause a decrease of the cutting speed. At a certain point, machining could not proceed due to the collision between the foil tool and the workpiece which could result in deformation of the foil tool. The reason for this was considered to be caused by the uneven tool length wear ratio along the reciprocating direction. In the reciprocating slicing method, the foil tool wear length was not uniform along the reciprocating direction because of the variable discharge gap conditions and the less standby-time of the workpiece at the start and end stage of the reciprocating motion. Therefore, eventually, the uneven foil tool wear caused the instability of the machining process in the reciprocating slicing method.

Chapter 4 Development of foil electrode running system for slicing SiC

4.1 Introduction

This chapter describes the development of foil electrode running system for EDM slicing of SiC and the characterizations of the slicing performance.

In the previous chapter, foil EDM reciprocating slicing method was proposed to slice SiC ingot aiming to improve the gap condition and disperse the tool wear. However, unfortunately, the tool wear length in the reciprocating stroke was not uniform. The collision between tool and workpiece during reciprocating slicing occurred easily due to the rapidly changing uneven discharge gap caused by the uneven tool wear during machining. Constant machining could not be conducted unless the reciprocating speed of the workpiece was adjusted timely according to the tool wear length at different position or the responding speed of servo system was improved.

In order to achieve a stable and constant slicing process, EDM of SiC by winding the band foil electrode in a unidirectional way was proposed in place of reciprocating worktable. **Fig. 4.1** is an illustration of the proposed winding foil electrical discharge slicing (EDS) method. Foil electrode (thickness less than 100μm) is winded in one direction at a constant speed *v*. The workpiece (SiC) is installed on the main feed axis and servo fed to the running foil electrode for machining. The feeding direction of workpiece is perpendicular to the foil running direction.

The advantage of this method is considered that a steady state tool wear model (which will be described later in detail) can be established to achieve a stable and continuous slicing process. In the meantime, it is considered that the discharge gap conditions can be improved since the running of foil will facilitate the removal of EDM debris, which can probably result in a higher slicing speed.

4.2 Mechanism of running foil EDM

The section describes the mechanism of running foil EDS which can realize a stable machining process.

In foil EDS, as described before, the foil tool electrode thickness could be 2-4 times smaller compared with the diameter of wire electrode in wire EDM process. On the other hand, however, with the decrease of foil thickness, the foil tool electrode wear becomes more significant compared with that of wire EDS where the wire electrode wear is usually insignificant and negligible. This is considered as a big difference between wire EDS and foil EDS.

In the proposed foil EDS method, if the foil is running at a very high speed, the foil electrode wear can be neglected owing to less machining time. Under this condition, the running foil EDS method is considered similar to that of the general wire EDM process in principle.

In the case that the foil is running at a very low speed, however, tool electrode wear will become large due to long stand-by time of machining. In this case, since the servo feed control is just in the Z direction, there is a probability of collision between tool and workpiece. To achieve a stable machining process, it
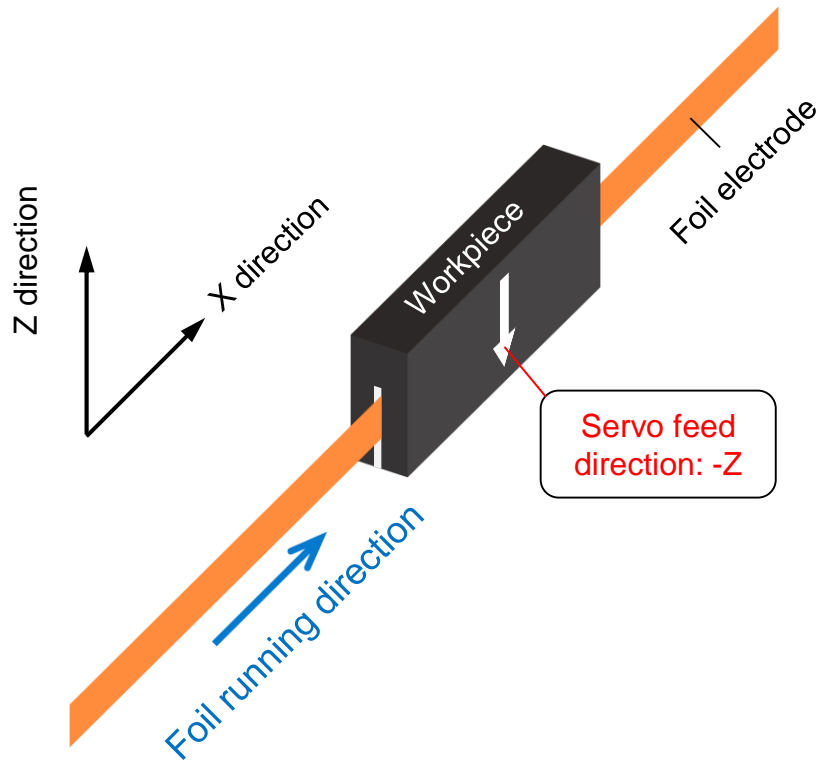
Fig. 4.1 Schematic diagram of EDM slicing method of SiC by running foil electrode
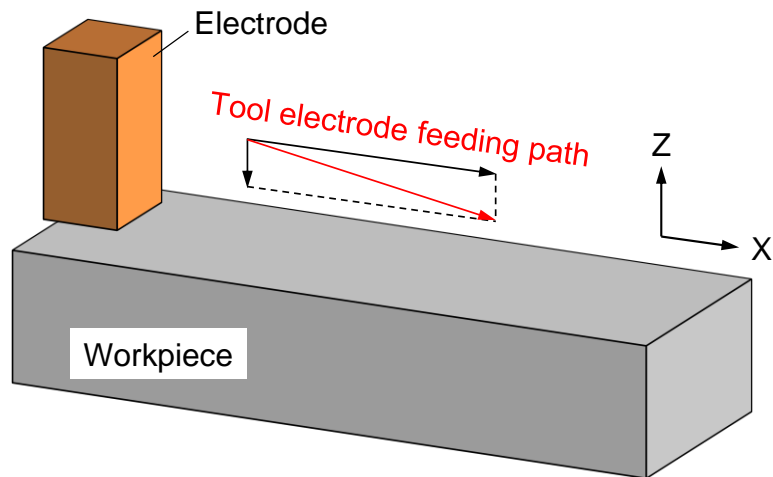
Fig. 4.2 Schematic diagram of EDM grooving by feeding tool electrode towards workpiece at a constant slope

is considered that the respond speed of servo feed control must be sufficiently high to adjust the feeding process. On the other hand, Sato et al. [56] reported an EDM grooving method by feeding the tool electrode towards the workpiece with a constant slope as shown in **Fig. 4.2**. The machining of grooves with uniform depths along the feeding direction could be conducted successfully by the slant feeding method because steady tool wear was achievable in this method. In the case of running foil EDS, the situation is considered to be similar to this EDM grooving process. The analysis of the steady state tool wear in foil EDS is described as in the following section.

4.2.1 Steady state tool wear model in running foil EDS

Considering the steady state in running foil EDS method, since the tool wear is supposed to be constant widthwise, the layout of the tool and the workpiece can be simplified to a two-dimensional model as shown in **Fig. 4.3**(a). In this model, to analyze the tool wear shape, the discharge gap distance is assumed to be zero for simplicity.

Assuming that the workpiece is machined $-\Delta z$ along Z axis while the tool electrode is worn Δx along X direction in a certain time Δt. If the feeding speed of the workpiece (workpiece removal length per unit time) is defined as v_w and the foil running speed (tool wear length per unit time) is defined as v, then Δz and Δx is given by the following equation

$$\Delta z = v_w \cdot \Delta t$$
$$\Delta x = v \cdot \Delta t$$

Eq. 4.1

If the point O marked in **Fig. 4.3**(a) is set as the origin point of the coordinates, then the boundary of the tool wear can be described by the following function

$$z = f(x)$$

Eq. 4.2

The infinitesimal machined volume of the workpiece, dW_w and the infinitesimal tool electrode wear volume dW_e can be expressed by the following equation:

$$dW_w = dx \cdot (-\Delta z)$$
$$dW_e = dz \cdot \Delta x$$

Eq. 4.3

Defining the tool electrode wear ratio as τ,

$$\tau = \frac{dW_e}{dW_w}$$

Eq. 4.4

Then the following equations can be obtained

$$dz = \tau \cdot \frac{\Delta z}{\Delta x} \cdot dx$$

Eq. 4.5

Since at point x=0, z=0, it can be derived that

$$z = \tau \cdot \frac{\Delta z}{\Delta x} \cdot x$$
$$= \tau \cdot \frac{v_w}{v} \cdot x$$

Eq. 4.6

$\frac{v_w}{v}$ is determined by the machining conditions such as foil running speed, discharge energy etc. Under the steady state condition, the value of $\frac{v_w}{v}$ is constant. Therefore, the boundary of tool electrode wear is supposed to be a straight line as shown in **Fig. 4.3**(b). The gradient of the boundary line is proportional to the tool electrode area wear ratio τ and the value of $\frac{v_w}{v}$. Moreover, if the workpiece width is L, then based on Eq. 4.6, the foil tool electrode wear length h can be derived as the following equation, which indicates that the foil tool wear length after machining is proportional to tool electrode area wear ratio and the slicing width of workpiece.

$$h = \tau \cdot \frac{v_w}{v} \cdot L$$

Eq. 4.7

4.2.2 Determination of optimal foil tool electrode width

It is of great importance to determine the optimal foil electrode width. This section describes the determination of foil electrode width during machining.

On one hand, foil electrode with larger foil width can sustain larger tension force due to the increased cross section area based on the following equation:

$$F = \sigma_{ts} \times A = \sigma_{ts} \times m \times n$$

Eq. 4.8

Here, σ_{ts} refers to the tension strength of foil material, A refers to the cross section area of foil electrode, m is the foil thickness and n is the foil width. On the other hand, however, with increasing the foil width, the side surface area of foil electrode will also increase. Due to the area effect in EDM, the probability of secondary discharge between the side surface of the foil electrode and the workpiece will increase, which will result in a larger kerf width. In principle, in order to reduce the kerf width, the foil electrode width should be reduced as smaller as possible.

Therefore, it is considered that the foil thickness m and the required tension force F should be determined first. Then based on Eq. 4.8, the foil width can be calculated easily. However, since there is tool wear during machining, as shown in Eq. 4.7, the tool wear length must be considered in the calculation. In conclusion, the foil width is determined by the following equation, which is considered as the optimal foil electrode width for foil EDM slicing.

128

$$n = \frac{F}{\sigma_{ts} \times m} + h \qquad\qquad \text{Eq. 4.9}$$
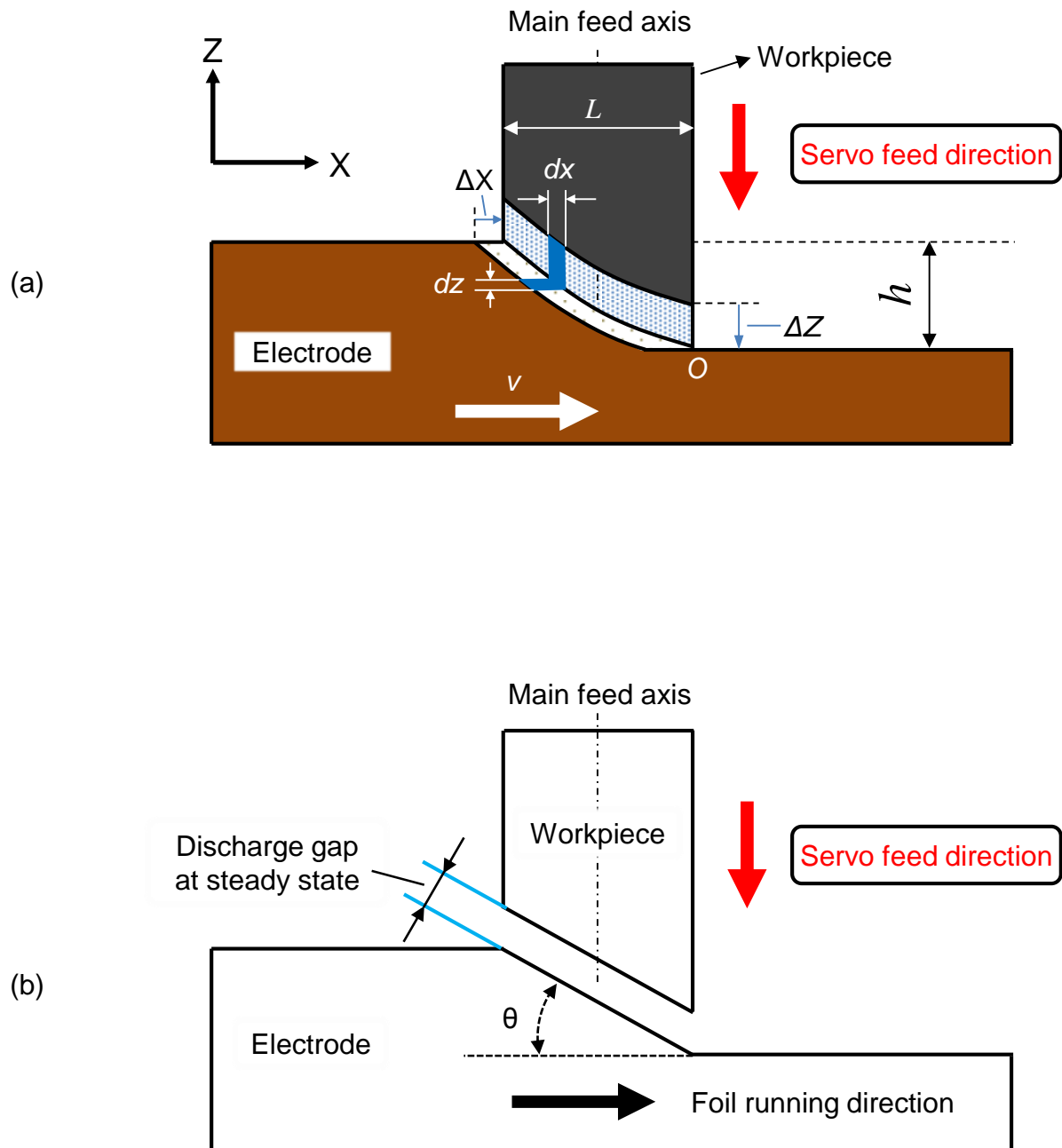
**Fig. 4.3** Two dimensional model of tool wear under steady state

4.3 Development of running foil EDS system

4.3.1 Manufacture of foil tool electrode

With regard to copper foil electrode, in order to reduce the kerf width, foils with thickness smaller than 100μm were selected as the electrodes in this research. The maximum tension force that foil could sustain could be calculated easily from the yield strength of the foil material.

Under the present conditions, however, no band shape foil electrode is available on the market. Therefore in this study the foil electrode was homemade by the procedures shown in **Fig. 4.4**. As the first step, copper foil of 100mm×10m (width×length, the maximum dimension of foil that can be purchased on market currently) was winded by hand to an aluminum rod on which two locating rings at a distance of 100mm (same to the width of foil) were fixed to position the copper foil and avoid malposition of foil. After the foil was winded orderly, the foil together with the rod was subjected to wire EDM process and ribbon shape foil electrode with the desired width could be cut out. To improve the foil electrode edge accuracy, the cut foil disc was polished, as shown in **Fig. 4.4(a)**. Then the foil was winded to the foil bobbin as shown in **Fig. 4.4**(b) and could be used for machining.

However, since the foil electrode was winded by hand in the manufacturing process, the foil flatness and dimension accuracy was probably affected by the manufacturing process. This will be discussed furthermore in later sections.
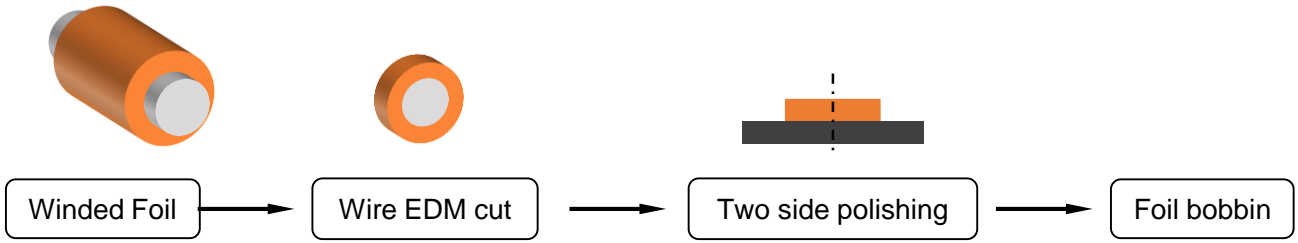
(a) Procedures for manufacturing the foil tool electrode
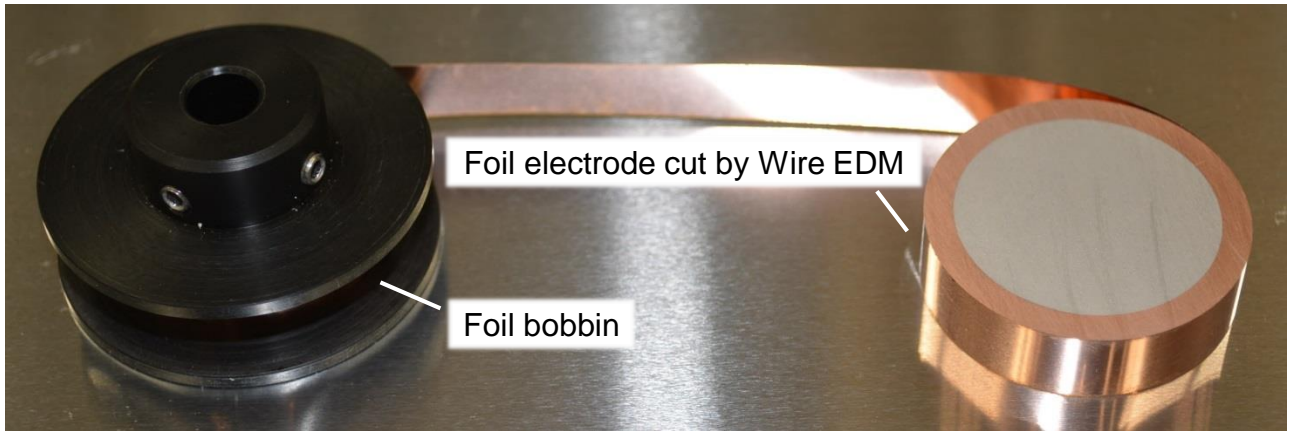
(b) Photograph of homemade copper foil electrode and foil bobbin

Fig. 4.4 Illustration of home-made copper foil electrode

4.3.2 Development of foil tool electrode winding system

The objective of the development of running foil EDS system was to realize foil EDM slicing of 6inch SiC ingot with a running foil tool electrode. This section describes the development of the experimental system.
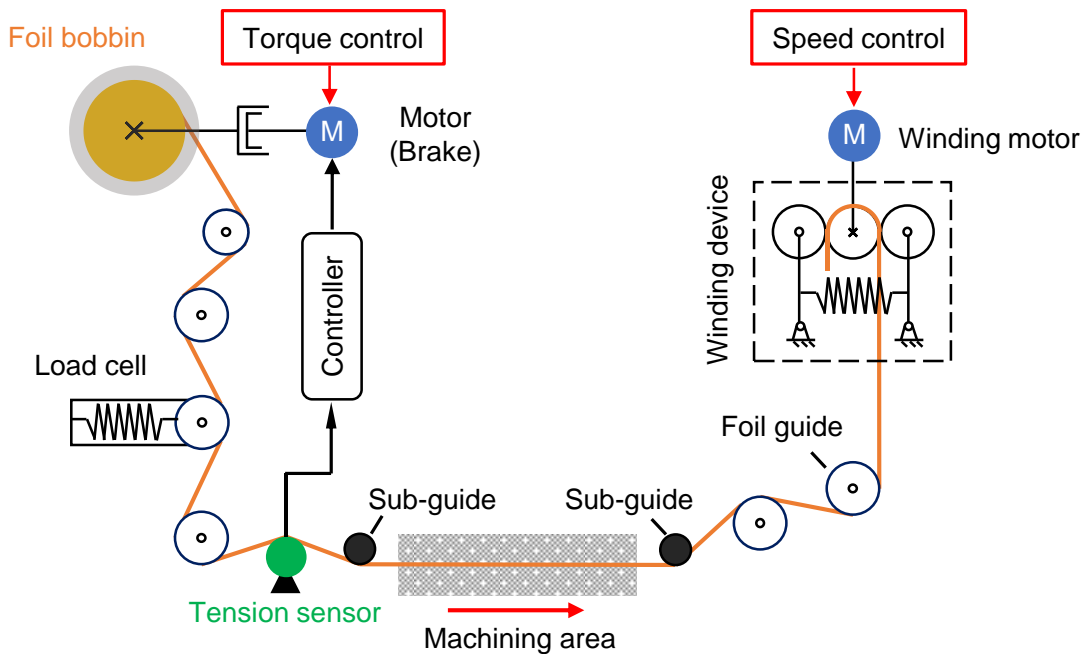
4.3.2.1 Structure of foil winding system

The schematic diagram of the designed foil winding system is shown in **Fig. 4.5**, which is mainly composed of four units: foil bobbin, unwinding devices, foil positioning guides and winding devices. The foil is tensioned with a constant tension force by controlling the output of velocity/torque of the unwinding and winding devices and winded at a constant speed. The foil winding mechanism, in concrete terms, is shown in **Fig. 4.6**(a) and (b), which is also the assemble drawing of the developed system.

As can be seen, two motors are used in the system, one for unwinding the foil bobbin (*Mitsubishi Electric Corporation, HG-KR13*), and one for winding the foil (*Oriental Motor Co., Ltd, BXS460A*). The foil is running along the periphery of the guide cams by the drag force of the winding device. In the winding unit, a knurled roller made of plastic, which is designed for increasing the grasp ability, is connected to the output shaft of the winding motor and used as the driving roller to drive the foil. On both sides of the driving roller, two idle knurl pulley were placed right next to the driving roller and they are pulled towards each other by a tension spring to generate press force. When the driving roller runs, foil can be winded along the driving roller by the friction force between the roller surface and the foil generated by the pressure.

There are flanges on the guide rollers keeping the vertical position of foil and the guide width can be adjusted to fit the width of foil electrode. The sub-guides are set at the nearest place to the machining area to improve the positioning accuracy. In this study, knock pins are used as the sub-guides. Two locating rings are fixed on each sub-guide by a locking screw to position the foil as shown in **Fig. 4.7**. All roller guides are made of plastic (Polyacetal/Nylon) to avoid the leak of current into inside bearings of roller while machining. Besides, a load cell which functions as a tensioner is set in the system serving as a compensator to reduce the change of tension force and stabilize the running of foil.
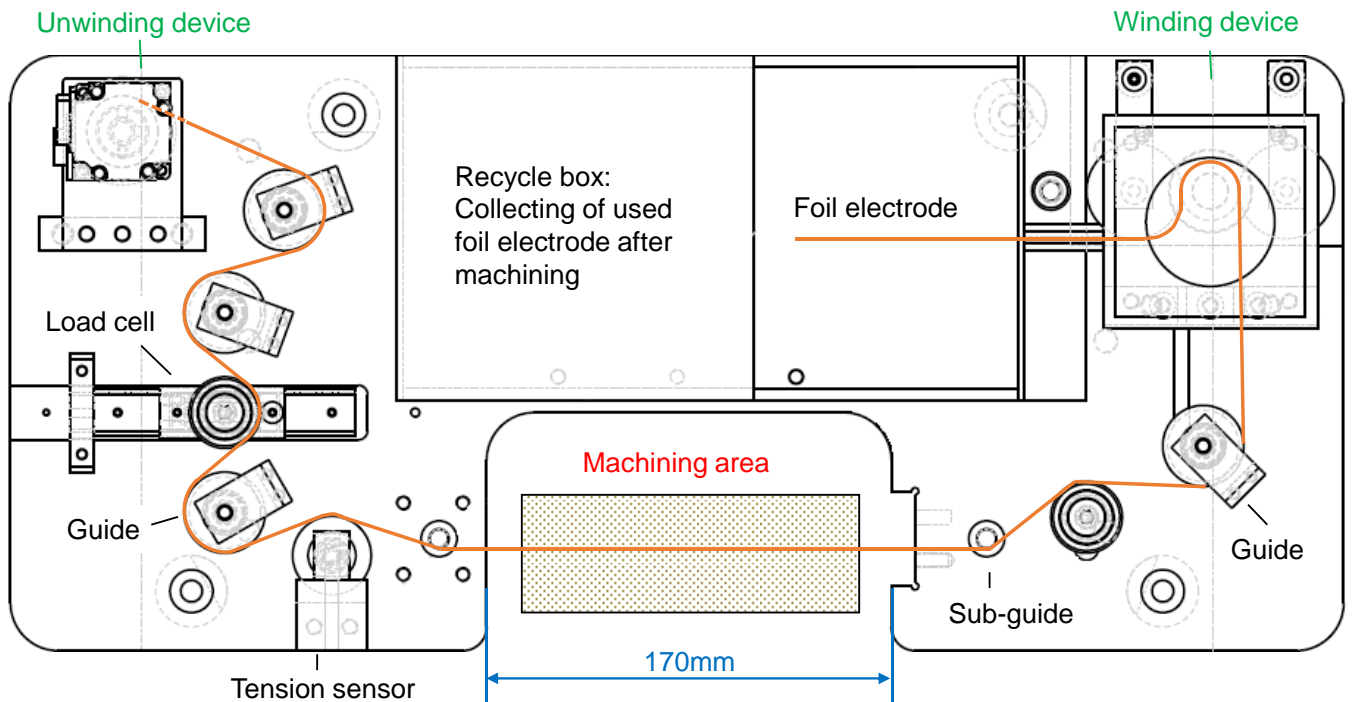
The length dimension of the machining area, which is marked in **Fig. 4.6**(b), is designed to be 170mm aiming to slice 6inch SiC ingot.

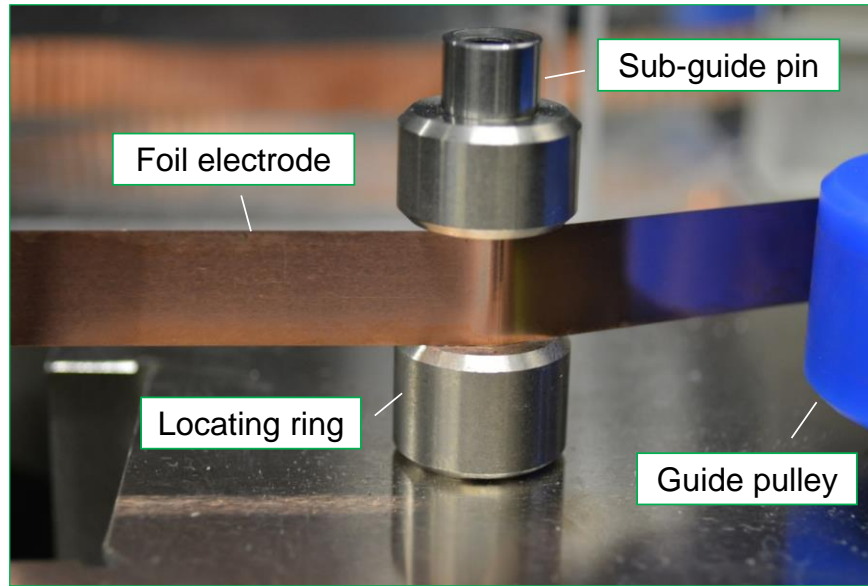**Fig. 4.5** Schematic diagram of foil tool winding system for EDM slicing of SiC
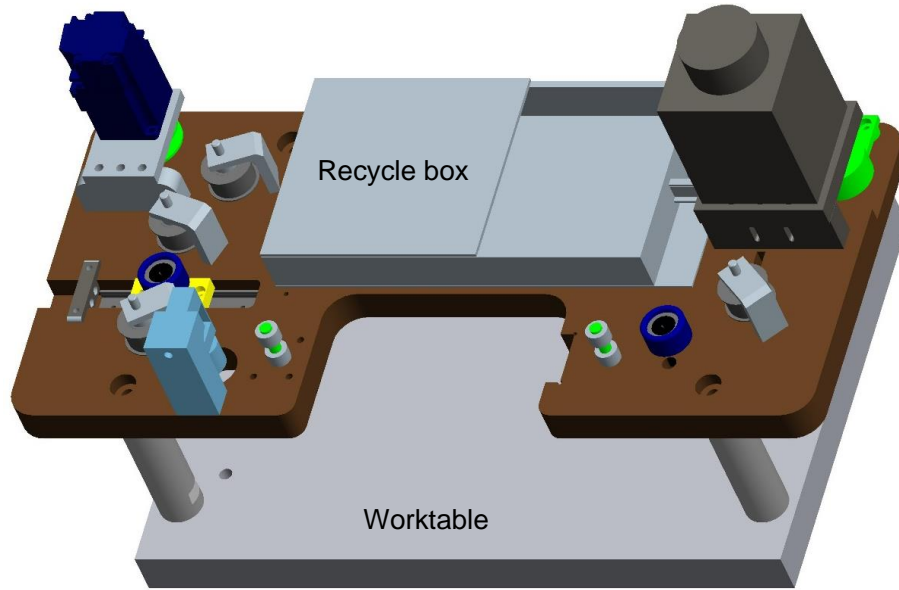
(a) 3D view of developed foil winding setup for slicing SiC

(b) Top view of the system structure

Fig. 4.6 Drawing of the designed foil winding system for EDM slicing of SiC

Fig. 4.7 Photograph of the developed foil guide used in the experiments

### 4.3.2.2 Detection of tension force

Tension force is a critical factor affecting the foil flatness during foil running. Keeping constant tension force is of great importance to improve the cutting accuracy. In order to detect the tension force of foil properly, a tension transducer, as shown in **Fig. 4.8**, was developed in the system using stain gauges based on the bending beam model. In the foil winding system, tensioned foil electrode ran along the surfaces of the guide pulley which was connected together with an aluminum beam. The tension force on the foil would deform the very thin Al beam by means of the shearing force F_r acting on the guide pulley. Two strain gauges, which were connected into a half "Wheatstone Bridge" circuit (see **Fig. 4.9**), were mounted on the deformed Al beam at the points where maximum strain was generated. By measuring the output voltage of the "Wheatstone Bridge" circuit as shown in **Fig. 4.9**, the strain of the strain gauges could be obtained. Thus, the tension force F can be calculated from the strain of the Al beam which is described in the following. The specifications of the designed tension sensor is shown in **Table 4.1**.

The relationship between the strain of the sensor beam, ε, and the force, F_r, was calculated based on a single bending beam model as shown in **Fig. 4.10**. Since there were two beams in the designed tension transducer, the exert tension force on single beam was $F_r/2$. The bending moment at cross section x was expressed as below:

$$M_z = \frac{F_r}{2} \times (l - x)$$

Eq. 4.10
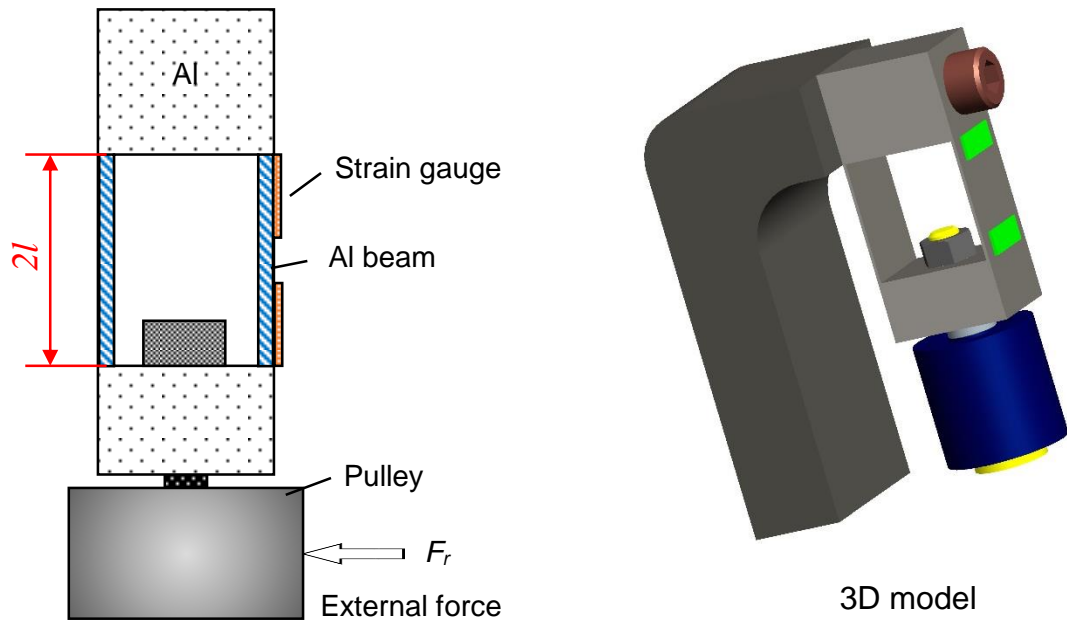
**Fig. 4.8** Illustration of the structure of tension sensor

$$\frac{\Delta R}{R} = K_s \cdot \varepsilon$$

$$V_0 = \frac{\Delta R}{2R} \times E_0 = \frac{K_s \cdot \varepsilon}{2} \times E_0$$
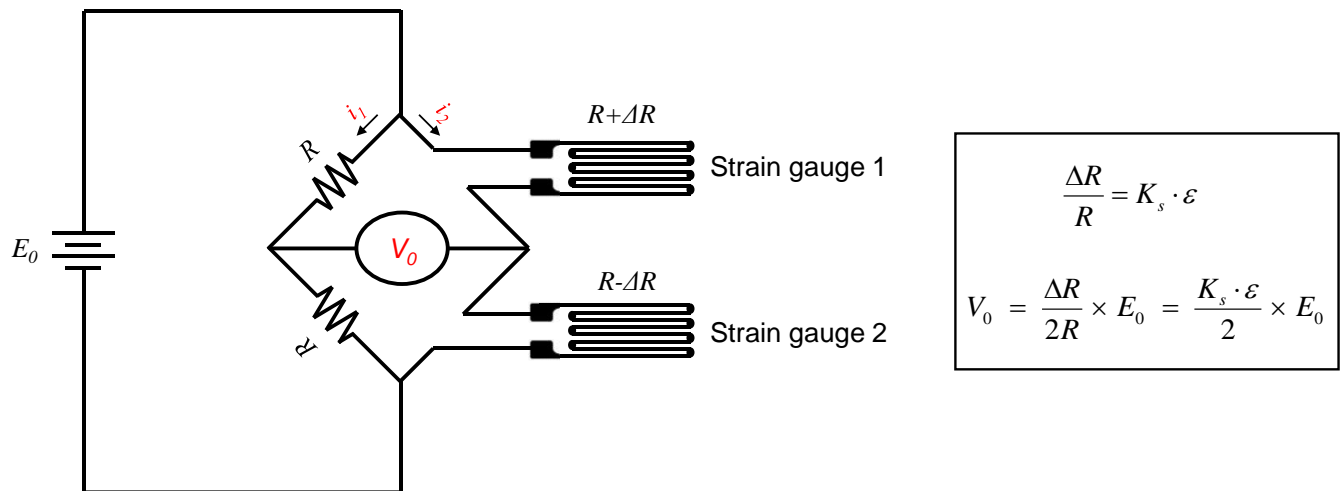
Fig. 4.9 Application of Wheatstone Half-Bridge for Strain Measurement

Table 4.1 Design specification of tension sensor

Gauge length [mm]	2
Gauge factor, K_s	2.11 (25°C, 50%RH)
Optimal strain range, ε	200μ< ε <800μ
External force, F_r [N]	3.6-7.6
Elastic modulus of aluminum, k [GPa]	69
Beam width, a [mm]	15
Beam thickness, b [mm]	1
Beam length, $2l$ [mm]	20
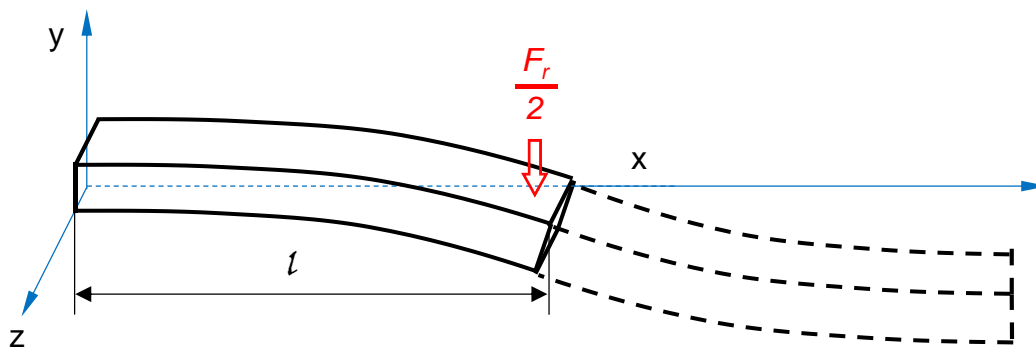
a) Bending deformation of the beam
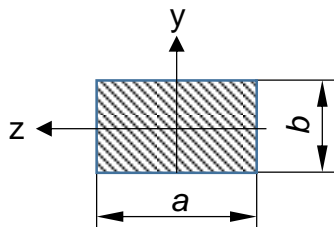
b) Cross section of the beam

Fig. 4.10 Bending beam model used for strain calculation.

The maximum normal stress $\sigma_{x_{\max}}$ in the beam was calculated by the following equation.

$$\sigma_{x_{\max}} = \frac{|M_z|}{I_z} y_{\max} = \frac{|M_z|}{W_z}$$

<div align="right">Eq. 4.11</div>

Here, I_z is the inertia moment, W_z is referred to as section modulus, which equals $\frac{I_z}{y_{\max}}$. In the case of rectangular cross-section shown in **Fig. 4.10**(b), $W_z = \frac{ab^2}{6}$.

According to Hooke's law, $\varepsilon_x = \frac{\sigma_x}{k}$, we can get the maximum normal stress

$$\varepsilon_{x_{\max}} = \frac{1}{k} \times \frac{|M_z|}{W_z} = \frac{1}{k} \times \frac{\dfrac{F_r}{2} \cdot l}{\dfrac{ab^2}{6}} = \frac{3F_r l}{kab^2}$$

<div align="right">Eq. 4.12</div>

Hence by measuring the strain of the beam of the designed sensor, the external force F_r can be determined. The tension force F applied to the foil electrode can be calculated by the method shown in **Fig. 4.11**, where the external force F_r is actually the resultant force of the tension force F.
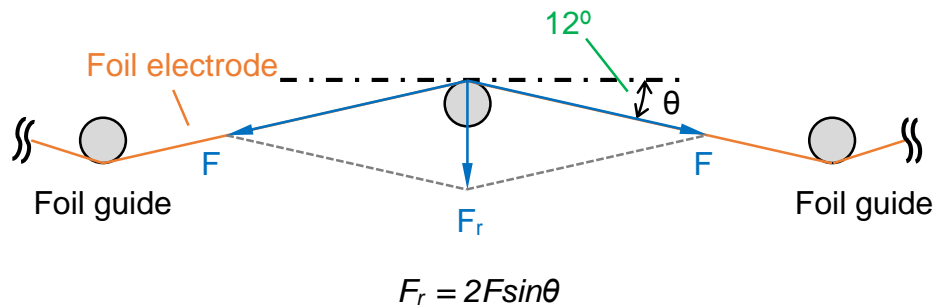
Fig. 4.11 Illustration of tension force calculation method

4.3.2.3 Tension force control method

As the tool electrode, foil flatness error is a critical factor determining the machining accuracy of foil EDM. To obtain a high flatness, it is necessary to apply a large tension force to the foil. In addition, in order to improve the foil running stability, it is important to keep the tension force constant during foil running.

Fig. 4.12 shows the schematic diagram of the method to apply tension force to the foil electrode in the developed experimental setup. The foil electrode was winded with a constant speed by the two winding rollers on the right side. To apply tension force to the foil, the unwinding roller was applied a torque in the reverse direction of foil running direction. Assuming that the foil bobbin diameter is B, the torque applied to the bobbin is P, then the tension force F can be obtained by the following equation:

$$F = 2P/B \hspace{4cm} \text{Eq. 4.13}$$

Since the diameter B of the foil bobbin was changing during winding, to keep a constant tension force, the torque must be changed with the change of the bobbin diameter B. Moreover, mechanical loss and effect of inertia at acceleration and deceleration stage contributed to the variation of tension force. Therefore, in order to get a stable tension force, in principle the tension force should be detected and fed back to the unwinding roller timely to servo control the output torque of the unwinding device. In this study, however, since the foil was running at a relatively low speed (around 1~750mm/min), for simplicity, the output torque of unwinding device was kept constant instead of the adaptive control.
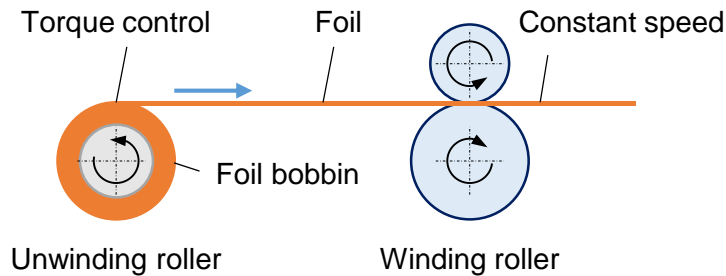

Fig. 4.12 Illustration of method for applying tension force to the foil electrode

### 4.3.3　Evaluation of accuracy of foil running system

1) Parallelism error between feed axis and foil surface

The accuracy of the foil running system mainly refers to the parallelism error between the feeding trajectory and the foil surface as illustrated in **Fig. 4.13**, which is decisive to the slicing accuracy. In the experiments, a laser displacement sensor was fixed to the main axis. The parallelism error between the feeding trajectory of the main axis and the foil surface was measured by the laser displacement sensor which was moving together with the main axis. **Fig. 4.14** shows the measured parallelism error in experiments which was around 40μm along foil width of 7mm, quite large compared to the foil thickness. It was considered that the parallelism error measured here was mainly composed of two parts: foil positioning error caused by the fixing method and the foil flatness error of itself. On the other hand, the knock pin with cylindricity error of 5μm was used as the foil guide in the developed foil running system, as shown in **Fig. 4.7**. Measurement showed that the parallelism error between the feed axis and the foil guide pin was less than 12μm. Therefore, it was considered that the foil flatness error was significant. This

was probably because that, all the foil electrodes and foil bobbins used in the experiments were homemade by hand, which probably caused a very large deviation of the foil flatness. Except for these reasons, the foil running system probably exerted influence on the foil flatness error during foil running due to the uneven tension force along the foil width direction by the foil winding unit.

A: Reference surface
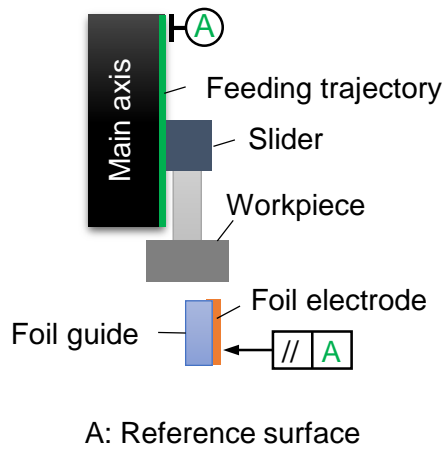
**Fig. 4.13** Schematic diagram of parallelism error between feeding trajectory and the foil surface
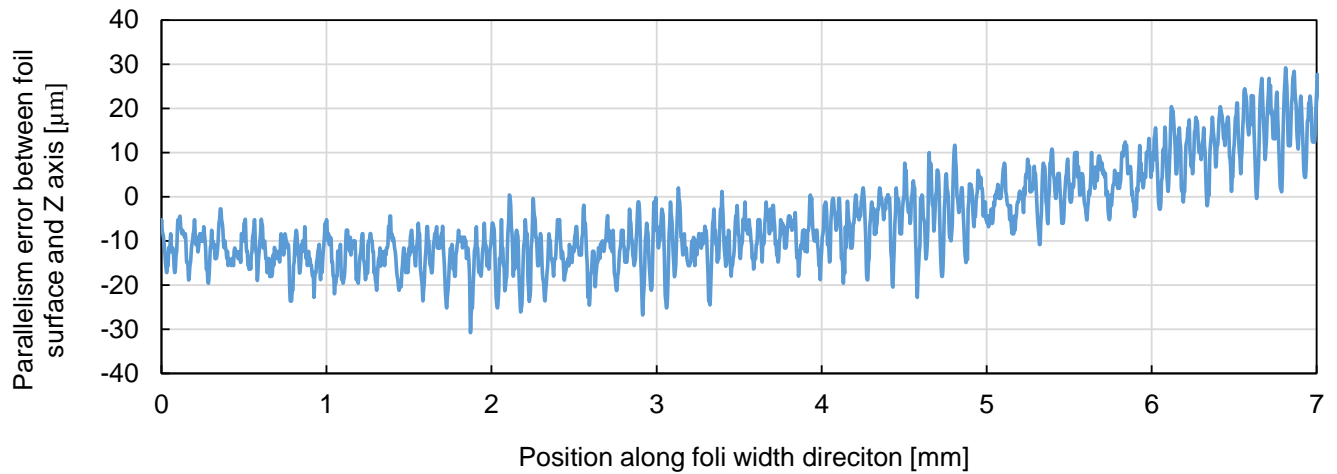
Fig. 4.14 Parallelism error between the feeding trajectory of the workpiece and the foil surface
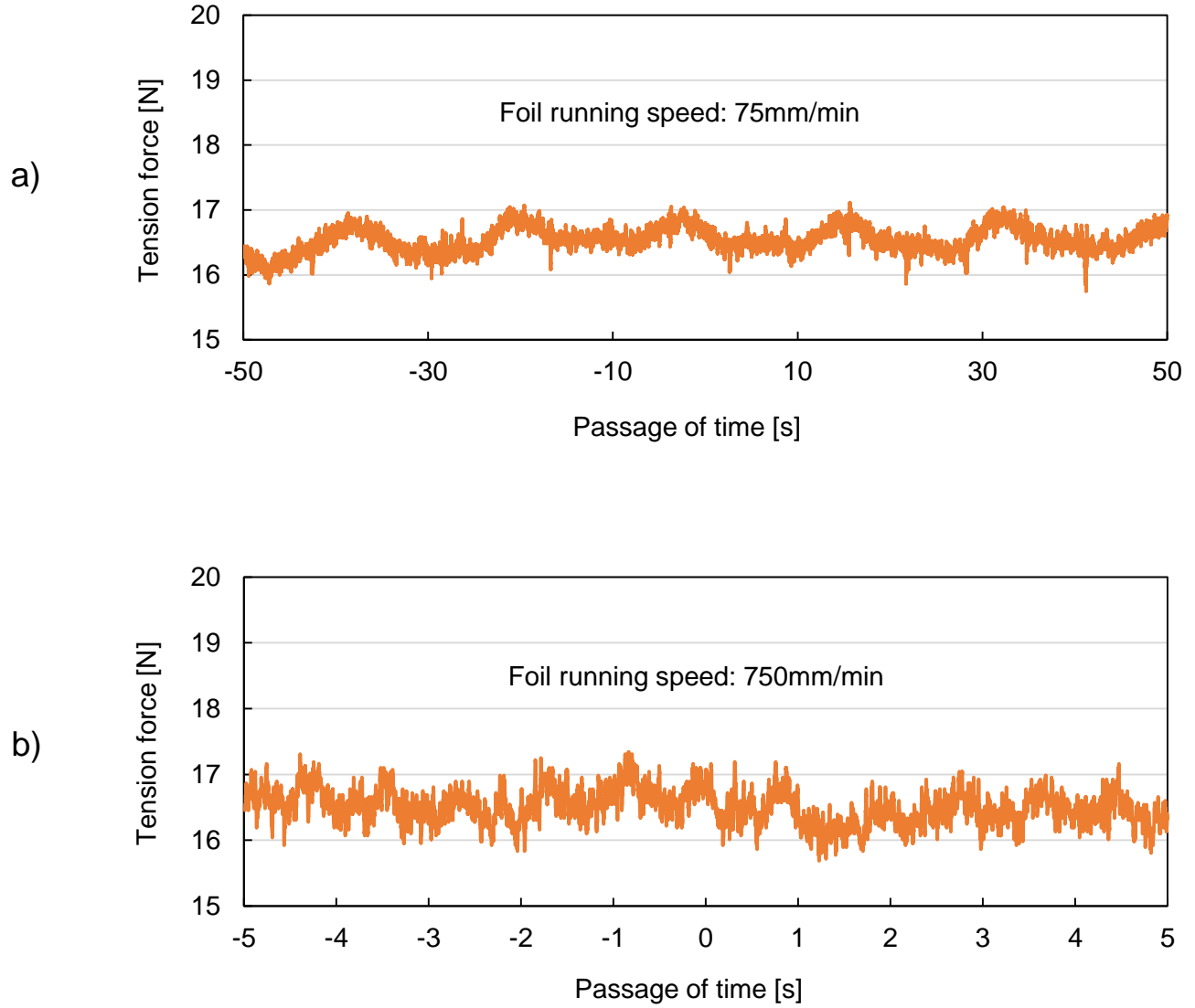
2) Foil displacement during foil running

The foil surface displacement along the displacement direction, as illustrated in **Fig. 4.15**, at a certain point during foil running was measured using a laser displacement sensor as shown in **Fig. 4.15**. The foil tool electrode width was 10mm in the measurement. The foil displacement here included not only the foil vibration amplitude during foil running but also the foil surface flatness error. The measurement was done when no machining was conducted. The measurement results, as shown in **Fig. 4.16**, showed that the displacement of the foil electrode surface increased with increasing the foil running speed and the displacement was around 10µm under the running speed of 1000mm/min. Except for the initial foil flatness error, insufficient tension force probably caused the foil displacement during the foil running. Although the foil tool electrode could sustain larger tension force, due to the limited conditions, the maximum tension force was no larger than 18N in the present work.

The fluctuation of tension force during foil running was also detected by the designed tension force transducer under different foil running speed without machining. The fluctuation of the tension force, as shown in **Fig. 4.17**, was around 1N during foil running. With increasing the foil running speed, the fluctuation of the tension force became more frequent, however, the fluctuation amplitude was still around 1N.
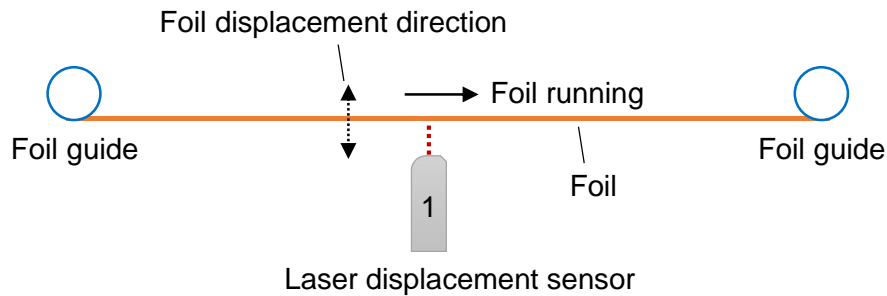
Fig. 4.15 Illustration of measurement of foil displacement during running with on machining (top view)

Fig. 4.16 Variations of tension force during foil running under different foil running speed
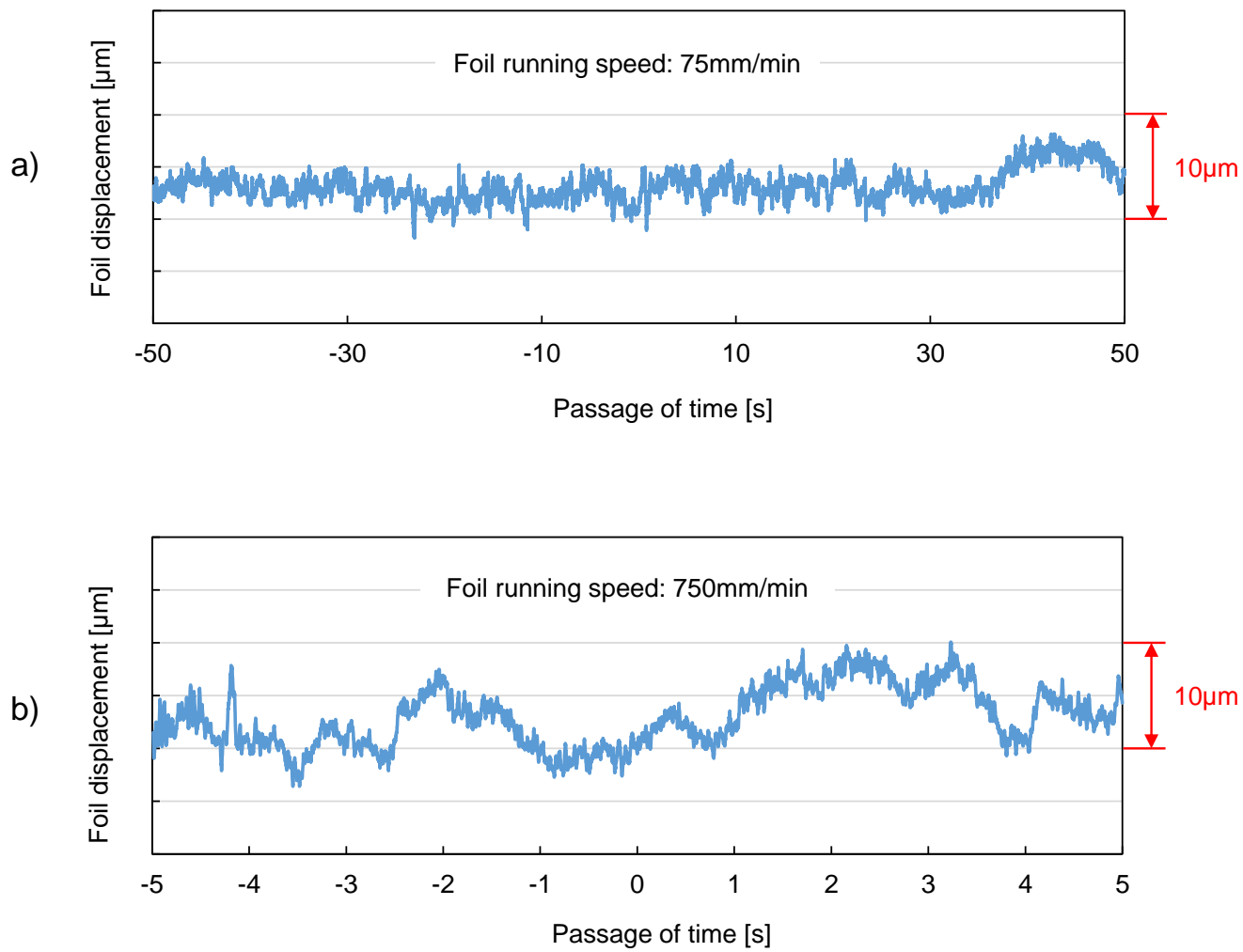
Fig. 4.17 Displacement of foil electrode during foil running under different foil running speed
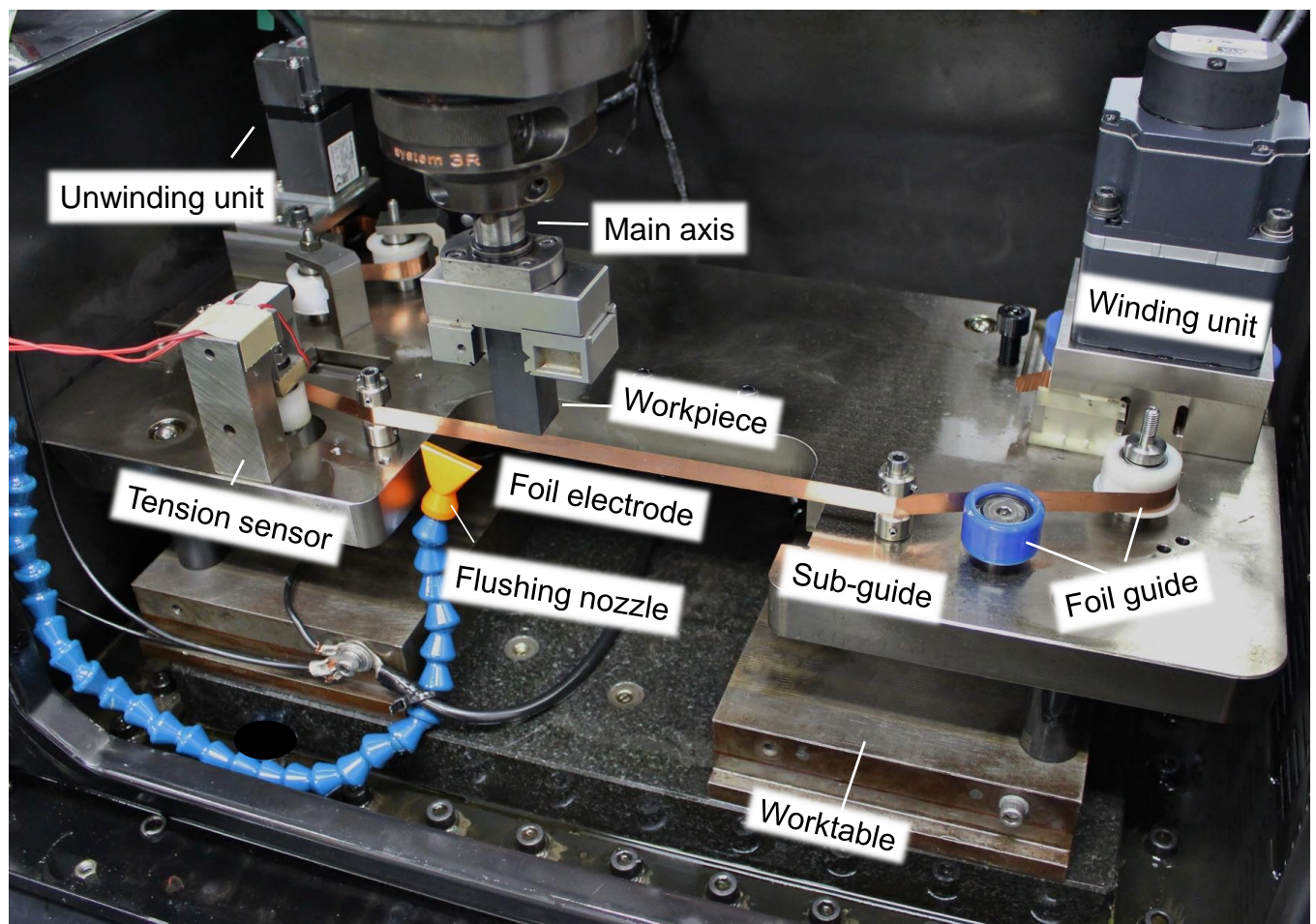
4.4 Experiments of running foil EDS

The present section describes the slicing performance of the developed running foil EDS method.

4.4.1 Experiment setup and method

Experiments of EDM slicing of SiC by running foil electrode was conducted on a commercialized sinking EDM machine (*Sodick C32*). The developed foil running system was placed on the worktable of sinking EDM machine as shown in **Fig. 4.18**. The foil was winded by the foil winding system independent of the EDM machine. A workpiece (SiC) was fixed on the main axis and servo fed downwards to the foil electrode to realize servo slicing process. All the machining area was submerged in EDM oil. **Table 4.2** shows the machining conditions used in the experiments.

Fig. 4.18 Photograph of experimental setup of running foil EDM slicing of SiC

Table 4.2 Experimental conditions

|	
Tool polarity	(-)
Tool electrode	Copper foil
Foil thickness [µm]	30
Slicing thickness of workpiece [mm]	20
Preset slicing depth [mm]	3
Slicing direction	⊥c axis
Measured pulse duration [µs]	2
Pulse interval [µs]	15
Discharge current [A]	14
Open voltage [V]	120
Servo voltage [V]	60
Dielectric	EDM oil

4.4.2 Machining stability

In the experiments, the machining speed and stability were investigated by measuring the feed of the main axis using an electrical micrometer. **Fig. 4.19** shows the measured displacement of the feed axis during machining. It can be seen that the feed of the main axis was not constant but accompanied with low frequency periodical retractions. The reason for the instability of the main axis feed was investigated. It was found that the fluctuation of the position of the foil electrode along the feed direction, as shown in **Fig. 4.20**, was the main reason for the retraction of the feed axis during machining. By comparing **Fig. 4.20** with that of **Fig. 4.19**, it can be found that the main axis retraction amplitude and frequency coincides with those of the fluctuation of the vertical position of the foil electrode.

The fluctuation of the foil electrode was found to be caused by the uneven width of the foil electrode resulted from the manufacturing process of the foil tool electrode. On the other hand, it was considered that the clearance gap between the foil tool and foil guide probably also contributed to the fluctuation of the foil electrode as shown in **Fig. 4.21**, which also shows the measurement method of foil movement in the feed direction by utilizing an electrical micrometer. However, if there was no clearance left, foil electrode would be deformed due to the interaction between the thin foil and the foil guide during running.
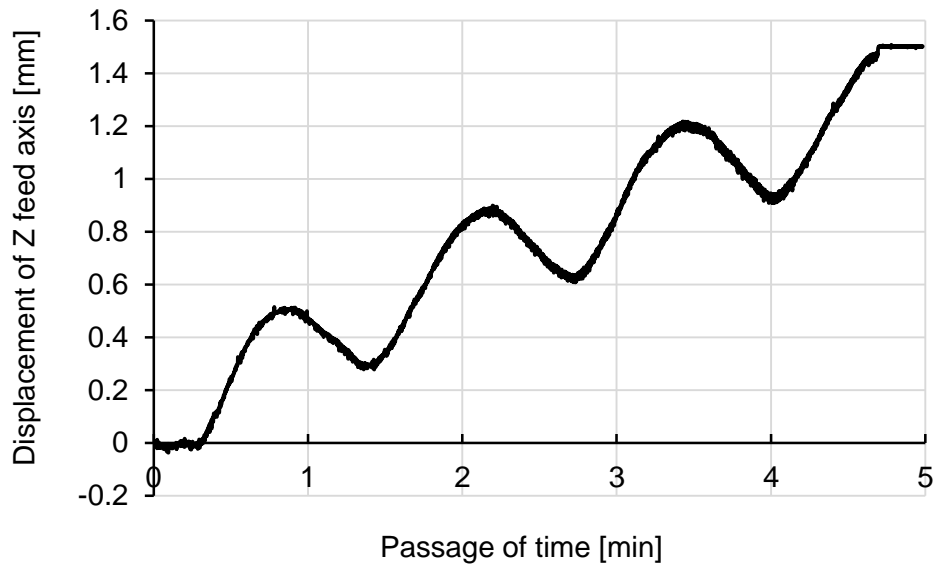
Fig. 4.19 Displacement of feed axis in running foil EDM slicing of SiC (Foil running speed: 75mm/min)
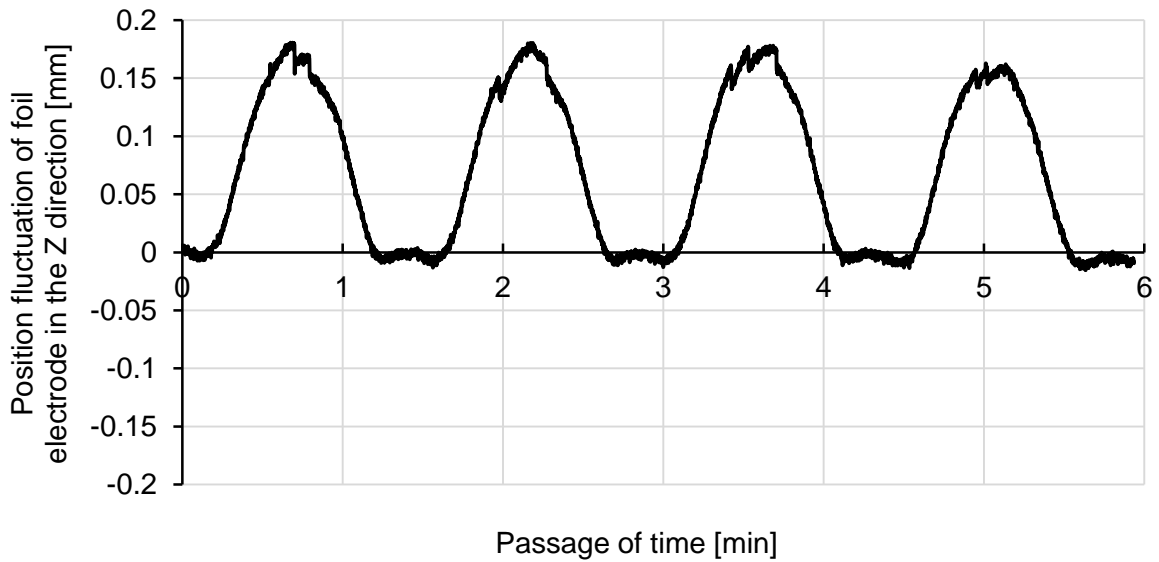

Fig. 4.20 Position fluctuation of foil electrode in the Z direction (Foil running speed: 75mm/min)

On the other hand, since the time period of the fluctuation was around 1min, the response speed of the servo feed control system was sufficiently high to response the fluctuation of the foil electrode. It was therefore considered that the fluctuation of the foil electrode did not affect the machining speed. However, the foil position error resulted from the foil winding system and the foil flatness error of itself etc. may bring about frequent short circuiting and influence the machining stability, which in consequence affected the slicing speed. It will be discussed furthermore with regard to the slicing speed of the wing foil EDS method in later sections.
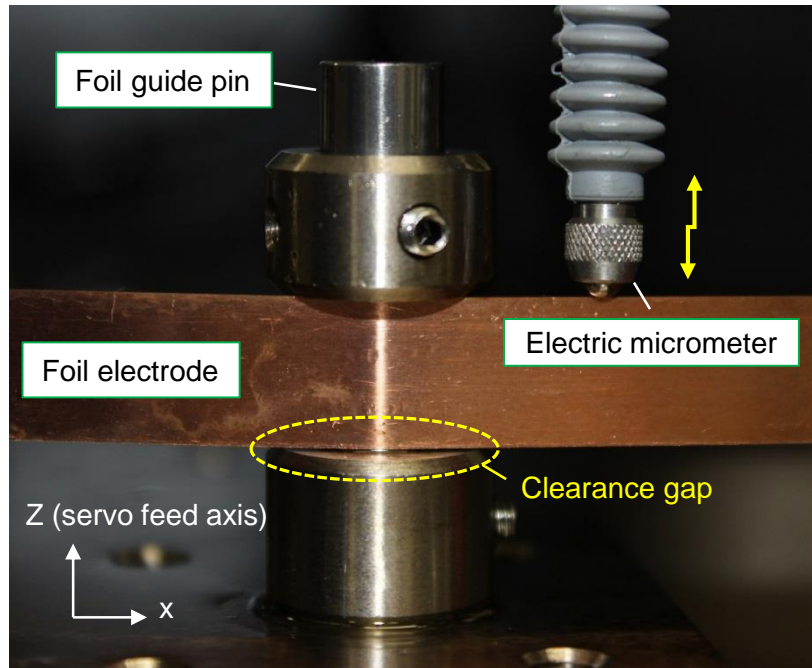
Fig. 4.21 Illustration of measurement of the fluctuation of foil electrode along the feed direction, Z

The machined slit depth along the workpiece thickness direction is shown in **Fig. 4.22**. It can be seen that after machining, the sliced slit depth was not uniform but changing, which confirmed the analysis model of discharge gap (refer to **Fig. 4.3**) in running foil EDS method. By substituting the tool wear ratio, workpiece removal length per unit time, the workpiece thickness and the foil running speed into Eq. 4.7, the angle θ can be calculated, which is shown as the red line in **Fig. 4.22**. It was found that, however, the experimental results did not coincide with the analysis result. Instability of machining was considered as the main reason. The analysis in Section 4.2.1 was based on steady state conditions. In the actual machining experiments, however, the machining was not always in steady state due to many influence factors such as the foil positioning error during foil running, the changing flushing conditions and discharge concentrations etc. which probably caused a large tool length wear ratio and a low machining rate.
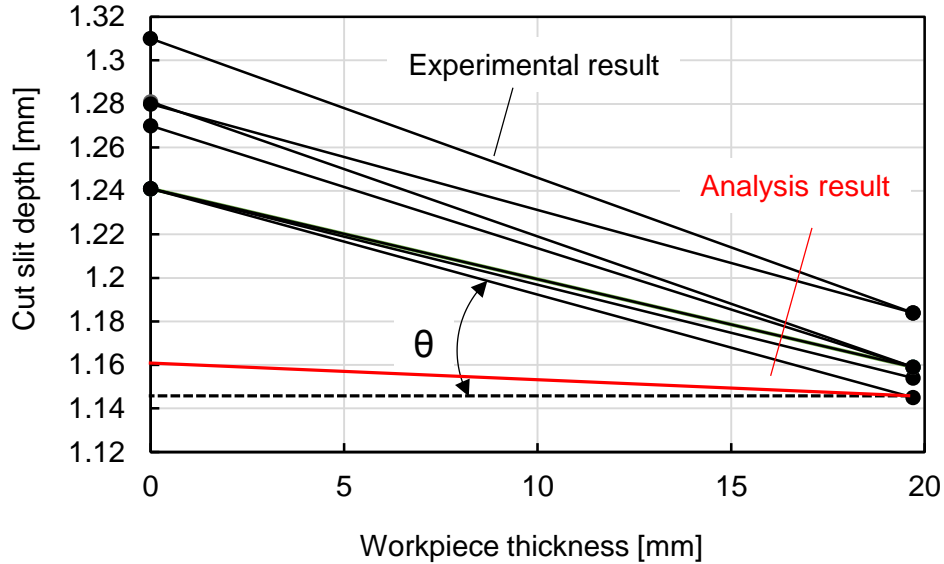
Fig. 4.22 Machined slit depth variation along workpiece thickness direction

4.4.3 Influence of workpiece position

In the running foil EDS method, the workpiece could be fed to the foil electrodes either downward or upward. In other words the workpiece position during machining could be set differently as shown in **Fig. 4.23**. It was considered that the workpiece position may influence the removal of EDM debris in the discharge gap, which consequently influenced the machining rate. Therefore, the influence of the workpiece position on the cutting speed was investigated. The experimental conditions were set the same as that shown in **Table 4.3** for both experiments. Specifically, the foil was kept no running in the experiments. Only the workpiece position and servo feed direction was changed. **Fig. 4.24** shows the experimental results. It can be seen that when the workpiece was upside, higher machining speed was obtained, which may indicate that when the workpiece was set upside, EDM debris in the discharge gap could be removed more easily due to the gravity. This probably resulted in a better gap conditions and was considered as the main reason for the higher machining speed when the workpiece was set upside.
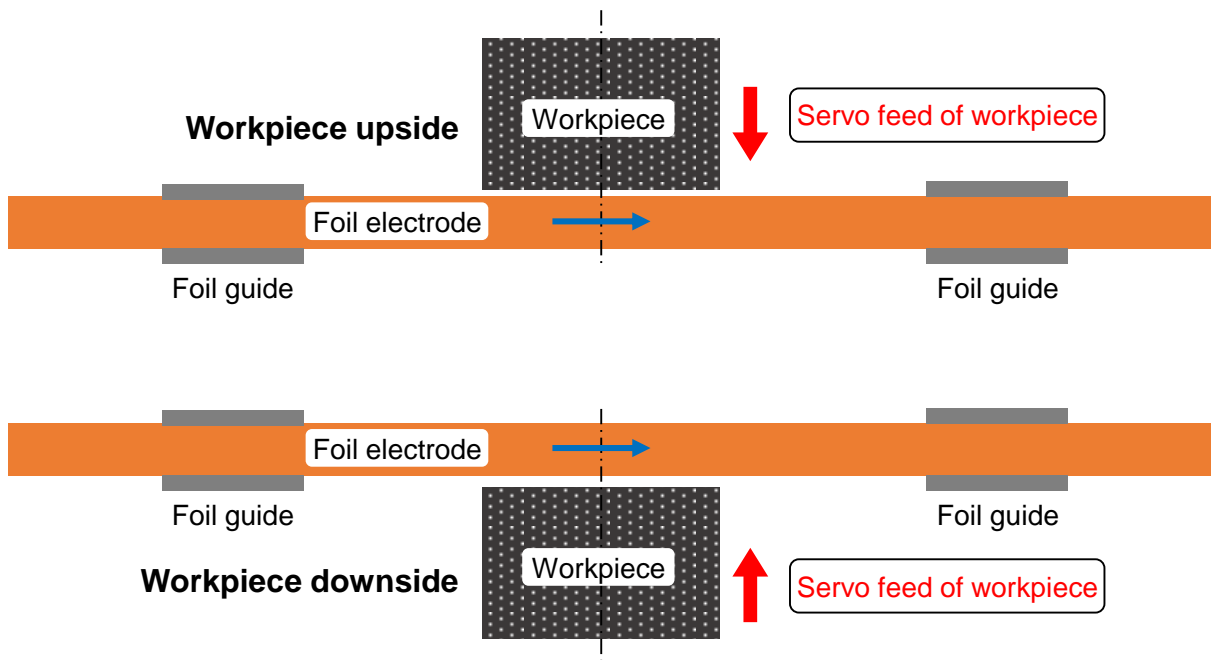
Fig. 4.23 Illustration of the workpiece position in running foil EDS
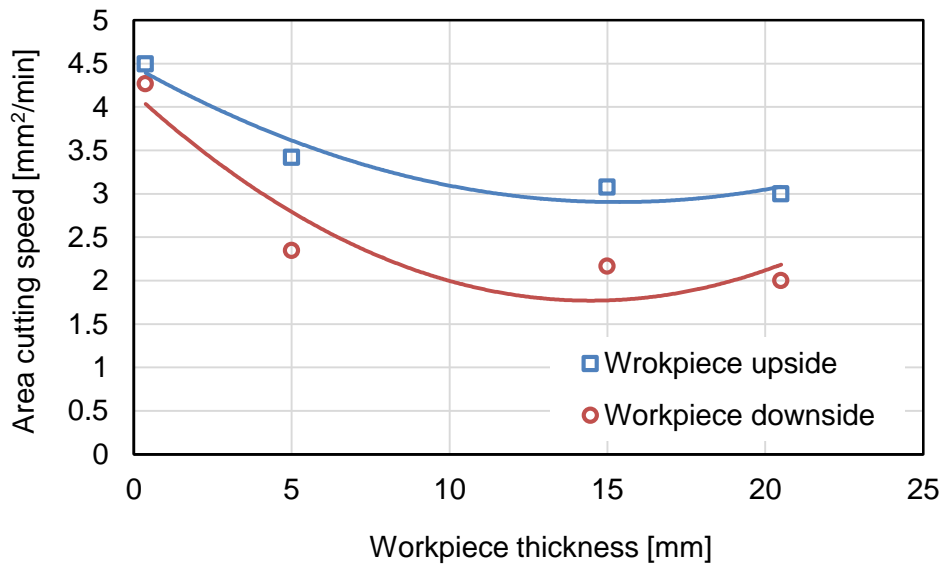

Fig. 4.24 Influence of workpiece position on the machining rate (Foil running speed: 0)
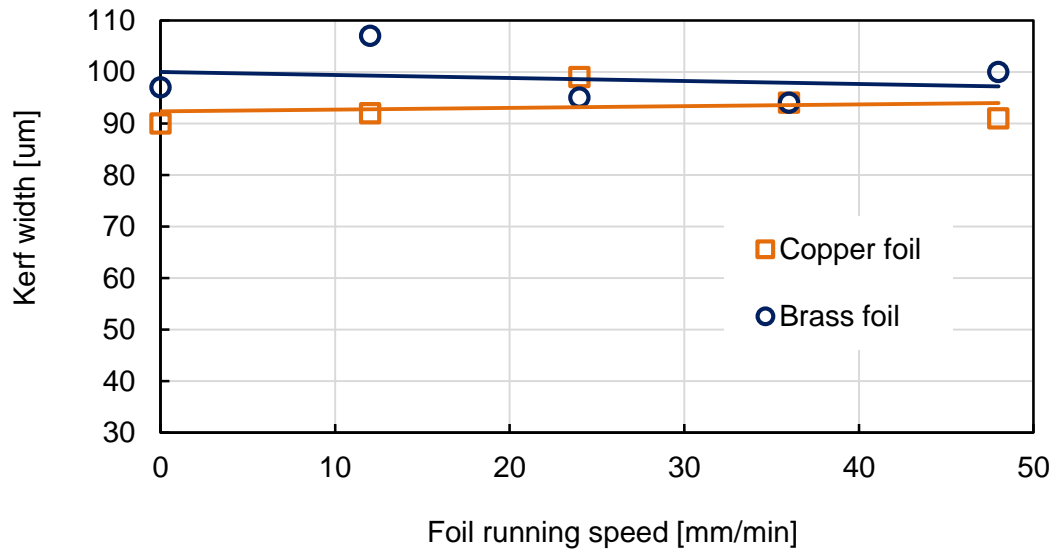
4.4.4 Influence of foil running speed

The influence of the foil running speed on the slicing speed and kerf width was investigated. Since the length of the foil electrode was limited, the foil running speed was changed from 0 to 50mm/min in the experiments. The workpiece position was set upside. Besides, both copper foil and brass foil were used in the experiments to investigate their performances. The experimental results of the machining speed and kerf width are shown in **Fig. 4.25** and **Fig. 4.26** respectively. With increasing the foil running speed, the foil EDM area cutting speed was increased in both cases, which indicated that the gap conditions were improved by the running of the foil tool electrode. However, since the foil running speed was very low (no higher than 50mm/min), the impact of the foil running speed was not significant. With regard to the cut kerf width, the average value was near 100μm, as shown in **Fig. 4.26**. The machined kerf shape was uniform, as shown in **Fig. 4.27**. However, the kerf was not totally straight which indicated that the foil electrode position was probably changed during machining due to short circuit etc.

On the other hand, it was confirmed that brass foil could also be applied for slicing SiC. However, copper foil electrode presented a higher cutting speed compared to that of brass foil electrode in the present work.
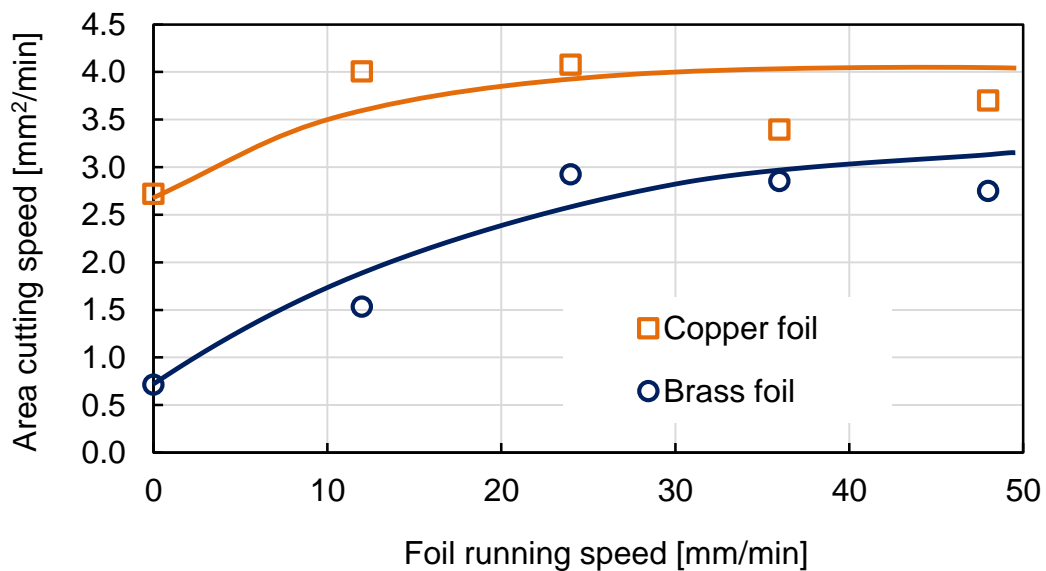
Fig. 4.25 Influence of foil running speed on the area cutting speed of SiC

Fig. 4.26 Inlet kerf width variation with increasing the foil running speed

Kerf width shape
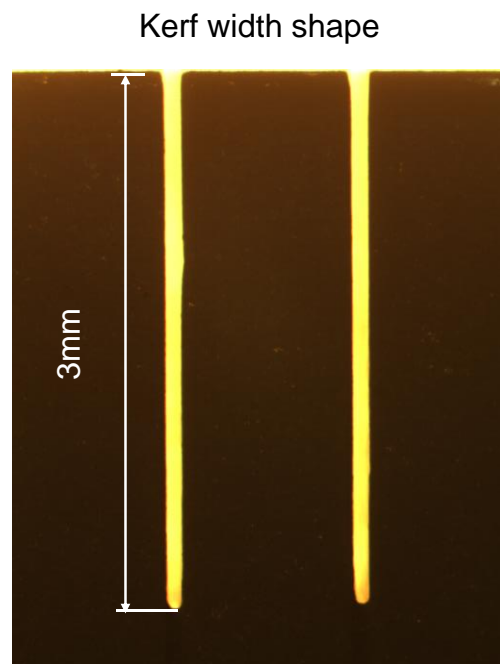
Fig. 4.27 Shape of the cut ke rf

4.4.5 Influence of flushing conditions

Fig. 4.28 shows a comparison of the feed speed between winding foil EDS with and without flushing. **Fig. 4.29** shows the flushing method used in the experiments. Dielectric was flushed from the bottom up into the slicing slit form one side of the workpiece using a nozzle. It was found that when flushing was applied to the working gap, at the very first, the workpiece feed speed did not show significant difference. With increasing the cut depth, the machining with flushing showed a higher feeding speed due to the improved gap conditions.
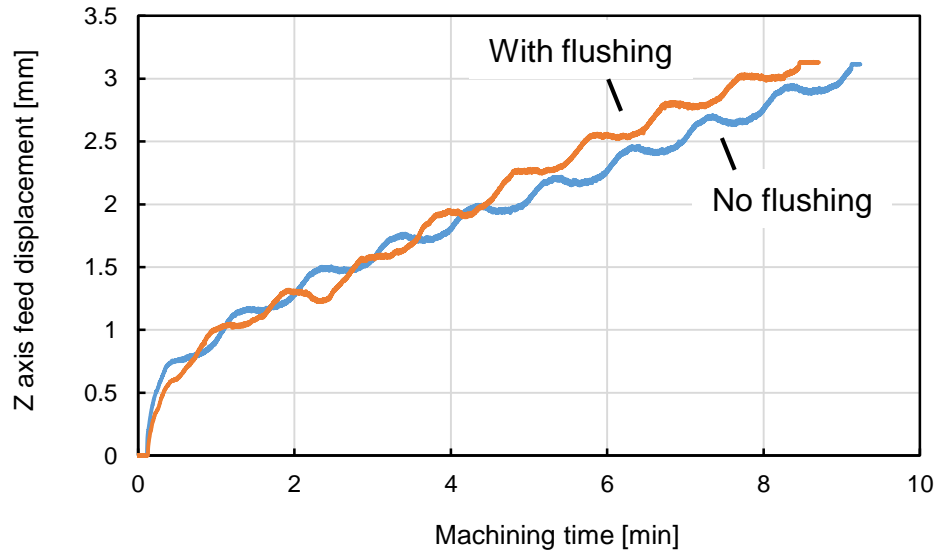
Fig. 4.28 Influence of flushing on the feed displacement of Z axis
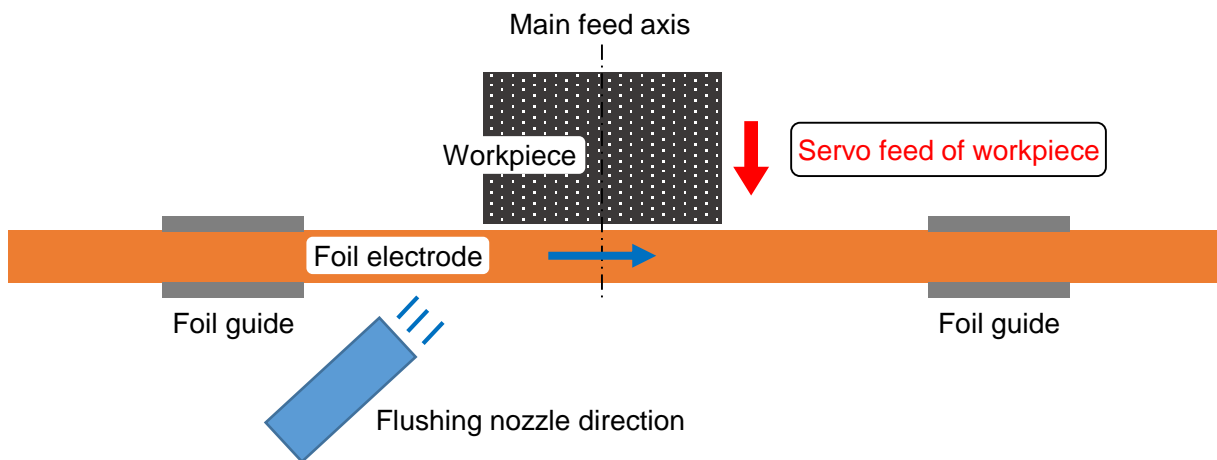
Fig. 4.29 Illustration of the flushing method in foil EDM slicing experiments

4.5 Conclusions of Chapter 4

In Chapter 4, EDM of SiC by winding the band foil electrode in a unidirectional way was proposed in place of the reciprocating slicing method aiming to achieve a stable and constant slicing process. With regard to the mechanism of the winding foil EDS process, when the foil running speed is sufficiently high, the foil tool wear can be neglected and the foil EDM slicing method functions in the same way as the wire EDM. On the other hand, however, under a low foil running speed, with decreasing the foil thickness, the tool wear of foil would increase due to higher average heat flux, which was considered as the most significant difference from that of wire EDM process. In order to clarify the feasibility and performance of this method, the experimental setup for realizing running foil EDM slicing of SiC was developed and the characteristics of running foil EDS were investigated based on the developed experimental setup. The main conclusions were as the following:

1) The development of the foil running system including foil unwinding unit, foil guides, load cell, tension sensor, winding unit etc. was accomplished in order to realize winding foil EDM slicing of SiC ingot. Running foil EDS of SiC was performed successfully using thin foil electrodes (copper/brass) with thickness of 30μm. Compared with the multi-wire EDS method, the newly developed foil EDS presented a smaller kerf width of less than 100μm.

2) It was found that the running foil EDS could be performed even under the low foil running speed. By theoretic analysis of the tool wear under steady state of machining, it was considered that steady state too wear model could be formed and the foil tool wear length should be proportional to the tool electrode wear ratio and the slicing thickness of the workpiece and inversely proportional to the foil running speed under steady state.

3) No foil tool electrode is available on market currently. Therefore, foil tool electrodes were homemade in this research. Due to the limited conditions, however, the manufactured foil tool electrode width had some deviation. In order to perform high accuracy cutting, the foil tool electrode accuracy (dimension accuracy and shape accuracy) must be improved in the future.

4) The workpiece fixing position exerted an influence on the machining rate. When the workpiece was fixed upside relative to the tool electrode on the main axis and fed downwards to the foil tool electrode, higher machining rate could be obtained because EDM debris in the gap could be removed out more easily due to gravity.

5) Both high foil running speed and flushing of dielectric liquid could improve the machining rate by enhancing the discharge gap flushing conditions under the conditions used in the present work.

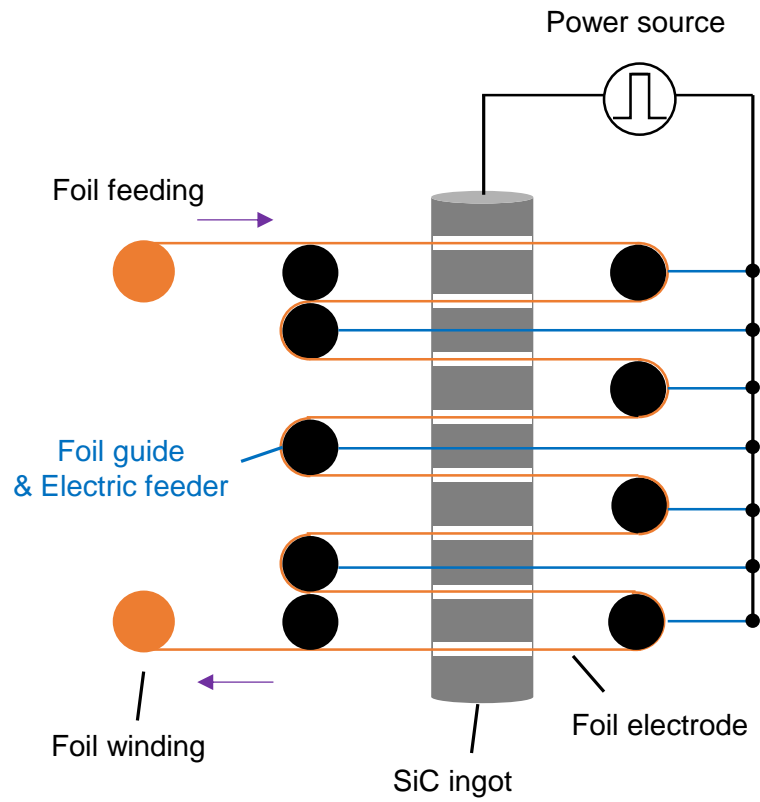# Chapter 5 Multi-discharge EDM of SiC by electrostatic induction feeding

5.1 Introduction

Even though the slicing speed of SiC by wire EDM is much higher than that of multi-wire saw method [26], only one wafer can be cut at one time, which results in a very low productivity. In order to improve the throughput of wire EDM slicing method, development of multi-wire EDM slicing method is inevitable which can realize multi-slice of wafers at the same time. As described in Chapter 1, the research and development of multi-wire EDS method have been started in the recent few years for the application of slicing SiC wafer [29-35]. However, this method is still under development and there are several problems that need to be enhanced and improved. Some of the main problems in multi-wire EDS which have been discussed in the previous chapters are listed as in the following:

1) Prevention of wire breakage

2) Increase of wire tension force

3) Improvement of wire running speed and stability

4) Reduction of wire diameter

In order to advance the multi-wire EDS method by overcoming its disadvantages in terms of wire breakage, wire vibration and wire diameter, multi-discharge EDS by utilizing foil electrode (hereafter referred to as multi-foil EDS) instead of wire was proposed in this study. **Fig. 5.1** shows the schematic diagram of the proposed multi-foil EDS method. In this method, a thin foil electrode is winded several turns along the foil guides to form a foil web. Slicing is conducted by feeding the workpiece towards the foil electrode web. The structure is similar to that of multi-wire EDS system except that the foil tool electrode guides are different from that of wire. The advantages of the proposed multi-foil EDS system are that: 1) by utilizing foil electrode, the frequent wire breakage problem can be reduced. 2) With the increased cross section area of foil electrode compared with that of wire electrode, the tension force of the tool electrode can be increased. 3) Consequently both the tool electrode running speed and the tool electrode vibration during running can be improved under the larger tension force. 4) The foil tool thickness can be several times smaller compared with the diameter of the currently used wire electrode [30, 35], which makes it possible to further reduce the kerf width of slicing SiC in the future.

On the other hand, with regard to the multi-discharge circuit, in the currently developed multi-wire EDS method, as described in Chapter 1, introduction of large impedance is necessary to realize multiple discharges. However, introduction of large impedance in the discharge circuit will cause low energy efficiency due to the consumption of energy of the resistance. Furthermore, the increased impedance (mainly inductance X_L) in the discharge circuit will make it difficult to generate discharges with short pulse duration. Therefore, in this research, multi-discharge EDM by utilizing the electrostatic induction feeding (EIF) method [57] was proposed in place of the conventional pulse power supply to realize multi-discharge EDM considering its simplicity. Moreover, multi-foil EDS slicing of SiC by utilizing the EIF method was proposed. The characteristics of multi-discharge EDM by the EIF method was experimentally investigated and the feasibility of the proposed multi-foil EDS method was discussed.

**Fig. 5.1** Schematic diagram of multi-foil EDM slicing method

5.2 Multi-discharge EDM of SiC by electrostatic induction feeding method

5.2.1 Introduction

It is known that EDM is a material removal process by mean of electrical discharges which are generated intermittently by a pulse generator. It is normal that only one discharge can occur in one pulse, which is considered as one principal factor resulting in one of the major problems of EDM process: low material removal rate. The machining rate in EDM is determined by the product of material removal volume of single discharge and the discharge frequency. To improve the machining rate, it has been a longstanding goal to generate multiple discharges in a single pulse duration in order to increase the total discharge frequency.

Kunieda et al. [58] firstly developed a multi-spark EDM system which consists of twin electrodes as shown in **Fig. 5.2**. In this method, in a single pulse, one discharge occurred in the gap between the tool on the left side and the workpiece and another discharge occurred in the gap at the same time between the tool on the right side and the workpiece, which could improve the machining rate and energy efficiency considerably. However, in this method the maximum number of electrodes was two and the maximum possible improvement of machining speed was at most two times higher than that of conventional EDM. Han et al. [59] proposed a parallel spark EDM method utilizing RC type discharge circuit as shown in **Fig. 5.3** which could generate multiple discharges at the same time. However, since there was no interval time between discharges in the RC type pulse generator, additional switching circuit was required to preset the discharge interval.

In the multi-wire EDS method that are being developed currently (refer to in Chapter 1), multiple discharges were generated by utilizing current limiting impedances introduced in the discharge circuits [29, 30, 31, 34, 35]. It is considered that, however, there are some disadvantages in this method. On one hand, the introduction of large impedance will cause low energy efficiency due to the consumption of energy of the resistance. Moreover, large impedance (mainly inductance X_L) in the discharge circuit will make it difficult to generate discharges with short pulse duration. On the other hand, introduction of large impedance requires a specifically developed pulse power source and electricity feed system. Taking the multi-wire EDS system developed by Mitsubishi Corporation for instance [34, 35], a high frequency AC pulse power supply is considered necessary to increase the impedance inside the wire electrode in order to realize multi-discharge EDM. Therefore, a new multi-discharge EDM method by the electrostatic induction feeding (EIF) was proposed in this study. With the electrostatic induction feeding method, it becomes easier to realize multiple discharges with just a simple bipolar pulse power source. The principle, advantages and machining characteristics of multi-discharge EDM by EIF are discussed in the following.
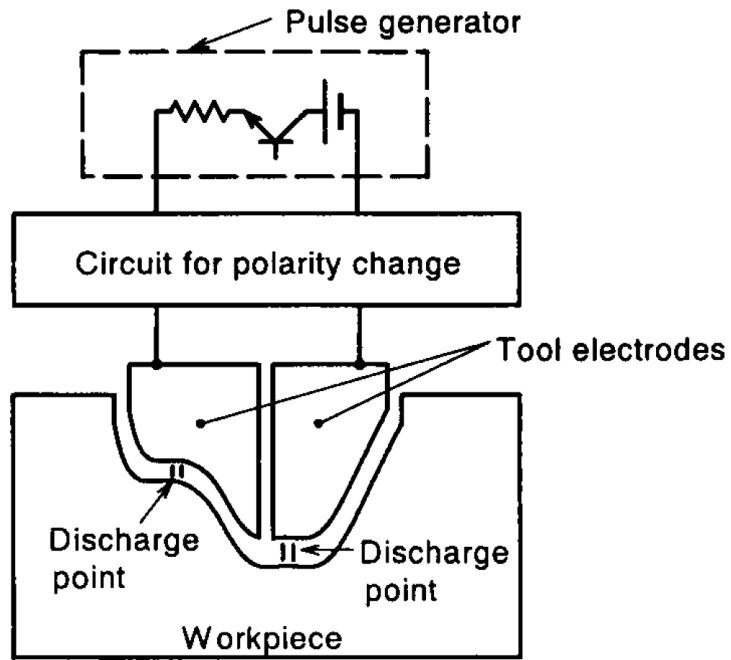
**Fig. 5.2** Principle of multi-spark EDM with two electrodes [58]
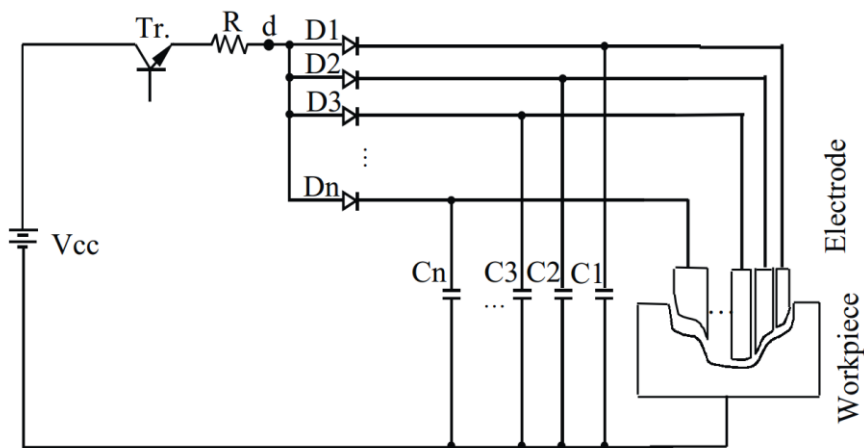
Fig. 5.3 Circuit of parallel-spark EDM by RC type pulse generator [59]

158

5.2.2 Principle and advantages of electrostatic induction feeding method [57, 60, 61]

Fig. 5.4 and **Fig. 5.5** shows the discharge circuit and principle of EDM by the electrostatic induction feeding method respectively. The pulse power source with amplitude E_0 is coupled to the discharge gap through the capacitor C_1 (hereafter referred to as feeding capacitor). C_2 indicates the capacitor formed in the discharge gap between the tool electrode and the workpiece. When the output voltage of the pulse power supply becomes E_0, capacitor C_1 and C_2 will be charged and electrical potential difference between the tool and the workpiece will be generated (i). Since no charging resistance exists, the gap voltage can rise up to the maximum in a very short time. The gap breaks down by the large gap voltage and discharge occurs (ii). During discharge, the gap voltage will be kept constant at 20V which is the discharge voltage of the arc plasma. The electric charges will flow due to the discharge in the circuit. The charges stored in C_2 will be transferred to the opposite electrode through arc plasma instantaneously. At the same time, new electric charges flows into the arc plasma through the power source E_0 and capacitor C_1. After the discharge, no charges flows in the circuit and the gap voltage is kept constantly the same as that of the discharge voltage. Next, after the polarity of the pulse power source is reversed and becomes zero, the electric charges in the circuit will be relocated and the tool will be negatively charged this time (iii). Due to this, the gap voltage becomes large and discharge occurs again with an opposite polarity (iv). After the discharge, the gap will be charged again as (i') when the next pulse of the power source is applied to the gap. Machining is conducted by repeating the cycle of (i)~(iv). From (ii) and (iv), it can be seen that the discharge current is bipolar in EDM by the electrostatic induction feeding method.

Based on the principle discussed above, it is known that electricity is fed to the discharge gap through the feeding capacitor, which makes it possible to feed electricity to the discharge gap without contact, as illustrated in **Fig. 5.6** [57]. This is considered as an exceptional advantage of this method.

In addition, compared to RC type pulse generator, the electrostatic induction feeding method provides discharge interval time between consecutive discharges because only one discharge occurs in each half cycle of the pulse power source and the gap voltage will keep constant as the discharge voltage, 20V, after the discharge until the output voltage of the pulse power supply is changed. While in RC type pulse generator, the gap voltage will increase right after the discharge.

a) RC type pulse generator   b) EDM by electrostatic induction feeding method
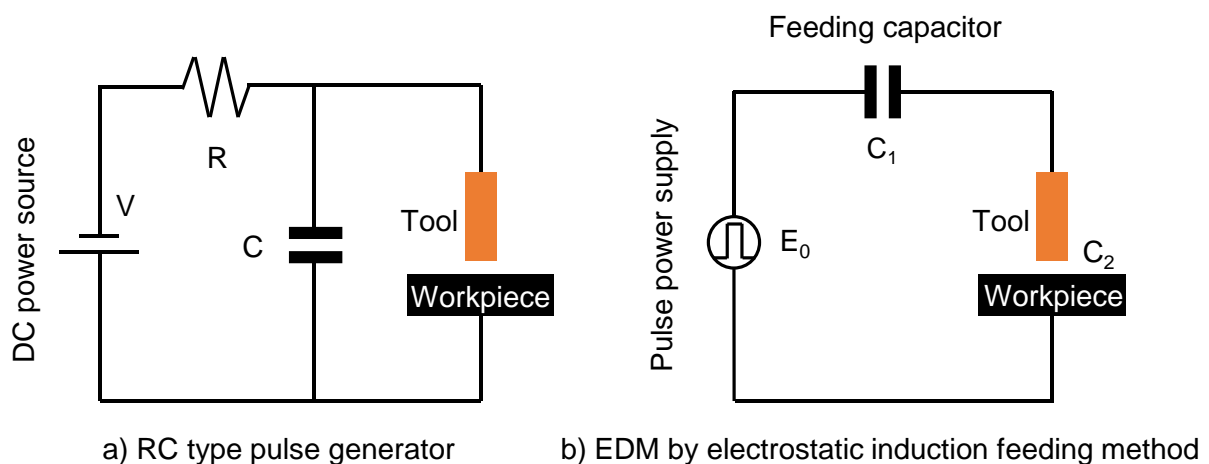
Fig. 5.4 Comparison of discharge circuit of EDM between different pulse generators
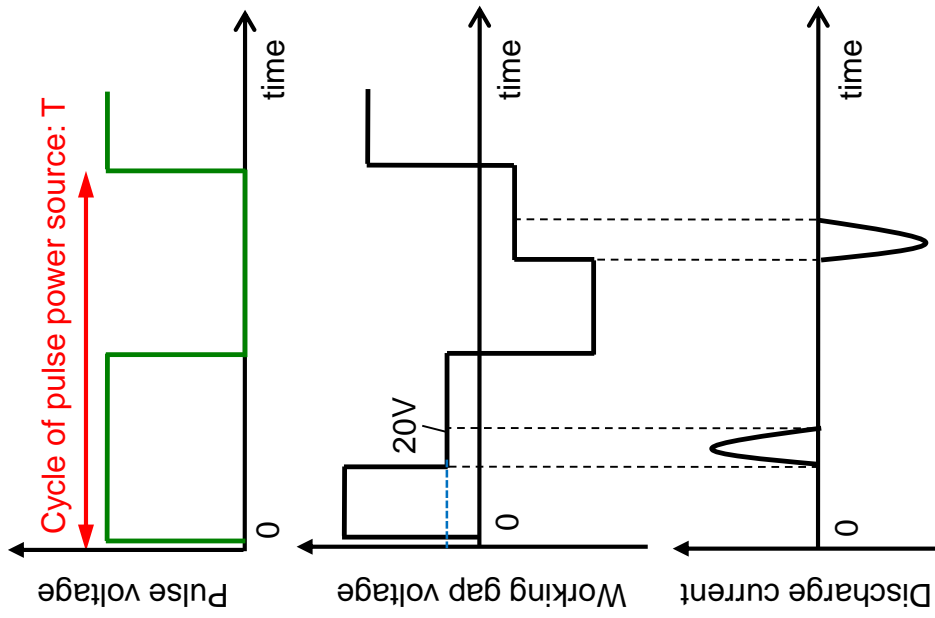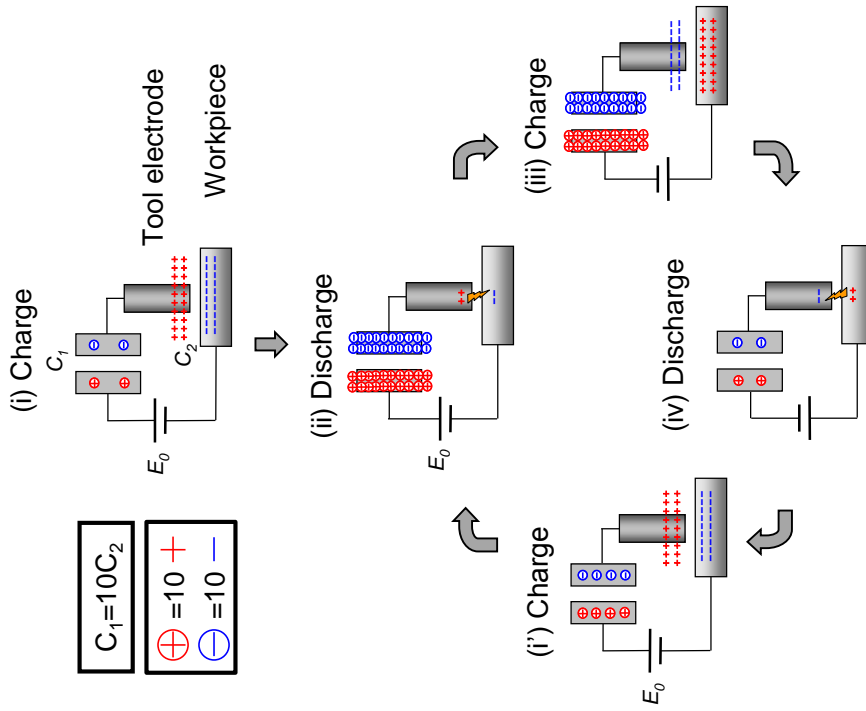
Fig. 5.5 Electrical discharge machining by electrostatic induction feeding method [57, 60, 61]

160
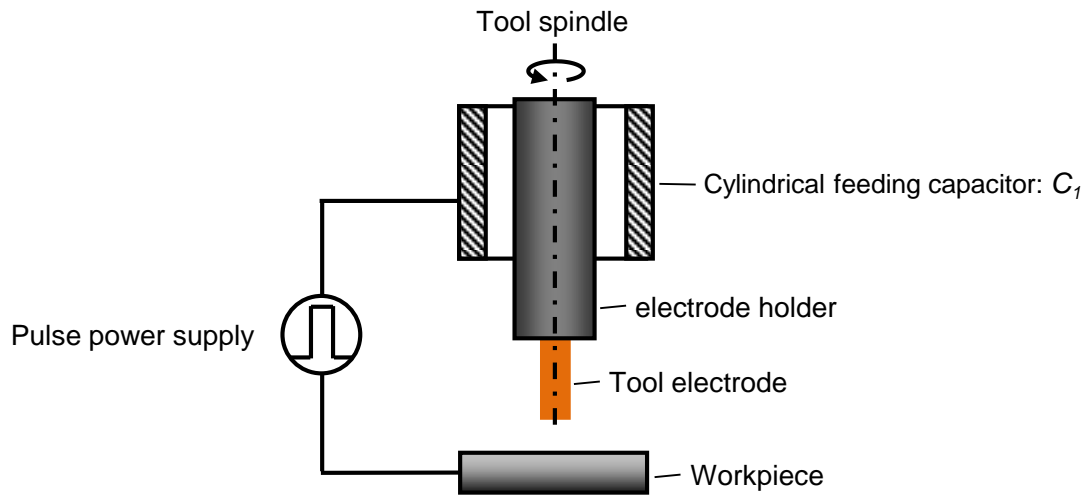
Fig. 5.6 Schematic diagram of non-contact feeding in EDM by electrostatic induction feeding [57]

5.2.3 Principle of multi-discharge EDM by EIF method

In EDM by the electrostatic induction feeding method, the electrical charges stored between the capacitor and the tool electrode are preserved as long as discharge does not occur. Based on this mechanism, multi-discharge EDM by the electrostatic induction feeding method can be realized by arranging multiple pairs of capacitor and tool electrode parallelly.

Fig. 5.7 shows the equivalent circuit of multi-discharge EDM by utilizing the electrostatic induction feeding method. Multiple tool electrodes are set parallelly and connected to the pulse power source through feeding capacitors C_1. Every tool electrode is electrically insulated to each other and the pulse power source is coupled to each working gap through each corresponding feeding capacitor respectively taking advantage of the electrostatic induction effect. Each working gap between the tool electrode and the workpiece is regarded as a discharge channel.

As shown in **Fig. 5.7**, during a half cycle, if one discharge occurs at the working gap G_1, the stored charges on the other discharge channels do not move because the output of the pulse power supply does not change. Therefore, the potential difference between the tool electrode and the workpiece can be preserved. In other words, occurrence of discharge at one discharge gap does not affect the gap voltage at other discharge channels. Therefore, with the change of the polarity of the pulse voltage, discharges can occur independently at each discharge channel and multiple discharges can be realized in the same single pulse duration by just arranging a number of tool electrodes parallelly. The fundamental principle of this method was firstly investigated by using two electrodes in parallel in micro EDM process which confirmed two discharges in a single pulse of power supply voltage [62]. In the present work, the multi-discharge EDM method has been improved further which enables to generate multiple discharges (more than two) by utilizing multiple tool electrodes for practical applications. Owing to the multiple discharges in a single

pulse, it is be expected that the machining speed can be improved greatly by increasing the discharge frequency.

On the other hand, in all the previous research, EDM by the electrostatic induction feeding method was applied for micro-machining with feeding capacitance in the order of pF. In the present work, however, electrical discharge machining by the electrostatic induction feeding method by using large feeding capacitance in the order of μF is proposed and the feasibility and characteristics of applying this method for rough machining is investigated.
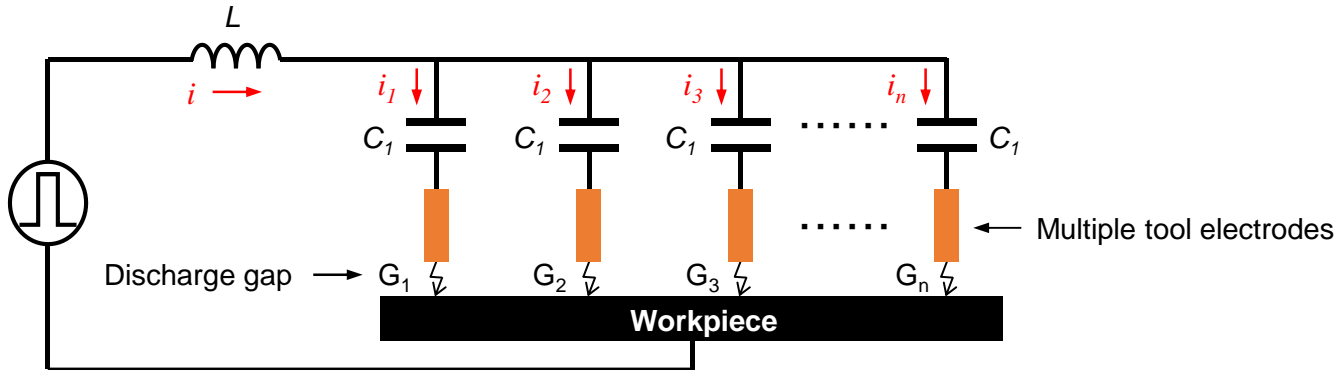
Fig. 5.7 Schematic diagram of multi-discharge EDM by electrostatic induction feeding method.

5.2.4   Advantages of multi-discharge EDM by EIF method

At first, multi-discharge EDM enables improvement of the machining speed. Theoretically the machining rate can be improved by only increasing the number of tool electrodes, with no need for extra complex circuit and dedicated pulse power source.

Second advantage of this method is that the machining speed and accuracy can be improved at the same time since total discharge energy per unit time can be very large, while single discharge energy can be kept small owing to separate feed of electricity.

Third, comparing with multi-discharge by RC pulse generator [59], the electrostatic induction feeding method enables interval time between discharges with no need for additional switching circuit.

At last, as discussed before, the electrostatic induction feeding enables no contact feeding of electricity, which is considered as a very important and unique merit of this method for multi-discharge EDM.

5.2.5   Proposal of multi-discharge EDS of SiC by EIF method

Based on the advantages discussed above, it is considered that the proposed multi-discharge EDM by the electrostatic induction feeding method (hereafter referred to as multi-discharge EIF EDM) can be applied

162

to slice SiC ingot as an alternative method. **Fig. 5.8** shows the schematic diagram of the proposed multi-foil EDM slicing of SiC ingot by using the electrostatic induction feeding method.

In this method, foil electrodes are separated with each other so that electricity can be fed separately to each foil electrode. Therefore, each separate foil electrode is winded by a separate foil winding system. Pulse power supply is coupled to the foil electrodes through the feeding capacitors as shown in the figure. In principle, the circuit is the same as that shown in **Fig. 5.7**.

However, due to the limited conditions in this research, the proposed multi-foil EDS experimental system could not be accomplished. In order to verify the feasibility of multi-foil EDS by EIF method and investigate the machining performances, multi-discharge EIF EDM coring, as an alternative method, was developed to conduct the multi-discharge EDM experiments. The developed multi-discharge EIF EDM coring method can be used for coring SiC ingot, which will be described in detail in the following sections.
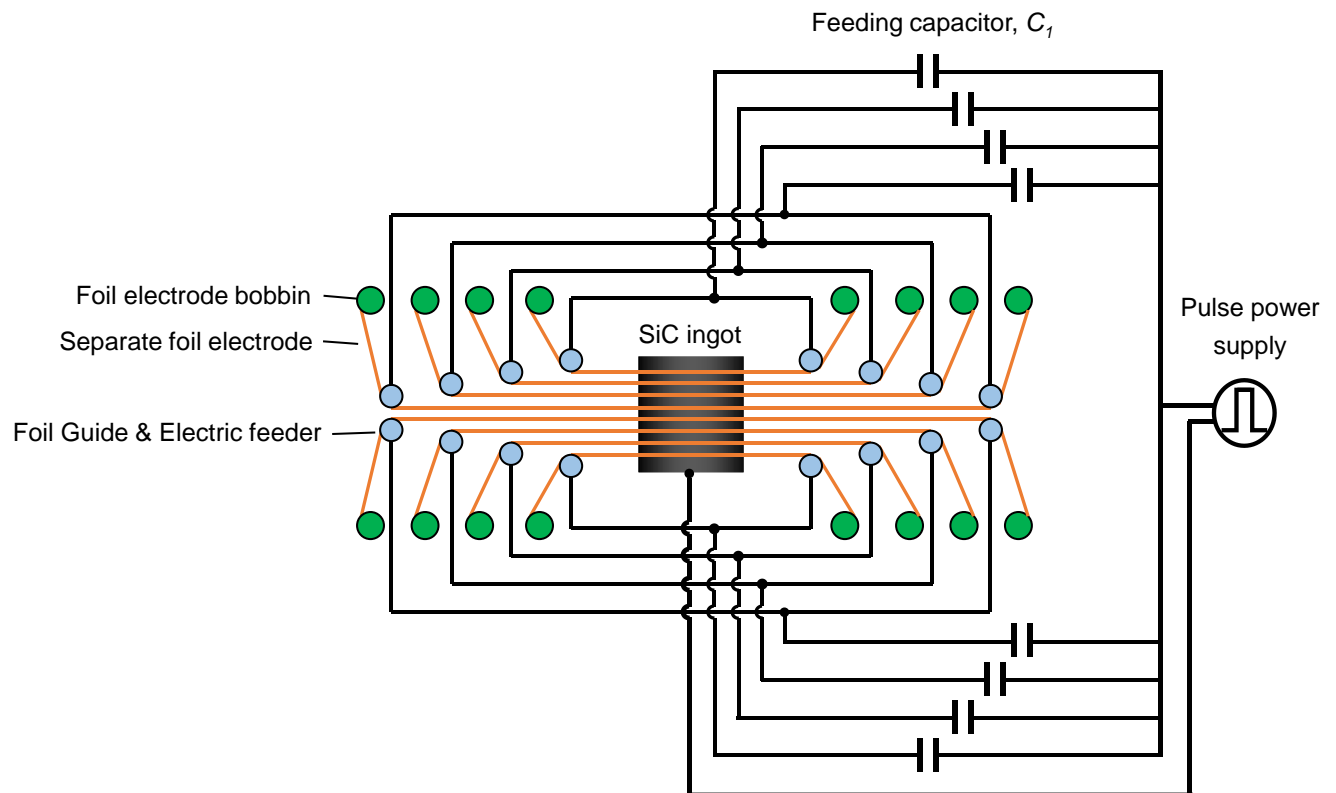
Fig. 5.8 Schematic diagram of multi-foil EDS by electrostatic induction feeding method

## 5.3 Application of multi-discharge EIF EDM on coring of SiC

5.3.1 Background

In the manufacturing process of SiC wafer, coring is another important subject. In the fabrication process of single crystal SiC ingot/wafer, cracks or defects are generated occasionally due to thermal or mechanical causes resulted from the manufacturing process, for example, crystal growth, multi-wire saw process and the like, as illustrated in **Fig. 5.9**. Since single crystal SiC material is very expensive, in order to maximize the material utilization and save the no defect part of ingot/wafer, demands for coring of SiC ingot has been increasing. On the other hand, due to the super high hardness of SiC, EDM was proposed to coring SiC material instead of conventionally used mechanical machining methods.

Normally wire EDM is considered as an easy and suitable method for coring an undamaged SiC cylinder from a larger damaged wafer/ingot. However, due to the high residual stress distributed in the peripheral region of the ingot resulted from the ingot manufacturing process, breakage of ingot along cleavage planes of SiC will occur easily when wire electrode is cutting into the ingot from the circumference of ingot. Therefore, instead of wire EDM, a new EDM coring method based on sinking EDM was proposed in this research to realize EDM coring of SiC ingot by utilizing a rotating tool electrode. By the developed method, multi-discharge EIF EDM was realized which will be described in the later sections.

On the other hand, with the purpose of practical application of the developed EDM coring method on normal sinking EDM machine, EDM coring experiments based on conventional pulse generator was also conducted to investigate its performance.
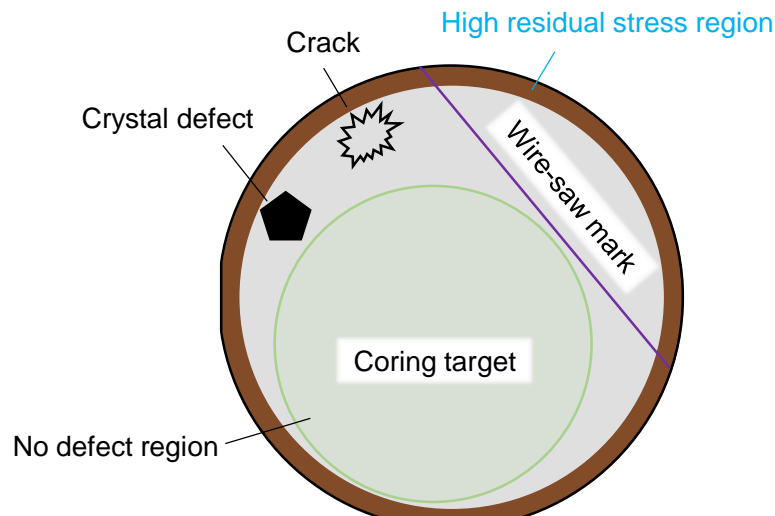
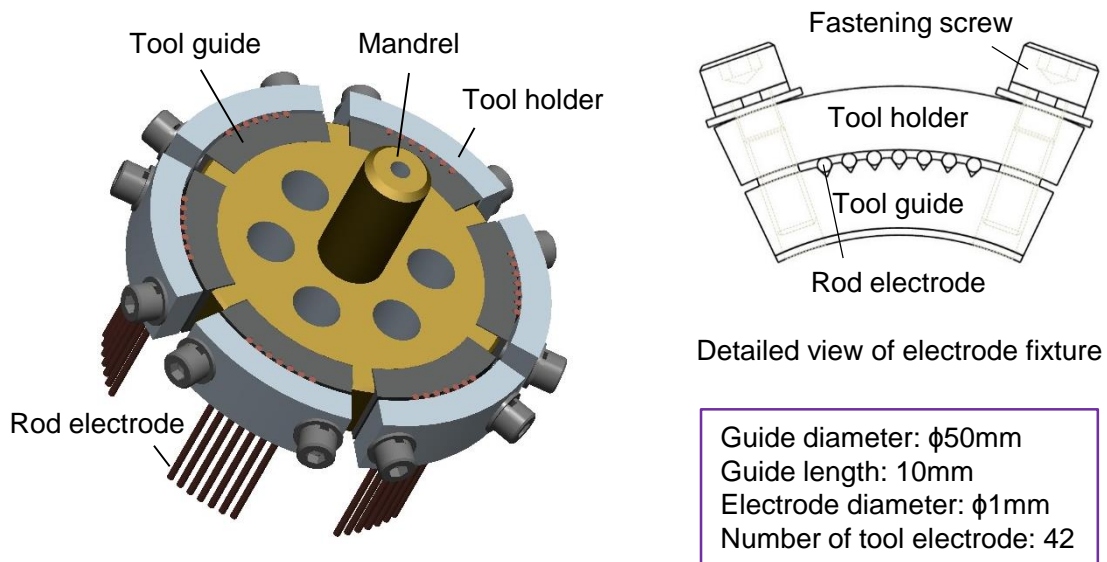**Fig. 5.9** Illustration of coring of SiC ingot/wafer

5.3.2 EDM coring of SiC by conventional pulse generator

Before the multi-discharge EIF EDM experiments, EDM coring experiments based on conventional pulse generator was firstly conducted to confirm the feasibility of the developed experimental setup.
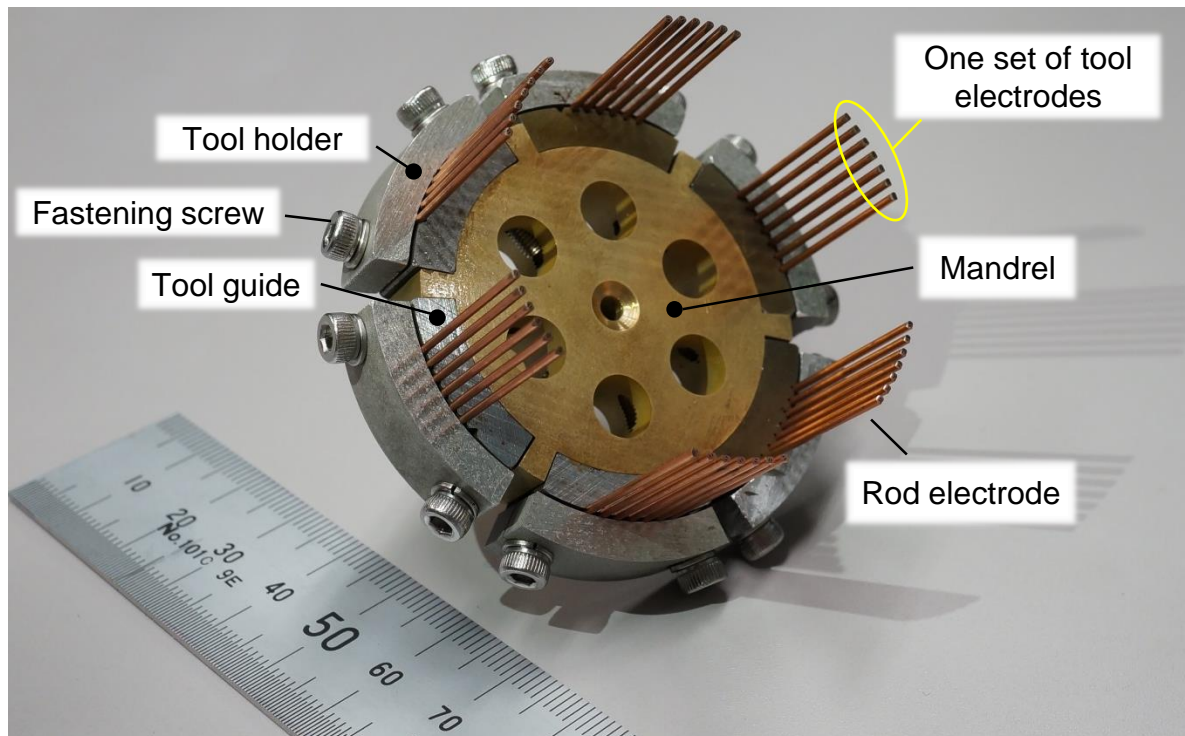
5.3.2.1 Experimental setup and machining method

For coring the SiC ingot, a tubular tool electrode (like coring bit) is necessary. However, manufacturing of a tubular copper tool electrode with a small wall thickness has great difficulty. Meanwhile, the flushing condition will become worse with increase of the cut depth when using a whole piece of tubular tool electrode. Therefore, a new rotatory tool electrode setup specifically designed for coring SiC ingot, as shown in **Fig. 5.10**, was developed in this research. Copper rod was selected as the tool electrode due to its simplicity and easy accessibility. The rod electrode was fixed by a specially designed tool fixture of which the detailed structure is shown on the right side of **Fig. 5.10**(a). The tool electrode fixture mainly consisted of 3 components: mandrel, circular electrode guide with V-shape grooves and the outside circular holders. The mandrel (yellow part in **Fig. 5.10**) was used as the base (support) for fixing and rotating the rod tool electrodes. The circular V-shape electrode guide was divided into 6 segments so that separate feed of electricity could be realized for multi-discharge EDM process which will be described in detail in later sections. Rod electrodes were positioned along the V-shape groove guides and clamped tightly towards the guides by the outside circular holders using bolt screws along the radial direction. Each set of the tool electrodes were electrically insulated to each other. When the tool fixture was rotated, the trajectory of the rod tool electrodes would be a circle. By feeding the rotating tool electrodes towards the workpiece at the same time, a cylinder could be cut out.

The advantage of this design is that the tool electrode can be easily replaced after being worn. In the event of collision between the rod tool electrodes and the workpiece, only the bent rod needs to be replaced by a new one, while in the case of the tubular tool electrode the whole electrode should be replaced. Another strong point of the setup is that it can provide better flushing effect and better gap condition compared with that of one whole piece of tubular tool electrode, owing to the interspace between any two rod electrodes.

Fastening screw

Tool holder

Tool guide

Rod electrode

Detailed view of electrode fixture

Guide diameter: φ50mm
Guide length: 10mm
Electrode diameter: φ1mm
Number of tool electrode: 42

(a) Structuring drawing of the tool setup

(b) Image of the tool setup

Fig. 5.10 Tool electrode setup for EDM coring.

166

Fig. 5.11 shows the schematic diagram of the experimental setup used in the study. The rotating apparatus, which was composed of a drive motor, a timing pulley and a conveyor belt and a support frame, was installed on the main axis of the sinking EDM machine tool (*Sodick C32*).The developed tool electrode setup was fixed to the rotating apparatus by a collet chuck (range of rotating speed: 50~250rpm) in order to realize rotation motion of the tool electrode setup. The electricity was fed to the tool electrode through the rotating apparatus utilizing two carbon brush feeders. The machining was conducted by feeding the tool electrode along the z axis towards the workpiece while keeps the tool electrode setup rotating. Since the rotating trajectory of the rod electrodes was a circle, EDM coring could be realized.
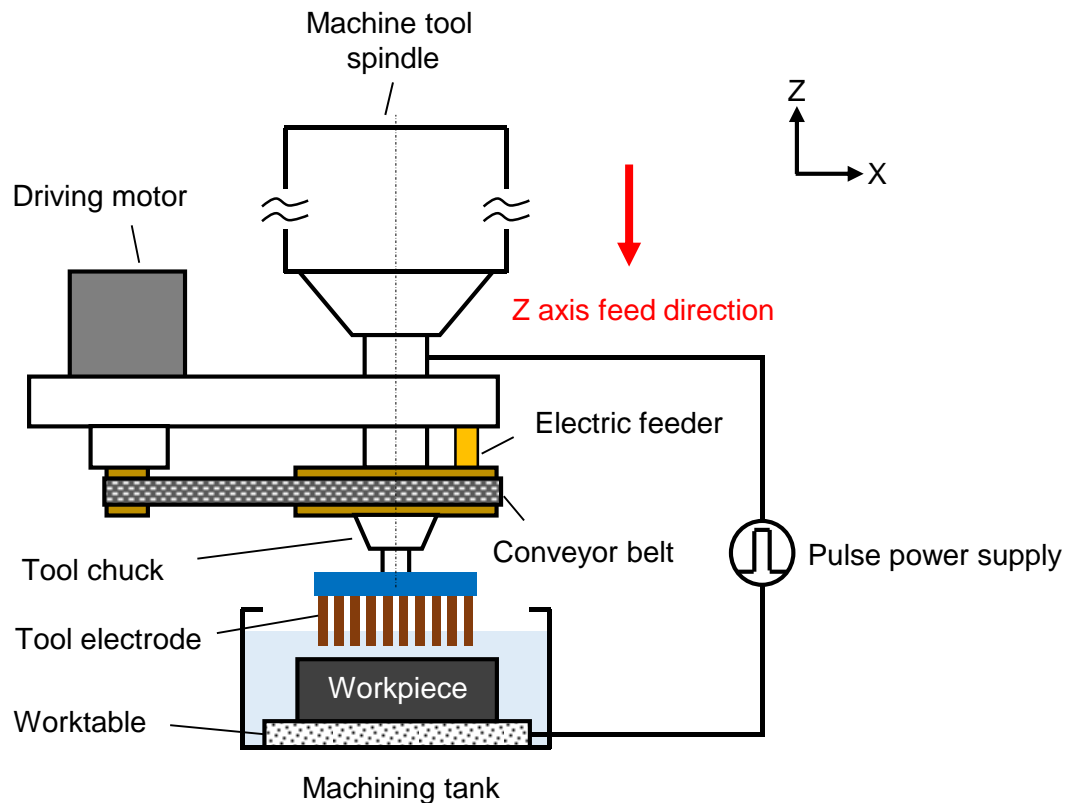
Fig. 5.11 Schematic diagram of the experiment setup of EDM coring of SiC ingot using the rotatory tool electrode setup.

5.3.2.2   Machining stability

Before machining SiC, carbon steel was subjected to the proposed EDM coring process to verify the feasibility. **Fig. 5.12**(a) shows a photograph of the machining experiment setup (workpiece: cold tool steel SKD11 plate). It was found out that steel material could be machined successfully with the developed EDM coring method. **Fig. 5.12**(b) shows the machined sample of steel workpiece. However, it should be noted here that appropriate machining conditions should be selected to perform the EDM coring process.

If not, thin copper rod electrodes may be deformed by collisions between the tool and the workpiece during machining due to, for example, too high feed speed etc.

The experimental conditions for machining SiC are shown in **Table 5.1**. In order to avoid collisions between the rotating tool electrode and the workpiece during feeding, an auxiliary high-voltage power source with large impedance, as illustrated in **Fig. 5.13**, was connected to the working gap in parallel with the conventional EDM pulse generator to enlarge the discharge gap and improve the discharge conditions. In addition, since the machining at the beginning stage was usually unstable due to a small gap width, jump motion of the tool electrode was applied at the beginning of machining. After the machining became stable, the jump motion was canceled to reduce the machining time. A stable machining process was achieved by this method as shown in **Fig. 5.14**, which shows that the increment of feed axis displacement is almost linear with the increase of the machining time.

Table 5.1 Experimental conditions

| Workpiece	SiC ingot
Tool electrode [mm]	Copper rod, $\phi 1$
Open voltage [V]	120
High-voltage synchronization [V]	240
Measured discharge current [A]	16
Preset pulse duration [µs]	2
Cut depth [mm]	2
Tool revolution number [rpm]	100
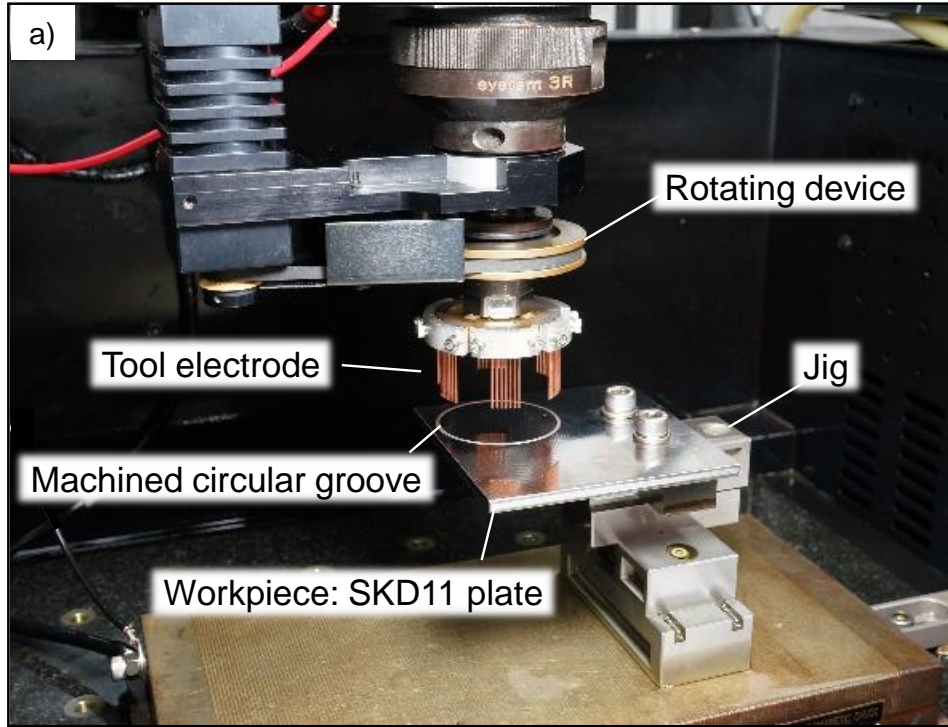
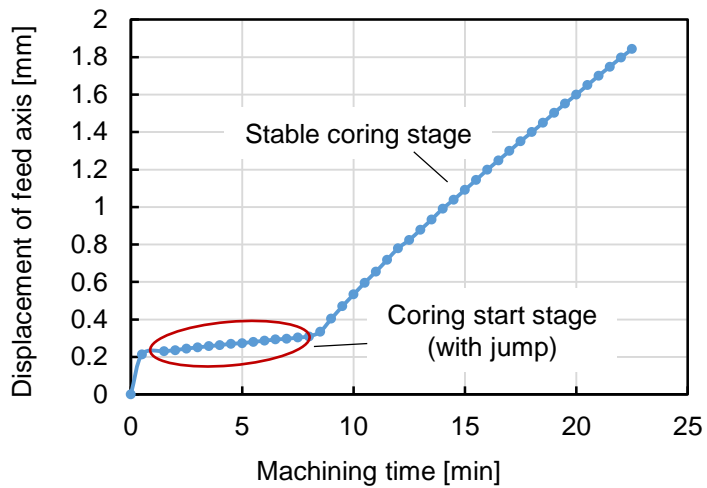a) Image of experimental setup of EDM coring

b) EDM coring sample: coring of steel workpiece

Fig. 5.12 Photograph of EDM coring example by the developed experimental setup
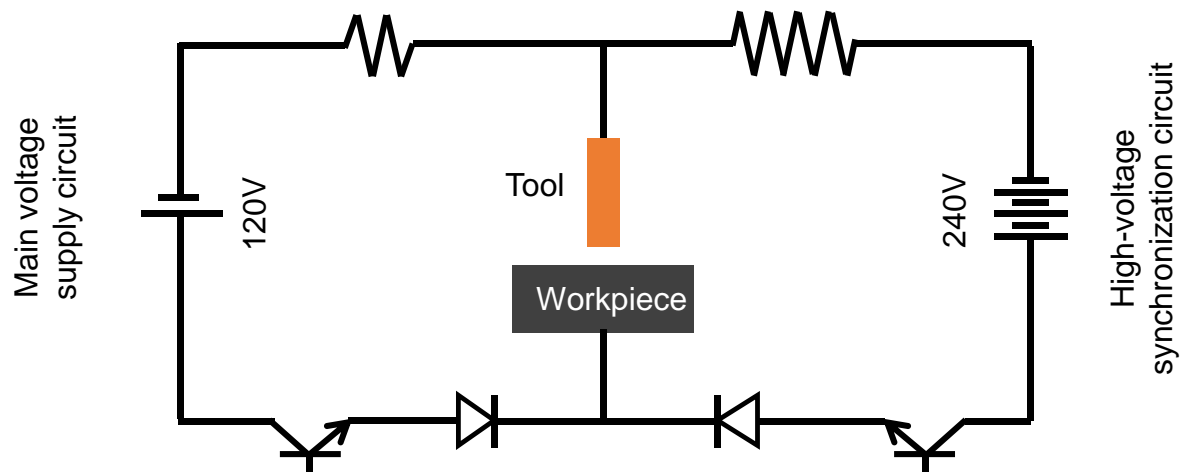
Fig. 5.13 Diagram of the discharge circuit used in the EDM coring experiments

Fig. 5.14 Displacement of the feed axis with the passage of the machining time during EDM coring of 2inch SiC ingot.

5.3.2.3 Cutting speed and tool wear

The typical discharge waveforms of EDM coring of SiC using the conventional pulse generator of sinking EDM machine are shown in **Fig. 5.15**. Due to the inductance existing in the circuit, the actual discharge duration was about 3.5µs, longer than the setting value, 2µs. Since SiC is a high resistivity material, the gap voltage measured was around 60V including the voltage drop in the workpiece, much higher than that in conventional EDM of metal materials, which is usually around 20V. Based on previous study, Joule heating effect playing an important role in EDM of SiC due to the high voltage drop. It was therefore considered that the pulse interval time should be set long enough for the plasma of every discharge to be completely extinguished to avoid discharge concentrations due to the Joule heating effect.
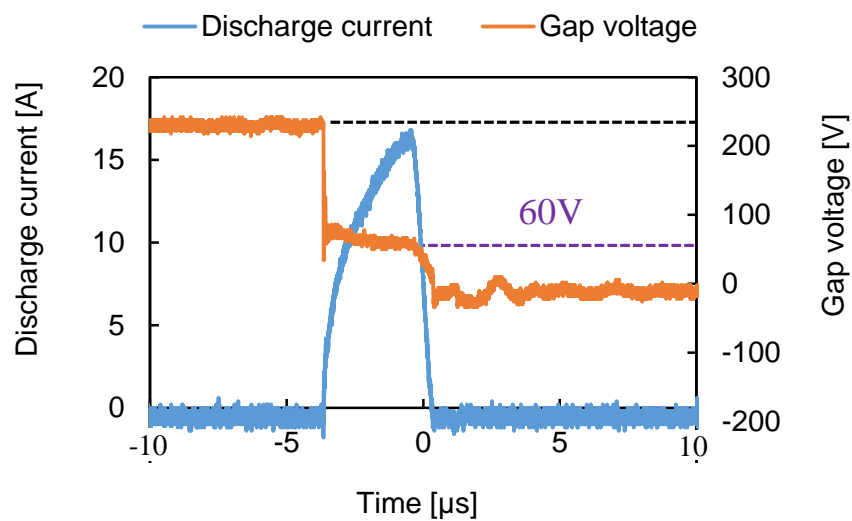
Fig. 5.15 Typical discharge waveform of EDM coring of SiC ingot by conventional pulse generator of sinking EDM machine (setting pulse duration: 2µs).

To clarify this, the influence of the duty factor on the machining performances was investigated by changing the duty factor value. The cutting speed (here refers to the feed speed per minute) variation with the variation of duty factor under different pulse duration is shown in **Fig. 5.16**. It should be noted here that under short pulse duration, 3µs, negative tool polarity was used to obtain a better machining rate based on the previous study and the energy distribution theory that more energy was distributed into anode than cathode [46, 47]. On the other hand, in order to reduce the tool wear as much as possible, experiments under conditions of long pulse duration, 30µs and positive tool polarity were also tried out, considering to take advantage of the deposition effect of carbon on the anode surface by the decomposition of working oil.
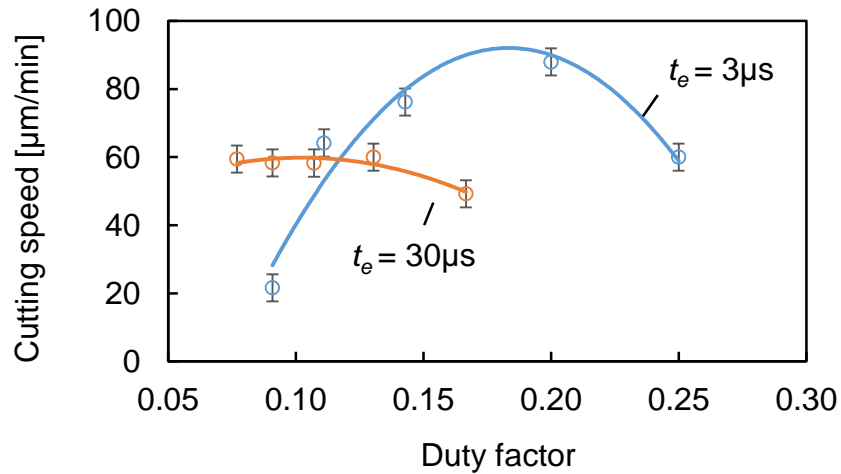
Fig. 5.16 Duty factor influence on the cutting speed under different pulse duration in EDM coring of SiC.

It was found by repeated trials that the D.F. should be set smaller than 0.2, otherwise stable machining could not proceed due to severe discharge concentrations. In addition, the long pulse duration required longer pulse interval time. **Fig. 5.16** shows that under the same duty factor, the long pulse duration resulted in a lower machining rate compared to that under the short pulse duration, which indicated that under the long pulse duration, material removal efficiency of single discharge was lower and stable machining became more difficult. The maximum feed speed was around 90μm/min taking into account the tool wear. Further increase of the duty factor would cause unstable machining. With respect to the tool electrode length wear ratio, according to **Fig. 5.17**, the long pulse duration under plus tool polarity did not help to obtain a lower tool wear ratio. On the contrary, the short pulse duration under minus tool polarity resulted in much lower tool wear ratio, which was around 30%.
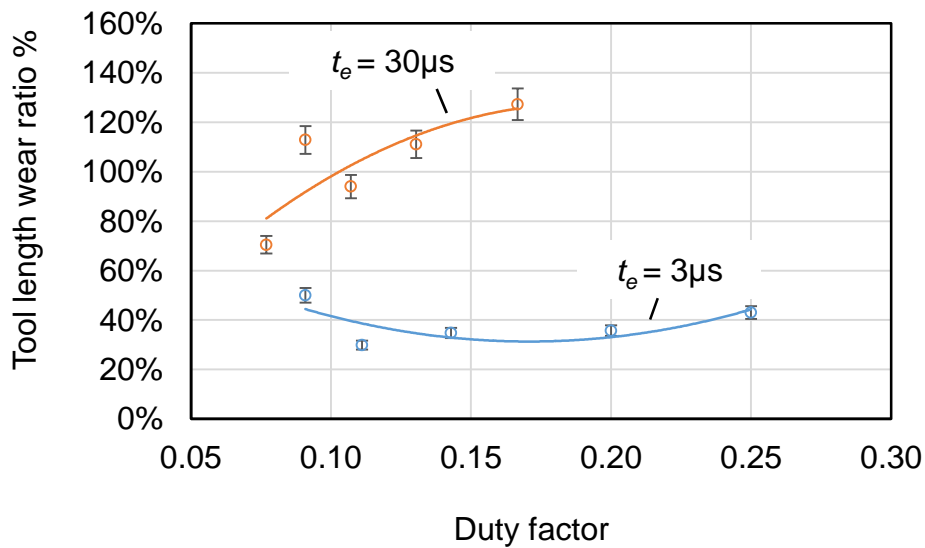
Fig. 5.17 Tool length wear ratio in EDM coring of SiC ingot.

172

5.3.3   Multi-discharge EDM coring of SiC by electrostatic induction feeding method

5.3.3.1   Tool electrode setup for multi-discharge EDM

The tool electrode setup used to realize multi-discharge EDM by the electrostatic induction feeding method (hereafter referred to as multi-discharge EIF EDM) is shown in **Fig. 5.18**. The structure was almost the same as the tool electrode setup illustrated in **Fig. 5.10**. The difference was that six insulated naflon sheets with thickness of 200μm were placed in the spaces between the mandrel and the circular tool guides to insulate each separate segment of tool electrodes so that separate feeding of electricity to each set of tool electrodes could be realized. In addition, copper rod electrodes were clamped tightly towards the V-shape tool guides using plastic bolt screws for insulation. Electricity was fed to each set of the tool electrodes by using 6 separate feeding capacitors. In this study, metallized polypropylene film capacitors (also referred to as plastic film capacitors), as shown in **Fig. 5.19**, were used as the feeding capacitors since they were suitable for high frequency charge and discharge circuit due to their excellent high frequency responsibility.
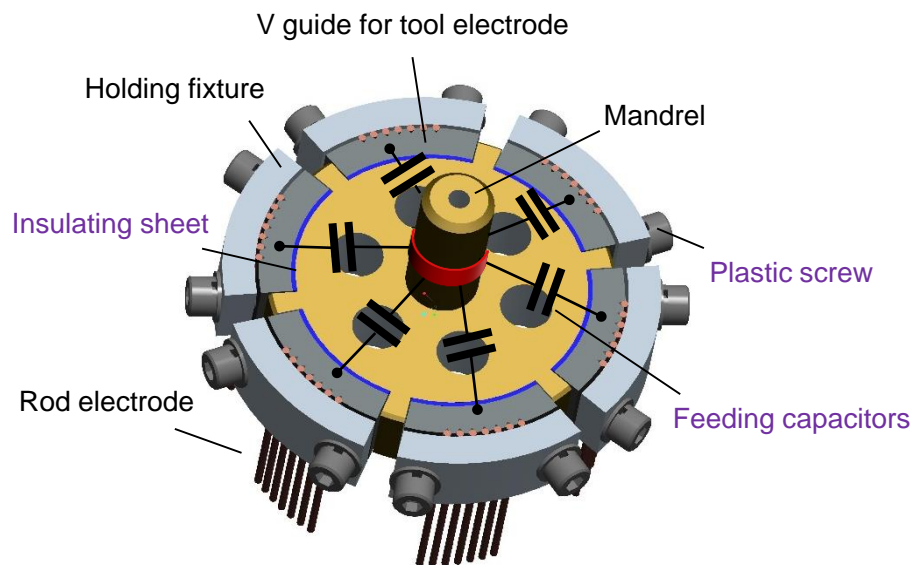
Fig. 5.18 Structure drawing of tool electrode fixture for realizing multi-discharge EDM by electrostatic induction feeding method.

Fig. 5.19 Image of the feeding capacitor used in experiments (plastic film capacitor)

5.3.3.2   Pulse voltage supply for multi-discharge EDM

Voltage supply with bipolar square waveform was used in the experiments to realize EDM by the electrostatic induction feeding method. The pulse power supply used in the machining was composed of two devices: a function/arbitrary waveform generator (*Agilent 33250A*) and a high power bipolar power source (*NF Corporation, BP4620*), as shown in **Fig. 5.20**. The waveform of the required voltage supply machining was firstly generated by the function generator and then the generated voltage signal was sent to the high power bipolar power source. The bipolar power source functioned as the pulse power supply by amplifying the voltage signal sent from the function generator to the required value of voltage for machining. **Table 5.2** shows the maximum capacity of the bipolar pulse power source. The output of the bipolar pulse power supply was applied to the discharge gap between the tool electrode and the workpiece as that shown in **Fig. 5.11**.

The machining was conducted on a sinking EDM machine with the same method as described in Section 5.3.2.1. However, since in multi-discharge EDM by EIF, the external power supply was used instead of the power supply of the sinking EDM machine, servo feed control could not be conducted. Therefore, in the following sections the multi-discharge machining experiments were conducted by feeding the tool electrode to the workpiece with a constant feed speed. On the other hand, it should be noted that when using the bipolar power source, either plus or minus voltage was applied to the working gap all the time. Due to effect of electrophoresis, usually there would be a high possibility of debris concentration in the discharge gap under the electrical field. In this method, this problem was avoided by rotating the tool electrode to improve the flushing conditions of the discharge gap.

Table 5.2 Output limits of the bipolar pulse power supply

Output mode	Constant voltage output mode
Output voltage limit [V]	± 52
Output current limit [A]	± 28
Rise / Fall time [μs]	≒ 2.5
Output impedance	3.5 mΩ +0.65 μH
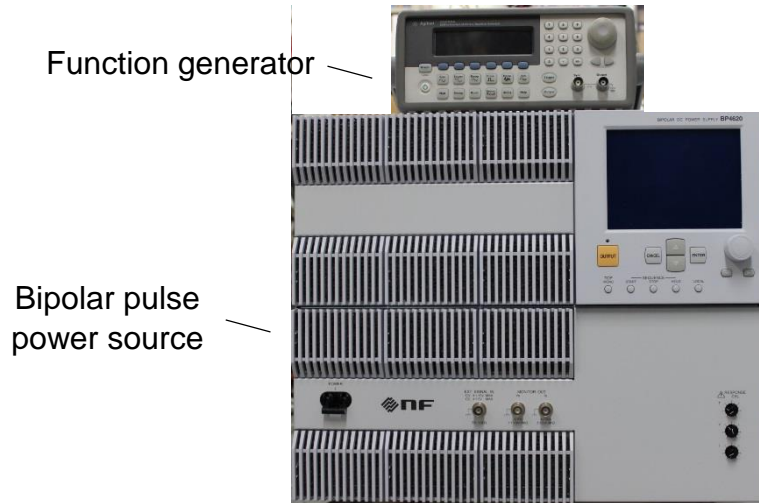
Fig. 5.20 Image of the pulse power supply: function generator + bipolar power source

5.3.3.3   Multi-discharge waveforms

Based on the experimental setup described above, multi-discharge EIF EDM of single crystal SiC was performed successfully. **Table 5.3** lists the machining conditions. The discharge waveforms of multi-discharge EDM with three and six separated feeding capacitors are shown in **Fig. 5.21**(b) and **Fig. 5.21**(c) respectively, which reveals the mechanism of multi-discharge EDM. For comparison, **Fig. 5.21**(a) shows the waveform of the conventional EDM by the electrostatic induction feeding method with single feeding capacitor EDM (hereafter referred to as single-discharge EIF EDM). **Fig. 5.21**(b) confirms that with three separate feeding capacitors, even though in a single pulse of the power source, three discharges can occur. **Fig. 5.21**(c) shows a waveform of six simultaneous or one-by-one discharges in a single pulse owing to the six separate feeding capacitors. Based on these phenomena, it was concluded that multiple discharges could be easily realized by controlling the number of the separate feeding capacitors and tool electrodes. It was therefore considered that the discharge frequency could be improved significantly by increasing the tool electrode numbers based on the developed multi-discharge EIF EDM method.

Table 5.3 Machining conditions

Pulse power source	
Amplitude [V]	±50
Frequency [Hz]	6k~12k
Duty factor [%]	50
Tool electrode	Copper rod
Workpiece	Single crystal SiC
Dielectric	EDM oil
Feeding capacity C [μF]	0.33
Set feed speed [μm/min]	5~100

(a)
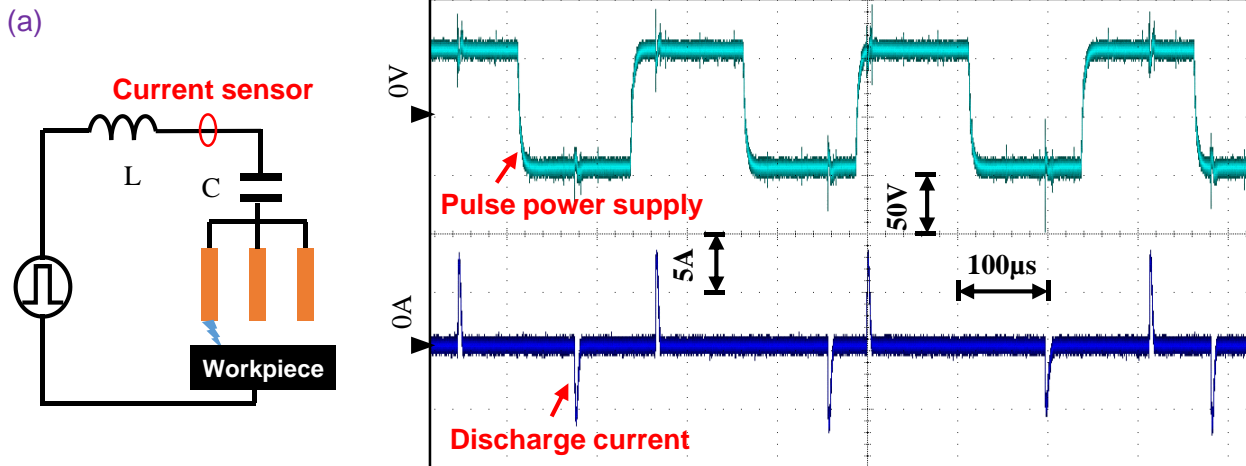
a) Schematic diagram of conventional EDM by EIF with single feeding capacitor and the corresponding discharge waveform
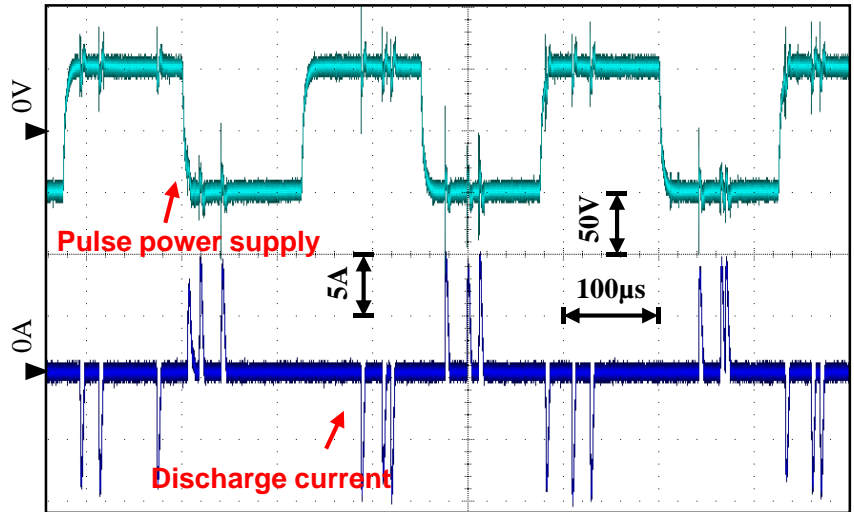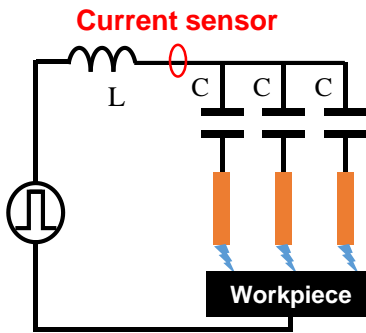
b) Schematic diagram of multi-discharge EDM by EIF with 3 feeding capacitors and the corresponding discharge waveform
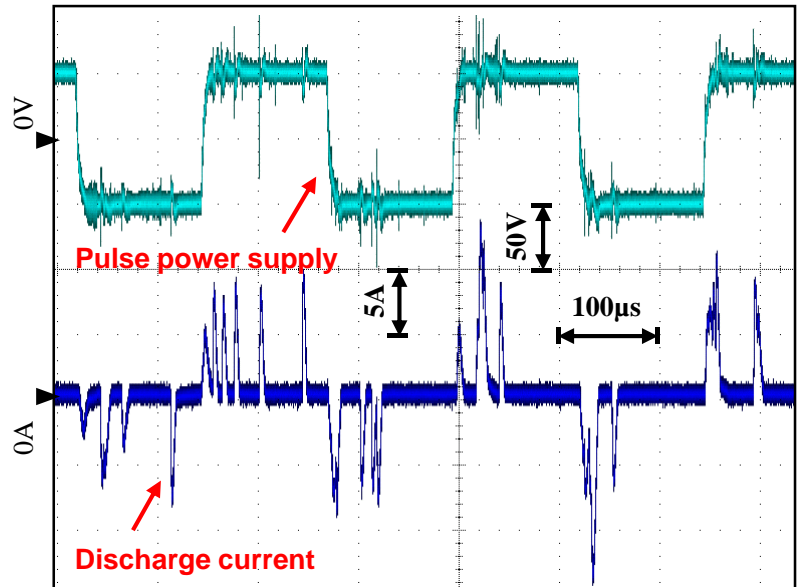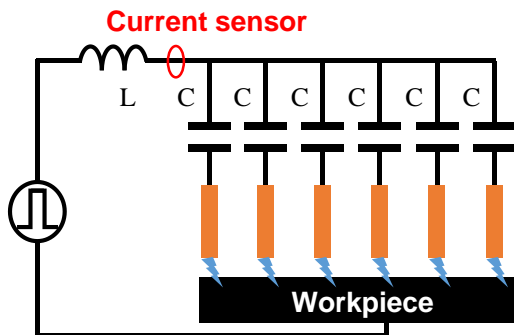
c) Schematic diagram of multi-discharge EDM by EIF with 6 feeding capacitors and the corresponding discharge waveform

Fig. 5.21 Discharge waveforms in multi-discharge EIF EDM with different number of feeding capacitors

Fig. 5.22 shows an enlarged view of the typical discharge waveform in multi-discharge EIF EDM with six separate feeding capacitors. It can be seen that with six separate feeding capacitors, six discharges can occur in a single pulse. The six discharges in a single pulse can occur simultaneously or sequentially one by one. In principle, the number of discharges per single pulse can be increased by increasing the number of separate tool electrodes. In practice, however, the number is limited by the capacity of the pulse power source, because the peak current may exceed the limit of the pulse power source when multiple discharges occur simultaneously.
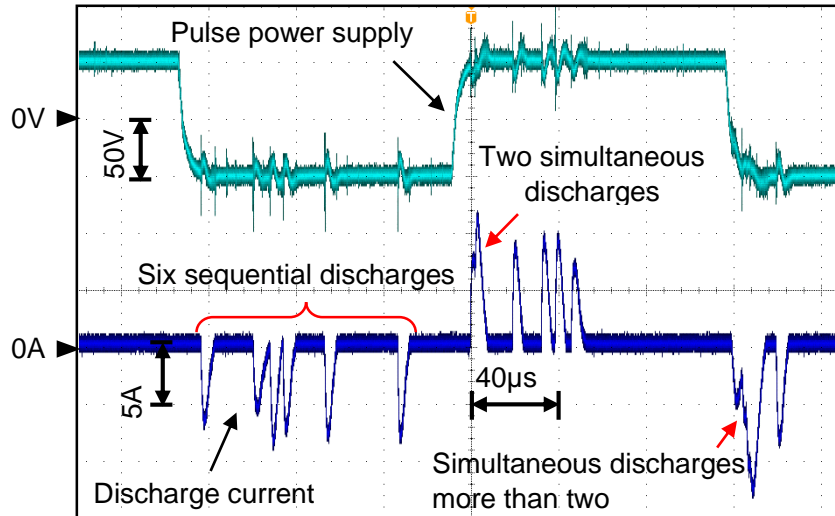
Fig. 5.22 Analysis of the discharge waveform of multi-discharge EDM with 6 discharges in one pulse

5.3.3.4   Increase of discharge frequency

Discharge frequency is one of the determining factors of machining rate. In the experiment, the discharge frequency difference between the conventional electrostatic induction feeding using one feeding capacitor and multi-discharge EDM using three separate feeding capacitors was investigated. Although the number of feeding capacitors was different, the total value of the feeding capacitance in the two cases was set the same as 3C (equal to 1μF) (refer to **Fig. 5.23**) to keep the total discharge energy the same. In addition, the total rod tool electrode number was kept the same. The single discharge energy could be decreased in multi-discharge EIF EDM method by the separate feed of electricity as shown in **Fig. 5.24**.

The machining experiments was performed successfully when using the feeding capacitor of 1μF. It was confirmed for the first time that EDM by the electrostatic induction feeding method can be used for not only micro-EDM machining but also for rough EDM machining.
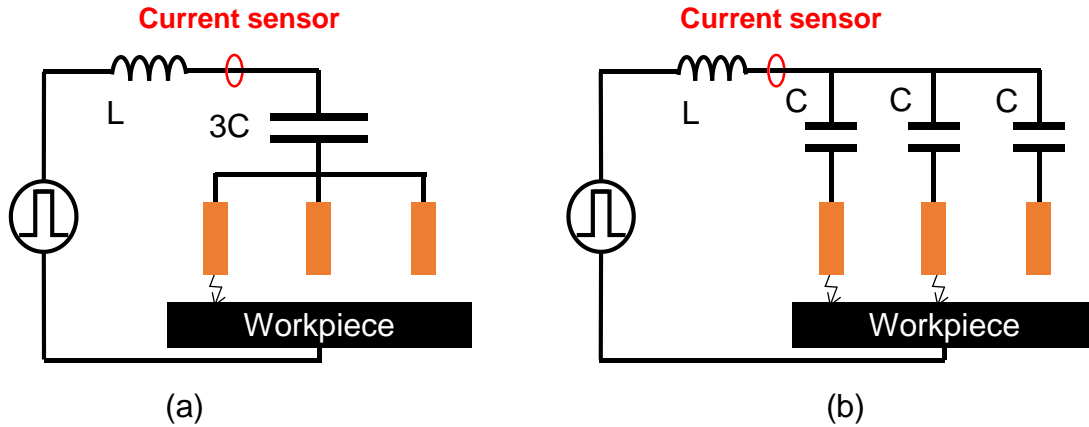
Fig. 5.23 Different methods of feeding electricity: a) Single-discharge EIF EDM with single feeding capacitor 3C; b) Multi-discharge EIF EDM with 3 separate feeding capacitors C
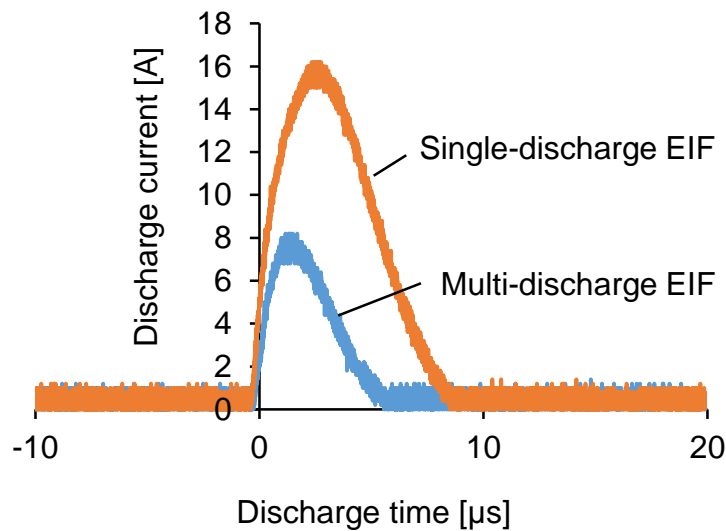
Fig. 5.24 Discharge current waveform differences between multi-discharge EIF EDM and single-discharge EIF EDM under the same total feeding capacitance

The total discharge frequency was measured utilizing a universal counter (*Hewlett-Packard Universal Counter, 53131A*). The total discharge number in two min was measured and the average discharge number per second was calculated and taken as the discharge frequency. **Fig. 5.25** shows the difference of the discharge frequency under the two different EDM methods. In the case of multi-discharge EIF EDM with 3 separate feeding capacitors, the discharge frequency, on average, was about 2.5 times of that of single-discharge EIF EDM method under the same feed speed. In terms of the maximum discharge frequency, it was about 4 times higher in the case of multi-discharge EDM compared to the case of single discharge EIF EDM method.
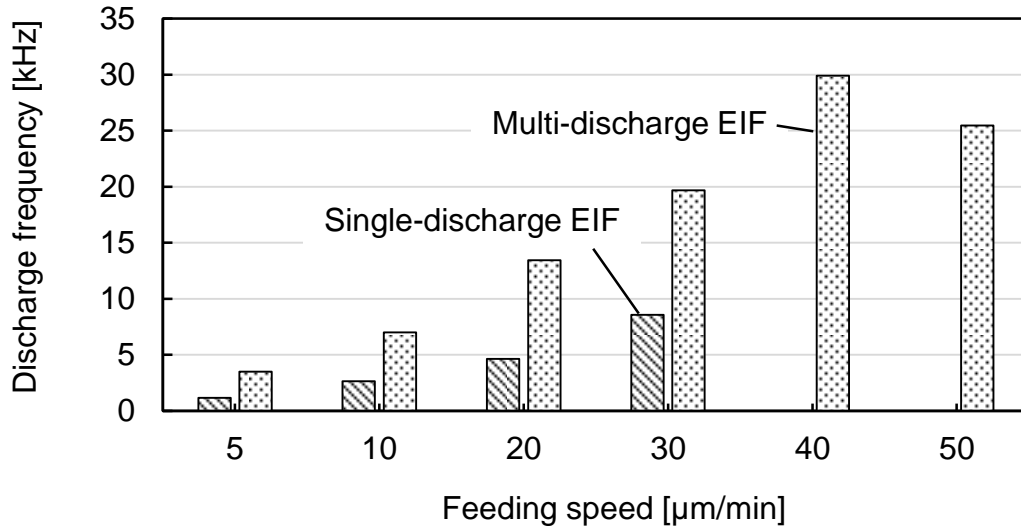
Fig. 5.25 Comparison of the discharge frequency between single-discharge EIF EDM and multi-discharge EIF EDM (Pulse power supply frequency: 8 kHz)

On the other hand, the maximum feed speed was around 25µm/min in the case of single discharge EIF EDM and 50µm/min in the case of multi-discharge EIF EDM with 3 separate feeding capacitors. Since the total feeding capacitance was the same, it may indicate that the machining efficiency of multi-discharge EDM method was higher.

In the case of multi-discharge EDM, the discharge frequency increased almost linearly with increasing the feed speed. However, the discharge frequency did not increase linearly after a threshold of the feed speed. The reason was considered that when the feed speed was high enough, probability of simultaneous discharges would become high due to smaller gap width. Discharges at each working gap would occur at the same time and the discharge current would be superimposed to each other in the main circuit. Therefore, only one discharge could be detected in a single pulse by the universal counter which detected the signal of the current sensor set at the main circuit (refer to **Fig. 5.23**).

In addition, it was found that in the multi-discharge EDM with 3 separate feeding capacitors, the actual measured discharge frequency at the maximum was about 4 times of the pulse power source frequency. Theoretically, the maximum discharge frequency may reach up to 6 times of the pulse power source frequency. Nevertheless, it could be confirmed that the discharge frequency can be increased by the multi-discharge EDM method. In single-discharge EIF EDM method, in order to realize high-frequency EDM, the general method is to increase the frequency of pulse power supply. However, if the pulse power supply frequency is increased too high, discharge concentration will occur due to too short discharge interval, resulting in an unstable machining process. In the multi-discharge EIF method, however, high frequency EDM can be realized by the multi-discharge mechanism even if the pulse power supply frequency is low, which is a considerable advantage of the multi-discharge EIF EDM method.

5.3.3.5   Material removal rate

Since the constant feed method was used in the experiment, the attainable maximum feed speed was investigated to evaluate the material removal rate of the multi-discharge EDM. In every experiment, the machining was conducted in two min with a constant feed speed. If the machining could be conducted stably without short circuit in the two min, the feed speed was increased furthermore. By this method the maximum feed speed was found out. **Fig. 5.26** shows the maximum feed speed obtained under the conditions used in the present work. It can be seen that the maximum feed speed increases with increasing the frequency of the pulse power source owing to the increased total discharge frequency and the maximum feed speed was around 75µm/min. Further increase of the pulse power source frequency was not possible because of the power limit of the bipolar power source used in the present work.
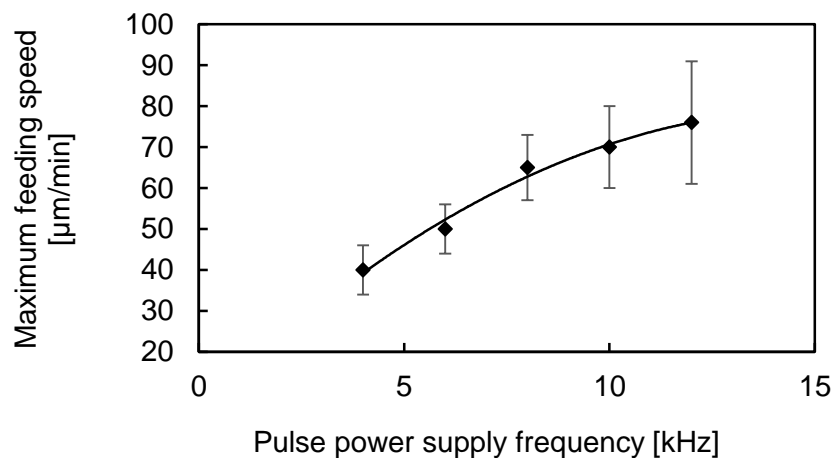
Fig. 5.26 Maximum feed speed increases with increasing the frequency of pulse power source.

5.3.3.6   EDM'd surface of rough machining by EIF method

The micro-topographies of the machined surfaces of SiC by the conventional single-discharge EIF EDM and multi-discharge EIF EDM are shown in **Fig. 5.27**(a) and (b) respectively. Under the two different methods, given the same total feeding capacitance, the machined surfaces showed totally different topography. Owing to the smaller energy of single discharge (refer to **Fig. 5.24**), the multi-discharge EDM'd surface presented a better surface integrity with smaller pits and less fracture compared with that of single discharge EIF EDM'd surface.

On the other hand, it was confirmed by experiments that increase of the number of feeding capacitors in the multi-discharge EIF EDM method did not influence the surface topography. **Fig. 5.28** presented an image of machined groove on SiC by the multi-discharge EIF EDM method with 3 separate feeding capacitors.

Fig. 5.27 EDM'd surface topography of SiC by electrostatic induction feeding method: a) single-discharge EIF EDM with one feeding capacitor; b) multi-discharge EIF EDM with 3 separate feeding capacitors.

Groove depth: 2mm

1.05mm

Material: SiC

Fig. 5.28 Photograph of machined groove on SiC by multi-discharge EIF EDM method (3 separate feeding capacitors)

182

5.3.3.7 Multi-discharge EDM coring of SiC wafer

The proposed EDM coring method can also be applied for coring SiC wafer. **Fig. 5.29** shows the designed experimental setup for EDM coring of a damaged SiC wafer resulted from abrasive wire saw process. SiC wafer (thickness: 0.5mm) was put on a flat support plate (S45C) to avoid the vibration during machining and to reduce the voltage drop inside the workpiece SiC by shortening the distance between the discharge spot of SiC and the electric feeder. In order to cut out the wafer completely, a circular groove was machined on the support plate right under the wafer cutting area. The wafer was fixed by a circular ring which was chucked by two precision fixtures. In addition, in order to avoid the displacement of the wafer after it is cut off, a magnet was put on the top center of the wafer for fixing.

Based on the setup, SiC wafer cylinder was cored successfully using the rotatory tool electrode. Before the experiments, the truing process of the copper rod electrode was accomplished by using a copper plate with the same fixture. The copper plate was fixed by the two precise fixtures to make sure that it was perpendicular to the Z axis. The truing was done by feeding the rotating electrode to the copper plate with a feeding depth of 2mm. After the truing process, the electrode was subjected to cut SiC wafer. By the truing process, the perpendicularity between the end surface of the electrode and the Z axis of the machine can be set. The run out error of the rotating tool, however, could not be eliminated.

Fig. 5.30 shows the micrograph and profile of machined groove taken by laser confocal microscope (*Olympus Lext Ols3000*). The groove shape was arc-shaped but not square probably due to larger tool wear at the edge of the copper rod electrode during machining. Therefore, in practical use, the fed depth must be larger than the wafer thickness so that no slope or burr exists at the edge of the wafer after coring. **Fig. 5.31** shows the micrograph and profile of cored wafer edge after complete coring. The edge of cut wafer was very straight without any burr.

The example of coring a 2inch wafer from a larger diameter (4inch) wafer by the developed method is shown in **Fig. 5.32**.

Fig. 5.29 Experimental setup for EDM coring of SiC wafer

Fig. 5.30 Machined groove on SiC wafer by EDM coring method (wafer thickness: 500µm)

Fig. 5.31 Edge of cored wafer by through cut

184

Fig. 5.32 Photograph of cored wafer by EDM coring method

5.3.3.8 Discussions

Based on the experimental results of multi-discharge EDM coring of SiC by the electrostatic induction feeding method, it can be considered that the same method can be successfully applied to the proposed multi-foil EDS method (refer to Section 5.2.5). However, it is considered that there are still several problems and subjects that should be solved before this method can be actually applied to practical use in the future.

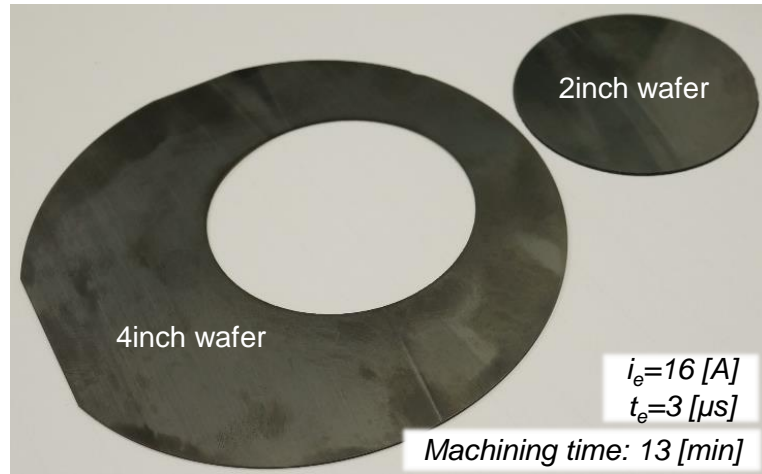1) In the multi-discharge EIF EDM method, the tool electrode must be separated so that separate feeding of electricity can be realized. However, separating of the tool electrodes will make the system very complex. In the case of multi-foil EDS of SiC, as shown in **Fig. 5.8**, with increasing the wafer number per slice, the machining system will become more complex due to the increased number of separate foil tool electrodes and the foil tool guiding and winding systems.

2) In the multi-discharge EIF EDM experiment, the machining was conducted by constant feeding method. In practical use, however, servo feed control system is considered necessary in order to improve the machining stability and the machining efficiency. Therefore, the servo feed control system should be developed in the future.

3) In the electrical discharge circuit by the electrostatic induction feeding method, the discharge energy can be increased by increasing the capacitance of the feeding capacitor C_1. However, the time constant of the discharge circuit ($= RC$) will also increase with increasing the feeding capacitance, which will result in a longer discharge duration. In other words, it is considered difficult to obtain a discharge waveform with a short pulse duration and a large peak current value by the electrostatic induction feeding method. From the previous study, however, it was known that short pulse duration was more suitable for high precision and high efficiency EDM of SiC. Therefore, this is considered as an important subject that should be improved and advanced in the future.

5.4   Conclusions of Chapter 5

In this chapter, in order to improve the slicing performances of multi-wire EDS method in terms of wire breakage, wire tension, wire running stability and wire diameter, multi-foil EDS method was proposed to slice SiC ingot. Moreover, multi-discharge EDM method by the electrostatic induction feeding method was developed to realize multi-discharge foil EDM slicing. The structure and the mechanism of realization of multi-foil EDS by the electrostatic induction feeding method was described. On the other hand, however, due to the limited conditions, the manufacturing of the experimental setup for multi-foil EDS could not be accomplished. Therefore, in order to investigate and verify the machining performance and feasibility of the proposed multi-discharge EDM method, a multi-discharge EDM coring experimental setup which could be used for coring SiC ingot was developed instead of multi-foil EDS setup. In the developed EDM coring setup, a dedicated tool electrode setup composed of 6 separate sets of rod electrodes (42 in total) was developed. Owing to this tool electrode setup, multi-discharge EDM by the electrostatic induction feeding method was realized successfully. Moreover, based on this setup, the machining feasibility and characteristics of multi-discharge EDM by the EIF were investigated. In addition, the coring performances of the developed experimental setup were investigated with regard to the coring speed and tool wear. The main conclusions were as the following:

1) The development of the experimental setup for multi-discharge EDM by the electrostatic induction feeding method was accomplished. Owing to the newly developed tool electrode setup, multi-discharge EDM by the electrostatic induction feeding method was conducted successfully. Six discharge pulses were generated simultaneously or sequentially one by one in a single pulse duration of the pulse power source by the six separate sets of tool electrodes. When using 3 separate sets of tool electrodes, the discharge frequency was improved to more than 4 times of the pulse power source frequency. Moreover, it was found out that under the same total discharge energy, multi-discharge EDM presented better surface integrity and machining stability compared to the conventional EDM method by EIF due to the separate feeding of electricity.

2) EDM coring of SiC ingot was performed successfully using the designed setup. The developed rotary tool electrode was advantageous for coring SiC because of its easy accessibility and better flushing conditions compared with those of the conventional tubular coring tool electrode. Under the conditions used in the present work, coring of 2inch SiC ingot could be performed with a machining feed speed of about 90µm/min. The EDM coring method of thin SiC wafer was also described and the coring results of SiC wafer were presented.

3) For the first time, EDM by the electrostatic induction feeding method was applied to rough machining process. Machining experiments of EDM of SiC by the EIF using feeding capacitance of 1µF were conducted successfully.

4) Due to the limited conditions, the experiments of multi-foil EDS method were not accomplished in this research. On the other hand, however, from the success of the multi-discharge EDM coring process using the electrostatic induction feeding method, it was considered that the proposed multi-foil EDS method could be performed successfully based on the same machining principle.

Chapter 6 Conclusions

Research and development of single crystal SiC semiconductor is advancing rapidly in recent years due to its superior properties over traditional Si semiconductor, such as high thermal conductivity, wide band-gap (3 times of that of Si), high critical electric field intensity (10 times of that of Si) and higher thermal conductivity etc. However the high cost of SiC has hindered the development and application of SiC based devices. The high cost of SiC is mainly caused by the manufacturing process of SiC. On one hand, the price of raw material is very high due to the difficulty in manufacturing high purity and low defects SiC bulk crystal. On the other hand, the manufacturing process of SiC wafer meets significant challenges due to its high hardness (approaching to that of diamond). The conventionally used manufacturing processes for making Si wafer are not suitable anymore to be used to produce SiC wafer. On the other hand, EDM slicing of SiC showed advantages over the conventional mechanical machining methods in terms of machining efficiency, slicing accuracy etc. Therefore, this research focused on the development of the EDM slicing process for manufacturing SiC wafer from the aspects of both the fundamental study and the practical application aiming to reduce the manufacturing cost and improve the machining efficiency of SiC wafer.

Chapter 2 mainly described the fundamental characteristics of EDM of SiC. At first, the differences of EDM characteristics between SiC and widely-used metal material were investigated by experiments. In addition, the material removal mechanisms of EDM of SiC were clarified. Heat conduction analysis taking into account Joule heating effect was conducted to investigate the influence of Joule heat on the EDM characteristics of SiC. At last, aiming to apply EDM for slicing SiC ingot, the wire EDM cutting performances of SiC were evaluated. The main conclusions were as the following:

1) The differences in machining characteristics between EDM of SiC and steel material were clarified. Under the same preset machining conditions, EDM of SiC showed a higher discharge voltage and lower discharge current compared with those of steel due to its high resistivity. Moreover, under the same preset servo voltage, EDM of SiC presented a higher discharge frequency compared to that of steel due to the higher discharge voltage of SiC. However, the material removal volume per single discharge in EDM of SiC was much higher than that of steel. In addition, the surface roughness was much higher in the case of SiC under the same discharge energy. Observation of EDM debris of SiC showed that the EDM debris of SiC included multi-angular particles, which indicated that EDM of SiC removed materials by not only decomposition and evaporation but also cracking and fracturing. This was considered as one reason for the higher machining efficiency of SiC compared with steel.

2) On the other hand, heat conduction analysis of single discharge of SiC showed that Joule heating effect considerably contributed to increase the discharge surface temperature near the discharge spot by one to two times. However, due to the high thermal conductivity of SiC, the surface temperature dropped quickly after the discharge ignition due to the expansion of plasma diameter. Under the same energy input of single discharge, the peak temperature on SiC discharge surface was lower compared with that of steel, but the working surface of SiC had a larger high temperature region. This was

considered as another mechanism for the higher material removal efficiency of SiC compared to that of steel.

3) Influence of the anisotropy properties of SiC on the EDM rate was investigated. No significant anisotropy of machining speed was found when machining was conducted in the *c* surface. However, it was found that higher machining speed could be obtained when the machining direction was parallel to the c axis compared with that perpendicular to the c axis. Moreover, fracture pits occurred more on the machined surface when the cutting direction was parallel with the crystal growth direction of SiC. The reason was considered to be caused by the difference of fracture strength along different crystal orientations.

4) Wire EDM cutting of SiC could achieve an area cutting speed of 5mm^2/min with a machined surface roughness of 4μm (R$_z$) under the discharge current of around 10A. The area cutting speed increased with increasing the discharge current, while the surface roughness deteriorated. The EDM'd surface of SiC presented a porous morphology with many holes on it. Fracture pits were occasionally generated on the machined surface of SiC probably caused by the thermal shock of discharges. A damage layer (thickness around 1-10μm) was found beneath the machined surface with many cracks in it.

5) Wire breakage was a significant problem of EDM cutting of SiC, especially when larger duty factor was applied. To avoid the wire breakage, small discharge current, small duty factor and high servo voltage were considered necessary, which, however, would influence the machining efficiency. In the case of multi-wire EDS method, since the load of machining time per unit length of wire is increased, the wire breakage problem will become more serious.

As discussed above, wire breakage was a significant problem limiting further improvement of wire EDM cutting performances of SiC. In addition to this, it was considered that there were still several other problems of wire electrode, especially in multi-wire EDS method such as limitation of wire tension force, wire running speed and wire diameter etc. which were considered critical to advance the wire EDM slicing process of SiC in terms of kerf width and cutting time etc. in the future. Based on these background, foil electrode was proposed in place of wire electrode for slicing SiC in Chapter 3. To perform foil EDM slicing of SiC, a foil tool electrode tension fixture was developed which could apply tension force to the foil and keep the foil flatness during machining. The performances of foil EDM cutting of SiC including the cutting speed, kerf width, foil tool wear etc. were experimentally investigated. In addition, the dielectric influences on the foil EDM performance of SiC were investigated. At last, aiming to reduce the foil tool electrode wear length, foil reciprocating slicing method, which was similar to conventional multi-blade diamond saw method, was proposed. The experimental setup of reciprocating slicing method was developed and the feasibility of this method was investigated. The main conclusions were as the following:

1) The development of foil tool electrode fixture was accomplished. The foil tool electrode fixture could apply tension force to the foil and keep the flatness of the foil electrode. Based on the developed setup, foil EDM cutting of SiC was performed successfully on a commercial sinking EDM machine. However, the machined kerf shape was not uniform. The kerf width at the entrance was larger than

that at the bottom. It was considered that the secondary discharges between the side surfaces of the foil tool electrode and the workpiece due to the existence of EDM debris and the large area effect of the foil electrode caused the large kerf width at the entrance side. A minimum kerf width of 100μm at the entrance was obtained by using 50μm thick foil electrode when the current was around 8A. On the other hand, the rectification characteristic of EDM of single crystal SiC semiconductor was not obvious.

2) Foil tool electrode length wear ratio was around 0.25~0.4 in foil EDM cutting when the discharge current is changing from 8A~20A with discharge duration of about 2μs (foil tool thickness: 50μm). It should be noted that jump motion of the foil tool electrode was applied here in the machining experiments. In addition, it was found that the tool wear ratio of SiC was more than 2 times lower compared with that of steel material under the same preset machining conditions. The higher material removal efficiency and higher thermal conductivity of SiC were considered as the reasons.

3) The optimal machining conditions of foil EDM of SiC on a sinking EDM machine were investigated. It was found that negative polarity of tool electrode and short pulse duration was better for foil EDM of SiC with higher machining speed and smaller tool wear ratio. On the contrary, long pulse duration was found not suitable for EDM SiC due to a larger tool wear ratio, larger kerf width and lower machining speed. In addition, it was found that the optimal pulse interval was around 15μs when pulse duration was 1μs in deionized water. Too short pulse interval would deteriorate the machining performances due to discharge concentration.

4) The foil EDM performances between in EDM oil and in deionized water were compared. It was found that under the same machining conditions, EDM in deionized water featured higher cutting speed, higher tool wear ratio and larger kerf width compared to those in EDM-oil. The EDM'd surfaces of SiC in deionized water and in EDM-oil were also significantly different. The surface machined in EDM-oil had a smoother surface topography while the surface machined in deionized water had many fracture pits on it. The surface roughness obtained from EDM in oil was much smaller compared to that in deionized water. In addition, the subsurface damaged layer depth in deionized water was slightly larger than that in EDM-oil. The reasons were considered as the following. Comparing with EDM oil, the higher permittivity of deionized water decreased the dielectric strength. In consequence, discharge occurred more easily in deionized water than in oil, which resulted in the larger kerf width of EDM of SiC in deionized water. In addition, it was considered that due to the better cooling effect of deionized water compared with that of EDM oil, the material removal efficiency of single discharge was higher in deionized water than in oil, which would result in a higher machining rate.

5) Since the foil tool wear length ratio was up to 0.2~0.4 in foil EDM cutting experiments when the foil thickness was 50μm, reciprocating slicing method was proposed in the research in order to disperse the foil tool length wear in foil EDM slicing of SiC. The development of the experimental setup of EDM slicing of SiC by foil tool electrode utilizing a reciprocating worktable was accomplished. Experiments showed that the foil tool electrode length wear could be decreased considerably due to the reciprocating motion. In addition, with increasing the reciprocating motion frequency, the average cutting speed increased due to the improved flushing conditions of the discharge gap. However, with further increasing the reciprocating frequency, the cutting speed decreased. At a certain point, machining could not proceed due to the collision between foil tool and workpiece, resulting in

deformation of foil tool. The reason for this was considered to be caused by the uneven tool length wear ratio along the reciprocating direction. In reciprocating slicing method, the foil tool wear length is not uniform along the reciprocating direction due to the variable discharge gap conditions and the less standby-time of the workpiece at the start and end stage of the reciprocating motion. Eventually, the uneven foil tool wear caused instability of the machining process in the reciprocating slicing method.

Based on the conclusions above, it was considered that a new method must be developed to achieve a constant and stable foil EDM slicing process. Therefore, in Chapter 4, EDM of SiC by winding the band foil electrode in a unidirectional way was proposed in place of the reciprocating slicing method aiming to achieve a stable and constant slicing process. With regard to the mechanism of the running foil EDM process, when the foil running speed is sufficiently high, the foil tool wear could be neglected and the foil EDM slicing method functions in the same way as wire EDM in terms of the slicing performances including machining speed, kerf loss, wire breakage, etc. On the other hand, when the foil electrode is running at a very low speed, tool electrode wear will become significant. With decreasing the foil thickness, the tool wear ratio will increase furthermore due to higher average heat flux. Based on theoretic analysis of the tool wear under steady state of machining, it was considered that steady state too wear model could be formed and the foil tool wear length should be proportional to the tool electrode area wear ratio and the slicing thickness of the workpiece and inversely proportional to the foil running speed under steady state. Therefore, the experimental setup for realizing running foil EDM slicing of SiC was developed. However, since no foil tool electrode is available on market currently, foil tool electrodes were homemade in this research. Due to the limited conditions, the manufactured foil tool electrode dimension accuracy was probably not high. In addition, since the foil electrode bobbin was hand-winded, the foil flatness error had some deviation. Nevertheless, based on the developed experimental setup, the feasibility and performance of the running foil EDS method were investigated. The main conclusions were as the following:

1) The development of the foil electrode running system which included foil unwinding unit, foil guides, load cell, tension sensor, winding unit etc. was accomplished in order to realize running foil EDM slicing of SiC ingot. Evaluation of the foil winding performance in terms of the tension force and the foil positioning accuracy etc. were conducted. Running foil EDS of SiC by thin foil electrodes with thickness of 30μm was performed successfully even under low foil running speed. Average kerf width less than 100μm was obtained in the experiments.

2) The workpiece fixing position had an influence on the machining rate. When the workpiece was fixed upside (relative to the tool electrode) on the main axis and fed downwards to the foil tool electrode, higher machining rate could be obtained. The reason was considered that when the workpiece was fixed upside, EDM debris in the discharge gap could be removed out more easily due to gravity.

3) Both high foil running speed and flushing of dielectric liquid could improve the machining rate by enhancing the discharge gap flushing conditions.

4) Compared with the currently developed multi-wire EDS, the newly developed foil EDS presented a smaller kerf width because thinner foil electrodes of 30μm in thickness were used. However, the machining speed by foil EDS did not show an obvious advantage. It was considered here that the foil electrode positioning accuracy resulted from the foil flatness error, the foil winding system etc. and

the insufficient flushing conditions may exert influence on the machining stability and affect the machining performances.

In Chapter 5, Multi-foil (instead of wire) electrical discharge slicing (EDS) of SiC was proposed to improve the slicing performances of multi-wire EDS in terms of wire breakage, wire tension and wire diameter. In order to realize multi-foil EDS of SiC, multi-discharge EDM by the electrostatic induction feeding method was proposed and the structure and mechanism of realization of multi-foil EDS by the electrostatic induction feeding method was described. However, due to the limited conditions, the manufacturing of the experimental setup for realization of the multi-foil EDS method was not accomplished. In order to investigate and verify the machining performance of the proposed multi-discharge EDM method, a multi-discharge EDM coring experimental setup which could be used for coring of SiC ingot was developed instead of multi-foil EDS setup. In the developed EDM coring setup, a dedicated tool electrode setup composed of 6 separate sets of rod electrodes (42 in total) was developed. Owing to this tool electrode setup, multi-discharge EDM by electrostatic induction feeding method was realized successfully. Based on this, the machining feasibility and characteristics of multi-discharge EDM by EIF were investigated. In addition, the coring performances of SiC ingot by the developed experimental setup were investigated in terms of the coring speed and the tool wear. The main conclusions were as the following:

1) The development of the experimental setup for multi-discharge EDM by the electrostatic induction feeding method was accomplished. However, due to the limited conditions, the developed experimental setup is used for EDM coring instead of EDM slicing. Owing to the newly developed rotary tool electrode setup with 6 separate sets of tool electrodes, multi-discharge EDM by the electrostatic induction feeding method was conducted successfully. In the developed multi-discharge EDM by the electrostatic induction feeding method, 6 discharges could be generated simultaneously or sequentially one by one (depending on the gap conditions) in a single pulse duration of the power source with 6 separate electrodes. When using 3 separate sets of tool electrodes, the discharge frequency was improved to more than 4 times of the pulse power source frequency. Moreover, it was found out that under the same total discharge energy, multi-discharge EDM presents better surface integrity and machining stability due to separate feeding of electricity.

2) EDM coring of SiC ingot was performed successfully using the designed setup. The developed rotary tool electrode was advantageous for coring SiC, because it was of easy accessibility and it provided better flushing conditions compared with the conventional tubular coring tool electrode. Under the conditions used in the present work, coring of 2inch SiC ingot could be performed with a machining feed speed of about 85μm/min. Thin SiC wafer was also cored successfully by the developed EDM coring method.

3) For the first time, EDM by electrostatic induction feeding method was successfully applied to rough machining process with the feeding capacitance of 1μF.

4) Due to the limited conditions, the development of multi-foil EDS system was not accomplished in this research. However, from the success of multi-discharge EDM coring process using the

electrostatic induction feeding method, it was considered that multi-foil EDS could be performed successfully based on the same machining principle.

In conclusion, in this research, the EDM characteristics and mechanism of EDM of SiC were clarified. The wire EDM performances of slicing of SiC were evaluated and the problems and disadvantages existing in the wire EDM slicing method, especially in the multi-wire EDM slicing method, such as wire breakage and wire vibration etc. were pointed out. To improve and advance the wire EDM slicing method, multi foil EDS method were proposed. In order to understand the basic characteristic of the foil EDM process, fundamental experiments of foil EDM of SiC were conducted. The feasibility of foil EDM cutting of SiC was confirmed. Moreover, based on the fundamental study, winding foil EDS method of slicing SiC ingot were proposed and the experimental setup was developed. The feasibility of the proposed running foil EDS method was confirmed. Furthermore, an alternative method for realizing multi-discharge EDM slicing was proposed to realize multi-foil EDM slicing of SiC. By the newly proposed multi-discharge EDM method, it was considered that the energy efficiency could be improved compared with the conventional multi-discharge wire EDM slicing method.

From the perspective of economy of practice use, however, the proposed multi-foil slicing method may increase the cost compared with the current multi-wire EDM slicing method. One of the reason is considered that the manufacturing cost of the foil tool electrode (band shape) with high dimension accuracy and shape accuracy is probably higher compared to wire electrode (round shape) due to the higher difficulty. In addition, as a new type of foil tool electrode, the foil guiding and winding system and the dielectric flushing system will be different from that of the wire electrode, which may bring about new challenges to the multi-foil EDS process. Considering reduction of cost, these aspects of the multi-foil EDS method should be discussed furthermore in the future practice.

Subjects and Perspectives:

Multi-foil EDS is considered to have a high potential to be applied for slicing SiC. Compared with multi-wire saw method and multi-wire EDS method, stable slicing of SiC with foil thickness of 30µm was accomplished which could achieve a thinner kerf width less than 100µm without foil breakage. This, under the present conditions, is considered as the main advantage of foil EDS compared to the other slicing method. On the other hand, due to the limited conditions in this research, high foil running speed and larger tension force was not realized. In addition, since the conventional pulse generator of sinking EDM machine was used for the machining, the machining speed of the foil EDS in the research did not show obvious advantages over multi-wire EDM slicing method which utilizes the pulse power supply of wire EDM machine.

In order to further advance the development of the multi-foil EDS in the future, there are several subjects that should be solved as described in the following:

1) Reduction of the area effect of foil electrode

   Under the same cross-section area, foil electrode with smaller thickness usually has a larger side surface area compared with that of wire electrode. Due to the area effect in EDM, side-surface discharge phenomena (also referred to as secondary discharge) will be considerable in foil EDM, which may cause a larger kerf width and a longer machining time. Therefore, the side-surface discharge phenomena must be suppressed so that both the slicing accuracy and the slicing time can be improved.

   A direct way to reduce the side surface area of the foil electrode is to make micro-holes on the foil electrode, as shown in **Fig. 6.1**. In addition to this, it is considered that the side surface area of the foil tool electrode (copper or brass) should be coated with a layer of high-resistance material to restrain the side surface discharges. Based on these considerations, an optimized foil tool electrode is proposed as shown in **Fig. 6.1**. The enlarged view of the cross-section of the proposed foil electrode is shown in **Fig. 6.2**. As noted here, except for the reduction of the foil side surface area, making holes on the foil can also help to improve the flushing conditions in the discharge gap by carrying out the EDM debris from the kerf.
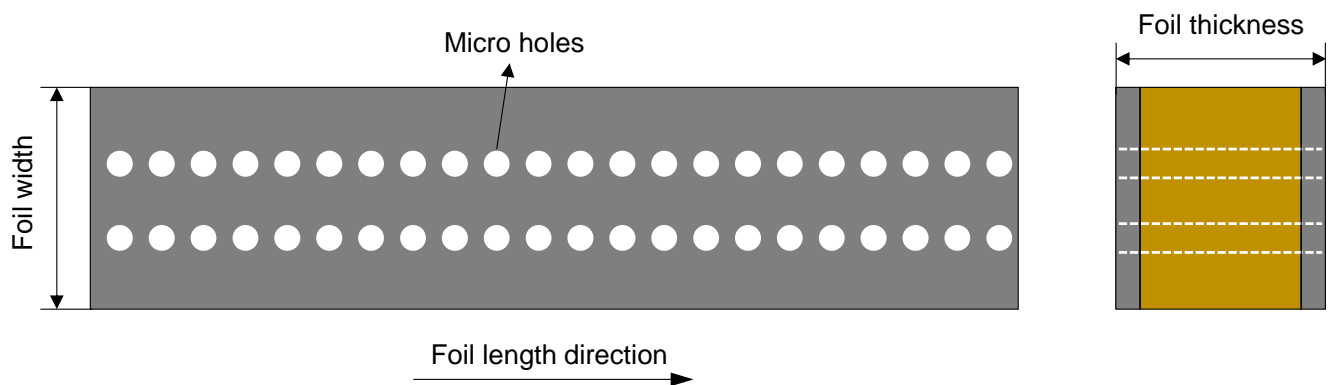
Fig. 6.1 Concept of optimal foil tool electrode
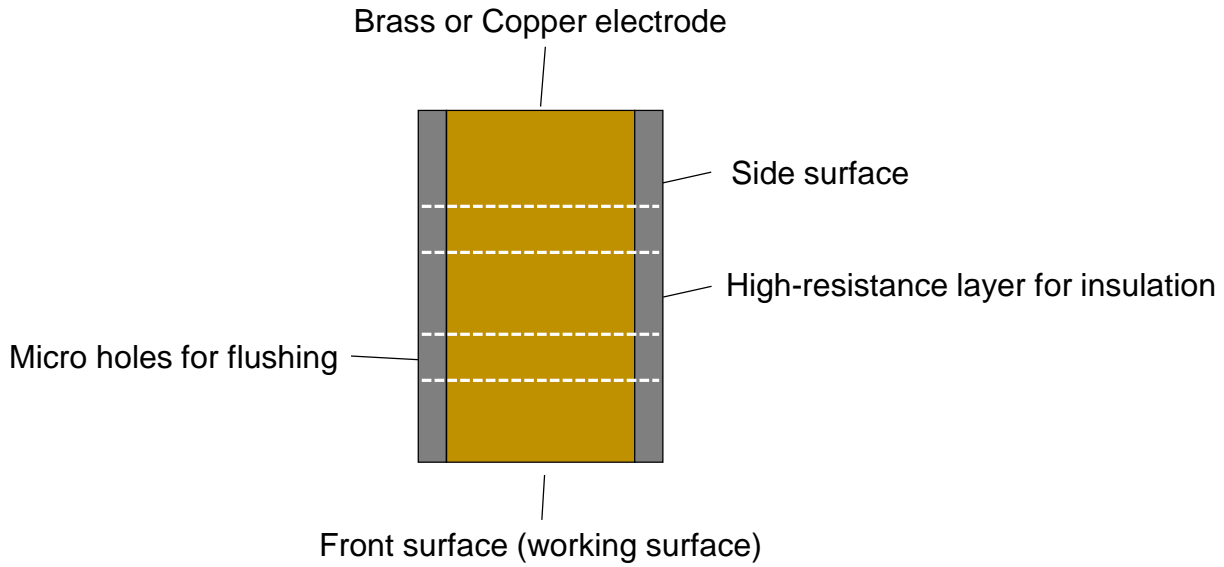
Fig. 6.2 Enlarged view of the cross-section of the proposed optimal foil tool electrode
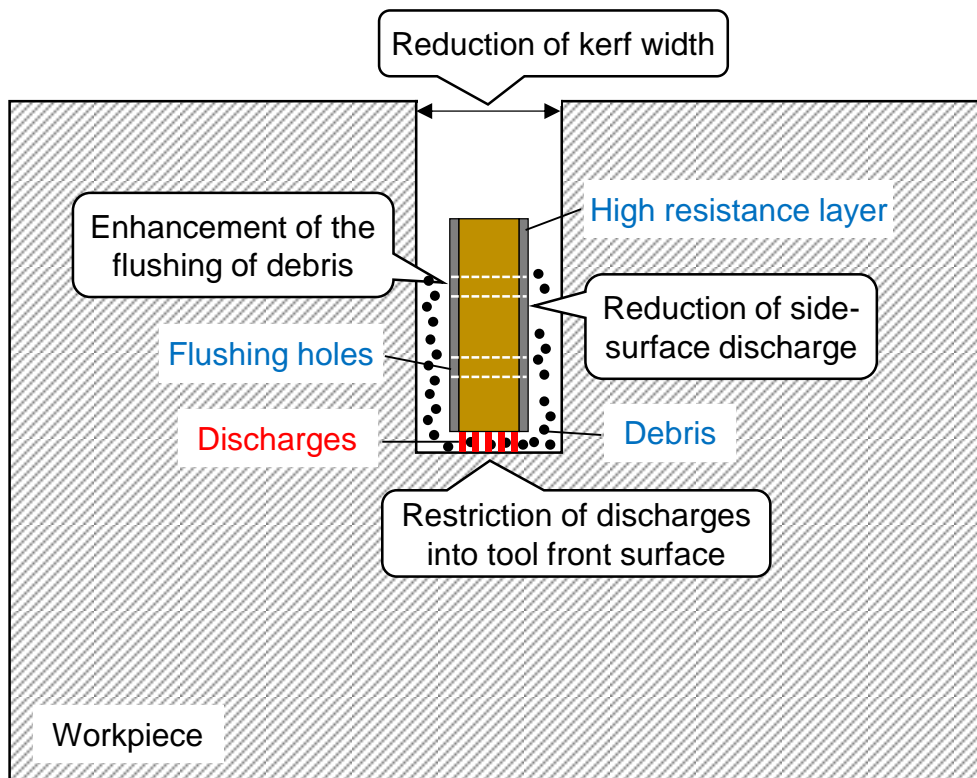

Fig. 6.3 Mechanism of the improvement of foil EDS by the proposed foil electrode

The mechanism of the improvement of the machining efficiency and accuracy by using the proposed foil tool electrode is illustrated in **Fig. 6.3**. If the side surface is coated with a high-resistance layer, most of the discharges will be concentrated to the uncoated front surface of the foil electrode. Therefore, the kerf width can be reduced and the machining stability can be improved due to the reduction of the side-surface discharges. In addition, the removal of EDM debris will be improved by the holes of the foil electrode during foil running.

2)   Development of foil EDM flushing system:

It is well known that in wire EDM process, the flushing conditions of the dielectric liquid, including the flushing pressure and the distance between the two flushing nozzles etc. have significant influence on the machining performances. Usually the machining rate can be increased by decreasing the distance between the two flushing nozzles owing to the better flushing conditions in the discharge gap. It is considered that this principle applies to the foil EDM slicing process. In foil EDM slicing of large diameter wafers in the future, it is considered that the removing out EDM debris from the discharge gap will become more difficult due to the increased slicing depth and thickness. Furthermore, when the wafer diameter or the slicing depth is large, it will has great difficulties to effectively inject the dielectric liquid into the small narrow discharge gap. Therefore, a well-developed flushing system is considered of significant importance to enhance the slicing performance of foil EDM slicing in the future. **Fig. 6.4** shows a proposal of the flushing method for foil EDM for the future study, which is similar to the flushing method in wire EDM process. The dielectric is flushed into the machining slit from both side of the ingot. To improve the flushing efficiency, it is better to make sure that the dielectric flow is surrounding all the surfaces of the foil tool electrode during flushing.
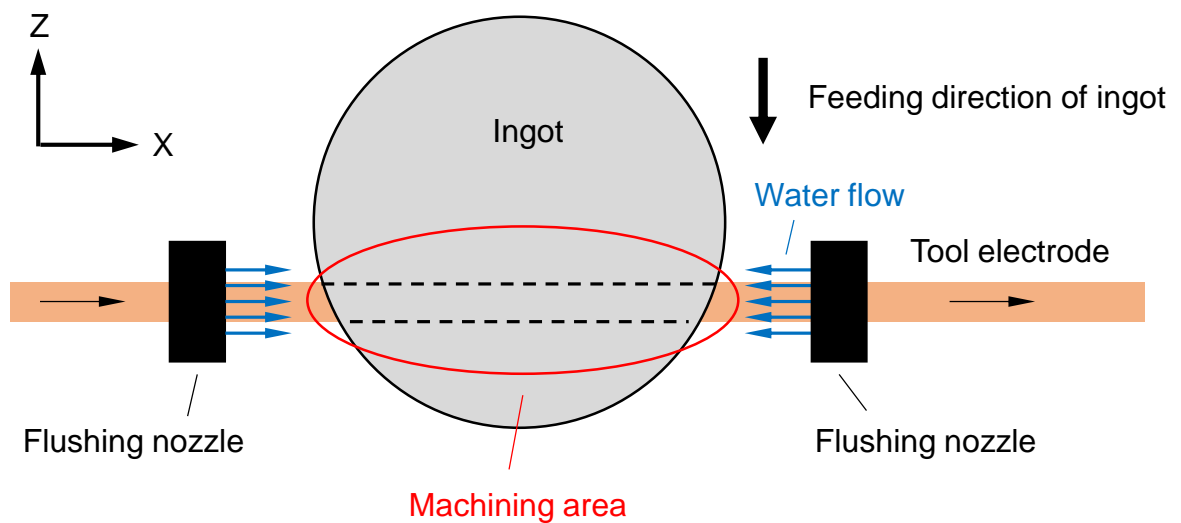

Fig. 6.4 Proposal of flushing system for foil EDM slicing of SiC ingot

3) Development of multi-foil EDS system with high foil running speed:

Higher foil running speed can facilitate the removal of EDM debris from the discharge gap and consequently improve the machining stability and efficiency. In this study, however, high foil running speed was not accomplished due to the limited conditions. Considering the band shape of the foil tool electrode, however, it is probably more difficult to realize high running speed (several tens to several hundred meters per min) compared with that of wire electrode which is round shape (axisymmetric). This is considered as a main and important subject for the future work.

4) In multi-discharge EIF EDM, the tool electrode must be separated so that separate feeding of electricity can be realized. However, separating the tool electrodes may make the system complex, especially when the tool electrode number is large. In the case of multi-foil EDS of SiC, with increasing the wafer number per slice, the machining system will become complex due to the increased number of separate foil tool electrodes and the foil guiding and winding systems. This is considered as a subject that should be improved and resolved in the future.

5) In this research, the multi-discharge EIF EDM was conducted by constant feeding method. In the practical use, however, a servo feed control system is considered necessary in order to improve the machining stability and efficiency in the future. **Fig. 6.5** shows a schematic diagram of the proposed servo control method which controls the discharge gap by controlling the total discharge current. In the multi-discharge EIF EDM, it is considered that the total average discharge current i is approximately proportional to the discharge gap width. When the gap is large, the total discharge frequency will be low. Since the average discharge current i in a certain time t is decided by the product of the peak discharge current and the discharge frequency, accordingly when the discharge frequency is low, the average discharge current value in a certain time (sampling time of servo system) will be low. On the other hand, when the discharge gap width is small, the probability of occurrence of multiple discharges in a single pulse will be high and the total discharge frequency will also be high, which can result in a larger average discharge current. In other words, the change of gap distance can be detected by measuring the average discharge current in a certain time. By comparing the preset reference current and the measured average discharge current, the difference can be obtained and the servo feed control of the main axis can be realized based on the difference.

6) In the electrical discharge circuit by the electrostatic induction feeding method, the discharge energy can be increased by increasing the capacitance of the feeding capacitor C_1. However, the time constant of the discharge circuit ($= RC$) also increases with increasing the feeding capacitance, which will result in a longer discharge duration. In other words, it is difficult to obtain a discharge waveform with a short pulse duration and a large peak current value by the electrostatic induction feeding method. From the previous study, however, it is known that short pulse duration is more suitable for high precision and high efficiency EDM of SiC. Therefore, this is considered as a subject that should be improved in the future.

(a)

(b)
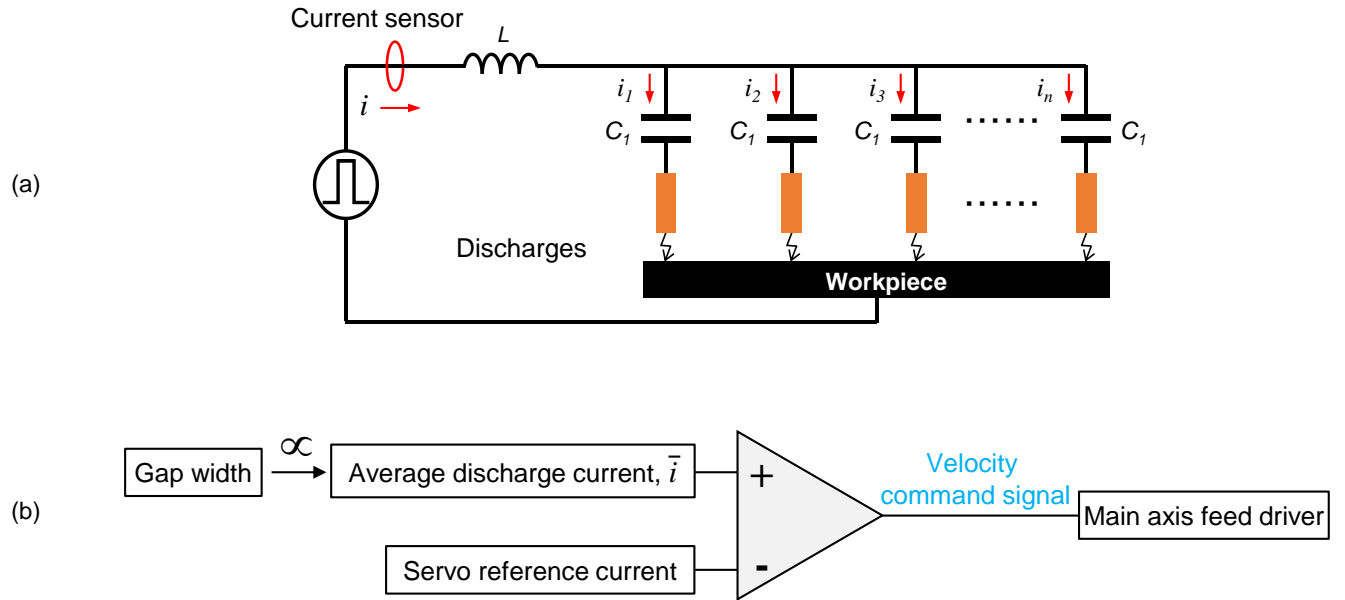
Fig. 6.5 Schematic diagram of servo feed control system for multi-discharge EDM by EIF

References

[1] 日本機械学会編，生産加工の原理，日刊工業新聞社 (1998).

[2] 斎藤長男，高鷲民生，毛利尚武，古谷政典，放電加工技術‐基礎から将来展望まで‐，日刊工業新聞社 (1997).

[3] 国枝正典，放電加工の原理と極間現象，精密工学会第 363 回講習会，東京大学 (2013).

[4] Handbook of Manufacturing Engineering and Technology, Springer-Verlag London (2013).

[5] M. Kunieda, B. Lauwers, KP. Rajurkar, BM. Schumacher, Advancing EDM through fundamental insight into the process, Annals of the CIRP. Vol. 54, Issue 2, pp. 64–87 (2005).

[6] H. Hashimoto, M. Kunieda, Spectroscopic Analysis of Temperature Variation of EDM Arc Plasma, Journal of the Japan Society of Electrical-machining Engineers. Vol. 31, Issue 68, pp. 32-40 (1997).

[7] S. Hayakawa, H. Kojima, M. Kunieda, N. Nishiwaki, Influence of Plasma Extinction on Machining Stability in EDM Process, Journal of the Japan Society for Precision Engineering. Vol. 62, Issue 5, pp. 686-690 (1996).

[8] Dhanaraj G, Byrappa K, Prasad V, Dudley M, Springer handbook of crystal growth, Springer, Berlin Heidelberg (2010).

[9] P. Friedrichs, T. Kimoto, L. Ley, G. Pensl, Silicon Carbide 1: Growth, Defects, and Novel Applications, Wiley-VCH Verlag GmbH&Co. KGaA, Weinheim (2010).

[10] P. Friedrichs, T. Kimoto, L. Ley, G. Pensl, Silicon Carbide 2: Power Devices and Sensors, Wiley-VCH Verlag GmbH&Co. KGaA, Weinheim (2010).

[11] W. Qian, M. Skowronsk, G. Augustine, R. C. Glass, H. McD. Hobgood, R. H. Hopkins, Characterization of Polishing-Related Surface Damage in (0001) Silicon Carbide Substrates, Journal of the Electrochemical Society. Vol. 142, Issue 12, pp. 4290-4294 (1995).

[12] 岩室憲幸，SiC パワーデバイスの開発と最新動向－普及に向けたデバイスプロセスと実装技術，第 1 版，S&T 出版，(2012).

[13] 加藤智久，SiC 単結晶の放電加工技術の現状と展望，日本学術振興会「結晶加工と評価技術第 145 委員会」第 122 回研究会資料, pp. 14-17 (2009).

[14] 加藤智久，大口径 SiC ウェーハ加工技術の最新動向，Electronic Journal 第 948 回 Technical Seminar, SiC ウェーハ製造技術の最前線徹底解説，(2011).

[15] I. Kao, Technology and research of slurry wire saw manufacturing systems in wafer slicing with free abrasive machining, International Journal of Advanced Manufacturing Systems, Vol.7, Issue 2, pp. 7–20 (2004).

[16] H.J. Moeller, Basic mechanisms and models of multi-wire sawing, Vol.6, Issue 7, pp. 501-513 (2004).

[17] 松波弘之，大谷昇，木本恒暢，中村孝，半導体 SiC 技術と応用　第 2 版，日刊工業新聞社 (2011).

[18] 前田弘人，出口喜宏，高鍋隆一，松田祥伍，加藤智久，高速マルチワイヤーソーによる SiC イン ゴットの高速切断，SiCおよび関連ワイドギャップ半導体研究会，第20回講演会予稿集，pp. 137- 138, (2011).

[19] 前田弘人，高鍋隆一，武田篤徳，松田祥伍，加藤智久，高速マルチワイヤーソーによる SiC イン ゴットの高速切断，2014 年度精密工学会秋季大会学術講演会講演論文集，pp. 751-752, (2014).

[20] A. Okada, Y. Uno, Y. Okamoto, A new slicing method of monocrystalline silicon ingot by Wire EDM, International Journal of Electrical Machining, No. 8, pp.21-26, (2003).

[21] W. Peng, Y. Liao, Study of electrical discharge machining technology for slicing silicon ingots, Journal of Materials Processing Technology, Vol. 140, No. 1-3, pp. 274-279, (2003).

[22] E. Bamberg, D. Rakwal, Experimental investigation of wire electrical discharge machining of gallium-doped germanium, Journal of Materials Processing Technology, Vol. 197, pp. 419–427, (2008).

[23] D. Rakwal, E. Bamberg, Slicing, cleaning and kerf analysis of germanium wafers machined by wire electrical discharge machining, Journal of Materials Processing Technology, Vol. 209, Issue 8, pp. 3740-3751, (2009).

[24] H. Takino, T. Ichinohe, K. Tanimoto, S. Yamaguchi, K. Nomura, M. Kunieda, High-quality cutting of polished single-crystal silicon by wire electrical discharge machining, Precision Engineering, Vol. 29, Issue 4, pp. 423-430 (2005).

[25] T. Kato, T. Noro, H. Takahashi, S. Yamaguchi, K. Arai, Characterization of electric discharge machining for silicon carbide single crystal, Materials Science Forum. Vols. 600-603, pp. 855-858, (2009).

[26] H. Yamada, S. Yamaguchi, N. Yamamoto, T. Kato, Cutting speed of electric discharge machining for SiC ingot, Mater Sci Forum, Vols. 717-720, pp. 861-864, (2012).

[27] S. Yamaguchi, T. Noro, H. Takahashi, H. Majima, Y. Nagao, K. Ishikawa, Y. Zhou, T. Kato, Electric discharge machining for silicon carbide and related materials, Materials Science Forum, Vol. 600-603, pp. 851-854 (2009).

[28] Y. Ishikawa, Y. Yao, Y. Sugawara, K. Sato, Y. Okamoto, N. Hayashi, B. Dierre, K. Watanabe, T. Sekiguchi, Comparison of slicing-induced damage in hexagonal SiC by wire sawing with loose abrasive, wire sawing with fixed abrasive, and electric discharge machining, Japanese Journal of Applied Physics, Vol. 53, No. 7, pp. 071301 (2014).

[29] Y. Okamoto, Y. Uno, A. Okada, S. Ohshita, T. Hirano, S. Takata, Development of multi-wire EDM slicing method for silicon ingot, Proceedings of ASPE 2008 Annual Meeting and the 12th ICPE, pp. 530-533 (2008).

[30] Y. Okamoto, A. Kimura, A. Okada, Y. Uno, J. Ohya, T. Yamauchi, Challenge to Development of Functional Multi-wire EDM Slicing Method using Wire Electrode with Track-shaped Section, Key Engineering Materials, Vols. 523-524, pp. 287-292 (2012).

[31] 鈴木彰隼，大谷卓也，岡本康寛，岡田 晃，栗原治弥，木戸正孝，グループ給電方式を用いたマルチワイヤ放電スライシング法の試み，電気加工学会全国大会（2014）講演論文集，pp. 95-98 (2014).

[32] 堀江 裕一郎，淵山正毅，多和靖展，吉川直樹，加藤智久，SiC 単結晶切断用マルチワイヤ放電加工機の開発，SiC および関連ワイドギャップ半導体研究会，第 20 回講演会予稿集，pp. 145-146 (2011).

[33] M. Ogawa, K. Mine, S. Fuchiyama, Y. Tawa, T. Kato, Development of multi-wire electric discharge machining for SiC wafer processing, Material Science Forum, Vols. 778-780, pp. 776-779 (2014).

[34] 糸数篤，橋本隆，福島和彦，湯澤隆，佐藤達志，シリコンカーバイドのマルチワイヤ放電加工，2012 年度精密工学会秋季大会学術講演会講演論文集，pp. 391-392 (2012).

[35] 糸数篤，三宅英孝，橋本隆，福島一彦，湯澤隆，シリコンカーバイドのマルチワイヤ放電加工 (第 2 報): 40 並列放電加工による薄板生産性の向上，2013 年度精密工学会春季大会学術講演会講演論文集，pp. 507-508 (2013).

[36] I. Cabanes, E. Portillo, M. Marcos, J.A. Sánchez, On-line prevention of wire breakage in wire electro-discharge machining, Robotics and Computer-Integrated Manufacturing, Vol. 24, Issue 2, pp. 287–298 (2008).

[37] N. Kinoshita, M. Fukui, G. Gamo, Control of Wire-EDM Preventing Electrode from Breaking, CIRP Annals - Manufacturing Technology, Vol. 31, Issue 1, pp. 111–114 (1982).

[38] K.H Ho, S.T Newman, S Rahimifard, R.D Allen, State of the art in wire electrical discharge machining (WEDM), International Journal of Machine Tools and Manufacture, Vol. 44, Issues 12–13, pp. 1247–1259 (2004).

[39] A. Okada, Y. Uno, M. Nakazawa, T. Yamauchi, Evaluations of spark distribution and wire vibration in wire EDM by high-speed observation, CIRP Annals - Manufacturing Technology, Vol. 59, Issue 1, 2010, pp. 231–234 (2010).

[40] 山下正英，北村朋生，山下健，福澤康，形彫り放電加工の加工速度に及ぼす材料物性の影響, 電気加工学会誌, Vol. 45, No. 109, pp. 71-79 (2011).

[41] T. Saeki, M. Kunieda, M. Ueki, Y. Satoh, Influence of Joule heating on EDM processes of high-electric-resistivity materials. American Society of Mechanical Engineers, Heat Transfer Division 366, pp. 95–103 (1996).

[42] C.S. Trueman, J. Huddleston, Material removal by spalling during EDM of ceramics, Journal of the European Ceramic Society, Vol. 20, Issue 10, pp. 1629-1635 (2000).

[43] A. Kojima, W. Natsu, M. Kunieda, Spectroscopic measurement of arc plasma diameter in EDM, CIRP Annals-manufacturing Technology, Vol.57, Issue 1, pp. 203-207 (2008).

[44] Saito N, Kobayashi K, Machining principle and characteristics of electric discharge machining. Mitsubishi Denki Giho 41(10), pp.1222-1230 (1967) [In Japanese].

[45] 猪飼健夫，藤田一郎，橋口清人，放電加工における放電痕形成の熱入力半径，電気学会論文誌 D（産業応用部門誌），Vol. 112, No. 10, pp. 943-949 (1992).

[46] H. Xia, M. Kunieda, N. Nishiwaki, Removal Amount Difference between Anode and Cathode in EDM Process, International Journal of Electrical Machining. Vol. 1, pp. 45-52 (1996).

[47] 早川伸哉，放電加工アークプラズマの熱流体解析による極間現象の解明，博士論文，東京農工大学 (1998).

[48] S. Hayakawa, M. Yuzawa, M. Kunieda, N. Nishiwaki, Mechanism of determining the power distribution in electrodes in EDM process, International Conference on Precision Engineering (ICPE), Taipei, (1997).

[49] M. Syvajarvi, R. Yakimova, E. Janzen, Cross-sectional cleavages of SiC for evaluation of epitaxial layers, Journal of Crystal Growth, Vol. 208, Issue 1-4, pp. 409–415 (2000).

[50] T. Kawakami, M. Kunieda, Study on Factors Determining Limits of Minimum Machinable Size in Micro EDM, CIRP Annals - Manufacturing Technology, Vol. 54, Issue 1, pp. 167-170 (2005).

[51] P. Wutimakun, H. Miyazaki, Y. Okamoto, J. Morimoto, T. Hayashi, H. Shiomi, Studies of thermal anisotropy in 4H-, 6H-SiC bulk single crystal wafers by photopyroelectric (PPE) method, Materials Science Forum, Vol. 600-603, pp. 521-524 (2008).

[52] J. Crofton, L. M. Porter, J. R. Williams, The Physics of Ohmic Contacts to SiC, Phys. Status Solidi B, Vol. 202, Issue 1, pp. 581–603 (1997).

[53] M. Kunieda, S. Ojima, Improvement of EDM efficiency of silicon single crystal through ohmic contact, Precision Engineering. Vol. 24, Issue 3, pp. 185-190 (2000).

[54] M. Kunieda, H. Takeuchi, U. Kusakabe: Clarifying EDM gap phenomena by gas chromatography analysis of bubbles, IJEM, No.16, pp.15-18 (2011).

[55] M. Kunieda, T. Takaya, S. Nakano, Improvement of Dry EDM Characteristics Using Piezoelectric Actuator, CIRP Annals - Manufacturing Technology, Vol. 53, Issue 1, pp. 183-186 (2004).

[56] T. Sato, Y. Imai, A. Goto, T. Magara, A. Takeuchi, K. Watanabe, A new grooving method based on steady wear model in EDM, International Journal of Electrical Machining, No. 5 (2000).

[57] M. Kunieda, A. Hayasaka, X.D. Yang, S. Sano, I. Araie, Study on nano EDM using capacity coupled pulse generator, CIRP Annals - Manufacturing Technology, Vol. 56, Issue 1, pp. 213-216 (2007).

[58] M. Kunieda, Muto. H, Development of multi-spark EDM, CIRP Annals - Manufacturing Technology, Vol. 49, Issue 1, pp. 119-122 (2000).

[59] F. Han, M. Kunieda, Development of parallel spark electrical discharge machining, Precision Engineering, Vol. 28, pp. 65-72 (2004).

[60] 花田倫宏，国枝正典，新家一朗，静電誘導給電を用いた微細放電加工法の開発，精密工学会誌, Vol. 72, No. 5, pp. 636-640 (2006).

[61] T. Koyano, M. Kunieda, Achieving high accuracy and high removal rate in micro-EDM by electrostatic induction feeding method, CIRP Annals - Manufacturing Technology, Vol. 59, Issue 1, pp. 219–222 (2010).

[62] N. Abbas，尾立真悟，国枝正典，静電誘導給電法を用いた微細放電加工における並列放電の試み，電気加工学会全国大会（2013）講演論文集, pp. 83-86 (2013).

Acknowledgements

Published papers related to this research

Peer-reviewed Journal Paper

1) Y. Zhao, M. Kunieda, K. Abe, Study of EDM cutting of single crystal silicon carbide, Precision Engineering, Vol. 38(1), pp. 92–99 (2014).

2) Y. Zhao, M. Kunieda, K. Abe, Multi-discharge EDM coring of single crystal SiC ingot by electrostatic induction feeding method, Precision Engineering, doi:10.1016/j.precisioneng.2014.12.007 (2015).

International Conference Paper

1) Y. Zhao, M. Kunieda, K. Abe, Experimental Investigations into EDM Behaviors of Single Crystal Silicon Carbide, Proceedings of the Seventeenth CIRP Conference on Electro Physical and Chemical Machining (ISEM), Procedia CIRP, Vol. 6, pp. 135–139 (2013).

2) Y. Zhao, M. Kunieda, K. Abe, Study on foil EDM of SiC single crystal in different dielectric liquids, 5th International Conference of Asian Society for Precision Engineering and Nanotechnology, November 2013, Taipei, Taiwan.

Domestic Conference Paper

1) Y. Zhao, M. Kunieda, K. Abe, T. Harada, Improvement of foil EDM slicing of SiC single crystal by utilizing reciprocating worktable, 電気加工学会全国大会(2013), 電気加工学会全国大会講演論文集, pp. 75-78 (2013).

2) Y. Zhao, M. Kunieda, K. Abe, T. Harada, Investigation of foil EDM slicing performances of single crystal SiC, 精密工学会秋季学術講演会, 精密工学会学術講演会講演論文集 (2013), pp. 967-968 (2013).

3) Y. Zhao, M. Kunieda, K. Abe, Experimental Studies of EDM Slicing of Single Crystal SiC Ingots by Band Copper Foil Electrodes, 電気加工学会全国大会 (2012), 電気加工学会全国大会講演論文集, pp. 81-82 (2012).

4) Y. Zhao, M. Kunieda, K. Abe, Fundamental Studies of EDM Characteristics of Single Crystal Silicon Carbide, 精密工学会秋季学術講演会, 精密工学会学術講演会講演論文集(2012) E43, pp. 359-360 (2012).

5) 趙永華，北村朋生，国枝正典，阿部耕三，単結晶 SiC の放電加工の基礎研究，第 205 回電気加工研究会，電気加工技術，Vol.36，No.113，pp. 1-6 (2012).